IMPROVING POLYSULFONE MEMBRANE RESISTANCE TO CARBON DIOXIDE INDUCED PLASTICIZATION DURING NATURAL GAS SEPARATION USING FUNCTIONALIZED CARBON NANOTUBES

Oluseyi Adebisi Aberefa

A thesis submitted to the Faculty of Engineering and the Built Environment, University of the Witwatersrand, Johannesburg, in fulfilment of the requirement for the Degree of Doctor of Philosophy.

May, 2019

DECLARATION

I declare that this thesis is my own unaided work. It is being submitted for the degree of Doctor of Philosophy in the University of Witwatersrand, Johannesburg. It has not been submitted before for any degree or examination to any other University.

_____

(Signature of candidate)

_____ Day of _____ year _____

ABSTRACT

Commercial natural gas, generally methane (CH_4), is described as the most efficient energy source with a calorific value per mass of approximate 50.1 MJ/kg. However, raw natural gas is made up of mostly methane and a considerable quantity of other components like C_{2+}, CO_2, water and hydrogen sulphide (H_2S) in varying composition from well to well depending on the geographical location and condition. Membrane technology for gas separation technology has become an acceptable method for CO_2 removal from natural gas. Majority of commercial natural gas separation membrane systems are polymeric due to processing feasibility and low cost. However, conventional polymeric membranes have reached a trade-off threshold between permeability and selectivity, and of great concern is CO_2 induced plasticization due to harsh industrial conditions such as high feed pressure. The addition of carbon nanotubes (CNTs) into polymers appears to offer a unique solution to the deficiencies of conventional polymeric membrane systems.

In this study, carbon nanotubes (CNTs) were produced using a catalyst-assisted chemical vapour deposition method. Ferrocene was used as the catalyst. Effects of carbon sources (acetylene and methane) and production conditions (temperature and type of carrier gas) on the physicochemical property of as-produced CNTs were investigated using field emission scanning electron microscopy (FESEM), energy-dispersive X-ray spectroscopy (EDS), electronic precision balance (EPB) and Raman spectroscopy. The best of as-produced CNTs was purified and functionalized using carboxylation protocol. The surface chemistry, thermal stability, textural property and crystallinity of the functionalized CNTs (FCNTs) were obtained using Fourier transform infrared spectroscopy (FTIR), thermo-gravimetric analysis (TGA), N_2 physisorption at 77 K and X-ray diffraction (XRD), respectively. CNT produced from methane and argon at 900 ^oC displayed the best quality with I_D/I_G ratio of 0.17 while the CNT produced from acetylene and mixture of argon and hydrogen at 1000 ^oC has the highest yield of 1.78 mg/s. FTIR confirms successful functionalization of CNTs. The degree of functionalization obtained from TGA is consistent with that of EPB. N_2

physisorption at 77 K indicates an increase in pore volume and average pore size of the FCNTs indicating more adsorption sites for the adsorbate. Thereby suggesting that FCNT could be a good filler in membrane synthesis for gas separation.

Dense mixed matrix membranes (MMMs) were synthesized by incorporating functionalized CNTs (FCNTs) at different wt. % (0.2, 0.5, 1.0, and 1.5) into polysulfone (PSF) using evaporation method. The MMMs were characterized using field emission scanning electron microscopy (FESEM), thermogravimetric analysis (TGA), differential scanning calorimetry (DSC), atomic force microscopy (AFM) and texture analysis (TA). Single gas permeation experiment was conducted using a custom-built permeation set-up via constant volume variable pressure technique while mixed gas permeability was measured on a constant pressure variable volume gas permeation apparatus. Surface and cross-section morphology of the MMMs as depicted by FESEM show that the membranes are dense, indicating that the membranes consist of dense structure whose porosity is not observable under an electron microscope. Depth-at-max analysis of AFM images of the synthesized membranes further supports that the pores of the MMMs possess dense structure. TGA indicates improved thermal stability of the MMMs with increasing wt. % loading of FCNTs. DSC results show that the glass transition temperature (T_g) of the MMMs was also improved with the addition of FCNTs. However, the increase in wt. % loading of FCNTs does not significantly increase the T_g of the MMMs. Tensile strength and Young's modulus of the MMM obtained from TA show an increase in these mechanical properties with the addition of FCNTs. Single gas permeation results indicate an increase in CO_2 permeability as the wt. % loading of FCNTs increases up to 1.0 wt. % loading. Mixed gas separation shows similar trend without sacrificing CO_2/CH_4 selectivity.

CO_2 induced plasticization of the membranes was investigated experimentally and by phenomenological modelling. The sorption isotherms showed a typical dual-mode sorption model behaviour for all the types of synthesized membranes with the CO_2 concentration increasing rapidly at low pressures, which indicated a hole-filling of the Langmuir sites. At higher pressure, the rate of increase in the concentration declines

due to the saturation of the Langmuir sites, the further increase in the concentration at higher pressure is because of the penetrant sorption in Henry's law sites. The permeation isotherm of pure PSF indicated plasticization onset at CO_2 pressure of 12 bar. The MMMs showed no sign of plasticization over the pressure range tested (0-20 bar). This indicated an improvement in the CO_2 plasticization resistance of PSF by the addition of FCNTs. The developed model assumed three possible interface interactions in the MMMs; polymer matrix – polymer matrix, CNT – polymer matrix, and aligned CNT – CNT interface interactions. The model also accounted for the plasticization of the membrane. The model equation was solved by using the Levenberg-Marquardt algorithm in the Matlab environment to obtain the plasticization potential and the fraction of the gas held in Langmuir sites that have mobility within the membrane. The model CO_2 permeability is in good agreement with CO_2 permeability obtained experimentally. The PSF plasticization potential obtained is similar to ones reported in the literature. The fraction of the gas held in Langmuir sites that have mobility within the membrane increases with an increase in FCNT wt. % loading which shows high diffusivity through the microvoids with respect to diffusivity through the polymer matrix. This is an indication of an increase in Langmuir sorption sites for the penetrant thereby improving gas permeability.

ACKNOWLEDGMENTS

I am a product of the grace of God and the privilege of working with some great men and women on this PhD journey. My heart is full of gratitude to God, the Father of light, with whom there is no variation or shadow of turning. Your help has brought me thus far. I am eternally thankful!

It an honour and a rare privilege for me to have Profs Sunny Iyuke and Michael Daramola as my supervisors. You believed so much in my abilities and you gave me ample opportunities to give expressions to my ideas. I cannot thank you enough for your great support and valuable contributions towards the success of this study. Sirs, I am grateful.

I wish to appreciate my host at the University of Melbourne (UoM), Australia, Dr. Colin Scholes and his research group for the warm welcome I received during my research visit to the department of chemical engineering, UoM. Special thanks to Bill Lu and Liang Liu for assisting me with gas permeation and sorption measurement equipment set-up at UoM.

I wish to thank National research foundation (NRF) and University of the Witwatersrand for funding this study. Special thanks to CHMT workshop team and MMU staff for fabrication of equipment and characterization of samples, respectively. Many thanks to my colleagues; Demilade, Ezinne, Damilola, Olawale, Ndangi, Veronica, Kelvin, and Kgothatso. I value your immense contributions to the success of this study.

My sincere thanks to my children; Praise, Wisdom, and Michelle. You understood with me during my many absences at home in the course of this study. You often stayed awake till late night just to say ‘welcome daddy’ to the daddy that always come home late due to his studies. You guys are the best!

To my wife, my love, the first lady federal republic of my home, princess Olufunke, words cannot express the immeasurable support you gave me during this study. You

encouraged me and you covered the missing gap due to my absence at home such that the children did not feel my absence so much. Thank you, my darling friend!

LIST OF PRESENTATIONS AT CONFERENCES, RESEARCH VISIT, PUBLISHED AND SUBMITTED PAPERS RELATED TO THIS WORK

1. **Aberefa**, O., Bedasie, K., Madhi, S., Daramola, M.O. and Iyuke, S.E. (2018) Production of carbon nanotube yarn from swirled floating catalyst chemical vapour deposition: a preliminary study. *Advances in Natural Sciences: Nanoscience and Nanotechnology*, *9*(3), p.035009

2. **Aberefa, O.A.,** Daramola, M.O. and Iyuke, S.E., 2019. Production and functionalization of carbon nanotubes for application in membrane synthesis for natural gas separation. Microporous and Mesoporous Materials, 280, pp.26-36.

3. **Aberefa**, O. A, Daramola, M. O., Scholes, C. A. and Iyuke, S. E. Synthesis and performance evaluation of functionalized carbon nanotube/polysulfone dense membrane for CO_2/CH_4 separation. ***Submitted to Separation Science and Technology.***

4. **Aberefa**, O. A, Daramola, M. O. and Iyuke, S. E. CO_2 induced plasticization study of functionalized carbon nanotube/polysulfone dense membrane: experimental and modelling. ***Submitted to Chemical Engineering Journal.***

5. **Aberefa**, O. A, Daramola, M. O. and Iyuke, S. E. *Synthesis of novel carbon nanotube infused polymeric membranes for improved resistance to carbon dioxide plasticization during natural gas separation: Prospects*, Centre for Renewable Energy and Water, International Conference, 24 November 2016, Vanderbijlpark, South Africa. **Oral Presentation.**

6. **Aberefa**, O. A, Daramola, M. O. and Iyuke, S. E. *Production and functionalization of carbon nanotubes for application in membrane natural gas separation*, School of Chemical and Metallurgical Engineering, Wits poster day, 28 September 2017, Johannesburg. **Poster Presentation.**

7. **Aberefa**, O., Bedasie, K., Madhi, S., Daramola, M.O. and Iyuke, S.E. *Production and characterization of yarn spun directly from carbon nanotube bundles,* Canadian Society for Chemical Engineering, International conference, 22 – 25 October 2017, Edmonton, Canada. **Oral Presentation.**

8. **Aberefa, O.A.,** Daramola, M.O. and Iyuke, S.E. *Synthesis and performance evaluation of functionalized CNT/PSF dense membrane for CO_2/CH_4 separation,* Gordon Research Conference, 11 – 17 August 2018, New London, NH, United States. **Discussion leader and Poster.**

9. ***Research visit**:* Peter Cook Centre for Carbon Capture and Storage research, University of Melbourne, Melbourne, Australia. 07 December 2017 – 10 January 2018.

TABLE OF CONTENTS

Contents Page

LIST OF FIGURES

Figures **Page**

LIST OF TABLES

Tables **Page**

NOMENCLATURE

A	Permeation area
A-Ar	Acetylene and argon
A-Ar/H	Acetylene and argon plus hydrogen
AFM	Atomic force microscopy
b	Langmuir affinity constant
BET	Brunauer-Emmett-Teller
BJH	Barrett-Johner-Halenda
BTU	British thermal unit
C	Total penetrants concentration
CCVD	Catalyst chemical vapour deposition
C_d	Concentration of gas molecules in Henry's law environment
CEE	Centre for energy economics
C_h	Concentration of gas molecules in Langmuir adsorption sites
C_h'	Polymer matrix saturation constant
CH_4	Methane
C_m	Concentration of the mobile gas
CNT	Carbon nanotube
CO_2	Carbon dioxide
CPVV	Constant pressure variable pressure
CVD	Chemical vapour deposition
CVVP	Constant volume variable pressure
DC	Direct current
DCM	Dichloromethane
D_d	Diffusion coefficient
D_o	diffusion coefficient as C_m tends to zero
DSC	Differential scanning calorimetry
DWCNT	Double-walled carbon nanotube
EDS	Energy-dispersive X-ray spectroscopy

EIA	Energy information administration
EPB	Electronic precision balance
F	Fraction of the gas held in Langmuir sites that have mobility
FCNT	Functionalized carbon nanotube
FESEM	Field emission scanning electron microscopy
FTIR	Fourier transform infrared radiation spectroscopy
H_2S	Hydrogen sulphide
H_2SO_4	Sulfuric acid
HCl	Hydrochloric acid
HNO_3	Nitric acid
IUPAC	International Union of Pure and Applied Chemistry
J	Gas flux
J_s	Gas flux at steady state
k_d	Henry's law solubility coefficient
L	Membrane thickness
M-Ar	Methane and argon
MMM	Mixed matrix membrane
MWCNT	Multi-walled carbon nanotube
N_2	Nitrogen
NMP	N-methyl-2-pyrrolidone
O_2	Oxygen
^oC	Degree Celsius
P	Permeability
p	Pressure
PCNT	Purified carbon nanotubes
P_{eff}	Effective permeability
PES	Polyethersulfone
PSF	Polysulfone
RBM	Radial breathing mode
RCNT	Raw carbon nanotube

STP	Standard temperature and pressure
SWCNT	Single-walled carbon nanotube
T	Temperature
TA	Texture analyzer
TEM	Transmission electron microscopy
T_g	Glass transition temperature
TGA	Thermo-gravimetric analysis
UoM	University of Melbourne, Australia
V	permeate constant volume
wt.	Weight
XRD	X-ray diffraction
α	Selectivity/separation factor
β	Plasticization potential
$\emptyset$	Fraction of FCNTs dispersed into the polymer matrix
%	Percentage
Δp	Transmembrane pressure

CHAPTER 1

1 INTRODUCTION

1.1 Background

Natural gas has become the most increasing energy source globally in terms of consumption. According to Energy information administration (EIA, 2016), natural gas world consumption projection will rise from 120 trillion cubic feet in 2012 to 203 trillion cubic feet in 2040. Commercial natural gas, generally methane (CH_4), is described as the world's cleanest and most efficient energy source with a calorific value per mass of approximate 50.1 MJ/kg (George et al., 2016). Furthermore, it has the lowest carbon dioxide (CO_2) emission upon combustion when compared to oil (30% less) and coal (43% less) (Langston and Lee, 2010).

Natural gas processing involves separation of acid gases, water (both free and saturated water), condensate and non-condensate from raw natural gas (Mokhatab et al., 2015), as shown in Figure 1.1. The objective is to produce a sales gas that conforms to market specifications. These specifications are primarily aimed at meeting pipeline requirements and the needs of industrial and domestic consumers (Poe and Mokhatab 2017). The specifications include the following:

- The gross heating value must be within a specified BTU content range. For instance, in the US, it should be 1035±50 Btu per standard cubic foot (CEE, 2004).
- It must be delivered at a specified hydrocarbon dew point. This would prevent liquid condensate and slugs formation which could damage the reticulation network (CEE, 2004).
- It should contain only trace amount of elements of compound such as CO_2, H_2S, N_2, mercury, organic sulfur products and O_2 (CEE, 2004).
- The gas must be dehydrated sufficiently to prevent corrosion and formation of gas hydrates in the processing plant or pipeline (CEE, 2004).

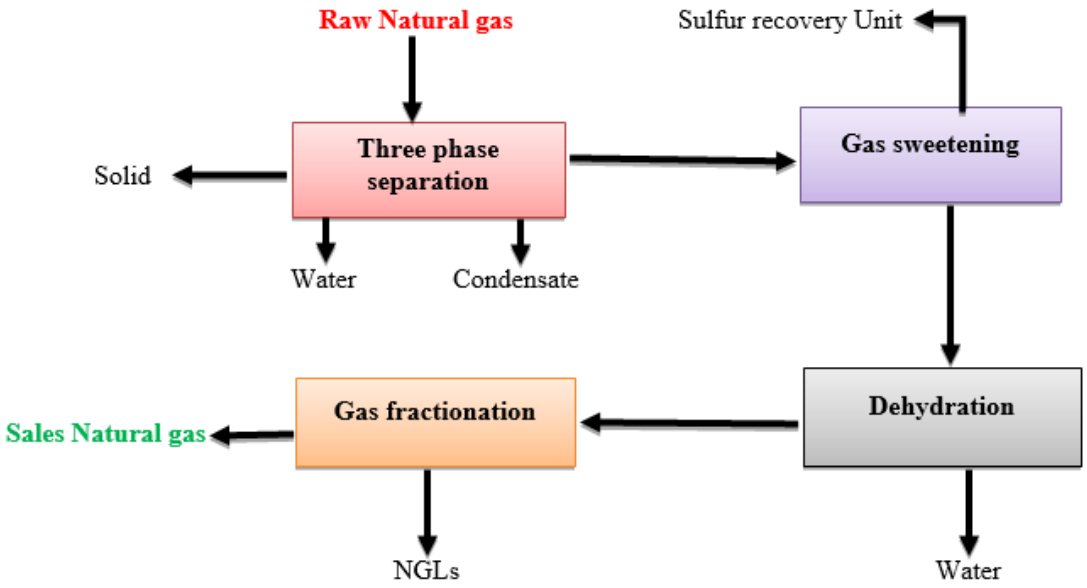

Figure 1.1: Overview of Natural gas processing (Adapted from Mokhatab et al., 2015)

Raw natural gas is made up of mostly methane and a considerable amount of other components like C_{2+}, CO_2, water and hydrogen sulphide (H_2S) in varying composition from well to well depending on its geographical condition (Mushtaq et al., 2013). Tables 1.1 and 1.2 show typical natural gas compositions and natural gas specifications for commercial applications. CO_2 is the most common impurity in raw natural gas (Baker and Lokhandwala, 2008) and needs to be separated to increase the calorific value of natural gas; reduce pipeline corrosion within the gas reticulation system (Xiao et al., 2009); prevent environmental effects such as global warming and ocean acidification (Mushtaq et al., 2013).

Traditional methods used for CO_2 removal are solvents absorption (basic solvents used include amine and hot aqueous potassium carbonate solution), pressure swing adsorption (Xiao et al., 2009) and by cryogenic distillation (Chen et al., 2015). However, these methods suffer some setbacks. The most developed and fully matured amine absorption method suffers need for solvent regeneration with a significant energy penalty, equipment corrosion, large footprint and flow assurance due to change in viscosity (Adewole et al., 2013; Ahmad et al., 2008).

Table 1.1: Natural gas compositions characteristic (Dung et al., 2008)

Component	**Composition range (mol%)**
CH_4	29.98 – 90.12
Ethane	0.55 – 14.22
Propane	0.23 – 12.54
Butanes	0.14 – 8.12
Pentanes and heavier hydrocarbons	0.037 – 3.0
CO_2	0.06 – 42.66
H_2S	0.0 – 3.3
Nitrogen	0.21 – 26.10
Helium	0.0 – 1.8

Table 1.2: Specifications of natural gas for commercial applications (Kidnay and Parrish, 2006)

Major components	**Minimum (mol%)**	**Maximum (mol%)**
CH_4	75	Nil
Ethane	Nil	10
Propane	Nil	5
Butanes	Nil	2
Pentanes and heavier hydrocarbons	Nil	0,5
Nitrogen and other inert	Nil	3
CO_2	Nil	2 – 3
Total diluents gases	Nil	4 - 5

Membrane technology has become an acceptable method of CO_2 removal from natural gas since its first use in 1981 (Dortmundt and Doshi, 1999). Membrane separation is reported to have the following advantages over traditional methods: smaller footprint, lower capital and operational costs, ease of operation, adaptability and environmental friendliness (Dortmundt and Doshi, 1999; Baker and Lokhandwala, 2008; Zhang et al., 2013). Therefore, several research works are being undertaken to harness viable advantages of membrane technology by improving the performance and durability of membrane systems.

1.2 Research problem and motivation

Majority of commercial natural gas separation membrane systems are polymeric due to processing feasibility and low cost. However, existing polymers have reached a trade-off threshold between permeability and selectivity, hence, are not viable for full commercial exploitation (Mushtaq et al., 2013). Figure 1.2 shows the relationship between permeability and selectivity. Also, of great concern is the plasticization problem associated with polymeric membranes due to harsh industrial conditions such as high feed pressure. Plasticization reduces polymer glass transition temperature (T_g) and selectivity of gases while increasing gas mobility and permeability (Ismail and Lorna, 2002). Figure 1.3 depicts the effect of plasticization on permeability. Generally, the performance of polymeric membranes is measured based on permeability and selectivity. Permeability measures intrinsic productivity of the membrane while selectivity measures the separation factor of the membrane during separation of mixed gases (Eguchi et al., 2015).

Carbon nanotubes (CNTs) have exceptional mechanical properties owing to the carbon-carbon bonds in the graphite layers, which are perhaps the most powerful chemical bond known (Ismail et al., 2009), light weight and its length to radius ratio. However, this also causes a dispersion problem in polymer matrix due to agglomeration. Functionalization of CNTs is believed to overcome this problem (Chen et al., 2008). The addition of functionalized carbon nanotubes into polymers appears to

offer a unique solution to the deficiencies of conventional polymeric membrane materials (Deng and Hagg, 2014). This is the primary motivation of this research.

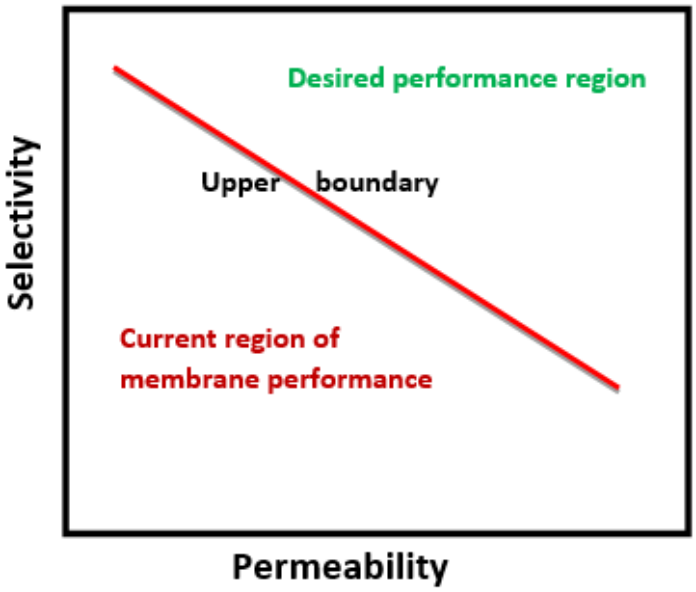

Figure 1.2: Relationship between membrane permeability and selectivity for polymeric membranes (adapted from Robeson, 2008)

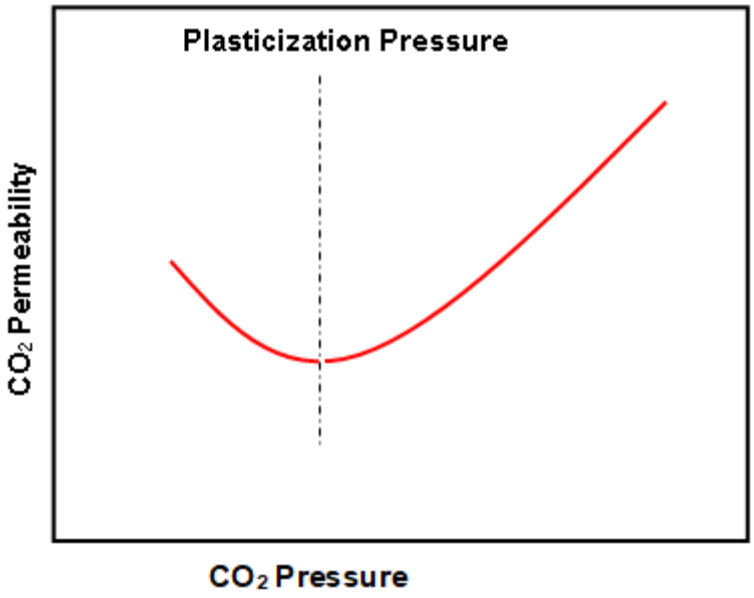

Figure 1.3: CO_2 induced plasticization isotherm (adapted from Dong et al., 2011)

One of the most widely researched polymeric membranes for CO_2/CH_4 separation is polysulfone due to its low cost, chemical resistance, mechanical strength and good transport properties (Scholes et al., 2010). Furthermore, the polysulfone membrane has been widely used as a commercial polymer for gas separation owing to its ease of synthesis with reproductive properties and controllable porosity (Shah and Murthy, 2013). When compared to state-of-the-art cellulose acetate, polysulfone has a lower CO_2 permeability and lower selectivity for CO_2/CH_4 but a higher plasticization pressure (Julian and Wenten, 2012; Momeni and Pakizeh, 2013). Therefore, the novel aspect of this research is to suppress CO_2 induced plasticization of polysulfone membrane by the addition of functionalized CNTs so as to withstand high feed pressure while achieving an improved permeability without sacrificing the selectivity during natural gas separation, particularly the separation of CO_2/CH_4 mixture.

1.3 Aim and Objectives of the study

The aim of this research was to synthesize functionalized CNT infused polysulfone membranes with an excellent balance of permeability, selectivity and carbon dioxide (CO_2) induced plasticization resistance during natural gas separations, particularly the separation of CO_2/CH_4 mixture. Also, to develop a mathematical model for CO_2 gas permeability in mixed matrix membranes in the presence of plasticization.

This aim was achieved by meeting the following objectives:

i. To produce CNTs and functionalize them using carboxylation protocol.
ii. To synthesize functionalized CNT-infused polysulfone membranes and characterize them.
iii. To evaluate gas permeation properties of the synthesized membranes at different loading of the functionalized CNTs.
iv. To investigate CO_2 induced plasticization resistance of the synthesized membranes using gas permeation properties.
v. To develop a mathematical model for CO_2 gas permeability in the mixed matrix membranes in the presence of plasticization.

1.4 Overview of the thesis

The thesis is divided into three broad sections: introduction, results, and conclusions. The introduction is further subdivided into three chapters, the result section is subdivided into three chapters in response to our five objectives, and the conclusion. The overview of the thesis is shown in Figure 1.4.

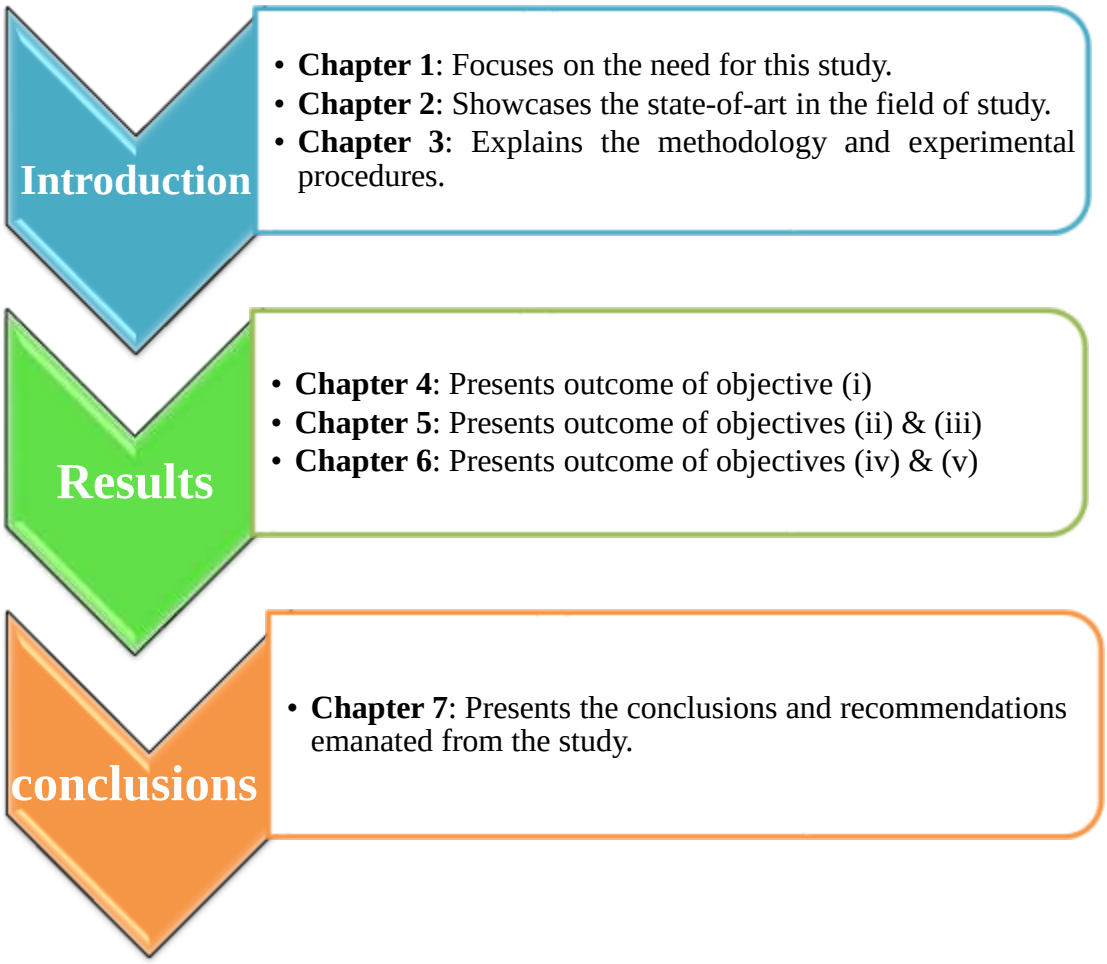

Figure 1.4: Overview of the thesis

References

Adewole, J. K., Ahmad, A. L., Ismail, S. and Leo, C.P. (2013) Current challenges in membrane separation of CO_2 from natural gas: A review, *International Journal of Greenhouse Gas Control*, vol. 17, pp. 46–65.

Ahmad, A.L., Sunarti, A., Lee, K., Fernando, W., (2008) Review of liquid absorbent behaviours in membrane gas absorption process. *In: 12th Asian Pacific Confederation of Chemical Engineering Congress, Dalian, China.*

Baker, R. W. and Lokhandwala, K. (2008) Natural Gas Processing with Membranes: An Overview, *Industrial & Engineering Chemistry Research*, vol. 47 (7), pp. 2109–2121.

Centre for Energy Economics (CEE) at Bureau of Economic Geology, (2004). Interstate Natural Gas Quality Specifications & Interchangeability. Texas.

Chen, L., Xie, H., Li, Y. and Yu, W. (2008) Surface Chemical Modification of Multi-walled Carbon Nanotubes by a Wet-Mechanochemical Reaction, *Journal of Nanomaterials*, Article ID 783981.

Chen, X.Y., Vinh-Thang, H., Ramirez, A.A., Rodrigue, D. and Kaliaguine, S. (2015) Membrane gas separation technologies for biogas upgrading. *RSC Advances*, *5*(31), pp.24399-24448.

Deng, L. and Hägg, M-B. (2014) Carbon nanotube reinforced PVAm/PVA blend FSC nanocomposite membrane for CO_2/CH_4 separation, *International Journal of Greenhouse Gas Control*, vol. 26 pp. 127–134.

Dong, G., Li, H. and Chena, V. (2011) Plasticization mechanisms and effects of thermal annealing of Matrimid hollow fiber membranes for CO2 removal, *Journal of Membrane Science*, vol. 369, pp. 206–220

Dortmundt, D. and Doshi, K. (1999) Recent developments in CO_2 removal membrane technology, *Technical paper*, Honeywell UOP LLC, Des Plaines, Illinois, USA.

Dung, E.J., Bombom, L.S., and Agusomu, T.D. (2008) The effects of gas flaring on crops in the Niger Delta Nigeria, *Geological Journal*, vol. 73, pp. 297–305.

Eguchi, H., Kim, D. J. and Koros, W. J. (2015) Chemically cross-linkable polyimide membranes for improved transport plasticization resistance for natural gas separation, *Polymer,* vol. 58, pp. 121-129.

Energy information administration, US department of energy. International energy outlook, 2016.

George, G., Bhoria, N., AlHallaq, S., Abdala, A. and Mittal, V (2016) Polymer membranes for acid gas removal from natural gas, *Separation and Purification Technology*, vol. 158, pp. 333–356.

Ismail, A. F. and Lorna, W. (2002) Penetrant-induced plasticization phenomenon in glassy polymers for gas separation membrane, *Separation and Purification Technology*, vol. 27, pp. 173–194.

Ismail, A. F., Goh, P. S., Sanip, S. M., and Aziz, M. (2009) Transport and separation properties of carbon nanotube-mixed matrix membrane, *Separation and Purification Technology*, vol. 70, pp. 12–26.

Kidnay, A. J. and Parrish, W. R. (2006) *Fundamental of Natural gas processing,* Taylor and Francis group, LLC, Florida, United States.

Langston, L. and Lee, S. L. (2010) A bright natural gas future, *Mechanical Engineering (New York, N.Y. 1919)*, vol. 132, pp. 49.

Linde Engineering (2012) Natural gas processing plants, *Technical paper,* Dr.-Carl-von-Linde-Strasse 6-14, 82049 Pullach, Germany.

Mokhatab, S., Poe, W. A. and Mak, J. Y. (2015) Basic Concepts of Natural Gas Processing Book, *Handbook of Natural Gas Transmission and Processing (Third Edition)*, Chapter 3, pp. 123-135.

Mushtaq, A., Mukhtar, H. B., Shariff, A. M. and Mannan, H. A. (2013) A Review: Development of Polymeric Blend Membrane for Removal of CO_2 from Natural Gas, *International Journal of Engineering & Technology*, vol. 13, No. 02, pp. 53-60.

Poe, W. A. and Mokhatab, S. (2017) Modeling, Control, and Optimization of Natural Gas Processing Plants, *Introduction to Natural Gas Processing Plants*, Chapter 1, pp. 1-72

Robeson, L. M. (2008) The upper bound revisited, *Journal of Membrane Science*, vol. 320, pp. 390–400

Scholes, C. A., Chen, G. Q., Stevens, G. W. and Kentish, S. E. (2010) Plasticization of ultra-thin polysulfone membranes by carbon dioxide, *Journal of Membrane Science*, vol. 346, pp. 208–214.

Shah, P. and Murthy, C.N. (2013) Studies on the porosity control of MWCNT/polysulfone composite membrane and its effect on metal removal, *Journal of Membrane Science*, vol. 437, pp. 90–98.

Xiao, Y., Low, B. T., Hosseini, S. S., Chung, T. S. and Paul, D. R. (2009) The strategies of molecular architecture and modification of polyimide-based membranes for CO_2 removal from natural gas—A review, *Progress in Polymer Science*, vol. 34, pp. 561–580.

Zhang, Y., Sunarso, J., Liu, S. and Wang, R (2013) Current status and development of membranes for CO2/CH4 separation: A review, *International Journal of Greenhouse Gas Control*, vol. 12, pp. 84–107.

CHAPTER 2

2 LITERATURE REVIEW

2.1 History of gas separation membranes

In 1823, a German chemist by the name Johann Doebereiner reported the escape of hydrogen gas through a crack in a bell jar that was left in a pneumatic trough (Mason, 1991). No consistent scientific explanation was given to this phenomenon until Thomas Graham postulated the law of gas diffusion in 1833 (Mason, 1991). However, no significant breakthrough was reported in membrane gas separation until 1943 during world war II, Graham's law of diffusion was exploited to enrich Uranium $^{235}UF_6$ from $^{238}UF_6$ in a project coded as Manhattan project (Baker, 2004). Since then many researchers have laid the foundation for the modern theories of membrane gas separation. Richard Barrer and Van Amerongen were the first to report the systematic gas permeability measurement in 1951 (Van Amerongen, 1950; Barrer, 1951).

The first commercial membrane for gas separation (PRISM® membranes) was commissioned in 1980 by Permea for hydrogen gas separation from flue gas streams of ammonia plants using polysulfone hollow fiber membranes (Bernardo and Clarizia, 2013). After the success of PRISM® membranes, other companies like Cynara, Separex, Medal, MTR and UOP commercialized cellulose acetate membranes for CO_2 removal during natural gas processing. Figure 2.1 shows the milestones of membrane gas separation systems during the early stage and in industrial application.

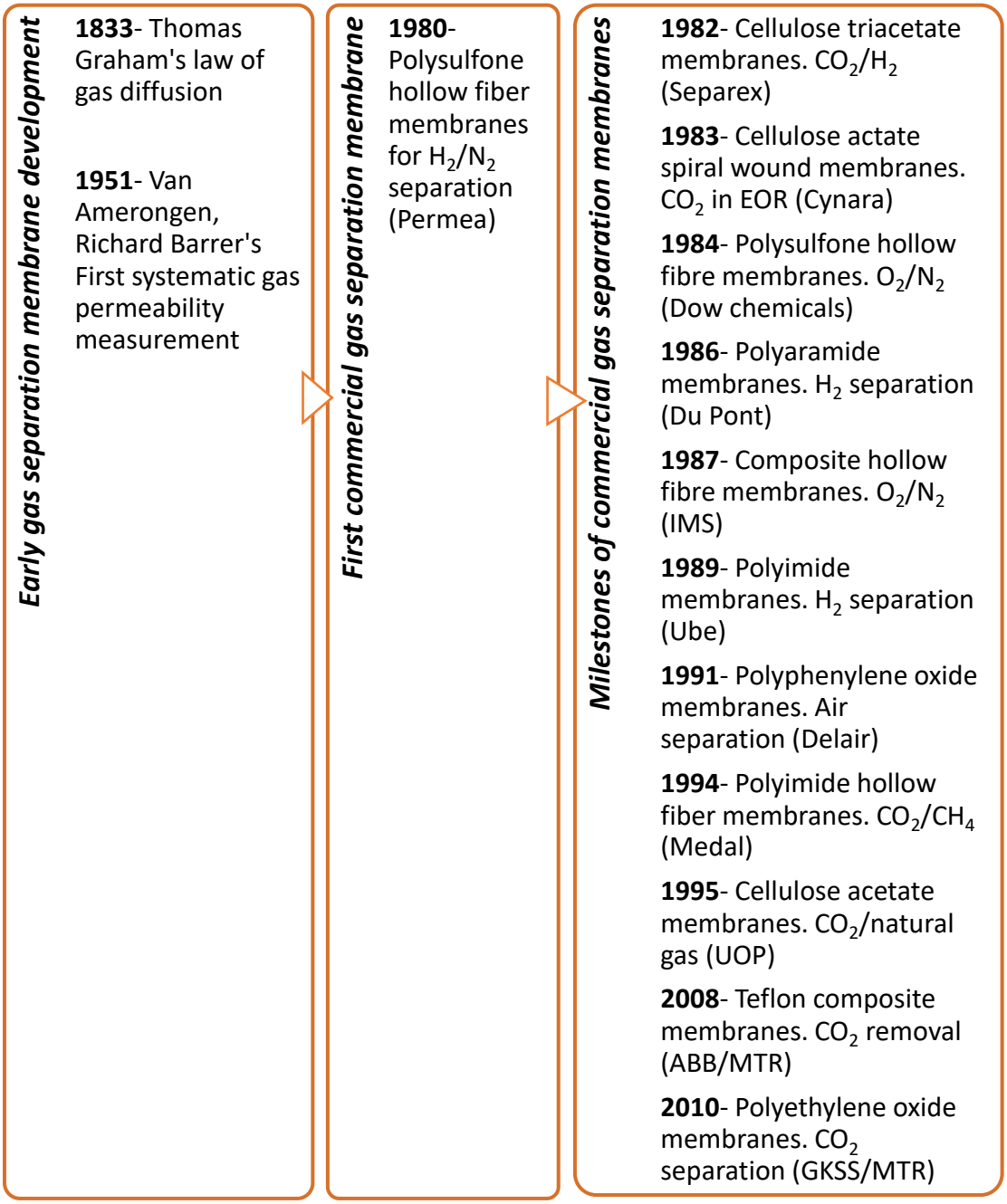

Figure 2.1: Milestones of membrane gas separation systems in industrial application (adapted from Bernardo and Clarizia, 2013)

2.2 Gas transport mechanisms in polymeric membranes

Polymeric membranes are generally classified in terms of morphology as symmetric, asymmetric, composite and mixed matrix membranes; and in terms of porosity as porous and non-porous dense membranes. The symmetric membrane is a homogenous structure with porosity approximately evenly distributed. Asymmetric membranes consist of an ultrathin selective layer placed on thicker and porous support of the same polymeric materials (Shusen et al., 1996). The composite membrane is an improved form of asymmetric membranes where the ultrathin selective layer is made of a polymeric material different from the polymeric material of the porous support (Dortmundt and Doshi, 1999). Mixed matrix membranes (MMM) consist of filler particles dispersed into the matrix of a polymer. The filler is immiscible with the matrix and they both have different transport properties (Wang et al., 2017). The classification scheme of polymeric membranes in terms of morphology and porosity is presented in Figure 2.2.

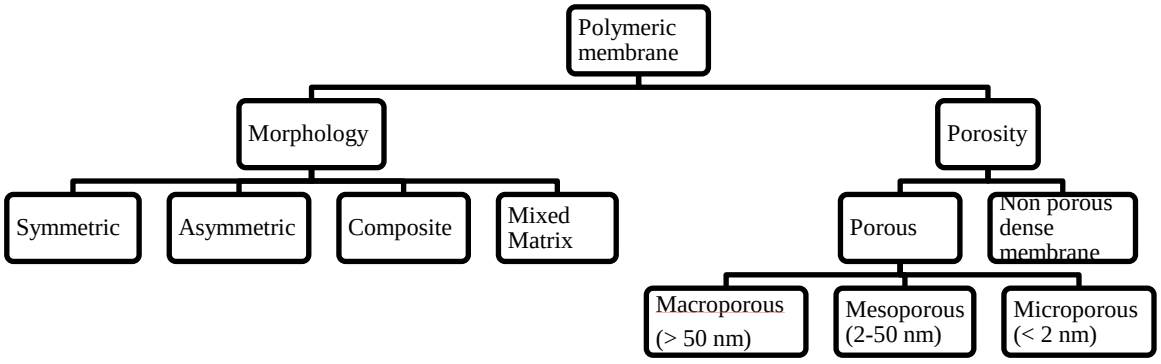

Figure 2.2: General classification scheme of polymeric membranes (Baker, 2007)

The gas transport mechanism in polymeric membranes is a controlling factor in membrane gas separation processes (George and Thomas, 2001). Some of the factors influencing the type of gas transport mechanisms in polymeric systems of membrane include the nature of the polymer, type of penetrant (George and Thomas, 2001), membrane pore structure and type of fillers (Bird and Trimm, 1983). The transport mechanisms in porous polymeric membranes include Poiseuille flow (viscous flow), Knudsen diffusion and molecular sieving mechanisms (Ismail et al., 2011) while the transport mechanism in the nonporous dense membrane is generally solution-diffusion mechanism (Kanehashi and Nagai, 2005). These mechanisms are represented schematically in Figure 2.3.

- **Poiseuille flow**: It occurs in macroporous membranes and it uses pressure gradient as a driving force. The penetrant molecules exert a mutual frictional force on one another due to the collision. As a result of the mutual frictional force, all the molecules pass the pores at an average drift velocity which is independent of their mass, size or shape (Bitter, 2012). Therefore, no gas separation occurs in Poiseuille flow regime.
- **Knudsen diffusion**: This takes place in mesoporous membranes. When the membrane pore diameter is very small with respect to the mean free path of the penetrant molecules, the tendency for these molecules to collide with one another is negligible relative to the tendency to collide with the pore wall. Therefore, each penetrant molecules will pass the membrane pores at its own molecular speed which is based on its own molecular weight (Present and Debethune, 1949). This means that lighter gases will penetrate through the membrane faster than heavier gases in the Knudsen diffusion regime. In a binary gas mixture, the separation factor from Knudsen diffusion is a function of the inverse square root of the two molecular weights (Koros and Fleming, 1993). It is important to state that Knudsen diffusion selectivity is generally low, hence its application is limited to separation systems that have large values for the molecular weight ratios e.g hydrogen separation from hydrocarbons mixture (Bitter, 2012).

- **Molecular sieving mechanism**: This happens in microporous membranes. According to the mechanism, separation of a gas mixture is based on the molecular size of the gases. When the membrane pore size is close to the molecular size of the penetrant, the membrane acts as a molecular sieve (Dos Santos, 2009). It implies that smaller molecules are given passage through the narrow pore and the larger molecules are obstructed. Molecular sieving mechanism has a balance of high selectivity and permeability (Ismail et al., 2011). However, condensible gases have been reported to cause pore blockage and fouling which alters the tortuosity of the membrane (Chen, 2002).
- **Solution-diffusion mechanism**: This mechanism involves three stages (Wijmans and Baker, 1995; Pandey and Chauhan, 2001): (a) dissolution of the gas into the high chemical potential upstream side of the membrane, (b) diffusion of the gas through the membrane and (c) desorption from the low chemical potential downstream side of the membrane. Separation is achieved in a gas mixture by this mechanism based on the differences in the amount of penetrants that dissolve in the membrane (solubility coefficient) and the rate at which the penetrants diffuse through the membrane (diffusivity coefficient) (Ismail et al., 2005). Solubility selectivity is a function of condensability of the penetrant, it favours penetrant with a higher critical temperature (Robeson et al., 2014). Diffusivity selectivity is based on the shape and size of the penetrant molecules, it favours smaller and linear molecules (Chung et al., 2003). In this study, the transport mechanism through the synthesized membranes is the solution-diffusion mechanism. Both solubility selectivity and diffusivity selectivity favour CO_2 over CH_4. This is because CO_2 is a more condensable gas with a critical temperature of 304.25 K, a kinetic diameter of 0.33 nm, and linear shape. CH_4, on the other hand, is less condensable with a critical temperature of 191.25 K, a kinetic diameter of 0.38 nm, and a tetrahedral shape.

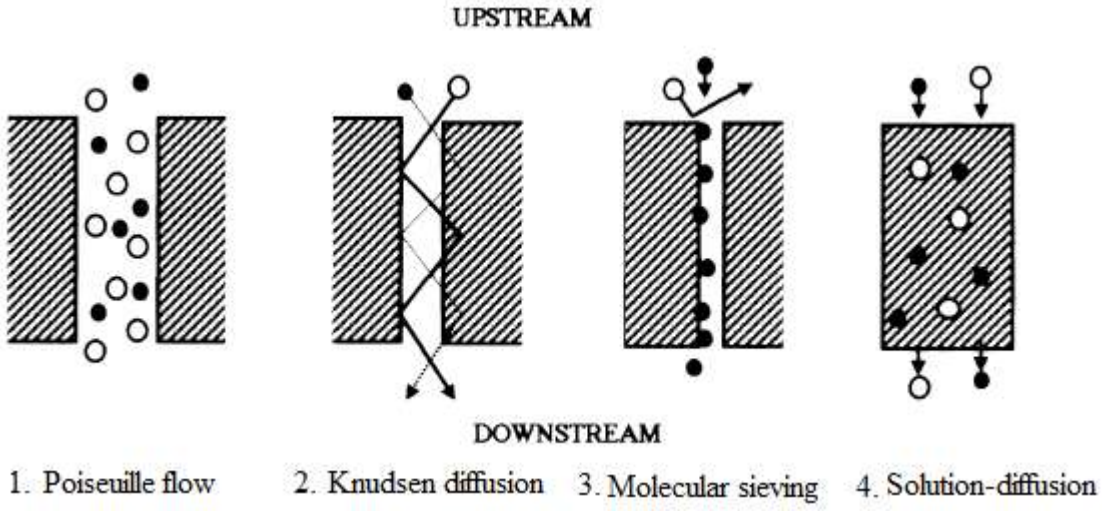

Figure 2.3: General gas transport mechanisms through polymeric membranes (used with permission from Stern and Trohalaki, 1990)

2.3 CO_2 induced plasticization in glassy polymeric membranes

2.3.1 Theory of plasticization

Plasticization phenomenon has been described as swelling and solvation of polymer due to disruption in chain packing and reduction in the interaction between the adjacent segments of polymer chains (Kesting and Fritzche, 1993; Scholes et al., 2010; Zhuang et al., 2018). This phenomenon occurs when the concentration of a very condensable gas e.g CO_2, reaches a critical point within the polymer matrix causing an increase in the segmental mobility and the free volume (Horn and Paul, 2011). CO_2 induced plasticization has been attributed to an increase in permeability, diffusivity (Dong et al., 2011) and the absolute value of the heat of sorption (Chung, 2004) of CO_2 through the membrane. However, plasticization phenomenon is reported to cause loss of selectivity (Yong et al., 2015) and a decrease in glass transition temperature (Chow, 1980) of the membrane. Let us take a closer look at the impact of CO_2 induced plasticization on these quantities in glassy polymeric membranes.

- **Permeability**: This is a measure of intrinsic productivity of a membrane (Eguchi et al., 2015). In glassy polymeric membranes, an increase in pressure is expected to cause a slight decrease in CO_2 permeability owing to the saturation of Langmuir environment of the membrane which reduces the solubility of CO_2 with increasing pressure (Wijmans and Baker, 1995). At plasticization, new free volumes are created in the membrane due to the mobility of the polymer matrix. This creates more sorption sites for CO_2 and causes an increase in the gas permeability with increasing pressure. Therefore, the plasticization pressure may be determined from the permeability isotherm. Plasticization pressure has been defined as the pressure at which permeability reaches its minimum value before it begins to increase (Dong et al., 2011).
- **Diffusivity**: Diffusivity of gas is said to be a measure of the energy required by the gas to achieve a diffusive jump through the polymer matrix (Ismail and Lorna, 2002). It is a function of the packing and motion of polymer segments and the size and shape of the gas molecules (Chung, 2004). When a membrane is plasticized, there is a disruption in the chain packing and an increase in the mobility of the polymer matrix. Hence, the amount of energy required by the gas to execute diffusive jump reduces and consequently, the diffusivity of the gas through the polymer matrix increases.
- **Heat of sorption**: Heat of sorption also described as isosteric heat is an indication of the affinity of a material for a given adsorbate (Roque-Malherbe, 2000). It measures the strength of interaction between a gas and the polymer matrix which could provide potential selectivity between a gas pair (White, 2017). The heat of sorption is exothermic, hence an increase in pressure of the gas is expected to reduce the absolute value of the heat of sorption which means less affinity for the gas as the sorption sites are getting saturated with increasing pressure. However, at plasticization, the absolute value of the heat of sorption increases. This depicts an increase in affinity for the gas by the polymer due to the formation of new free volume in the polymer matrix as a result of plasticization. Chung et al. (2004) reported that plasticization pressure could be

determined from the turning point at which the gradient of the absolute value of the heat of sorption against pressure changes from a negative value to a positive one. This approach for determining the plasticization pressure is still at a preliminary stage; further research is needed to support this claim.

- **Selectivity**: This is a measure of membrane's separation efficiency (Eguchi et al., 2015). Selectivity of polymeric membranes for a gas pair is defined as the ratio of their permeability. During plasticization of membranes, the permeability of all gases is enhanced which leads to a loss in separation efficiency of the membrane. Conversely, the use of loss of selectivity to determine the onset plasticization of membranes especially in a gas mixture has been discouraged by many researchers (Sanders et al., 1984; Dong et al., 2011). Owing to the fact that in the separation of a gas mixture, there is the tendency for selectivity to reduce without plasticization due to competitive sorption and bulk flow effect of the mixed gas (Kraftschik et al., 2013).
- **Glass transition temperature (T_g)**: T_g is a measure of the rigidity of the polymer matrix (Xue et al., 2013). During CO_2 induced plasticization, the polymer matrix swells due to the condensability of CO_2. This causes a reduction in the rigidity of the polymer matrix and consequently, a decrease in T_g is observed. However, there is a limitation to the use of T_g to determine membrane plasticization due to T_g measurement technique. Plasticization could be temporal if the plasticizer is removed in good time, the polymer may immediately return to its original state. Since the T_g measurement technique is not in-situ, the T_g of the membrane after plasticization may remain unchanged except where membrane conditioning has taken place. Conditioning of a membrane occurs when the plasticizer is removed and the polymer did not immediately return to its original state (Horn and Paul, 2011).

2.3.2 Techniques for improving CO_2 induced plasticization resistance of polymeric membranes

Several techniques have been reported in the literature for suppressing CO_2 induced plasticization of polymeric membranes. These techniques include thermal annealing, cross-linking, polymer blending, and mixed matrix membrane.

- **Thermal annealing**: The plasticization of membranes may be suppressed by thermal annealing of the membranes owing to a densification of the polymer matrix which results in a reduction of chain mobility through the heating process (Kusworo et al., 2013). Chung et al. (2004) observed an improvement in CO_2 induced plasticization resistance of dense poly [2,6-toluene-2,2-bis(3,4-dicarboxylphenyl)hexafluoropropane diimide] membranes by thermal annealing at 250 ^oC for 24 h. Thermal annealing of polysulfone membranes at 140 ^oC and 160 ^oC for 1 h was reported to have successfully suppressed CO_2 induced plasticization of the membrane (Ismail and Lorna, 2003). In the work of Dong et al. (2011), the effect of thermal annealing of Matrimid hollow fiber membrane was investigated. According to their report, superior CO_2 induced plasticization of the membrane was achieved at 250 ^oC for 30 min heating protocol. However, densification of the polymer matrix by thermal annealing has been reported to cause loss of permeability (Ismail and Lorna, 2003).
- **Cross-linking**: Cross-linking process involves thermally and chemically joining of two or more molecules of cross-linkable membrane materials together by using cross-linking agents such as glycidol and 1,3-propandiol (Eguchi et al., 2015; Qiu et al., 2011). Cross-linked polymeric membranes have been reported to enhance CO_2 induced plasticization resistance of glassy polymers. Wind et al. (2003) investigated the covalent cross-linking of 6FDA-based polyimide membranes with different cross-linking agents. Cross-linking with cyclohexanedimethanol and butylene glycol at 295 ^oC was effective in suppressing CO_2 induced plasticization up to 40 atm feed pressure without sacrificing sorption. Qiu et al. (2011) studied sub-T_g cross-linking of 6FDA-

2,4,6-trimethyl-1,3-diaminobenzene(DAM):3,5-diaminobenzoic acid (DABA) (3:2) membranes with glycidol as cross-linker. Their study showed that excellent balance of selectivity, permeability and anti-plasticization was achieved with decarboxylation-induced thermal cross-linking of 6FDA-DAM:DABA (3:2) polymeric membranes at temperatures below the polymer T_g.

- **Polymer blending**: Blending of a polymer with high CO_2 induced plasticization propensity with another that is less plasticized by CO_2 has tendencies to improve plasticization resistance of the blended polymer. Bos et al. (2001) investigated the effect of homogeneous polymer blending on the balance of CO_2 plasticization resistance, permeability and separation factor. Their results showed that homogeneous blending of the polyimide matrimid and polysulfone (50/50) enhanced the plasticization resistance of the membrane but at the expense of both permeability and separation factor. However, blending of the polyimide matrimid with a copolyimide P84 (60/40) improved the plasticization resistance without sacrificing the separation factor. Furthermore, Kapantaidakis et al. (2003) reported that the plasticization pressure of polyimide ultrathin hollow-fiber membrane was improved by the addition of polyethersulfone.
- **Mixed matrix membrane (MMM)**: Since plasticization causes mobility of polymer matrix, the addition of fillers with excellent mechanical properties to rigidify the polymer chains has been reported to suppress CO_2 induced plasticization of the membrane. Some of the inorganic fillers used include metal-organic frameworks (MOFs) (Shahid and Nijmeijer, 2014), zeolitic imidazolate frameworks (ZIFs) (Zhuang et al., 2018), mesoporous silica (Khan et al., 2015) and zeolites (Adams et al., 2011). However, the use of CNTs as fillers for the synthesis of MMMs for CO_2 plasticization suppression is yet to be reported in open literature to the best of our knowledge. Therefore, the focus of this study is to leverage the exceptional mechanical properties, light weight,

and length to radius ratio of CNTs to fabricate MMMs that can withstand high CO_2 feed pressure without plasticizing.

2.4 Carbon nanotubes

2.4.1 Structure and properties

The structure of a CNT has been described as a rolled up sheet of graphene with carbon atoms distributed in a planar-hexagonal lattice (Rastogi et al., 2014). CNTs are classified into single-walled, double-walled, and multi-walled carbon nanotubes depending on the number of graphene sheets that the rolling layers contained (Peponi et al., 2011). Figure 2.4 shows the basic structure of single-walled carbon nanotube (SWCNT) and multi-walled carbon nanotube (MWCNT).

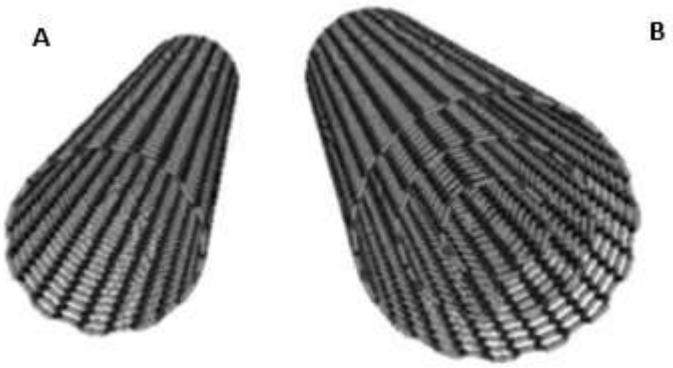

Figure 2.4: Basic structure of (A) SWCNT (B) MWCNT (used with permission from Ismail et al., 2009)

CNTs have also been group into an armchair, zigzag and chiral with respect to the angle of rolling layers of the graphene sheet (Ma et al., 2010). Figure 2.5 depicts the formation of different types of CNTs from planar-hexagonal graphene sheet as determined by the chiral vector Equation (2.1):

$$C_h = na_1 + ma_2 \tag{2.1}$$

Where:

a_1, a_2 = unit vectors of the hexagonal lattice.

Integers (n, m) = number of movements along the unit vectors.

If $n = m$;

The CNTs are called armchair.

If $m = 0$;

The CNTs are called zigzag.

The CNTs that do not fall into these two categories are called chiral.

Kirtania and Chakraborty (2012) determined the circumference of CNTs by using Equation (2.2):

$$L = a\sqrt{n^2 + m^2 + nm} \tag{2.2}$$

Where:

a = length of the unit vector.

The angle (θ) of the rolling layers of the graphene sheet is given by Equation (2.3):

$$\cos\theta = \frac{(n+m)/2}{\sqrt{n^2+m^2+nm}} \tag{2.3}$$

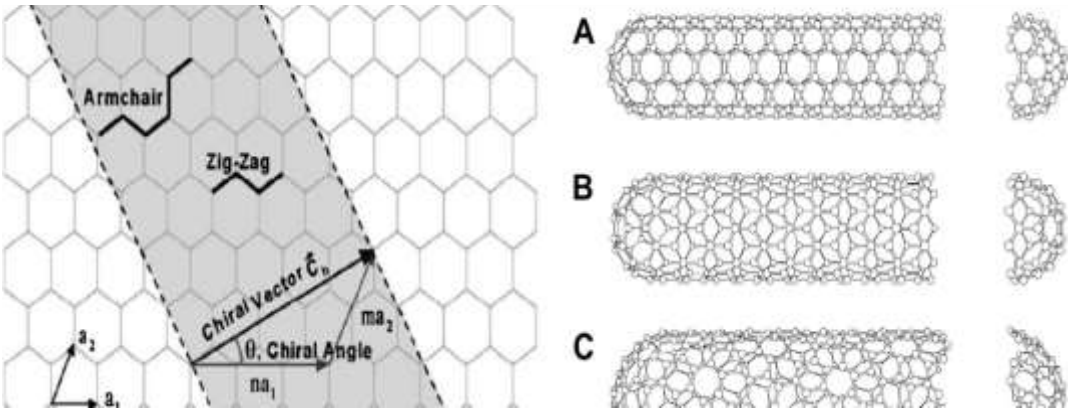

Figure 2.5: Formation of different types of CNTs (A: armchair; B: zigzag; C: chiral) (used with permission from Ma et al., 2010)

2.4.2 Production methods

Several methods have been reported in the literature for the production of CNTs. These methods include but not limited to arc-discharge (Sharma et al., 2015; Ando and Zhao, 2006), laser ablation (Chrzanowska et al., 2015) and chemical vapour deposition (Iyuke and Simate, 2011).

- **Arc discharge**: Arc discharge set-up is one of the oldest methods of production of CNTs. The set-up entails two electrodes and a DC power supply with current and voltage rating of 100-200 A and 20-30 V, respectively (Sharma et al., 2015). The arc-containing CNTs and other forms of carbon are produced between the two graphite rods that are used as anode and cathode electrodes (Ando and Zhao, 2006). Furthermore, the set-up consists of three component systems containing argon, methane, and iron for CNT synthesis (Rafique and Iqbal, 2011). The vessel can contain deionized water to provide an environment favourable for the reaction, as well as cooling due to extremely high temperatures. It further creates an insulation of the reaction from atmospheric oxygen. The produced carbon soot settles upon termination, by bringing the electrodes a certain distance apart, and is collected on the cathode (Sharma et al., 2015).

- **Laser ablation**: Laser ablation method uses a pulsed laser, striking at a graphite target in a reactor at a very high temperature. This is done in the presence of an inert gas which then vaporizes the graphite target. CNTs are said to develop at the cooler end of the reactor. According to Rafique and Iqbal (2011), this physical process has some short-comings which include extensive energy use that makes it economically unfavourable. It also requires graphite to be evaporated so as to produce the desired nanotubes. This limits large-scale production in industrial processes.
- **Chemical vapour disposition (CVD)**: CVD method is said to be the most preferred and widely used method (Awadalla et al., 2012) with great potential for large-scale and continuous CNT production (Yah., 2011). This method uses transition metals as catalyst and hydrocarbon as a carbon source (Awadallah et al., 2012; Hou et al., 2008). CVD method has low energy input requirements in terms of CNT production, as well as lower reaction temperatures (Yah, 2011). This makes it a preferred method for large-scale production. The production quantity and quality are influenced by reaction parameters such as temperature, catalytic systems, carrier gas composition and type of carbon source used (Aberefa et al., 2019; Biris et al., 2006). Even though arc discharge and laser ablation are well-established processes that produce high quality and near perfect CNTs, they have scale-up limitations. The use of temperatures and pressures of over 1200^{o}C and 10 atm, respectively, make production costs too high and thus not economically viable (Hou et al, 2008). In this study, the CVD method was used to produce CNTs from acetylene and methane as carbon sources and ferrocene served as a catalyst. Table 2.1 shows the advantages and disadvantages of different CNT production methods.

Table 2.1: The advantages and disadvantages of different CNT production methods (as reported by Rafique and Iqbal (2011)).

Process/Property	***Arc Discharge***	***Laser Ablation***	***Chemical Vapour Deposition***
Raw material availability	Difficult	Difficult	Easy, abundantly available
Energy requirement	High	High	Moderate
Process control	Difficult	Difficult	Easy, can be automated
Reactor Design	Difficult	Difficult	Easy, can be designed as large-scale process
Production rate	Low	Low	High (CoMoCAT, HiPco)
Purity of product	High	High	High
Yield of process	Moderate (70%)	Moderate (80%-85%)	High (95%-99%)
Post-treatment requirements (refining e.t.c.)	Require refining	Require refining	No extensive refining required
Process Nature (Batch or Continuous type)	Batch	Batch	Continuous
Per unit cost	High	High	Low

2.4.3 Functionalization techniques

The presence of strong carbon-carbon bonds in the graphite layers of CNTs cause agglomeration of CNTs in both aqueous and non-aqueous solvents, and in polymer matrix even when a dispersing agent is used (Inam and Peijs, 2007). This creates a major limitation to the commercial application of CNTs. Hence, the functionalization chemistry of CNTs has become a growing area of research. Functionalization of CNTs

reduces the strong Van der Waal force of attraction between carbon-carbon atoms of CNTs and enhances separation of CNT bundles into individual CNT when dispersed in solvents. This improves the CNT-polymer matrix interface interaction (Chen et al., 2008). Furthermore, CNT functionalization could be modified to have particular interactions with specific gases to enhance molecular sieving by chemical recognitions (Corry, 2011). Several functionalization protocols for joining CNTs and functional groups have been reported in the literature (Ma et al., 2010). These protocols are classified into two groups viz; physical and chemical functionalization, according to the interfaces between the molecules of the functional group and carbon-carbon atoms of the CNTs (Rafiee and Pourazizi, 2014).

Physical functionalization of CNTs involves self-arrangement of individual CNTs held together by non-covalent bonds to form thermodynamically stable structures (Lin et al., 2003). Some of the physical functionalization methods that are mostly used include polymer wrapping, surfactant adsorption, and endohedral filling.

- **Polymer wrapping**: Several species of polymers, especially the high molecular weight and conjugated polymers, have the capacity to wrap through the surface of CNTs to form supermolecular complexes of CNTs (Yang et al., 2011). This could be attributed to the dispersion of CNTs in the polymers matrix. Examples of such polymers include polypropylene and polyethylene (Tasis et al., 2006). The process involves the non-covalent interaction of the van der Waals and p–p stacking between CNTs and polymer matrix with aromatic rings (Ismail et al., 2009). The advantage of this method is that it does not damage the structure and the physicochemical properties of the CNTs.
- **Surfactant adsorption**: Rahimpour et al. (2012) reported the surfactant-assisted functionalization of CNTs. In this process, the surface tension of CNTs is lessened by the physical adsorption of surfactant onto the surface of CNTs thereby suppressing the agglomeration of CNTs. Furthermore, the surfactant-assisted CNTs prevent the attraction due to van der Waals forces through electrostatic repulsive forces (Wang et al., 2014). The effectiveness of

surfactant-assisted functionalization of CNTs is based on the surfactant properties, the chemistry of the medium, and polymer matrix (Bekou and Mattia, 2011).

- **Endohedral filling**: Endohedral method operates on the principle of the capillary effect. In this principle, foreign atoms such as fullerene derivatives and metal halides are implanted into the tubes of CNTs (Tasis et al., 2006). Examples of metal halides used for the functionalization by Endohedral filling include $AgCl_xBr_y$, CdI_2 and $ThCl_4$, $CdCl_2$, $TbCl_3$, $TiCl_4$ and PbI_2 (Hirsch, 2002). The disadvantages of this method as compared to other physical functionalization methods include the possible re-agglomeration of CNTs in the polymer matrix and the method is not easy to use (Ma et al., 2010).

Chemical functionalization involves covalent interaction between the molecules of functional groups and the carbon-carbon atoms of CNTs. This functionalization could be achieved using direct covalent sidewall or using defect transformation.

- **Direct covalent sidewall**: Direct sidewall method involves the conversion of the hybridized carbon atoms from sp^2 to sp^3 and an immediate loss of π-conjugation alignment on the graphene layer. The disadvantages of this method, however, include the damage of the physicochemical properties of CNTs and possible re-agglomeration of CNTs in a polymer matrix (Inam and Peijs, 2007; Chen et al., 2008).
- **Defect transformation**: This method entails pre-oxidation of CNTs by using strong acids such as nitric acid, sulfuric acid, or a mixture of them; or with strong oxidants such as potassium per manganite in acidic medium, ozone or reactive plasma (Dyachkova et al., 2013), in order to create a site defect on the CNTs. The defect sites are covalently stabilized by bonding with functional groups such as carboxylic and hydroxyl groups (Ma et al., 2010).

2.5 Recent developments in CNT infused polymeric membranes for gas separation

CNT infused polymeric membranes have become an emerging technology for gas separation which has been keenly discussed in the literature. Several research works have shown that polymeric membrane embedded with well-dispersed CNTs has enhanced gas permeability and selectivity while improving physiochemical properties of the membrane.

In the work of Sanip et al. (2011), cyclodextrin functionalized multi-walled carbon nanotubes (FMWCNTs) were dispersed in *N*-methyl-2-pyrrolidone (NMP) solvent with polyimide membrane, pure gas permeation measurements were done at 35^{o}C with feed pressure up to 10 bars. It was reported that the mixed matrix membrane showed 100% improvement for the selectivity of CO_2/CH_4 at optimum FMWCNT load of 0.7% ratio compared to pure polyimide membrane. Also, CO_2 permeance was said to be highly favoured compared to other pure gases like CH_4, O_2, and N_2 due to stronger adsorption of CO_2 through the channels of CNTs.

The effects of single-walled CNTs (SWCNTs) and multi-walled carbon nanotubes (MWCNTs) on brominated poly(2,6-diphenyl-1,4-phenylene oxide) (BPPO) for CO_2/N_2 separation were investigated by Cong et al. (2007). According to the report, 4.8 wt. % of BPPO was dissolved in chloroform and pristine CNTs (SWCNTs or MWCNTs) were slowly added to the polymer solution at varying wt. % (2, 5, 9 and 17 wt. %), pure gas permeation measurements were conducted at 25^{o}C with 10 psig feed pressure. Their results showed an optimum CNT load of 5 wt. %. It was reported that at 5 wt. % of SWCNTs and MWCNTs, the CO_2 permeability increased by 58% and 91% respectively without compromising CO_2/N_2 selectivity, while the tensile modulus of BPPO increased by 67% and 44%, respectively.

Ismail et al. (2011) studied the effect of purification and functionalization of MWCNTs loading on gas separation performance of polyethersulfone (PES) at varying MWCNTs loading from 0.5 - 3.0 wt. %. They purified MWCNTs with HNO_3/H_2SO_4 acid mixture

and surface functionalized using 3-aminopropyltriethoxylsilane (APTES), the PES/MWCNTs membranes were then synthesized by dry-wet phase inversion method and gas permeation measurements conducted at 27ºC with a feed pressure of 4 bar. They reported that the highest CO_2/CH_4 selectivity was achieved at 0.5 wt. % MWNTs loading ($\alpha = 250$) but decreased with increasing MWNTs loading from 1.0 – 3.0 as a result of the possible existence of interface voids which became significant at increasing MWNTs loading.

Ranjbaran et al. (2015) synthesized a novel Elvaloy4170/ FMWCNT membranes for CO_2/CH_4 separation. In their study, raw MWCNTs were treated with a mixture of concentrated acid comprising 3/1 volumetric ratio of H_2SO_4/HNO_3 so as to purify and have carboxyl/hydroxyl groups on their surfaces, then were solution-blended with Elvaloy4170 in toluene, pure gas permeability tests were conducted at 35ºC with the feed pressures of 2, 4 and 6 bars. Their results showed that CO_2 permeability and CO_2/CH_4 selectivity increased by 30% and 14% respectively as the feed pressure increased from 2 to 6 bars in pure Elvaloy4170 membrane, while with 1 wt. % FMWCNT loading, CO_2 and CH_4 permeabilities increased by 30% and 40% respectively in comparison to pure Elvaloy4170 membrane, CO_2/CH_4 selectivity increased with increasing FMWCNTs loading from 1 - 4 wt. % in the polymeric membrane.

2.6 Membrane gas permeation models

Membrane-based gas separation is economically and environmentally viable than conventional gas separation processes (Balçık and Ahunbay, 2018). Hence, varieties of polymeric and mixed matrix membranes need to be screened to develop a membrane with an excellent balance of permeability, selectivity and penetrant induced plasticization resistance. Experimental screening of these membranes is quite tedious especially with the need for high-pressure equipment for determination of penetrant induce plasticization pressure of these membranes. Therefore, model-based determination of the membrane gas transport properties has become necessary to

facilitate accelerated development of novel membrane for commercial gas separation (Adewole et al., 2015). Several models have been reported in the literature for predicting gas permeability and subsequently determining plasticization pressure of the membranes. These models could be classified as empirical, phenomenological, mechanistic and atomistic models.

The empirical model is developed using experimental data. It requires minimal investment in modeling but needs a greater number of experimental data to improve the predictability of the model (Neumann et al., 2006). According to a concise dictionary of physics, a phenomenological model is defined as 'a theory which expresses mathematically the results of observed phenomena without paying detailed attention to their fundamental significance' (Thewlis, 1973). Phenomenological models are expected to have a better predictive capacity than empirical models (Neumann et al., 2006). In mechanistic modeling, detailed fundamental principles and physical theories governing a process are used to develop mathematical equations for the prediction of different phenomena (Zhang et al., 2010). Atomistic molecular modeling enables direct observation of some properties of membrane gas separation system such as the mobility of penetrant atoms and the distribution of free volume (Hölck et al., 2006).

Adewole et al. (2015) developed a semi-empirical model for estimating plasticization pressure and gas permeability at plasticization, from permeation experimental data. In their report, the permeability-pressure relationship was represented by Equation (2.4);

$$P = \emptyset e^{f(p)} \tag{2.4}$$

Where

P = permeability

p = pressure

Expanding Equation (2.1) using Taylor series up to 2nd order gives:

$$P_{(p)} = a_1 p^2 + a_2 p + a_3 \tag{2.5}$$

Where a_1, a_2 and a_3 are the model parameters.

Since plasticization is the pressure at which gas permeability is at a minimum (Dong et al., 2011), then;

$$\frac{dP}{dp} = 0 \tag{2.6}$$

Applying Equation (2.6) to Equation (2.5) gives:

$$p_i = \frac{-a_2}{2a_1} \tag{2.7}$$

$$P_{(p_i)} = a_3 - \frac{a_2^2}{4a_1} \tag{2.8}$$

Where:

p_i = plasticization pressure

$P_{(p_i)}$ = permeability at plasticization

The values of a_1, a_2 and a_3 were estimated using experimental data from about 90 polymeric membranes available in litthe erature.

Dual mode sorption phenomenological model is widely used to describe gas sorption in glassy polymers (Vieth and Sladek, 1965; Petropoulos, 1970; Paul and Koros, 1976; Barrer, 1984; Zhou and Stern, 1989). Dual mode sorption model is the summation of Henry's law and the Langmuir equation (Koros et al., 1976). Equations (2.9) – (2.11) illustrate the dual mode sorption mechanism;

$$C_d = k_d p \tag{2.9}$$

$$C_h = \frac{C_h' bp}{1+bp} \tag{2.10}$$

$$C = C_d + C_h = k_d p + \frac{C_h' bp}{1+bp} \tag{2.11}$$

Where C_d is the concentration of gas molecules in Henry's law environment, k_d is Henry's law solubility coefficient, p is pressure, C_h is the concentration of gas molecules in Langmuir adsorption sites, C_h' is the polymer matrix saturation constant, b is the ratio of the rate of gas adsorption and desorption into the polymer matrix (also known as Langmuir affinity constant) and C is the total penetrants concentration.

In the work of Paul and Koros (1976), it was observed that a fraction of the gas in C_h and all the gas in C_d are mobile within the membrane. Therefore, the concentration of the mobile gas, C_m, and the permeability of gas, P, within the polymeric membrane are expressed by Equations (2.12) and (2.13) respectively (Zhou and Stern, 1989; Koros et al., 1981).

$$C_m = C_d + FC_h = k_d p\left(1 + \frac{FC_h' b}{k_d(1+bp)}\right) \tag{2.12}$$

$$P = k_d D_d\left(1 + \frac{FC_h' b}{k_d(1+bp)}\right) \tag{2.13}$$

Where F is the fraction of the gas held in Langmuir sites that have mobility within the membrane, D_d is the diffusion due to the local concentration gradient. k_d, b and C_h' can be determined from independent gas sorption measurement. D_d and F can be obtained graphically by plotting P against $1/(1+bp)$.

Mechanistic model on the basis of continuity and momentum equations was developed by Gilassi and Rahmania (2015). The overall conservation of mass, momentum and concentration equations for the gas as reported are as follows;

$$\frac{\partial u_x}{\partial x} + \frac{\partial u_y}{\partial y} = 0 \tag{2.14}$$

$$\frac{\partial n_x}{\partial x} + \frac{\partial n_y}{\partial y} = 0 \tag{2.15}$$

$$u_x \frac{\partial C}{\partial x} + u_y \frac{\partial C}{\partial y} + D\left(\frac{\partial^2 C}{\partial x^2} + \frac{\partial^2 C}{\partial y^2}\right) = 0 \tag{2.16}$$

$$\rho\left(u_x \frac{\partial u_x}{\partial x} + u_y \frac{\partial u_y}{\partial y}\right) = -\frac{\partial p}{\partial x} + \mu\left(\frac{\partial^2 u_x}{\partial x^2} + \frac{\partial^2 u_x}{\partial y^2}\right) + \rho g_x \tag{2.17}$$

$$\rho\left(u_x \frac{\partial u_x}{\partial x} + u_y \frac{\partial u_y}{\partial y}\right) = -\frac{\partial p}{\partial y} + \mu\left(\frac{\partial^2 u_y}{\partial x^2} + \frac{\partial^2 u_y}{\partial y^2}\right) + \rho g_y \tag{2.18}$$

Where u_x, u_y, ρ, D and p represent velocity in x and y directions, density, diffusivity and pressure, respectively. Applying appropriate concentration and velocity boundary conditions, the equations were solved using a numerical scheme.

Other mathematical models used to predict gas permeability include; Maxwell equation (Maxwell, 1954) and Bruggeman model (Bruggeman, 1935). Maxwell equation, represented by Equation (2.19), was originally developed for electrical conductivity and adapted for gas flux through a membrane. Bruggeman model, denoted by Equation (2.20), was initially developed to determine the dielectric constant of a particulate composite.

$$P_r = \frac{1+2\emptyset\left(\frac{P_d}{P_m}-1\right)/\left(\frac{P_d}{P_m}+2\right)}{1-\emptyset\left(\frac{P_d}{P_m}-1\right)/\left(\frac{P_d}{P_m}+2\right)} \tag{2.19}$$

$$(P_r)^{1/3}\left(\frac{\frac{P_d}{P_m}-1}{\frac{P_d}{P_m}-P_r}\right) = (1-\emptyset)^{-1} \tag{2.20}$$

Where P_r is the relative permeability of species, P_m is the permeability of species in the matrix (continuous phase), $\emptyset$ is volume fraction of the filler particles, P_d is the permeability of species in the dispersed phase.

2.7 Concluding remarks

This chapter reviews recent developments in production and functionalization of CNTs, separation performance of CNT infused polymeric membranes and techniques for suppressing CO_2 induced plasticization in glassy polymeric membranes. Some challenges have been identified. Currently, there is a concern about the production of quantity and quality CNTs at lowest cost possible. CNTs production techniques that yield quality CNTs do so at a lower quantity and at a higher cost, while the techniques that yield a higher quantity of CNTs do so at lower quality. Hence the need to balance these three factors. Furthermore, CNT infused membranes have shown an improved gas permeability as compared to conventional polymeric membranes with little compromise of ideal selectivity. However, the selectivity of mixed gas separation is sacrificed due to the competitive sorption of different gas molecules in a mixed gas. In addition, the majority of techniques for suppressing CO_2 permeability in membranes tend to sacrifice CO_2 permeability of the membrane.

With the aforementioned challenges in mind, the remaining chapters of this thesis will show the promising potential of CNTs-PSF membrane for an excellent balance of permeability, selectivity and carbon dioxide (CO_2) induced plasticization resistance during natural gas separations, particularly the separation of CO_2/CH_4 mixture.

References

Aberefa, O.A., Daramola, M.O. and Iyuke, S.E., 2019. Production and functionalization of carbon nanotubes for application in membrane synthesis for natural gas separation. Microporous and Mesoporous Materials, 280, pp.26-36.

Adams, R.T., Lee, J.S., Bae, T.H., Ward, J.K., Johnson, J.R., Jones, C.W., Nair, S. and Koros, W.J., 2011. CO_2–CH_4 permeation in high zeolite 4A loading mixed matrix membranes. *Journal of Membrane Science*, *367*(1-2), pp.197-203.

Adewole, J.K., Ahmad, A.L., Sultan, A.S., Ismail, S. and Leo, C.P., 2015. Model-based analysis of polymeric membranes performance in high pressure CO 2 removal from natural gas. *Journal of Polymer Research*, 22(3), p.32.

Ando, Y. and Zhao, X., 2006. Synthesis of carbon nanotubes by arc-discharge method. *New Diamond and Frontier Carbon Technology*, *16*(3), pp.123-138.

Awadallah, A.E., Abdel-Hamid, S.M., El-Desouki, D.S., Aboul-Enein, A.A. and Aboul-Gheit, A.K., 2012. Synthesis of carbon nanotubes by CCVD of natural gas using hydrotreating catalysts. *Egyptian Journal of Petroleum*, *21*(2), pp.101-107.

Baker, R.W., 2007. Membrane technology and applications. 2004. *England: John Wiley and Sons*.

Balçık, M. and Ahunbay, M.G., 2018. Prediction of CO2-induced plasticization pressure in polyimides via atomistic simulations. *Journal of Membrane Science*, 547, pp.146-155.

Barrer, R.M., 1984. Diffusivities in glassy polymers for the dual mode sorption model. *Journal of Membrane Science*, *18*, pp.25-35.

Barrer, R.M., 1951. *Diffusion in and through Solids*. Cambridge University Press, London

Bekou, S. and Mattia, D., 2011. Wetting of nanotubes. *Current Opinion in Colloid & Interface Science*, *16*(4), pp.259-265.

Bernardo, P. and Clarizia, G., 2013. 30 years of membrane technology for gas separation. *Chemical Engineering Transactions*, *32*, pp.1999-2004.

Bird, A.J. and Trimm, D.L., 1983. Carbon molecular sieves used in gas separation membranes. *Carbon*, *21*(3), pp.177-180.

Biris, A.R., Biris, A.S., Lupu, D., Trigwell, S., Dervishi, E., Rahman, Z. and Marginean, P., 2006. Catalyst excitation by radio frequency for improved carbon nanotubes synthesis. *Chemical Physics Letters*, *429*(1-3), pp.204-208.

Bitter, J.G.A., 2012. *Transport mechanisms in membrane separation processes*. Springer Science & Business Media.

Bos, A., Pünt, I., Strathmann, H. and Wessling, M., 2001. Suppression of gas separation membrane plasticization by homogeneous polymer blending. *AIChE Journal*, *47*(5), pp.1088-1093.

Bruggeman, V.D., 1935. Berechnung verschiedener physikalischer Konstanten von heterogenen Substanzen. I. Dielektrizitätskonstanten und Leitfähigkeiten der Mischkörper aus isotropen Substanzen. Annalen der physik, 416(7), pp.636-664.

Chen, J.C.Y., 2002. *Evaluation of Polymeric Membranes for Gas Separation Processes: Poly (ether-b-amide)(PEBAX® 2533) Block Copolymer* (Master's thesis, University of Waterloo).

Chen, L., Xie, H., Li, Y. and Yu, W., 2008. Surface chemical modification of multiwalled carbon nanotubes by a wet-mechanochemical reaction. *Journal of Nanomaterials*, *2008*, p.63.

Chow, T.S., 1980. Molecular interpretation of the glass transition temperature of polymer-diluent systems. *Macromolecules*, *13*(2), pp.362-364.

Chrzanowska, J., Hoffman, J., Małolepszy, A., Mazurkiewicz, M., Kowalewski, T.A., Szymanski, Z. and Stobinski, L., 2015. Synthesis of carbon nanotubes by the laser ablation method: Effect of laser wavelength. *Physica Status Solidi (b)*, *252*(8), pp.1860-1867.

Chung, T.S., Cao, C. and Wang, R., 2003. Pressure and temperature dependence of the gas-transport properties of dense poly [2, 6-toluene-2, 2-bis (3, 4-dicarboxylphenyl) hexafluoropropane diimide] membranes. *Journal of Polymer Science Part B: Polymer Physics*, *42*(2), pp.354-364.

Chung, T.S., Cao, C. and Wang, R., 2004. Pressure and temperature dependence of the gas-transport properties of dense poly [2, 6-toluene-2, 2-bis (3, 4-dicarboxylphenyl) hexafluoropropane diimide] membranes. *Journal of Polymer Science Part B: Polymer Physics*, *42*(2), pp.354-364.

Cong, H., Zhang, J., Radosz, M. and Shen, Y., 2007. Carbon nanotube composite membranes of brominated poly(2,6-diphenyl-1,4-phenylene oxide) for gas separation, *Journal of Membrane Science*, vol. 294, pp. 178–185.

Corry, B., 2011. Water and ion transport through functionalised carbon nanotubes: implications for desalination technology. *Energy & Environmental Science*, *4*(3), pp.751-759.

Dong, G., Li, H. and Chen, V. (2011) Plasticization mechanisms and effects of thermal annealing of Matrimid hollow fiber membranes for CO2 removal. *Journal of Membrane Science*, *369*(1-2), pp.206-220.

Dortmundt, D. and Doshi, K., 1999. Recent developments in CO2 removal membrane technology. *UOP LLC*, pp.1-30.

Dos Santos, M.M.C.C., 2009. *Carbon Molecular Sieve Membranes for Gas Separation: Study, Preparation and Characterization* (Doctoral dissertation, Universidade do Porto (Portugal)).

Dyachkova, T.P., Melezhyk, A.V., Gorsky, S.Y., Anosova, I.V. and Tkachev, A.G., 2013. Some aspects of functionalization and modification of carbon nanomaterials. *Nanosystems: Physics, Chemistry, Mathematics, 4,* pp. 605–621.

Eguchi, H., Kim, D.J. and Koros, W.J., 2015. Chemically cross-linkable polyimide membranes for improved transport plasticization resistance for natural gas separation. *Polymer*, *58*, pp.121-129.

George, S.C. and Thomas, S., 2001. Transport phenomena through polymeric systems. *Progress in Polymer Science*, *26*(6), pp.985-1017.

Gilassi, S. and Rahmanian, N., 2015. Mathematical modelling and numerical simulation of CO2/CH4 separation in a polymeric membrane. Applied Mathematical Modelling, 39(21), pp.6599-6611.

Hirsch, A., 2002. Functionalization of single-walled carbon nanotubes. *Angewandte Chemie International Edition*, *41*(11), pp.1853-1859.

Hölck, O., Siegert, M.R., Heuchel, M. and Böhning, M., 2006. CO2 sorption induced dilation in polysulfone: comparative analysis of experimental and molecular modeling results. *Macromolecules*, 39(26), pp.9590-9604.

Horn, N.R. and Paul, D.R., 2011. Carbon dioxide plasticization and conditioning effects in thick vs. thin glassy polymer films. *Polymer*, *52*(7), pp.1619-1627.

Hou, P.X., Liu, C. and Cheng, H.M., 2008. Purification of carbon nanotubes. *Carbon*, *46*(15), pp.2003-2025.

Inam, F. and Peijs, T., 2007. Re-agglomeration of carbon nanotubes in two-part epoxy system; influence of the concentration.

Ismail, A. F., Rahim, N. H., Mustafa, A., Matsuura, T., Ng, B.C., Abdullah, S. and Hashemifard, S.A. (2011) Gas separation performance of

polyethersulfone/multi-walled carbon nanotubes mixed matrix membranes, *Separation and Purification Technology*, vol. 80, pp. 20–31.

Ismail, A.F. and Lorna, W., 2002. Penetrant-induced plasticization phenomenon in glassy polymers for gas separation membrane. *Separation and Purification Technology*, *27*(3), pp.173-194.

Ismail, A.F., Goh, P.S., Sanip, S.M. and Aziz, M., 2009. Transport and separation properties of carbon nanotube-mixed matrix membrane. *Separation and Purification Technology*, *70*(1), pp.12-26.

Ismail, A.F., Kusworo, T.D., Mustafa, A. and Hasbulla, H., 2005. Understanding the solution-diffusion mechanism in gas separation membrane for engineering students. In *Regional Conference on Engineering Education RCEE* (Vol. 20052005).

Ismail, A.F., Rana, D., Matsuura, T. and Foley, H.C., 2011. *Carbon-based membranes for separation processes*. Springer Science & Business Media.

Iyuke, S.E. and Simate, G.S., 2011. Synthesis of carbon nanomaterials in a swirled floating catalytic chemical vapour deposition reactor for continuous and large scale production. In *Carbon Nanotubes-Growth and Applications*. InTech.

Kanehashi, S. and Nagai, K., 2005. Analysis of dual-mode model parameters for gas sorption in glassy polymers. *Journal of Membrane Science*, *253*(1-2), pp.117-138.

Kapantaidakis, G.C., Koops, G.H., Wessling, M., Kaldis, S.P. and Sakellaropoulos, G.P., 2003. CO2 Plasticization of polyethersulfone/polyimide gas-separation membranes. *AIChE Journal*, *49*(7), pp.1702-1711.

Kesting, R. E. and Fritzche, A. K. (1993) *Polymeric Gas Separation*, Wiley, New York.

Khan, A.L., Sree, S.P., Martens, J.A., Raza, M.T. and Vankelecom, I.F., 2015. Mixed matrix membranes comprising of matrimid and mesoporous COK-12:

Preparation and gas separation properties. *Journal of Membrane Science*, *495*, pp.471-478.

Kirtania, S. and Chakraborty, D., 2012. Multi-scale modeling of carbon nanotube reinforced composites with a fiber break. *Materials & Design*, *35*, pp.498-504.

Koros, W.J. and Fleming, G.K., 1993. Membrane-based gas separation. *Journal of Membrane Science*, *83*(1), pp.1-80.

Koros, W.J., Paul, D.R. and Rocha, A.A., 1976. Carbon dioxide sorption and transport in polycarbonate. *Journal of Polymer Science: Polymer Physics Edition*, *14*(4), pp.687-702.

Kraftschik, B., Koros, W.J., Johnson, J.R. and Karvan, O., 2013. Dense film polyimide membranes for aggressive sour gas feed separations. *Journal of Membrane Science*, *428*, pp.608-619.

Kusworo, T.D., Ismail, A.F. and Mustafa, A., 2013. Budiyono. Studies of Thermal annealing on Suppression of Plasticization of the Asymmetric Hollow Fiber Mixed Matrix Membranes. *World Applied Sciences Journal*, *28*, pp.09-19.

Lin, T., Bajpai, V., Ji, T. and Dai, L., 2003. Chemistry of carbon nanotubes. *Australian Journal of Chemistry*, *56*(7), pp.635-651.

Ma, P.C., Siddiqui, N.A., Marom, G. and Kim, J.K., 2010. Dispersion and functionalization of carbon nanotubes for polymer-based nanocomposites: a review. *Composites Part A: Applied Science and Manufacturing*, *41*(10), pp.1345-1367.

Mason, E.A., 1991. From pig bladders and cracked jars to polysulfones: an historical perspective on membrane transport. *Journal of Membrane Science*, *60*(2-3), pp.125-145.

Maxwell, J. C., 1954. A Treatise on Electricity and Magnetism, Dover Publications, New York, United States.

Neumann, G.A., Finkler, T.F., Cardozo, N.S. and Secchi, A.R., 2006. Comparison between phenomenological and empirical models for gas-phase polymerization process control. *Industrial & Engineering Chemistry Research*, 45(8), pp.2651-2660.

Pandey, P. and Chauhan, R.S., 2001. Membranes for gas separation. *Progress in Polymer Science*, *26*(6), pp.853-893.

Paul, D. R. and Koros, W. J., 1976. Effect of partially immobilized sorption on permeability and the diffusion time lag, *Journal of Polymer Science Part B: Polymer Physics*, vol. 14, pp. 675–685.

Peponi, L., Tercjak, A., Martin, L., Mondragon, I. and Kenny, J.M., 2011. Morphology-properties relationship on nanocomposite films based on poly (styrene-block-diene-block-styrene) copolymers and silver nanoparticles. *Express Polymer Letters*, *5*(2), pp.104-118.

Petropoulos, J.H., 1970. Quantitative analysis of gaseous diffusion in glassy polymers. *Journal of Polymer Science Part A-2: Polymer Physics*, *8*(10), pp.1797-1801.

Present, R.D. and Debethune, A.J., 1949. Separation of a gas mixture flowing through a long tube at low pressure. *Physical review*, *75*(7), p.1050.

Qiu, W., Chen, C.C., Xu, L., Cui, L., Paul, D.R. and Koros, W.J., 2011. Sub-T g cross-linking of a polyimide membrane for enhanced CO2 plasticization resistance for natural gas separation. *Macromolecules*, *44*(15), pp.6046-6056.

Rafiee, R. and Pourazizi, R., 2015. Influence of CNT functionalization on the interphase region between CNT and polymer. *Computational Materials Science*, *96*, pp.573-578.

Rafique, M.M.A. and Iqbal, J., 2011. Production of carbon nanotubes by different routes-a review. *Journal of Encapsulation and Adsorption Sciences*, *1*(02), p.29.

Rahimpour, A., Jahanshahi, M., Khalili, S., Mollahosseini, A., Zirepour, A. and Rajaeian, B., 2012. Novel functionalized carbon nanotubes for improving the surface properties and performance of polyethersulfone (PES) membrane. *Desalination*, *286*, pp.99-107.

Ranjbaran, F., Omidkhah, M. R. and Amooghin, A. E., 2015. The novel Elvaloy 4170/functionalized multi-walled carbon nanotubes mixed matrix membranes: Fabrication, characterization and gas separation study, *Journal of the Taiwan Institute of Chemical Engineers*, vol. 49, pp. 220–228.

Rastogi, V., Yadav, P., Bhattacharya, S.S., Mishra, A.K., Verma, N., Verma, A. and Pandit, J.K., 2014. Carbon nanotubes: an emerging drug carrier for targeting cancer cells. *Journal of Drug Delivery*, *2014*.

Robeson, L.M., Smith, Z.P., Freeman, B.D. and Paul, D.R., 2014. Contributions of diffusion and solubility selectivity to the upper bound analysis for glassy gas separation membranes. *Journal of Membrane Science*, *453*, pp.71-83.

Roque-Malherbe, R., 2000. Complementary approach to the volume filling theory of adsorption in zeolites. *Microporous and Mesoporous Materials*, *41*(1-3), pp.227-240.

Sanders, E.S., Koros, W.J., Hopfenberg, H.B. and Stannett, V.T., 1984. Pure and mixed gas sorption of carbon dioxide and ethylene in poly (methyl methacrylate). *Journal of Membrane Science*, *18*, pp.53-74.

Sanip, S. M., Ismail, A. F., Goh, P.S., Soa, T., Tanemura, M. and Yasuhiko, H. (2011) Gas separation properties of functionalized carbon nanotubes mixed matrix membranes, *Separation and Purification Technology*, vol. 78, pp. 208–213.

Scholes, C. A., Chen, G. Q., Stevens, G. W. and Kentish, S. E. (2010) Plasticization of ultra-thin polysulfone membranes by carbon dioxide, *Journal of Membrane Science*, vol. 346, pp. 208–214.

Shahid, S. and Nijmeijer, K., 2014. Performance and plasticization behavior of polymer–MOF membranes for gas separation at elevated pressures. *Journal of Membrane Science*, *470*, pp.166-177.

Sharma, R., Sharma, A.K. and Sharma, V., 2015. Synthesis of carbon nanotubes by arc-discharge and chemical vapor deposition method with analysis of its morphology, dispersion and functionalization characteristics. *Cogent Engineering*, *2*(1), p.1094017.

Shusen, W., Meiyun, Z. and Zhizhong, W., 1996. Asymmetric molecular sieve carbon membranes. *Journal of Membrane Science*, *109*(2), pp.267-270.

Stern, S.A. and Trohalaki, S., 1990, January. Fundamentals of gas-diffusion in rubbery and glassy-polymers. In *ACS Symposium Series* (Vol. 423, pp. 22-59). 1155 16TH ST, NW, WASHINGTON, DC 20036 USA: AMER CHEMICAL SOC.

Tasis, D., Tagmatarchis, N., Bianco, A. and Prato, M., 2006. Chemistry of carbon nanotubes. *Chemical Reviews*, *106*(3), pp.1105-1136.

Thewlis, J., 1973. Concise dictionary of physics, Pergamon press, Oxford, United Kingdom, pp. 248.

Van Amerongen, G.J., 1950. Influence of structure of elastomers on their permeability to gases. *Journal of Polymer Science*, *5*(3), pp.307-332.

Vieth, W.R. and Sladek, K.J., 1965. A model for diffusion in a glassy polymer. *Journal of Colloid Science*, *20*(9), pp.1014-1033.

Wang, M., Wang, Z., Zhao, S., Wang, J. and Wang, S., 2017. Recent advances on mixed matrix membranes for CO2 separation. *Chinese Journal of Chemical Engineering*, *25*(11), pp.1581-1597.

Wang, T., Shen, J.N., Wu, L.G. and Van der Bruggen, B., 2014. Improvement in the permeation performance of hybrid membranes by the incorporation of

functional multi-walled carbon nanotubes. *Journal of Membrane Science*, *466*, pp.338-347.

White, K.A., 2017. *Direct determination of isosteric heats of sorption using pressure-gradient differential scanning calorimetry* (Doctoral dissertation, Stellenbosch: Stellenbosch University).

Wijmans, J.G. and Baker, R.W., 1995. The solution-diffusion model: a review. *Journal of Membrane Science*, *107*(1-2), pp.1-21.

Wijmans, J.G. and Baker, R.W., 1995. The solution-diffusion model: a review. *Journal of Membrane Science*, *107*(1-2), pp.1-21.

Wind, J.D., Staudt-Bickel, C., Paul, D.R. and Koros, W.J., 2003. Solid-state covalent cross-linking of polyimide membranes for carbon dioxide plasticization reduction. *Macromolecules*, *36*(6), pp.1882-1888.

Xue, Q., Lv, C., Shan, M., Zhang, H., Ling, C., Zhou, X. and Jiao, Z., 2013. Glass transition temperature of functionalized graphene–polymer composites. *Computational Materials Science*, *71*, pp.66-71.

Yah, C.S., Simate, G.S., Moothi, K., Maphutha, K.S. and Iyuke, S.E., 2011. Synthesis of large carbon nanotubes from ferrocene: the chemical vapour deposition technique. *Trends in Applied Sciences Research*, *6*(11), pp.1270-1279.

Yang, Y.K., Xie, X.L. and Mai, Y.W., 2011. Functionalization of carbon nanotubes for polymer nanocomposites. In *Polymer–Carbon Nanotube Composites* (pp. 55-91).

Yong, W.F., Kwek, K.H.A., Liao, K.S. and Chung, T.S., 2015. Suppression of aging and plasticization in highly permeable polymers. *Polymer*, *77*, pp.377-386.

Zhang, L., Xiao, Y., Chung, T.S. and Jiang, J., 2010. Mechanistic understanding of CO2-induced plasticization of a polyimide membrane: A combination of experiment and simulation study. Polymer, 51(19), pp.4439-4447.

Zhou, S. and Stern, S. A., 1989. The effect of plasticization on the transport of gases in and through glassy polymers, *Journal of Polymer Science Part B: Polymer Physics,* vol. 27, pp. 205.

Zhuang, G.L., Tseng, H.H., Uchytil, P. and Wey, M.Y. (2018) Enhancing the CO_2 plasticization resistance of PS mixed-matrix membrane by blunt zeolitic imidazolate framework. *Journal of CO2 Utilization*, *25*, pp.79-88.

CHAPTER 3

3 MATERIALS AND EXPERIMENTAL PROCEDURES

3.1 Materials

Nitrogen (purity: 99.99%), argon (purity: 99.99%), hydrogen (purity: 99.99%), acetylene (purity: 99%), methane (purity: 99.95%), carbon dioxide (purity: 99.99%) and carbon dioxide/methane mixture (50%/50%) gases were purchased from Afrox, South Africa. The following chemicals were purchased from Sigma Aldrich, South Africa: hydrochloric (wt. 37%), sulfuric (wt. 98 %) and nitric (wt. 70%) acids, ferrocene (purity: 98%), dichloromethane (purity ≥ 99.8%) and Polysulfone pellets (transparent, average M_w ~ 35 000). All the materials were used as supplied without any further purification.

3.2 Production of carbon nanotubes

The catalyst chemical vapour deposition (CCVD) system used for this study comprised of a vertical quartz tube reactor in a furnace and a temperature controller is attached to the reactor. Furthermore, the system is equipped with a set of four Supelco rotameter to regulate the flow of gases into the reactor. The process flow diagram of the CCVD system set-up employed in this study is shown in Figure 3.1.

The CCVD system was first tested for leaks and thereafter purged using nitrogen gas to create an inert environment in the reactor. 7 g of ferrocene was fed into the vapourizer for each of the experimental runs. Subsequently, the reactor was set to the desired temperature (800 ^{o}C – 1000 ^{o}C) using the temperature controller attached to the reactor furnace. When the desired reactor temperature was reached, the ferrocene vapourizer was heated up to the melting point of ferrocene (~ 173 ^{o}C) while the carrier gas, argon (150 ml/min) or argon/hydrogen (125/25 ml/min) was introduced to transport the ferrocene vapour into the reactor. Simultaneously, the carbon source, acetylene (150 ml/min) or methane (150 ml/min), was also introduced into the reactor. In order to adequately compare the production yields at different conditions, the

reaction was terminated at the end of 15 minutes for each experimental run by shutting down the system.

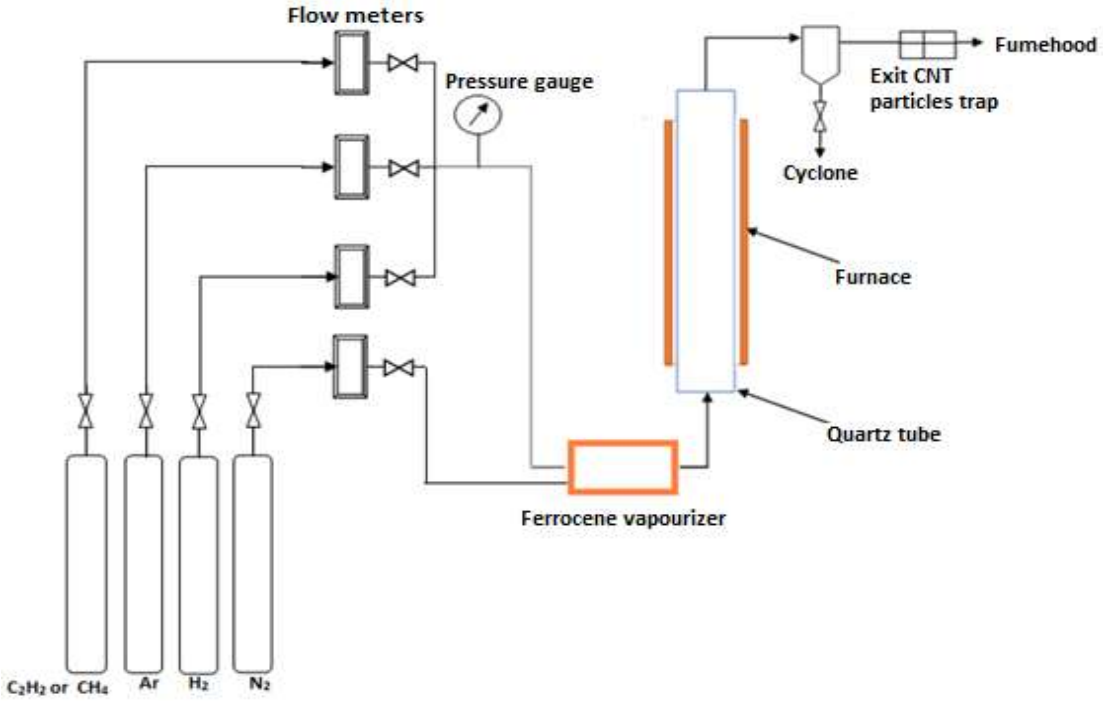

Figure 3.1: Process flow diagram of the CCVD system set-up

3.3 Functionalization of as-produced carbon nanotubes

CNTs produced at optimum quality condition was first purified to remove iron particle residues attached to the CNTs from the catalyst used and possible presence of amorphous carbon due to incomplete nucleation of the carbon source (Humphries et al., 2009). 1 g of raw CNTs (RCNTs) was added to 100 ml of hydrochloric acid and ultrasonicated for 4 h at 40 ^{o}C bath temperature. The mixture was thereafter washed with distilled water and centrifuge 3 times. Afterward, the purified CNTs (PCNTs) was washed again with distilled water and filter until the filtrate pH approaches neutral. The filtered PCNTs was dried at 100 ^{o}C for 24 h to remove the water content present in the PCNTs. PCNTs were functionalized using carboxylation protocol. 1 g of PCNTs were added to 75 ml of sulfuric acid and 25 ml of nitric acid. The mixture was ultrasonicated

for 1 h at 40 ^{o}C. Drying, washing and recovery determination procedure were the same as that of the purification process.

3.4 Membrane preparation procedures

Dense flat sheet membranes were synthesized by solvent evaporation. For pristine PSF membrane preparation, 1 g of polysulfone (PSF) beads were added to 10 ml dichloromethane (DCM) and stirred using magnetic stirrer until a homogeneous solution was formed. The solution was transferred to a flat bottom petri dish and left in a vacuum oven at room temperature for 6 h for controlled evaporation of DCM. Afterward, the oven temperature was increased to 40 ^{o}C (boiling point of DCM) for 24 h for complete removal of the solvent.

With respect to FCNT/PSF membrane preparation, desired wt. % of FCNTs were added to 5 ml of DCM and ultrasonicated for 30 min in a cold water bath to control agglomeration temperature. 1 g of PSF beads were added to 5 ml of DCM and stirred to form a homogeneous solution. PSF solution was transferred to FCNT solution and stirred for 12 h. Solvent evaporation steps of FCNT/PSF dope were the same as that of pristine PSF dope. The thickness of the membranes was measured using digital micrometer at 10 different points on the membrane and the average thickness was used for permeability calculations. Some of the thicknesses were verified by scanning electron microscope (SEM). A sample of the measurement of membrane thickness using SEM is presented in Appendix C. The thicknesses were between 60 – 90 μm.

3.5 Characterization of produced CNTs and membranes

3.5.1 Field emission scanning electron microscopy (FESEM)

SEM micrographs of as-produced CNTs and synthesized membranes were obtained using FESEM operated at 10 kV to check the morphology. A spatula tip of each sample was mounted onto an aluminum stub using carbon tapes. Two layers of gold-palladium coating, each of 10 nm in thickness, were applied to the mounted samples before taking images of the samples using the microscope.

3.5.2 Raman spectroscopy

Raman spectra were obtained using a Horiba LabRAM HR Raman spectrometer equipped with an Olympus BX41 microscope to check the existence of sp^2 carbon and to obtain the degree of disorder of the as-produced CNTs. A Lexel argon ion laser at a wavelength of 514.5 nm (green line) was used to excite raman scattering in the samples. A 100x objective was used to collect the backscattered light, which was dispersed via a 600 lines/mm grating onto a liquid nitrogen cooled charge coupled device (CCD) detector. The laser power at the samples was ~0.4 mW to prevent localized heating.

3.5.3 Fourier transform infrared (FTIR) spectroscopy

The presence of functional groups on the FCNTs was checked by PerkinElmer FTIR spectrometer equipped with a high-performance deuterated triglycine sulphate (DTGS) detector and a KBr beam splitter to establish successful functionalization of the CNTs. 2 mg of CNT sample was mixed with 300 mg potassium bromide (KBr) and pressed to form a self-supporting pellet (Scholze and Meier 2001). The spectra of RCNTs, PCNTs, and FCNTs were recorded from 4000 and 500 cm^{-1} wavenumbers.

3.5.4 Nitrogen physisorption

Nitrogen physisorption of CNT samples was conducted at 77 K using Tristar 3000 v6.05A to obtain the textural properties of the CNTs. Brunauer-Emmett-Teller (BET) equation was used to evaluate the surface area of RCNTs, PCNTs, and FCNTs. Barrett-Johner-Halenda (BJH) equation was used to determine the pore volume and average pore size of all the types of CNTs (Zaine et al., 2016).

3.5.5 X-ray diffraction (XRD)

The crystalline structure of RCNTs, PCNTs, and FCNTs was analyzed using Bruker XRD D2 Phaser with a Cu Kα target at a wavelength of 0.154184 nm, a tube voltage of 30 kV and a tube current of 10 mA to check the effect of functionalization on the crystallinity of the CNTs. The samples were scanned at a stepsize of 0.02^o and a rate

of 8.5º/min from 5º to 90º of 2θ. The Miller indices (hkl) were obtained from the reference library of Diffrac.EVA software.

3.5.6 Thermo-gravimetric analysis (TGA)

TGA was used to determine the degree of functionalization of the CNTs and check the thermal stability of the synthesized membranes. TA instrument SDT Q600 simultaneous DSC/TGA analyzer with balance sensitivity of 0.1 µg was used. The heating rate was 20 ºC/min from 25 ºC to 800 ºC. Nitrogen gas at 70 ml/min flowrate was used to create an inert environment in the instrument. Thermal stability of CNTs as a function of weight % loss with respect to temperature was used to quantitatively evaluate the degree of functionalization of the CNTs (Momeni and Pakizeh, 2013). For the synthesized membrane, thermal stability was determined using the graphs of weight % loss against temperature and derivative of weight with respect to temperature (Darabi et al., 2012).

3.5.7 Differential scanning calorimetry (DSC)

DSC analyzer incorporated into TA instrument SDT Q600 was used to measure the glass transition temperature (T_g) of synthesized membranes. T_g of synthesized membranes was calculated from heat flow against temperature curve using the half C_p (heat capacity at constant pressure) extrapolated method (Ranjbaran et al., 2015). To conduct DSC analysis, membranes samples were subjected to two heating cycles. The first heating cycle was to eliminate the thermal history of the membrane (Lappe et al., 2017). 15 mg of the sample was placed in alumina pan and heated at a heating rate of 10 ºC/min from 25 ºC – 300 ºC under a nitrogen atmosphere with a flowrate of 70 ml/min. Thereafter, the sample was cooled back to the initial temperature. For the second heating cycle, the sample was heated up to 350 ºC under the same conditions as the first heating cycle.

3.5.8 Atomic force microscopy (AFM)

Veeco Dimension 3100 atomic force microscopy (AFM) was used to study the surface topography of the membranes so as to determine if the pores in the membranes are continuous and to check the effect of FCNTs on the pore depth of the membranes. The membranes were cut into 1 cm x 1 cm size and mounted unto the instrument by attaching them to a steel disk using double-sided tape. Air duster was used on the mounted sample to minimize dust on the sample surface. For surface imaging, tapping mode was selected as imaging option. The scan size used was 10 µm x 10 µm at a scan rate of 1.5 Hz, except for pure PSF where scan size of 50 µm x 50 µm was used because its detailed surface topography could not be observed at 10 µm x 10 µm scan size. The tip resonant frequency is 75 kHz with a spring constant of 2.8 N/m. The number of data points captured during each extend-retract operation was 256. The Z range for amplitude data type was set at 1.5V while the Z range for height data type was set at 400 nm. AFM Nanoscope software was used to process the data and to obtain 2-D and 3-D views of the membrane surface images.

3.5.9 Texture Analysis

Bulk mechanical properties of the membranes were evaluated using TA XT Plus texture analyzer at ambient temperature to determine the effect of FCNTs on the tensile strength and Young's Modulus of the synthesized membranes. The membranes were cut into a 30 mm x 10 mm size and fixed into the sample holder of the instrument. Force and distance data at a rate of 500 points per second were captured and analyzed using integrated Exponent 32-bit software. Tensile strength and Young's Modulus of the membranes were calculated from the data using Equations (3.1) and (3.2), respectively. Tensile strength is the maximum amount of tensile stress a material can withstand before breaking. Young's Modulus is a measure of the stiffness of a solid material.

$$\sigma = \frac{F}{A} \tag{3.1}$$

$$E = \frac{Fl}{A\Delta l} \tag{3.2}$$

Where σ is the tensile strength, E is the Young's modulus, F is the uniaxial force, A is cross-sectional area of the sample (width x thickness), Δl is the elongation of the sample and l is the original gauge length.

3.6 Evaluation of gas transport property of the membranes

Gas separation performance of membranes is generally evaluated by single and mixed gas permeation measurements. Single gas permeation measurement provides an ideal gas separation performance of a membrane. It serves as a platform for improving the fabrication conditions of the membrane for better performance. Mixed gas permeation measurement, on the other hand, provides real gas separation of a membrane which is lower than the single gas permeation measurement in most cases. The reason being that in mixed gas separation, all penetrants compete for Langmuir sorption sites of the membrane which decreases their permeabilities (Kraftschik et al., 2013).

3.6.1 Single gas permeation measurements

Pure gas permeation measurements were carried out at the department of chemical engineering, University of Melbourne (UoM), Australia. The pure gas permeation experiment was conducted using a custom-built permeation set up via constant volume variable pressure (CVVP) technique (Scholes et al., 2010). The system temperature was kept constant at 35 ^{o}C and the feed pressure was between 2 and 20 bar. The permeate side contained 0.5 L sample cylinder. Before each experiment, the system together with the membrane to be tested was evacuated overnight to ~ 75 mtorr vacuum. The measured leakage rate was below 10^{-5} torr/s during permeability measurements. The rate of pressure increase on the permeate side due to the gas flux across the membranes was monitored using e-Baratron digital manometer. The output of the manometer was captured through a National instrument data logging card and the data were recorded electronically using LabVIEW X at 1s intervals. The pictures of pure gas permeation apparatus are shown in Figure 3.2.

For each experimental run, CH_4 was tested first followed by CO_2. Permeability measurement was determined after 1 h 30 min to ensure that solution-diffusion equilibrium was reached for each gas. The equation for calculating pure gas permeability was derived from the first principle as follows:

According to Yasuda (1975):

$$Permeability = \frac{membrane\ flux}{membrane\ permeation\ area \times driving\ force\ gradient} \tag{3.3}$$

Permeant flux is generally measured by either rate of pressure change at a fixed volume or rate of volume change at a fixed pressure (Yasuda, 1975). Also, the driving force gradient in our experiment is the differential pressure of the gas with respect to the thickness of the membrane. Equation (3.3) can then be written mathematically as:

$$P = \frac{J}{A \times \Delta p / \Delta L} \tag{3.4}$$

Where:

P = permeability

J = permeant flux

A = permeation area

Δp = differential pressure of the gas

L = membrane thickness

Since the technique used is CVVP,

$$J = V \frac{dp}{dt} \tag{3.5}$$

Substituting Equation (3.5) into Equation (3.4)

$$P = \frac{VL}{A \times \Delta p} \frac{dp}{dt} \tag{3.6}$$

Permeability unit used is Barrer (1 Barrer = 10^{-10}cm^3 (STP) cm/cm^2 .s. cmHg). Therefore, the permeate variables need to be changed from process conditions to STP. Using the ideal gas equation:

$$\frac{p_1 V_1}{T_1} = \frac{p_2 V_2}{T_2} \tag{3.7}$$

p = rate of change of pressure for the permeate $(\frac{dp}{dt})$

V = permeate constant volume

T = operating temperature

Subscript 1 = process condition

Subscript 2 = STP (273 K and 76 cmHg)

$$V_2 = \frac{273}{76}\frac{V_1}{T_1}\frac{dp}{dt} \tag{3.8}$$

Equation (3.6) becomes;

$$P\ (in\ Barrer) = \frac{273}{76} \times \frac{VL}{T \times A \times \Delta p} \times \frac{dp}{dt} \times 10^{10} \tag{3.9}$$

Δp = absolute feed pressure – permeate pressure

Since absolute feed pressure >>> permeate pressure

Δp ≈ absolute feed pressure (p)

$$\therefore P = \frac{273}{76} \times \frac{VL}{TA\,p} \times \frac{dp}{dt} \times 10^{10} \tag{3.10}$$

To account for the leak in the system, permeate variable pressure was obtained from Equation (3.11)

$$\frac{dp}{dt} = \left[\frac{dp}{dt}\right]_{ss} - \left[\frac{dp}{dt}\right]_{leak} \quad (3.11)$$

$\left[\frac{dp}{dt}\right]_{ss}$ = rate of change of permeate pressure at steady state

$\left[\frac{dp}{dt}\right]_{leak}$ = rate of change of pressure of the system leakage

The ideal selectivity was calculated using Equation (3.12) (Alaslai et al., 2016):

$$\alpha^{id}_{CO_2/CH_4} = \frac{P_{CO_2}}{P_{CH_4}} \quad (3.12)$$

P_{CO_2} = Permeability of CO_2

P_{CH_4} = Permeability of CH_4

Figure 3.2: Pictures of the pure gas permeation apparatus at UoM [A – Full view of the equipment. B – Oven that housed the membrane module and permeate sample cylinder. C – Close view of e-Baratron digital manometer]

3.6.2 Mixed gas separation

The mixed gas separation experiments were carried out at UoM and WITs laboratories. For the experiment conducted at UoM, the mixed gas composition was 10%/90% of CO_2/CH_4 with a feed pressure between 2 – 10 bar at 35 ^oC. The experiment at WITs was conducted with a feed pressure between 2 – 6 bar (based on the limit on the equipment) at 35 ^oC, the mixed gas composition was 50%/50% of CO_2/CH_4. The mixed gas permeability was measured on a constant pressure variable volume (CPVV) gas permeation apparatus (Scholes et al., 2015).

To ensure no concentration polarization on both sides of the membrane, the retentate flow rate was kept at about 200 ml/min on the feed side. For the permeate side, nitrogen was used as a sweep gas with a flow rate of 26 ml/min at 1 bar. The permeate gas was passed through a sample cylinder that was immersed in a water bath at ambient

temperature. The pictures of mixed gas permeation equipment used at UoM and Wits are shown in Figure 3.3 and Figure 3.4 respectively.

The flow rate of gas permeate was measured through a universal flowmeter (Agilent Technologies ADM 3000). The permeate gas was compositionally analyzed using pre-calibrated online gas chromatography equipped with a thermal conductivity detector. Permeability was determined after 3 h for each experimental run. The Equation for calculating mixed gas permeability was derived as follows:

From Equation (3.4)

$$P = \frac{J}{A \times \Delta p/L}$$

Since the technique used is CPVV,

$$J = p\frac{dV}{dt} \tag{3.13}$$

Substituting Equation (3.13) into Equation (3.4)

$$P = \frac{pL}{A \times \Delta p}\frac{dV}{dt} \tag{3.14}$$

Converting the process condition to STP as previously discussed

$$P = \frac{273}{76} \times \frac{p_p L}{TA \times \Delta p} \times \frac{dV}{dt} \times 10^{10} \tag{3.15}$$

p_p = permeate pressure ≈ 76 cmHg

T = permeate Temperature ≈ 273 K

Δp = absolute feed pressure (p_f) - p_p

$$\therefore P = \frac{L}{A(p_f - p_{p)}} \times \frac{dV}{dt} \times 10^{10} \quad (3.16)$$

The permeability of CO_2 and CH_4 was calculated using Equations (3.17) and (3.18), respectively:

$$P_{CO_2} = \frac{y_{CO_2} L}{A(x_{CO_2} p_f - y_{CO_2} p_{p)}} \times \frac{dV}{dt} \times 10^{10} \quad (3.17)$$

$$P_{CH_4} = \frac{y_{CH_4} L}{A(x_{CH_4} p_f - y_{CH_4} p_{p)}} \times \frac{dV}{dt} \times 10^{10} \quad (3.18)$$

The mixed gas separation factor was determined using Equation (3.19) (Alaslai et al., 2016):

$$\propto_{CO_2/CH_4} = \frac{(y_{CO_2}/y_{CH_4})_{permeate}}{(x_{CO_2}/x_{CH_4})_{feed}} \quad (3.19)$$

$\frac{dV}{dt}$ = permeate flow rate (cm^3/s).

Where x and y are the mole fractions.

Figure 3.3: Pictures of the mixed gas permeation apparatus at UoM [A – Full view of the equipment. B – Oven that housed the membrane module. C – Gas chromatography]

Figure 3.4: Pictures of the mixed gas permeation apparatus at WITs [A – Full view of the equipment. B – Oven that housed the membrane module. C – Gas chromatography]

3.6.3 CO_2 gas sorption measurements

Sorption measurement of CO_2 gas was carried out at UoM. The measurements were conducted on a gravimetric sorption analyzer (GHP-FS, with a Cahn D-200 balance, VTI Scientific Instruments, Florida) operated in a static mode at 35 ^oC with 10 pressure points between 0 - 20 bar. Prior to sorption measurement, a sample of the membrane was placed in the sample chamber and the system was purged for 360 min at 35 ^oC to remove all air from the polymer matrix. Thereafter, CO_2 was introduced into the sample chamber at incremental pressure. At each pressure point, the system was allowed to equilibrate for 1 h until a constant mass of adsorbed CO_2 by the membrane was achieved. CO_2 sorption isotherms as a function of feed pressure were determined. The system was then evacuated for another 300 min. For buoyancy correction, the above procedure was repeated with Helium gas, which can be assumed to have no adsorption onto the membrane. The picture of the sorption analyzer used is shown in Figure 3.5.

Figure 3.5: Picture of the gravimetric sorption analyzer at UoM [A- sample chamber, B- control panel]

References

Alaslai, N., Ghanem, B., Alghunaimi, F., Litwiller, E., and Pinnau, I. (2016) Pure-and mixed-gas permeation properties of highly selective and plasticization resistant hydroxyl-diamine-based 6FDA polyimides for CO_2/CH_4 separation, *Journal of Membrane Science*, vol. 505, pp. 100–107

Darabia, H. R., Tehrania, M. J., Aghapoora, K., Mohsenzadeha, F. and Malekfarb, R. (2012) A new protocol for the carboxylic acid sidewall functionalization of single-walled carbon nanotubes, *Applied Surface Science*, vol. 258, pp. 8953–8958

Humphries W, Huynh C, Lucas S, Smith S and Tran C (2009) Improving the Tensile Strength of Carbon Nanotube Spun Yarns Using a Modified Spinning Process *Carbon.* **47** 2662

Kraftschik, B., Koros, W.J., Johnson, J.R. and Karvan, O., 2013. Dense film polyimide membranes for aggressive sour gas feed separations. *Journal of Membrane Mcience*, 428, pp.608-619.

Lappe, S., Mulac, D. and Langer, K. (2017) Polymeric nanoparticles – Influence of the glass transition temperature on drug release, *International Journal of Pharmaceutics*, vol. 517, pp. 338–347

Momeni, S. M. and Pakizeh, M. (2013) preparation, characterization and gas permeation study of Psf/MgO nanocomposite membrane, *Brazilian Journal of Chemical Engineering*, vol. 30, no. 03, pp. 589 – 597

Ranjbaran, F., Omidkhah, M. R. and Amooghin, A. E. (2015) The novel Elvaloy 4170/functionalized multi-walled carbon nanotubes mixed matrix membranes: Fabrication, characterization and gas separation study, *Journal of the Taiwan Institute of Chemical Engineers*, vol. 49, pp. 220–228

Scholes, C. A., Chen, G. Q., Stevens, G. W. and Kentish, S. E. (2010) Plasticization of ultra-thin polysulfone membranes by carbon dioxide, *Journal of Membrane Science*, vol. 346, pp. 208–214

Scholes, C. A., Kanehashi, S., Stevens, G. W. and Kentish, S. E. (2015) Water permeability and competitive permeation with CO2 and CH4 in perfluorinated polymeric membranes, *Separation and Purification Technology,* vol. 147, pp. 203–209

Scholze, B and Meier, D (2001) Characterization of the water-insoluble fraction from pyrolysis oil (pyrolytic lignin). Part I. PY–GC/MS, FTIR, and functional groups, *Journal of Analytical and Applied Pyrolysis*, vol. 60, pp. 41–54

Yasuda, H. (1975) Units of gas permeability constants, *Journal of Applied Polymer Science*, Vol. 19, pp. 2529-2536

Zaine, I. S., Fahdil, S., Napiah, N. A. M., Yusof, A. M., Alias, A. N., Ali, A. M. M. and Khalid, S. H. (2016) Preliminary Analysis on Pore Structure of Modified Multi-Walled Carbon Nanotubes, *IJCTA*, vol. 9(6), pp. 2949-2955

CHAPTER 4

4 PRODUCTION AND FUNCTIONALIZATION OF CARBON NANOTUBES

The work presented in this chapter has been published in Microporous and Mesoporous Materials journal as "Aberefa, O.A., Daramola, M.O. and Iyuke, S.E., 2019. Production and functionalization of carbon nanotubes for application in membrane synthesis for natural gas separation. *Microporous and Mesoporous Materials*, *280*, pp.26-36".

4.1 Introduction

CNTs have exceptional mechanical properties owning to their light weight, length to radius ratio and the carbon-carbon (C-C) bonds in the graphite layers, which are perhaps the most powerful chemical bond known (Ismail et al., 2011). Furthermore, several literature have reported simulation studies of gas transport through CNTs (Skoulidas et al., 2002; Sokhan et al., 2004). CNTs have shown superior gas permeability and selectivity as compared to other fillers of similar pore sizes owing to the inherent smoothness of CNTs (Ismail et al., 2009). Addition of CNTs as a filler in polymeric mixed matrix membrane (MMM) has been reported to improve the mechanical strength (Sanip et al., 2011) and gas permeability and selectivity (Aroon et al., 2010; Sanip et al., 2011) of the membrane. Generally, the performance of polymeric membranes is measured based on permeability and selectivity. Permeability measures intrinsic productivity of the membrane while selectivity measures the membrane's separation efficiency (Eguchi et al., 2015).

The transfer of excellent mechanical and transport properties of a filler particle to the polymer matrix depends largely on the effective dispersion of the filler particles into the polymer matrices (Bastani et al., 2013). However, the C-C bonds cause a dispersion problem for CNTs in the polymer matrix due to the agglomeration of CNTs (Ma et al., 2010). Functionalization of CNTs has been proposed as a solution to this problem (Chen et al., 2008). The addition of functionalized carbon nanotubes (FCNTs) into

polymers appears to offer a unique solution to the deficiencies of conventional polymeric membrane systems (Deng and Hägg, 2014). Chemical functionalization of CNTs reduces the strong Van der Waal force of attraction between CNTs and enhances separation of CNT bundles into individual CNT thereby improving CNT-polymer matrix interface interaction (Balasubramanian and Burghard, 2005). Furthermore, functionalization of CNTs could be modified to have particular interactions with specific gases to enhance molecular sieving of MMMs by chemical recognitions during gas separation (Corry, 2011).

In this study, CNTs were produced by CCVD method using methane and acetylene as carbon sources, hydrogen and argon served as carrier gas and ferrocene used as catalyst. The effect of carbon sources and production conditions (temperature and type of carrier gas) on the yield and quality of produced CNTs are presented. Finally, CNT with optimum quality was purified and functionalized using carboxylation protocol to enhance its dispersion and adsorption properties for use in membrane synthesis for natural gas separation. Physicochemical properties of the as-produced and as-functionalized CNTs were checked to evaluate the influence of the aforementioned conditions on the yield and quality of them.

4.2 Experimental

4.2.1 Materials

Nitrogen (purity: 99.999%), argon (purity: 99.999%), hydrogen (purity: 99.999%), acetylene (purity: 99%) and methane (purity: 99.95%) gases were purchased from Afrox, South Africa. Hydrochloric (37 wt. %), sulfuric (98 wt. %) and nitric (70 wt. %) acids were purchased from Sigma Aldrich, South Africa. In addition, ferrocene (98%) used as catalyst was also purchased from Sigma Aldrich, South Africa. All the materials were used as supplied without any further purification.

4.2.2 Production and characterization of CNTs

CNTs were produced using chemical vapour deposition method. Methane and acetylene were used as carbon source, argon and hydrogen served as carrier gases while ferrocene acted as catalyst. The reactor temperature was varied between 800^{o}C and 1000^{o}C. Detailed production protocol is stated in chapter 3, section 3.2. Table 4.1 describes the variation in production conditions for the CNT samples.

The morphology and elemental composition of as-produced CNTs were obtained using field emission scanning electron microscope (FESEM) equipped with energy-dispersive X-ray spectroscope (EDS), degree of defect and graphitization were determined using raman spectroscope equipped with Olympus BX41 microscope and electronic precision balance (EPB) with readability of 0.1 mg was used to measure the yield of each experimental run.

Table 4.1: CNT production conditions

Sample	***Carbon Source***	***Reactor Temperature (^{o}C)***	***Carrier Gas***	***Notation C-T-G***
1	Acetylene	800	Argon	A-800-Ar
2	Acetylene	850	Argon	A-850-Ar
3	Acetylene	900	Argon	A-900-Ar
4	Acetylene	950	Argon	A-950-Ar
5	Acetylene	1000	Argon	A-1000-Ar
6	Acetylene	800	Argon/Hydrogen	A-800-Ar/H
7	Acetylene	850	Argon/Hydrogen	A-850-Ar/H
8	Acetylene	900	Argon/Hydrogen	A-900-Ar/H
9	Acetylene	950	Argon/Hydrogen	A-950-Ar/H
10	Acetylene	1000	Argon/Hydrogen	A-1000-Ar/H
11	Methane	800	Argon	M-800-Ar
12	Methane	900	Argon	M-900-Ar
13	Methane	1000	Argon	M-1000-Ar

C-T-G: C = carbon source; T = reactor temperature; G = carrier gas; A = Acetylene; M = Methane; Ar = Argon; H = Hydrogen

4.2.3 CNTs functionalization protocol and characterization

Extensive CNT functionalization procedure is given in chapter 3, section 3.3. In summary, 1 g of raw CNTs (RCNTs) was added to 100 ml of hydrochloric acid and ultrasonicated for 4 h at 40 ^{o}C. The mixture was rinsed with distilled water and filtered until the filtrate pH nears seven. The filtered PCNTs was dried at 100 ^{O}C for 24 h. Thereafter, 1 g PCNTs was added to 75 ml of sulfuric acid and 25 ml of nitric acid. The mixture was ultrasonicated for 1 hr at 40 ^{O}C. Rinsing, filtering, and drying were repeated as previously mentioned.

In order to confirm successful functionalization of PCNTs and to investigate the effect of functionalization; RCNTs, PCNTs, and FCNTs were characterized using TGA to quantify the degree of functionalization, Fourier transform infrared spectroscopy (FTIR) was used to check the presence of functional groups and Brunauer-Emmett-Teller (BET) analysis to obtain the textural properties and X-ray diffraction (XRD) was used to investigate the change in the crystallinity of CNTs due to functionalization.

4.3 Results and discussion

4.3.1 Morphology of as-produced CNTs

Figure 4.1 depicts the SEM images of CNTs produced from acetylene and argon at varying reactor temperature. The images show that carbon nanoballs are predominant at all the investigated temperatures. This observation is similar to the one obtained by Iyuke et. al (2009) where acetylene and argon were used but without a catalyst. The expectation is that the use of catalyst would provide nucleation sites for CNTs to grow (Liu et al., 2004). However, Figure 4.1 does not support this theory. We, therefore, looked at the growth mechanism of CNTs, the most acceptable growth mechanism of CNTs involves three stages (Iyuke and Simate, 2011; Meyyappan, 2004): (i) decomposition of the carbon source on the catalyst surface; (ii) dissolution and diffusion of the carbon atoms through the bulk of the catalyst particles; (iii) precipitation of CNTs on the other side of the catalyst particles. Hence, we postulated that, since acetylene is highly reactive (Soneda, 2002), there could be the formation of

carbon deposits on the surface of the catalyst which might deactivate the catalyst active sites (Ning et al., 2005; Kuwana et al., 2005). In order to substantiate our postulation, hydrogen gas, which is known to reduce catalyst deactivation (Bahome et al., 2005), was added to argon to serve as a carrier gas. The result shows the presence of more CNTs in all the reactor temperature as depicted in Figure 4.2.

Figure 4.3 shows the SEM results of CNTs produced from methane and argon. Methane being less reactive than acetylene (Soneda, 2002), supports the growth mechanism of CNTs without the addition of hydrogen to the carrier gas. This could be seen in the presence of more CNTs in the samples produced from methane. Figure 4.3a displays the existence of amorphous carbon in the sample which could be attributed to non-nucleation of some of the carbon atoms at a lower temperature (Gomez-Ballesteros et al., 2015). CNTs were predominant in Figure 4.3b, this was also confirmed with a transmission electron microscope (TEM) and presented in Figure 4.3d. Figure 4.3c depicts thermal degradation of the CNTs at a higher temperature (Duong et al., 2008).

4.3.2 Effect of production conditions on the yield of as-produced CNTs

The effect of production conditions on the rate of production of CNTs is depicted in Figure 4.4. CNTs production rate for acetylene and argon (A-Ar) shows a decrease in CNTs yield with an increase in temperature. This could be attributed to the deactivation of the catalyst active site with an increase in temperature (Sivakumar et al., 2010). However, with the addition of hydrogen to argon as carrier gas (A-Ar/H), the CNT yield increases with increase in temperature. This further support our initial postulate about the deactivation of catalyst active site due to the formation of carbon deposits on the surface of the catalyst owing to the high reactivity of acetylene, which is reduced by the addition of hydrogen gas (Ning et al., 2005; Kuwana et al., 2005). CNTs production rate of Methane and argon (M-Ar) shows an optimum yield at 900 ^{o}C.

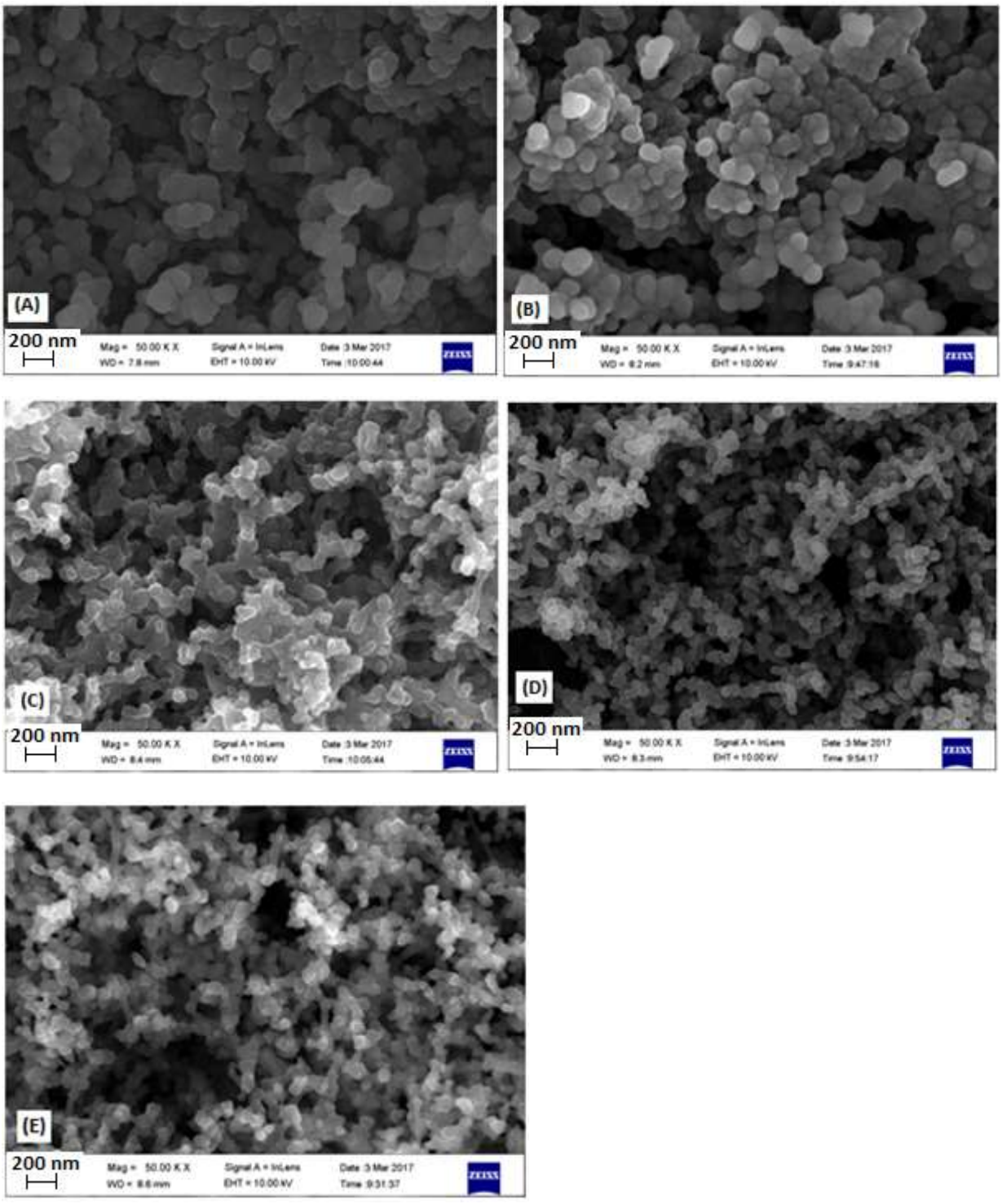

Figure 4.1: SEM micrograph of CNTs produced from acetylene as carbon source and argon as carrier gas (A = A-800-Ar, B = A-850-Ar, C = A-900-Ar, D = A-950-Ar, E = A-1000-Ar). Experimental conditions: acetylene flow rate = 150 ml/min; argon flow rate = 150 ml/min; amount of catalyst = 7 g; reaction time = 15 min

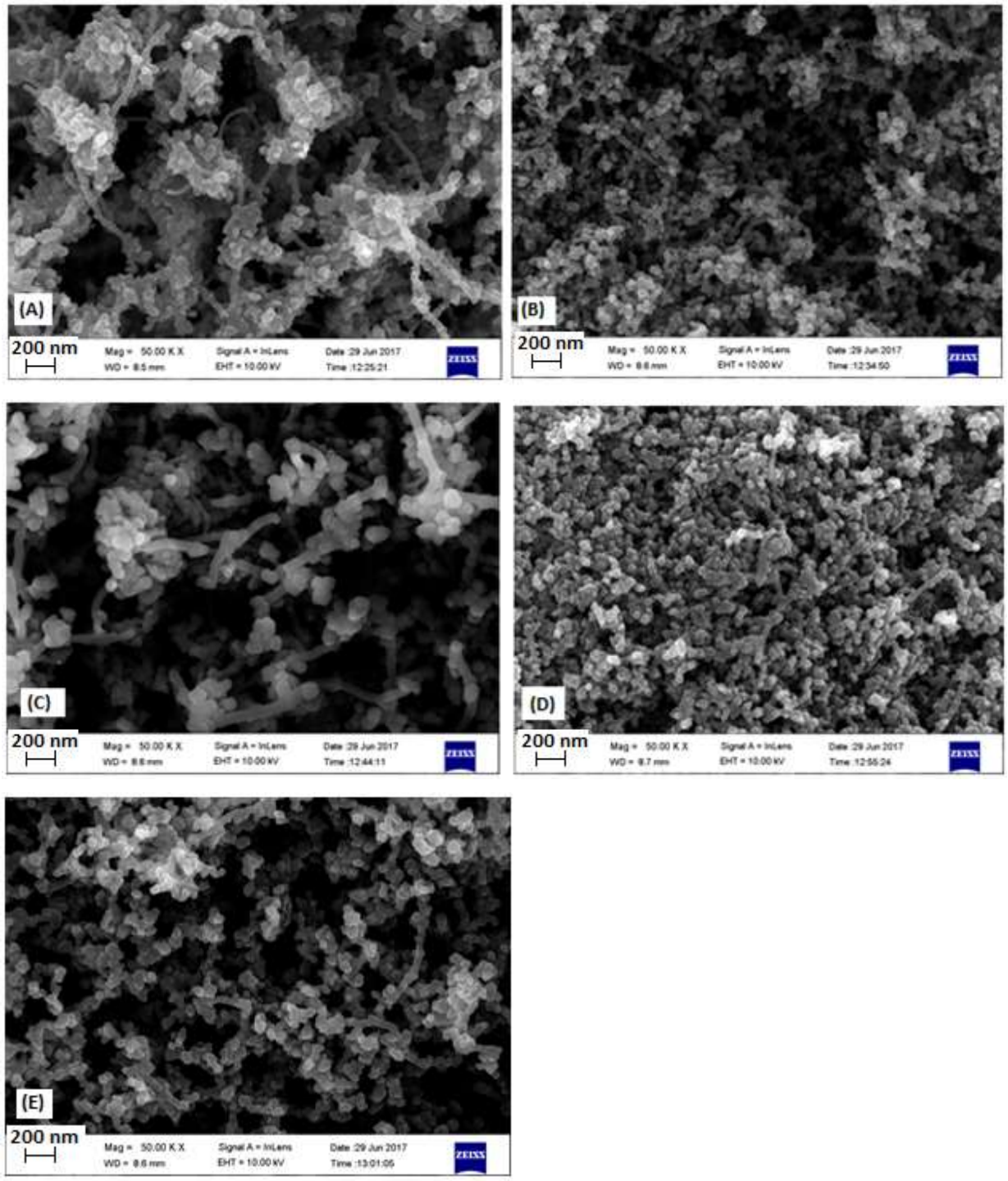

Figure 4.2: SEM micrograph of CNTs produced from acetylene as carbon source and argon/hydrogen as carrier gas (A = A-800-Ar/H, B = A-850-Ar/H, C = A-900-Ar/H, D = A-950-Ar/H, E = A-1000-Ar/H). Experimental conditions: acetylene flow rate = 150 ml/min; argon flow rate = 125 ml/min; hydrogen flow rate = 25 ml/min; amount of catalyst = 7 g; reaction time = 15 min

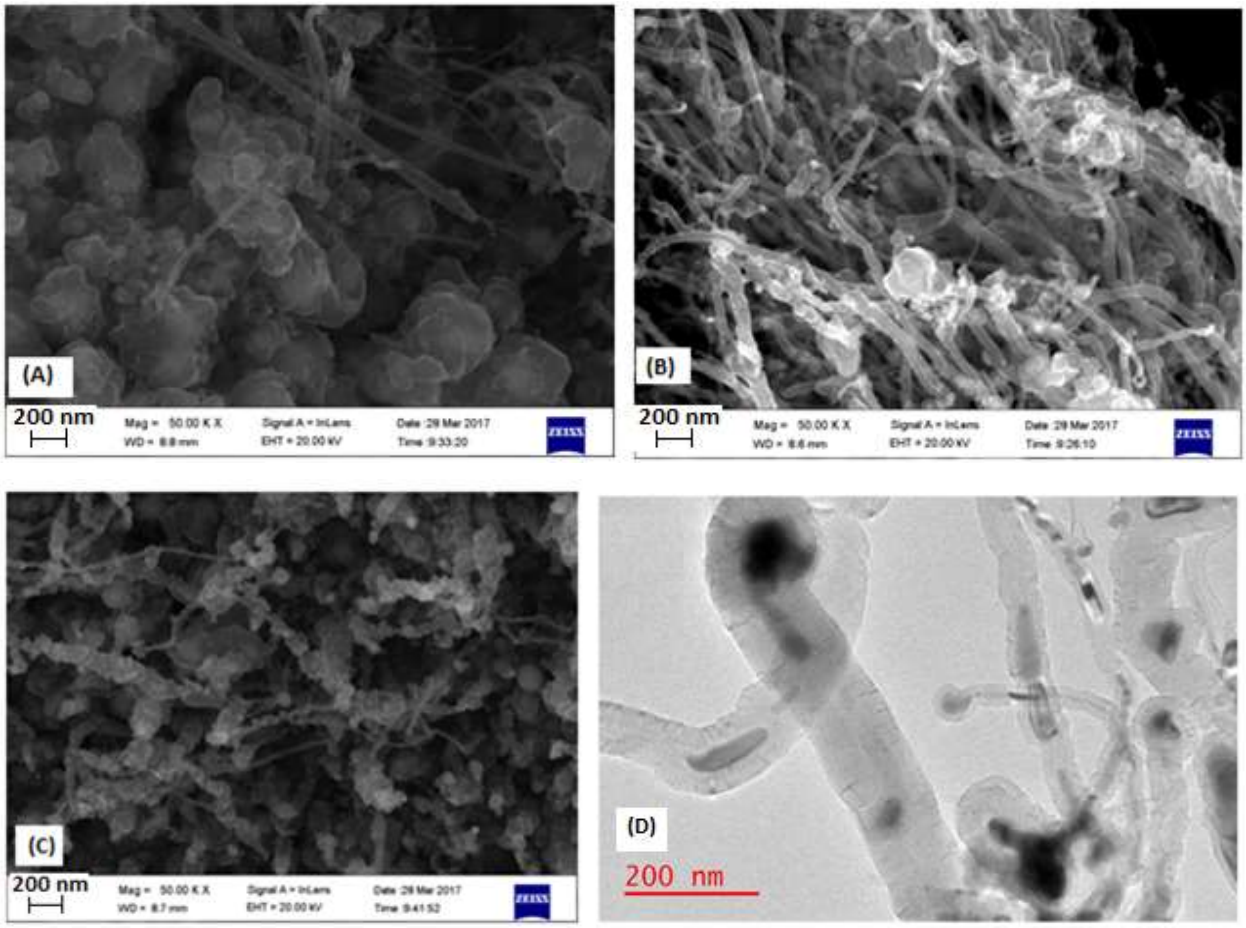

Figure 4.3: SEM micrograph of CNTs produced from methane as carbon source and argon as carrier gas: A = M-800-Ar; B = M-900-Ar; C = M-1000-Ar. D = TEM image of M-900-Ar. Experimental conditions: methane flow rate = 150 ml/min; argon flow rate = 150 ml/min; amount of catalyst = 7 g; reaction time = 15 min

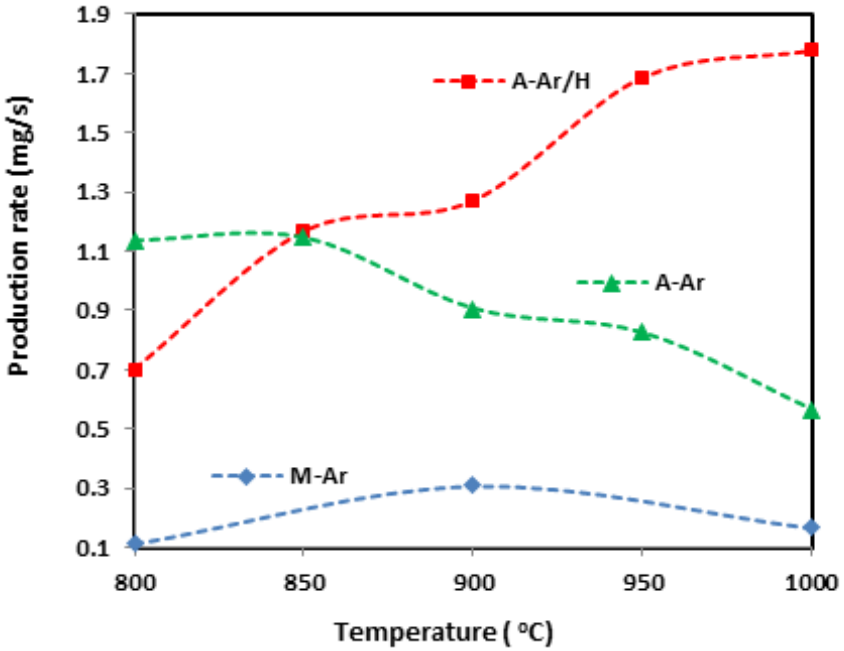

Figure 4.4: Production rate of CNTs

To further substantiate the effect of production conditions on CNTs production rate, EDS analysis was carried out on all the samples. EDS gives the elemental composition of a material. The weight percent (wt. %) of carbon in each sample is presented in Table 4.2. The results are consistent with the results obtained from EPB. Wt. % of carbon in A-Ar/H is the highest, followed by A-Ar. M-Ar shows the least wt. % of carbon. The full elemental compositions and spectra of all the as-produced CNTs are presented in Appendix A.

Table 4.2: EDS of the as-produced CNTs showing wt. % of Carbon

Sample	Wt. % of Carbon
A-800-Ar	85.34
A-850-Ar	87.03
A-900-Ar	90.51
A-950-Ar	88.32
A-1000-Ar	92.56
A-800-Ar/H	95.96
A-850-Ar/H	94.76
A-900-Ar/H	89.08
A-950-Ar/H	98.45
A-1000-Ar/H	98.94
M-800-Ar	79.39
M-900-Ar	78.43
M-1000-Ar	70.74

4.3.3 Raman spectroscopy of as-produced CNTs

Raman spectra in Figure 4.5 through Figure 4.7 show the existence of sp^2 carbon in all the samples due to peaks of high symmetry present in the spectra and this is a characteristic of CNTs (Dresselhaus et al., 2010). Three main characteristic peaks of CNTs are: (i) low-frequency peak also known as radial breathing mode (RBM) which is present in spectra range of 100-400 cm^{-1} (Toni et al., 2015). This is one of the main signatures of single-wall CNTs because it depends only on CNT diameter and can usually be detected for CNT diameter < 2 nm (Lehman et al., 2011); (ii) disorder-induced peak known as D-band which is observed around 1340 cm^{-1} (Lehman et al., 2011) and this is a measure of structural defect in CNTs (Miyata et al., 2010); (iii) G-band which is a measure of graphitization of CNTs and is present in spectra range of 1550-1600 cm^{-1} (Lehman et al., 2011). Furthermore, the ratio of the intensity of D-band to the intensity of G-band (I_D/I_G) is used as an indication of the degree of defect

in the CNTs (Wepasnick et al., 2010). The smaller the ratio is the lesser the structural defect in the CNTs (Liu et al., 2003).

The spectra depicted in Figures 4.5 – 4.7 show the presence of D-band and G-band in all the samples around the expected spectra ranges. RBM is noticed in all the samples from methane while the samples from acetylene show RBM at low temperatures. Also, the I_D/I_G ratio of samples from methane show the least CNTs sidewall defect, with M-900-Ar exhibiting the best quality. This result corroborated with SEM micrograph in Figure 4.3b. Addition of hydrogen to the carrier gas does not improve the sidewall defect in as-produced as shown in Table 4.3.

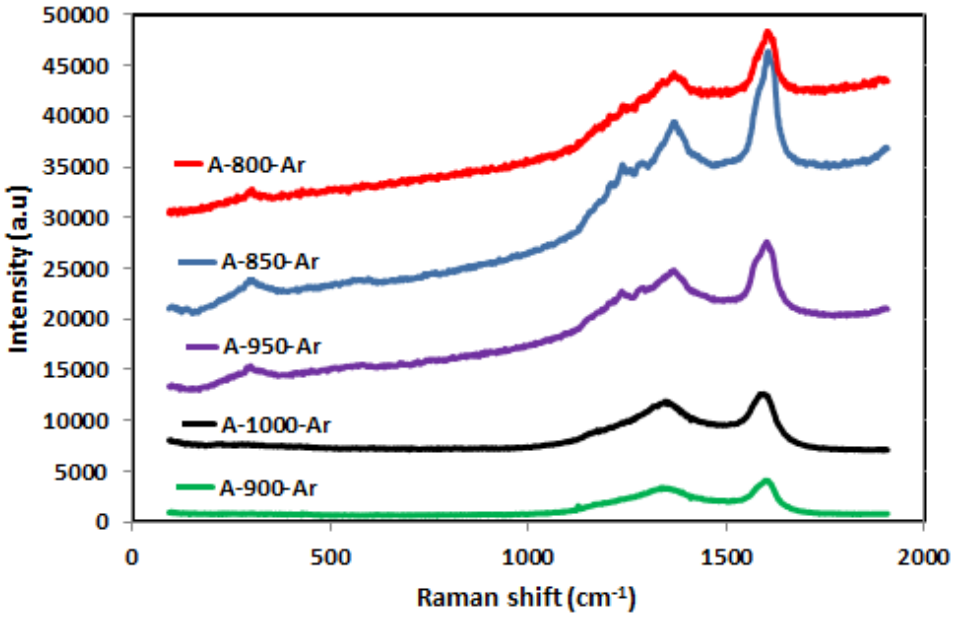

Figure 4.5: Raman spectra of CNTs produced from acetylene as carbon source and argon as carrier gas. Experimental conditions: acetylene flow rate = 150 ml/min; argon flow rate = 150 ml/min; amount of catalyst = 7 g; reaction time = 15 min

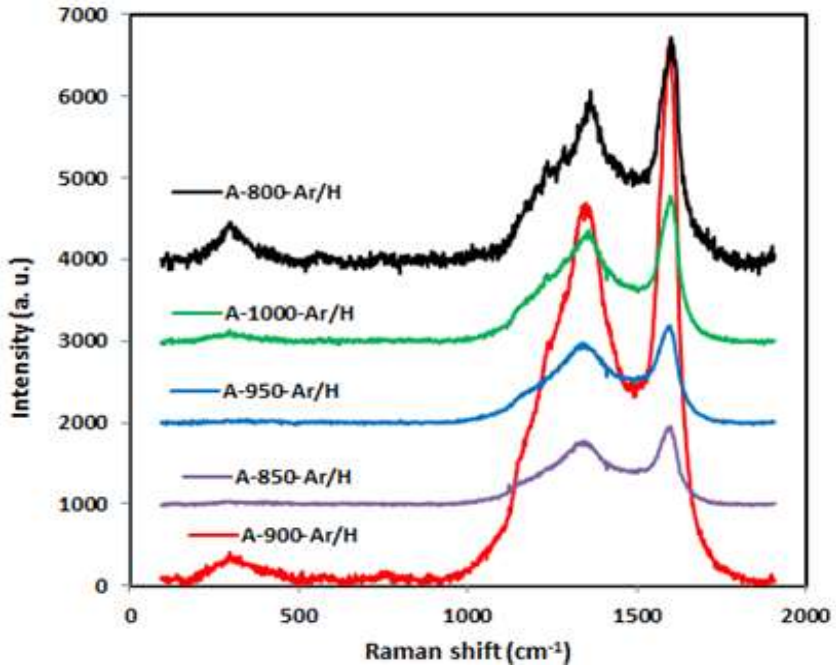

Figure 4.6: Raman spectra of CNTs produced from acetylene as carbon source and argon/hydrogen as carrier gas. Experimental conditions: acetylene flow rate = 150 ml/min; argon flow rate = 125 ml/min; hydrogen flow rate = 25 ml/min; amount of catalyst = 7 g; reaction time = 15 min

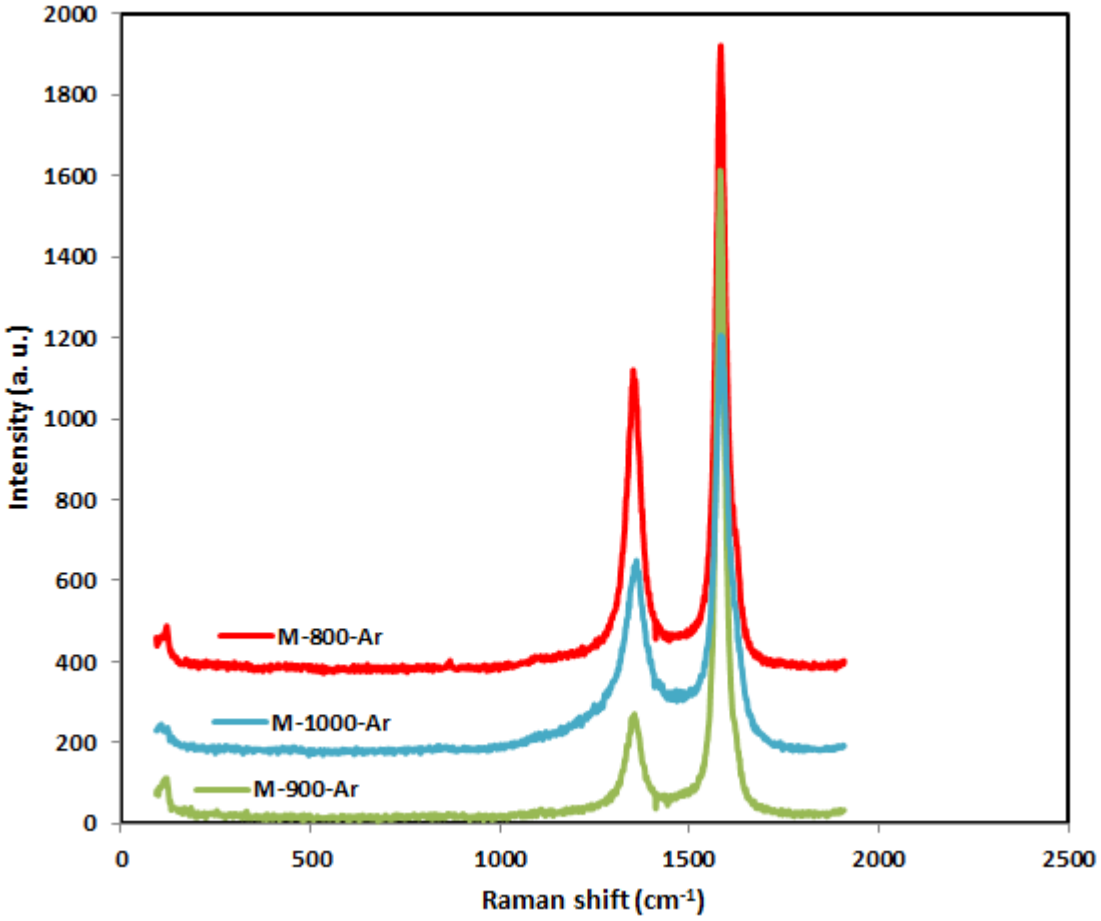

Figure 4.7: Raman spectra of CNTs produced from methane as carbon source and argon as carrier gas. Experimental conditions: methane flow rate = 150 ml/min; argon flow rate = 150 ml/min; amount of catalyst = 7 g; reaction time = 15 min

Table 4.3: Main raman signals of the produced CNTs

Sample	RBM (cm^{-1})	D-band (cm^{-1})	G-band (cm^{-1})	I_D/I_G
A-800-Ar	306	1368	1604	0.85
A-850-Ar	301	1370	1605	0.82
A-900-Ar	-	1342	1602	0.80
A-950-Ar	299	1368	1602	0.89
A-1000-Ar	-	1346	1600	0.89
A-800-Ar/H	299	1362	1600	0.90
A-850-Ar/H	-	1335	1600	0.90
A-900-Ar/H	299	1349	1600	0.71
A-950-Ar/H	-	1342	1600	0.93
A-1000-Ar/H	-	1358	1600	0.91
M-800-Ar	120	1351	1582	0.49
M-900-Ar	120	1354	1580	0.17
M-1000-Ar	122	1359	1582	0.47

4.3.4 Analysis of the degree of functionalization of CNTs

TGA and EPB were used to explore the degree of functionalization of as-produced CNTs (M-900-Ar). Figure 4.8 displays the effect of purification and functionalization on the thermal stability of the CNTs. The result shows that the onset degradation temperature of raw CNTs (RCNTs) was improved by purification. This could be attributed to the removal of amorphous carbon from the RCNTs by the purification process. A similar observation was reported by Hou et. al (2008). The percentage change in weight of purified CNTs (PCNTs) is less than that of RCNTs which confirmed an enhancement in the purity of PCNTs (Ling et al., 2013). The onset degradation temperature of functionalized CNTs (FCNTs) decreased significantly. This could be attributed to the decomposition of carboxylic chain covalently bounded to the PCNTs (Ling et al., 2013). The degree of functionalization is a measure of mass loss due to thermal degradation of functional group attached to CNTs (Salam and Burk,

2017). For FCNTs, the degree of functionalization was obtained from mass loss between the onset and endset degradation temperatures on the TGA curve as shown in Figure 4.9. A similar trend was obtained from EPB analysis and presented in Table 4.4.

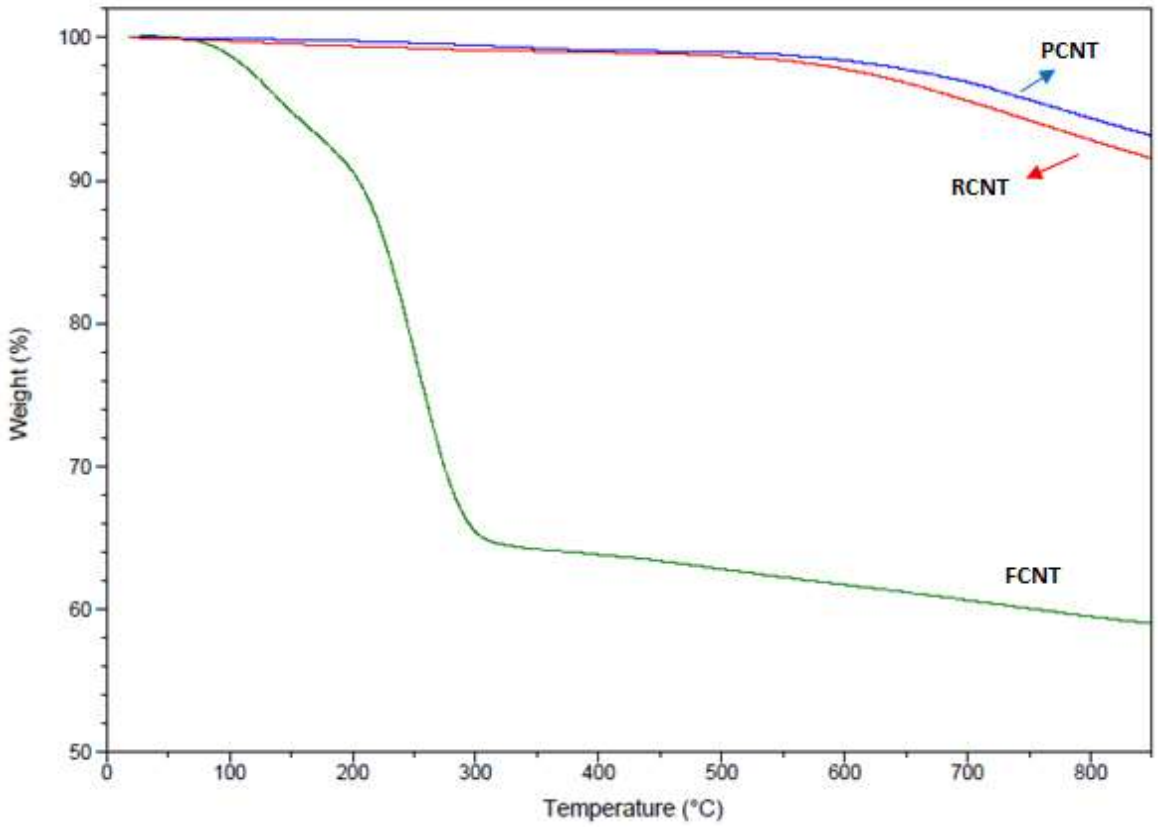

Figure 4.8: TGA quantitative analysis of raw CNTs (RCNT), purified CNTs (FCNT) and functionalized CNTs (FCNT)

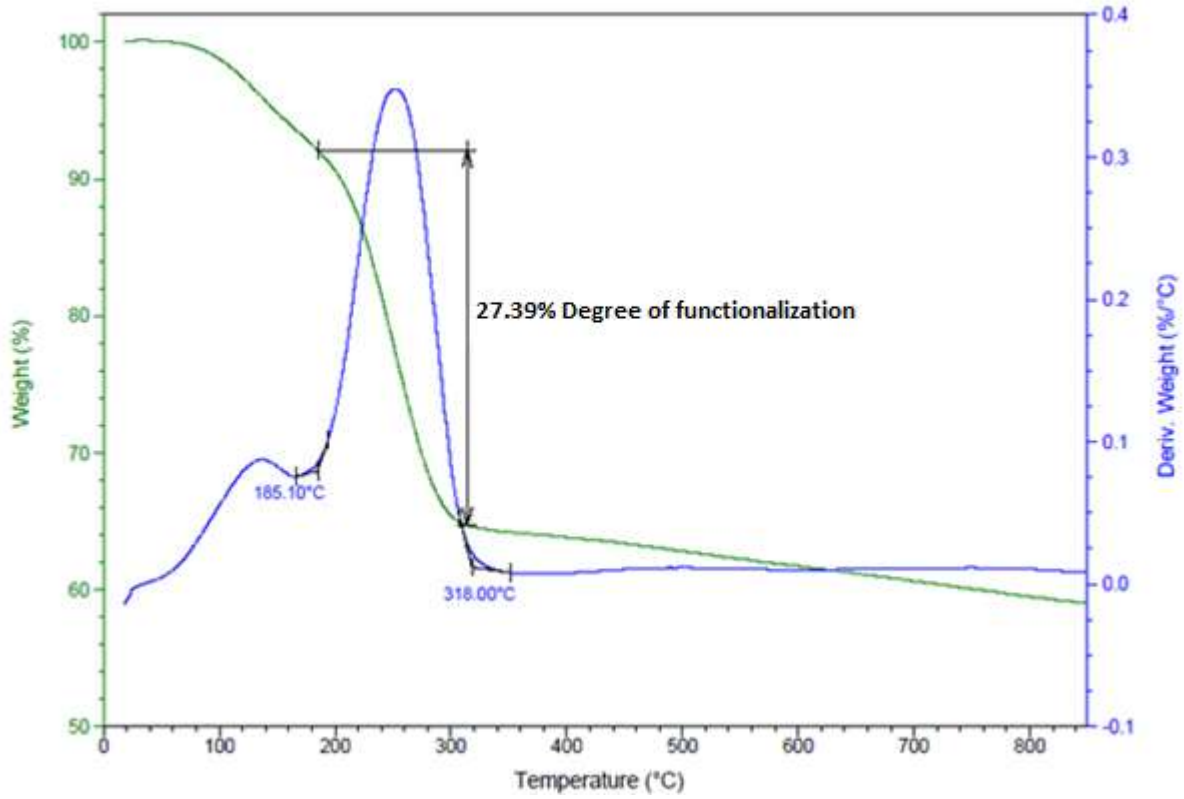

Figure 4.9: TGA quantitative analysis of degree of functionalization of FCNT

Table 4.4: Gravimetric analysis of degree of functionalization of M-900-Ar using EPB

Process	Initial weight (g)	Final weight after drying (g)	Change in weight (g)	Change in weight (%)
Purification	1.60	1.57	0.03 ▼	1.88
Functionalization	1.00	1.24	0.24 ▲	24.00

4.3.5 FTIR analysis of the functionalized CNTs

A FTIR spectrum comprises two regions: the fingerprint region with the spectrum range of 1500-400 cm^{-1} and functional group region between 4000-1500 cm^{-1} (Sahil et al., 2011). The fingerprint region comprises overlapping peaks of series of absorption due to bending vibration within a molecule (Danilczuka et al., 2011). Functional group region has distinctive peaks due to vibration of the functional group (Danilczuka et al., 2011). The FTIR spectra presented in Figure 4.10 show similar spectra for RCNTs and PCNTs. This confirms that the purification process does not add any functional group to the CNTs. The FCNT spectrum has five distinctive peaks at the functional group regions. The peak at 1614 cm^{-1} represents C=O stretch from COOH, that of 2347 cm^{-1} signifies OH stretch from H-bonded COOH, the peak at 2937 cm^{-1} represents C-H stretch and the broad peak at 3425 cm^{-1} denotes OH stretch from COOH (Titus et al., 2006). These peaks confirm successful carboxylic functionalization of CNTs. Furthermore, asymmetric and symmetric C-H vibration band at 2855 cm^{-1} and 2937 cm^{-1} are usually located at defect sites on the CNT sidewall (Ling et al., 2013).

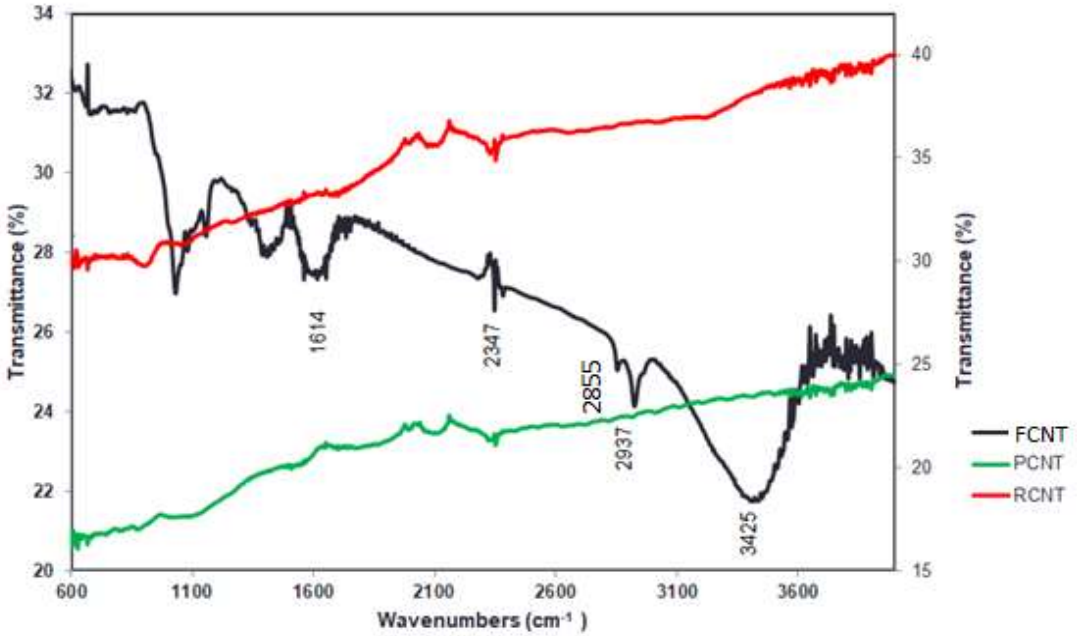

Figure 4.10: FTIR spectra of raw CNTs (RCNT), purified CNTs (PCNT) and functionalized CNTs (FCNT)

4.3.6 Effect of functionalization on the adsorption and textural properties of CNTs

Despite the shortcomings in the theoretical foundation of BET theory, it remains the most widely used method for studying the textural properties of nanoporous materials (Lehman et al., 2011; Thommes et al., 2015). According to IUPAC technical report (Thommes et al., 2015), nanoporous materials are classified, with respect to their pore sizes, as macropores (> 50 nm), mesopores (between 2 nm and 50 nm) and micropores (< 2 nm). As shown in Table 4.5, the average pore size of RCNTs, PCNTs, and FCNTs as determined by Barrett-Johner-Halenda (BJH) equation is within mesopore classification. Physisorption mechanisms in mesopore materials are monolayer-multilayer adsorption at a low relative pressure of adsorbate and pore condensation as the relative pressure of the adsorbate approaches unity (Sing, 1995). BET surface area of RCNTs, PCNTs, and FCNTs was estimated within the region of monolayer-multilayer adsorption up to a relative pressure of 0.29 (see Appendix B for detailed BET analysis). The pore volume was determined within the pore condensation region up to a relative pressure of 0.99 for all the types of CNTs.

Figure 4.11 depicts nitrogen adsorption and desorption isotherms of the CNTs at 77 K. The amount of nitrogen molecules adsorbed onto PCNTs and FCNTs within the pore condensation region is higher than that of RCNTs as shown in Figure 4.11b, indicating an increase in the porosity of PCNTs and FCNTs (Chen et al., 2006; Zaine et al., 2016). This is further supported by an increase in the pore volume and average pore size of PCNTs and FCNTs as presented in Table 4.5. From Figure 4.11a, the isotherms for all the types of CNTs showed Type IV physisorption isotherms with a characteristic H1 hysteresis as classified by IUPAC (Thommes et al., 2015). This means that most of the pores of RCNTs, PCNTs, and FCNTs are in mesopore sizes (Ziegler et al., 2005). Increase in the pore volume and the average pore size of PCNTs could be attributed to the removal of amorphous carbon and iron impurities constituting occluded materials in the inner wall of RCNTs (Li et al., 2004). Furthermore, the decrease in the surface areas of PCNTs and FCNTs with respect to RCNTs could be due to the removal of

amorphous carbon attached to CNTs after acid treatment (Salam and Burk, 2017). Increase in the pore volume and the average pore size of FCNTs as compare to PCNTs could be attributed to the etching of FCNTs sidewall by the acid, creating new pores (Salam and Burk, 2017; Wu et al., 2014).

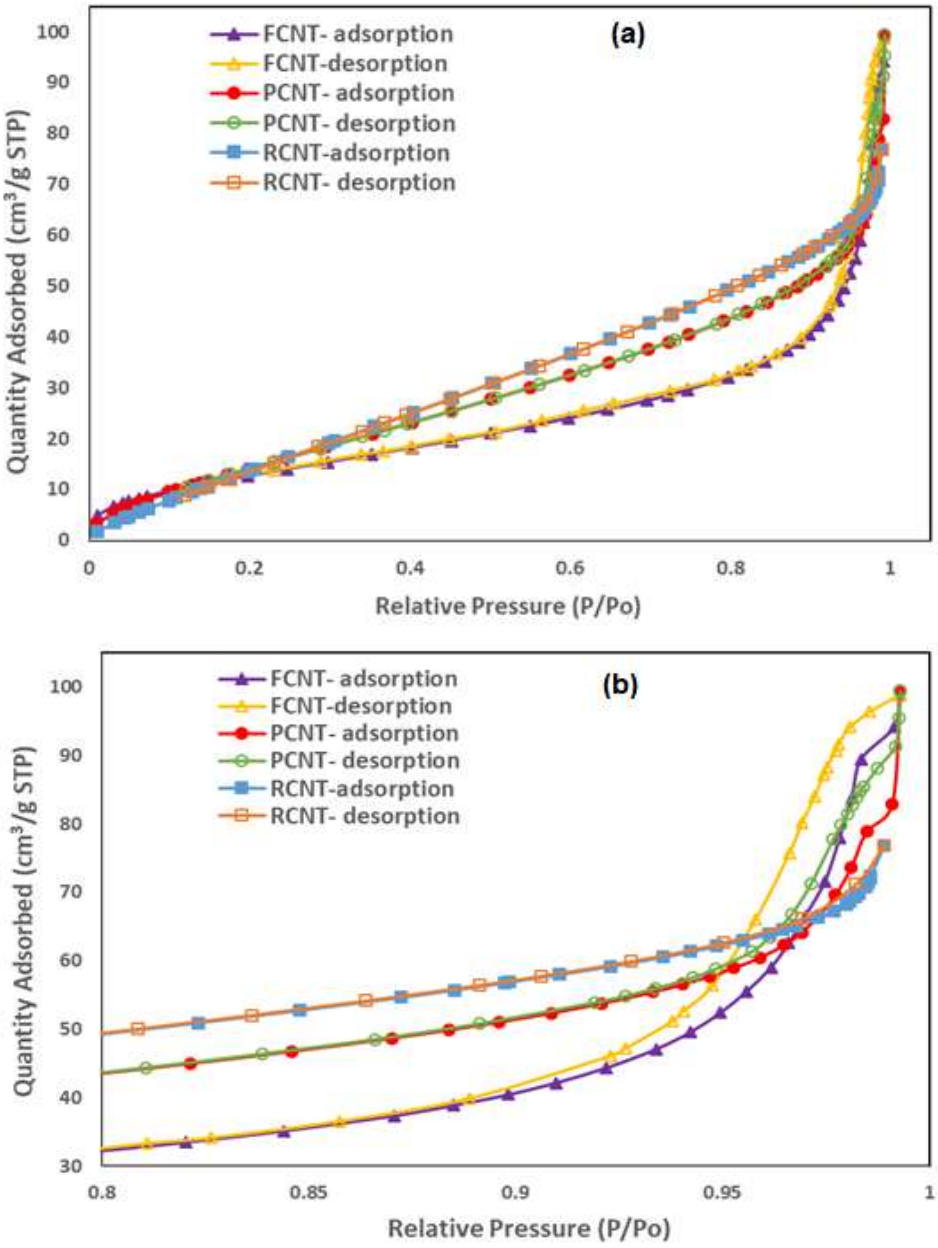

Figure 4.11: Nitrogen adsorption-desorption isotherms of raw CNT (RCNT), purified CNT (PCNT) and functionalized CNT (FCNT) at 77 K. (a) Full Isotherm (b) Expanded view of the pore condensation region

Table 4.5: Effect of functionalization on textural properties of the produced M-900-Ar

Sample	[a]Surface Area (m^2/g)	[b]Pore Volume (cm^3/g)	[b]Average pore size (nm)
Raw CNT	74.548 ± 4.077	0.107	5.504
Purified CNT	61.606 ± 2.357	0.142	7.706
Functionalized CNT	49.182 ± 0.871	0.145	10.372

a = determined using BET equation, b = determined using BJH equation

4.3.7 Effect of functionalization on the crystallinity of CNTs

Figure 4.12 shows the diffraction patterns of RCNTs, PCNTs, and FCNTs obtained using Bruker XRD D2 Phaser. Reference pattern from Diffrac.EVA software was used to obtain the Miller indices (hkl). Similar diffraction patterns were observed for RCNT and PCNT. This shows that purification of RCNT did not change its crystallographic characteristics and interatomic distances. The RCNT and PCNT diffraction patterns consist of two peaks at 2θ values of 25.6° (002 plane) and 44.0° (110 plane), corresponding to interatomic distances (d_{hkl}) of 0.348 nm and 0.206 nm, respectively.

The high-intensity peak at angle 25.6° represents the presence of graphitic particles. However, XRD is not sufficient to differentiate between pure graphite structure and other graphitic carbon like CNT (Zhu et al., 2003; Peigney et al., 1998). The low-intensity peak at angle 44.0° corresponds to α-Fe based on the match from Diffrac.EVA reference library. Mallakpou and Zacchnazari (2013) reported a similar result. This could be attributed to iron particles present in the CNT structure during synthesis with ferrocene catalyst. FCNT diffraction pattern depicts a similar number of peaks like that of RCNT and PCNT but with a slight shift in the 2θ angles. This shows that functionalization did not change the crystallographic characteristic of the CNTs but alters the interatomic distances. The high-intensity peak shifted to 2θ angle of 25.9°

which corresponds to d_{hkl} of 0.344 nm and the low-intensity peak shifted to 2θ angle of 44.6^{o} corresponding to d_{hkl} of 0.203 nm.

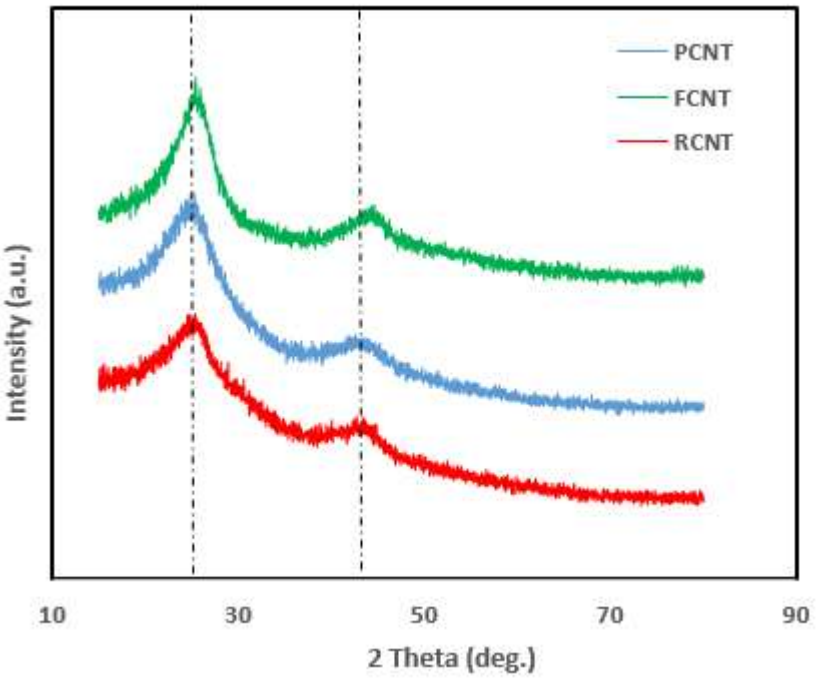

Figure 4.12: XRD patterns of raw CNT (RCNT), purified CNT (PCNT) and functionalized CNT (FCNT)

4.4 Concluding remarks

This work demonstrates the impacts of the type of carbon source and production conditions on the quantity and quality of CNTs produced by CCVD method. It also establishes the effect of hydrogen in reducing the deactivation of the catalyst active site during the production of CNTs. The SEM micrographs of CNTs produced from the mixture of acetylene and argon show the presence of more carbon nanoballs than CNTs. This is attributed to the deactivation of catalyst active site owing to the high reactivity of acetylene forming carbon nanoshells that reduce the activity of the catalyst. Addition of hydrogen to the carrier gas facilitated the production of CNTs present in the sample as well as the CNT yield. However, the presence of carbon nanoballs is minimal in the samples produced from the mixture of methane and argon

without the addition of hydrogen. This is because methane is less reactive than acetylene and the stoichiometric ratio of hydrogen during decomposition of methane is twice that of acetylene. The highest production rate was achieved with a mixture of acetylene, argon, and hydrogen at 1000 ^{o}C while the mixture of methane and argon at 900 ^{o}C gives the best quality.

FTIR spectra of FCNTs show the presence OH, C-H, and C=O groups at wavenumbers of 3425 cm^{-1}, 2937 $cm^{-1,}$ and 2347 cm^{-1}, respectively. This confirms the successful functionalization of as-produced CNTs. Nitrogen physisorption isotherm for RCNTs, PCNTs, and FCNTs show an increase in the quantity of nitrogen adsorbed by FCNTs which indicates that functionalization improves the adsorption sites of CNTs. Furthermore, BET analysis of the textural properties showed an increase in pore volume and average pore size of FCNTs as compared to PCNTs and RCNTs. These characteristics could enhance the transport properties of FCNT reinforced polymeric membranes when compared to that of non-reinforced polymeric membranes. The XRD patterns reveal that purification and functionalization of RCNT preserve its crystallographic characteristics. Purification did not alter the interatomic distances of the RCNT, but functionalization altered them.

References

Ando, Y. and Zhao, X., 2006. Synthesis of carbon nanotubes by arc-discharge method. *New Diamond and Frontier Carbon Technology*, 16(3), pp.123-138.

Aroon, M.A., Ismail, A.F., Montazer-Rahmati, M.M. and Matsuura, T., 2010. Morphology and permeation properties of polysulfone membranes for gas separation: Effects of non-solvent additives and co-solvent. *Separation and Purification Technology*, 72(2), pp.194-202.

Bahome, M.C., Jewell, L.L., Hildebrandt, D., Glasser, D. and Coville, N.J., 2005. Fischer–Tropsch synthesis over iron catalysts supported on carbon nanotubes. *Applied Catalysis A: General*, 287(1), pp.60-67.

Balasubramanian, K. and Burghard, M., 2005. Chemically functionalized carbon nanotubes. *Small*, 1(2), pp.180-192.

Bastani, D., Esmaeili, N. and Asadollahi, M., 2013. Polymeric mixed matrix membranes containing zeolites as a filler for gas separation applications: A review. *Journal of Industrial and Engineering Chemistry*, 19(2), pp.375-393.

Chen, L., Xie, H., Li, Y. and Yu, W., 2008. Surface chemical modification of multiwalled carbon nanotubes by a wet-mechanochemical reaction. *Journal of Nanomaterials*, 2008, p.63.

Chen, Y., Liu, C., Li, F. and Cheng, H.M., 2006. Pore structures of multi-walled carbon nanotubes activated by air, CO 2 and KOH. *Journal of Porous Materials*, 13(2), pp.141-146.

Chrzanowska, J., Hoffman, J., Małolepszy, A., Mazurkiewicz, M., Kowalewski, T.A., Szymanski, Z. and Stobinski, L., 2015. Synthesis of carbon nanotubes by the laser ablation method: Effect of laser wavelength. P*hysica Status Solidi (b)*, 252(8), pp.1860-1867.

Corry, B., 2011. Water and ion transport through functionalised carbon nanotubes: implications for desalination technology. *Energy & Environmental Science*, 4(3), pp.751-759.

Danilczuk, M., Lin, L., Schlick, S., Hamrock, S.J. and Schaberg, M.S., 2011. Understanding the fingerprint region in the infra-red spectra of perfluorinated ionomer membranes and corresponding model compounds: Experiments and theoretical calculations. *Journal of Power Sources*, 196(20), pp.8216-8224.

Deng, L. and Hägg, M.B., 2014. Carbon nanotube reinforced PVAm/PVA blend FSC nanocomposite membrane for CO2/CH4 separation. *International Journal of Greenhouse Gas Control*, 26, pp.127-134.

Dresselhaus, M.S., Jorio, A., Souza Filho, A.G. and Saito, R., 2010. Defect characterization in graphene and carbon nanotubes using Raman spectroscopy. *Philosophical Transactions of the Royal Society A: Mathematical, Physical and Engineering Sciences*, 368(1932), pp.5355-5377.

Du, J., Bai, J. and Cheng, H., 2007. The present status and key problems of carbon nanotube based polymer composites. *Express Polymer Letters*, *1*(5), pp.253-273.

Duong, H.M., Einarsson, E., Okawa, J., Xiang, R. and Maruyama, S., 2008. Thermal degradation of single-walled carbon nanotubes. *Japanese Journal of Applied Physics*, 47(4R), p.1994.

Eguchi, H., Kim, D.J. and Koros, W.J., 2015. Chemically cross-linkable polyimide membranes for improved transport plasticization resistance for natural gas separation. *Polymer*, 58, pp.121-129.

Gomez-Ballesteros, J.L., Burgos, J.C., Lin, P.A., Sharma, R. and Balbuena, P.B., 2015. Nanocatalyst shape and composition during nucleation of single-walled carbon nanotubes. *RSC Advances*, 5(129), pp.106377-106386.

Grissom, G., Jaksik, J., McEntee, M., Durke, E.M., Aishee, S.T., Cua, M., Okoli, O., Touhami, A., Moore, H.J. and Uddin, M.J., 2018. Three-dimensional carbon nanotube yarn based solid state solar cells with multiple sensitizers exhibit high energy conversion efficiency. *Solar Energy*, 171, pp.16-22.

Hao, J., Pan, L., Zhang, H., Chi, C., Guo, Q., Zhao, J., Yang, Y., Liu, X., Ma, X. and Li, Y., 2018. A general method for high-performance Li-ion battery Ge composites electrodes from ionic liquid electrodeposition without binders or conductive agents: The cases of CNTs, RGO and PEDOT. *Chemical Engineering Journal*, 346, pp.427-437.

Hou, P.X., Liu, C. and Cheng, H.M., 2008. Purification of carbon nanotubes. *Carbon*, 46(15), pp.2003-2025.

Ismail, A.F., Goh, P.S., Sanip, S.M. and Aziz, M., 2009. Transport and separation properties of carbon nanotube-mixed matrix membrane. *Separation and Purification Technology*, 70(1), pp.12-26.

Ismail, A.F., Rahim, N.H., Mustafa, A., Matsuura, T., Ng, B.C., Abdullah, S. and Hashemifard, S.A., 2011. Gas separation performance of polyethersulfone/multi-walled carbon nanotubes mixed matrix membranes. *Separation and Purification Technology*, *80*(1), pp.20-31.

Ismail, A.F., Rahim, N.H., Mustafa, A., Matsuura, T., Ng, B.C., Abdullah, S. and Hashemifard, S.A., 2011. Gas separation performance of polyethersulfone/multi-walled carbon nanotubes mixed matrix membranes. *Separation and Purification Technology*, 80(1), pp.20-31.

Iyuke, S.E. and Simate, G.S., 2011. Synthesis of carbon nanomaterials in a swirled floating catalytic chemical vapour deposition reactor for continuous and large scale production. In Carbon Nanotubes-Growth and Applications. InTech.

Iyuke, S.E., Mamvura, T.A., Liu, K., Sibanda, V., Meyyappan, M. and Varadan, V.K., 2009. Process synthesis and optimization for the production of carbon nanostructures. *Nanotechnology*, 20(37), p.375602.

Jia, X., Zhang, Q., Zhao, M.Q., Xu, G.H., Huang, J.Q., Qian, W., Lu, Y. and Wei, F., 2012. Dramatic enhancements in toughness of polyimide nanocomposite via long-CNT-induced long-range creep. *Journal of Materials Chemistry*, 22(14), pp.7050-7056.

Jin, Z.H., Liu, Y.L., Chen, J.J., Cai, S.L., Xu, J.Q. and Huang, W.H., 2017. Conductive polymer-coated carbon nanotubes to construct stretchable and transparent electrochemical sensors. *Analytical Chemistry*, 89(3), pp.2032-2038.

Kazemi, Y., Kakroodi, A.R., Ameli, A., Filleter, T. and Park, C.B., 2018. Highly stretchable conductive thermoplastic vulcanizate/carbon nanotube nanocomposites with segregated structure, low percolation threshold and improved cyclic electromechanical performance. *Journal of Materials Chemistry C*, 6(2), pp.350-359.

Kuwana, K., Endo, H., Saito, K., Qian, D., Andrews, R. and Grulke, E.A., 2005. Catalyst deactivation in CVD synthesis of carbon nanotubes. *Carbon*, 43(2), pp.253-260.

Lehman, J.H., Terrones, M., Mansfield, E., Hurst, K.E. and Meunier, V., 2011. Evaluating the characteristics of multiwall carbon nanotubes. *Carbon*, 49(8), pp.2581-2602.

Lekawa-Raus, A., Patmore, J., Kurzepa, L., Bulmer, J. and Koziol, K., 2014. Electrical properties of carbon nanotube based fibers and their future use in electrical wiring. *Advanced Functional Materials*, 24(24), pp.3661-3682.

Li, F., Wang, Y., Wang, D. and Wei, F., 2004. Characterization of single-wall carbon nanotubes by N2 adsorption. *Carbon*, 42(12-13), pp.2375-2383.

Li, Y., Zhou, B., Zheng, G., Liu, X., Li, T., Yan, C., Cheng, C., Dai, K., Liu, C., Shen, C. and Guo, Z., 2018. Continuously prepared highly conductive and stretchable SWNT/MWNT synergistically composited electrospun thermoplastic polyurethane yarns for wearable sensing. *Journal of Materials Chemistry C*, 6(9), pp.2258-2269.

Ling, X., Wei, Y., Zou, L. and Xu, S., 2013. The effect of different order of purification treatments on the purity of multiwalled carbon nanotubes. *Applied Surface Science*, 276, pp.159-166.

Liu, B.C., Lyu, S.C., Jung, S.I., Kang, H.K., Yang, C.W., Park, J.W., Park, C.Y. and Lee, C.J., 2004. Single-walled carbon nanotubes produced by catalytic chemical vapor deposition of acetylene over Fe–Mo/MgO catalyst. *Chemical Physics Letters*, 383(1-2), pp.104-108.

Liu, B.C., Lyu, S.C., Lee, T.J., Choi, S.K., Eum, S.J., Yang, C.W., Park, C.Y. and Lee, C.J., 2003. Synthesis of single-and double-walled carbon nanotubes by catalytic decomposition of methane. *Chemical Physics Letters*, 373(5-6), pp.475-479.

Ma, P.C., Siddiqui, N.A., Marom, G. and Kim, J.K., 2010. Dispersion and functionalization of carbon nanotubes for polymer-based nanocomposites: a review. *Composites Part A: Applied Science and Manufacturing*, *41*(10), pp.1345-1367.

Mallakpour, S. and Zadehnazari, A., 2013. Functionalization of multiwalled carbon nanotubes with S-valine amino acid and its reinforcement on amino acid-containing poly (amide-imide) bionanocomposites. *High Performance Polymers*, 25(8), pp.966-979.

Meyyappan, M., 2004. *Growth: CVD and PECVD*. In Carbon Nanotubes (pp. 137-159). CRC press.

Miyata, Y., Mizuno, K. and Kataura, H., 2011. Purity and defect characterization of single-wall carbon nanotubes using Raman spectroscopy. *Journal of Nanomaterials*, 2011, p.18.

Ning, G., Wei, F., Luo, G. and Jin, Y., 2005. Online BET analysis of single-wall carbon nanotube growth and its effect on catalyst reactivation. *Carbon*, 43(7), pp.1439-1444.

Peigney, A., Laurent, C., Dumortier, O. and Rousset, A., 1998. Carbon nanotubes–Fe–alumina nanocomposites. Part I: influence of the Fe content on the synthesis of powders. *Journal of the European Ceramic Society*, 18(14), pp.1995-2004.

Peponi, L., Tercjak, A., Martin, L., Mondragon, I. and Kenny, J.M., 2011. Morphology-properties relationship on nanocomposite films based on poly (styrene-block-diene-block-styrene) copolymers and silver nanoparticles. *Express Polymer Letters*, 5(2), pp.104-118.

Rafique, M.M.A. and Iqbal, J., 2011. Production of carbon nanotubes by different routes-a review. *Journal of Encapsulation and Adsorption Sciences*, 1(02), p.29.

Sahil, K., Prashant, B., Akanksha, M. Premjeet, S. and Devashish, R. 2011. Gas chromatography-mass spectrometry: applications. *International Journal of Pharmaceutical & Biological Archive.* 2(6): 1544–1560

Salam, M.A. and Burk, R., 2017. Synthesis and characterization of multi-walled carbon nanotubes modified with octadecylamine and polyethylene glycol. *Arabian Journal of Chemistry*, 10, pp.S921-S927.

Sanip, S.M., Ismail, A.F., Goh, P.S., Soga, T., Tanemura, M. and Yasuhiko, H., 2011. Gas separation properties of functionalized carbon nanotubes mixed matrix membranes. *Separation and Purification Technology*, *78*(2), pp.208-213.

Sharma, R., Sharma, A.K. and Sharma, V., 2015. Synthesis of carbon nanotubes by arc-discharge and chemical vapor deposition method with analysis of its morphology, dispersion and functionalization characteristics. *Cogent Engineering*, 2(1), p.1094017.

Sing, K.S., 1995. Physisorption of nitrogen by porous materials. *Journal of Porous Materials*, 2(1), pp.5-8.

Sivakumar, V.M., Mohamed, A.R., Abdullah, A.Z. and Chai, S.P., 2010. Role of reaction and factors of carbon nanotubes growth in chemical Vapour decomposition process using methane: a highlight. *Journal of Nanomaterials*, 2010, p.11.

Skoulidas, A.I., Ackerman, D.M., Johnson, J.K. and Sholl, D.S., 2002. Rapid transport of gases in carbon nanotubes. *Physical Review Letters*, 89(18), p.185901.

Sokhan, V.P., Nicholson, D. and Quirke, N., 2004. Transport properties of nitrogen in single walled carbon nanotubes. *The Journal of Chemical Physics*, 120(8), pp.3855-3863.

Soneda, Y., Duclaux, L. and Béguin, F., 2002. Synthesis of high quality multi-walled carbon nanotubes from the decomposition of acetylene on iron-group metal catalysts supported on MgO. *Carbon*, 6(40), pp.965-969.

Thommes, M., Kaneko, K., Neimark, A.V., Olivier, J.P., Rodriguez-Reinoso, F., Rouquerol, J. and Sing, K.S., 2015. Physisorption of gases, with special reference to the evaluation of surface area and pore size distribution (IUPAC Technical Report). *Pure and Applied Chemistry*, 87(9-10), pp.1051-1069.

Titus, E., Ali, N., Cabral, G., Gracio, J., Babu, P.R. and Jackson, M.J., 2006. Chemically functionalized carbon nanotubes and their characterization using thermogravimetric analysis, fourier transform infrared, and raman

spectroscopy. *Journal of Materials Engineering and Performance*, 15(2), pp.182-186.

Toni, F., Xing, H., Walter, J., Strauß, V., Nacken, T.J., Damm, C., Wirth, K.E., Guldi, D. and Peukert, W., 2015. Production of well dispersible single walled carbon nanotubes via a "floating catalyst"-method. *Chemical Engineering Science*, 138, pp.385-395.

Tran, C.D., Humphries, W., Smith, S.M., Huynh, C. and Lucas, S., 2009. Improving the tensile strength of carbon nanotube spun yarns using a modified spinning process. *Carbon*, 47(11), pp.2662-2670.

Wepasnick, K.A., Smith, B.A., Bitter, J.L. and Fairbrother, D.H., 2010. Chemical and structural characterization of carbon nanotube surfaces. *Analytical and Bioanalytical Chemistry*, 396(3), pp.1003-1014.

Wu, H., Li, X., Li, Y., Wang, S., Guo, R., Jiang, Z., Wu, C., Xin, Q. and Lu, X., 2014. Facilitated transport mixed matrix membranes incorporated with amine functionalized MCM-41 for enhanced gas separation properties. *Journal of Membrane Science*, 465, pp.78-90.

Yah, C.S., Simate, G.S., Moothi, K., Maphutha, K.S. and Iyuke, S.E., 2011. Synthesis of large carbon nanotubes from ferrocene: the chemical vapour deposition technique. *Trends in Applied Sciences Research*, 6(11), pp.1270-1279.

Zaine, I.S., Fahdil, S., Napiah, N.A., Yusof, A.M., Alias, A.N., Ali, A.M. and Khalid, S.H., 2016. Preliminary analysis on pore structure of modified multi-walled carbon nanotubes. *International Journal of Control Theory and Applications*, 9(6), pp.2949-2955.

Zhang, S., Yue, L., Wang, M., Feng, Y., Li, Z. and Mi, J., 2018. SnO 2 nanoparticles confined by N-doped and CNTs-modified carbon fibers as superior anode material for sodium-ion battery. *Solid State Ionics*, 323, pp.105-111.

Zhu, W.Z., Miser, D.E., Chan, W.G. and Hajaligol, M.R., 2003. Characterization of multiwalled carbon nanotubes prepared by carbon arc cathode deposit. *Materials Chemistry and Physics*, 82(3), pp.638-647.

Ziegler, K.J., Gu, Z., Shaver, J., Chen, Z., Flor, E.L., Schmidt, D.J., Chan, C., Hauge, R.H. and Smalley, R.E., 2005. Cutting single-walled carbon nanotubes. *Nanotechnology*, 16(7), p.S539.

CHAPTER 5

5 SYNTHESIS AND PERFORMANCE EVALUATION OF FUNCTIONALIZED CARBON NANOTUBE REINFORCED POLYSULFONE MEMBRANES FOR CO_2/CH_4 SEPARATION

5.1 Introduction

Several advanced classes of polymeric membranes have been reported in the literature for the enhancement of productivity and separation efficiency of conventional polymeric membranes. The classes include mixed matrix membranes (Rezakazemi, et. al., 2014; Wang et. al., 2017, Liu, et. al., 2018), membranes of polymers of intrinsic microporosity (Swaidan, et. al., 2015; Hart and Colina, 2014) and thermally rearranged polymer membranes (Li, et. al., 2013; Liu, et. al., 2016; Comesaña-Gándara, et. al., 2015). Mixed matrix membrane (MMM) has attracted more research attention than other classes of advanced polymeric membrane owing to its processability and reproducibility (Aroon et. al., 2010). MMMs consist of inorganic particles dispersed into polymer matrices in order to alter the structure of the matrices thereby improving permeability, selectivity, mechanical and thermal properties of the polymeric membranes (Vinoba, et. al., 2017). CNT has outstanding mechanical and thermal properties owing to the presence of strong Van der Waal force between carbon-carbon (C-C) atoms of its graphite layers (Du et. al., 2007; Ismail et. al., 2011). Furthermore, simulation studies of gas transport through CNTs have shown that CNTs have exception gas permeability and selectivity when compared to other inorganic particles of similar pore sizes due to the inherent smoothness of CNTs (Skoulidas et. al., 2002; Sokhan et. al., 2004; Ismail et. al., 2009).

Hence, incorporation of CNTs into polymer matrices to form a MMM has been reported to improve the productivity and separation efficiency of the conventional polymeric membrane (Cong et al., 2007). However, the transfer of outstanding mechanical, thermal and transport properties of CNTs into polymer matrices is greatly dependent on the effective dispersion of the CNT into the polymer matrix. The presence

of strong Van der Waal force between C-C atoms of CNT causes inadequate dispersion of CNTs into the polymer matrices due to aggregation of CNTs. Functionalization of CNTs has been proposed as a solution to this problem (Chen et. al., 2008). The addition of functionalized carbon nanotubes (FCNTs) into polymers appears to offer a unique solution to the deficiencies of conventional polymeric membrane systems (Deng and Hägg, 2014). Chemical functionalization of CNTs reduces the strong Van der Waal force of attraction between CNTs and enhances separation of CNT bundles into individual CNT thereby improving CNT-polymer matrix interface interaction (Balasubramanian and Burghard, 2005).

In this study, polysulfone (PSF) was used as the base polymer because of its low cost, mechanical strength, good transport properties (Scholes et. al. 2010), and ease of synthesis with reproductive properties (Shah and Murthy, 2013). The aim of the study was to enhance physicochemical properties and CO_2 permeability of PSF without sacrificing separation factor of CO_2/CH_4, by the addition of FCNTs to PSF. The working theory is that introduction of the carboxyl group to the walls of the CNTs will enhance the dispersion of CNTs into PSF matrices and perhaps give sorption competitive advantage to CO_2 over CH_4 during mixed gas separation.

5.2 Experimental

5.2.1 Materials

Polysulfone pellets (transparent, average M_w ~ 35 000), dichloromethane (purity ≥ 99.8%), ferrocene (purity: 98%), hydrochloric (37 wt. %), sulfuric (98 wt. %) and nitric (70 wt. %) acids were purchased from Sigma Aldrich, South Africa. Nitrogen (purity: 99.999%), argon (purity: 99.999%), and methane (purity: 99.95%) gases were purchased from Afrox, South Africa. All the materials were used as supplied without any further purification.

5.2.2 Membrane synthesis and characterization

Dense flat sheet pure and mixed matrix membranes were synthesized by solvent evaporation. For pristine PSF membrane preparation, 1 g of polysulfone (PSF) pellets were added to 10 ml dichloromethane (DCM) and stirred using magnetic stirrer until a homogeneous solution was formed. With respect to FCNT/PSF membrane preparation, wt. % FCNT loading was calculated using Equation (5.1). Desired wt. % of FCNTs were added to 5 ml of DCM and ultrasonicated for 30 min in a cold water bath to control CNT agglomeration temperature. 1 g of PSF pellets were added to 5 ml of DCM and stirred to form a homogeneous solution. PSF solution was transferred to FCNT solution and stirred for 12 h. Detailed casting and solvent evaporation steps are stated in chapter 3, section 3.4.

$$FCNT\ loading\ (wt.\%) = \frac{mass\ of\ FCNT}{mass\ of\ FCNT + mass\ of\ PSF} \times 100 \quad (5.1)$$

Physicochemical properties of the synthesized membranes were checked using field emission scanning electron microscopy (FESEM), thermogravimetric analysis (TGA), differential scanning calorimetry (DSC), atomic force microscopy (AFM) and texture analysis (TA). Permeation measurement of pure CO_2 and CH_4 was carried out using a custom-built permeation set up via constant volume variable pressure (CVVP) technique. The mixed CO_2/CH_4 permeability was measured on a constant pressure variable volume (CPVV) gas permeation apparatus. Elaborated explanations of characterization and permeability determination are contained in chapter 3, sections 3.5 and 3.6.

5.3 Results and discussion

5.3.1 Membrane morphology

The morphology of a membrane influences the gas transport mechanism through the membrane (George and Thomas, 2001). Figures 5.1 and 5.2 show the FESEM surface and cross-sectional morphologies of synthesized membranes, respectively. From the figures, the PSF membrane has a smooth, homogeneous and dense structure with non-continuous pores. The MMMs also have a dense structure with non-continuous pores. Hence, the gas transport through the membranes is expected to be governed by a solution-diffusion mechanism (Kanehashi and Nagai, 2005). The surface morphology of the MMMs shows that the FCNTs were well dispersed into the polymer matrices up until 1.0 wt. % loading. However, at 1.5 wt. % loading, agglomeration of FCNTs become evident. A probe into the pores of 1.5 wt.% loading of FCNT-PSF at higher magnification (HM) of 50,000x shows the agglomeration of FCNTs as depicted in Figure 5.2 (HM 1.5 wt.% FCNT-PSF).

5.3.2 Surface topology

The AFM images depicting the surface topography of the synthesized membranes are shown in Figure 5.3. From the height images (2D and 3D), some bright and dark regions can be observed which are ascribed to the peaks and valleys (or pores) of the surface of membranes, respectively (Prokopowicz, 2016). Furthermore, the amplitude and height images of 0.2 wt. % FCNT-PSF show that FCNTs were well dispersed into the polymer matrices with no visible particles. However, 1.5 wt. % FCNT-PSF images show evidence of FCNT agglomeration. This is similar to the FESEM micrographs depicted in Figures 5.1 and 5.2. The pores of pure PSF appears to be reduced with the addition of FCNTs.

Depth-at-max of height images (2D) of the synthesized membranes were analyzed to determine if the pores are continuous and the influence of FCNTs on the pore depth. The result is presented in Table 5.1. From the result, the depth-at-max of the

membranes are far smaller than the thickness of the membranes (60 µm – 90 µm). Hence, the pores are non-continuous. This further corroborates the results from FESEM

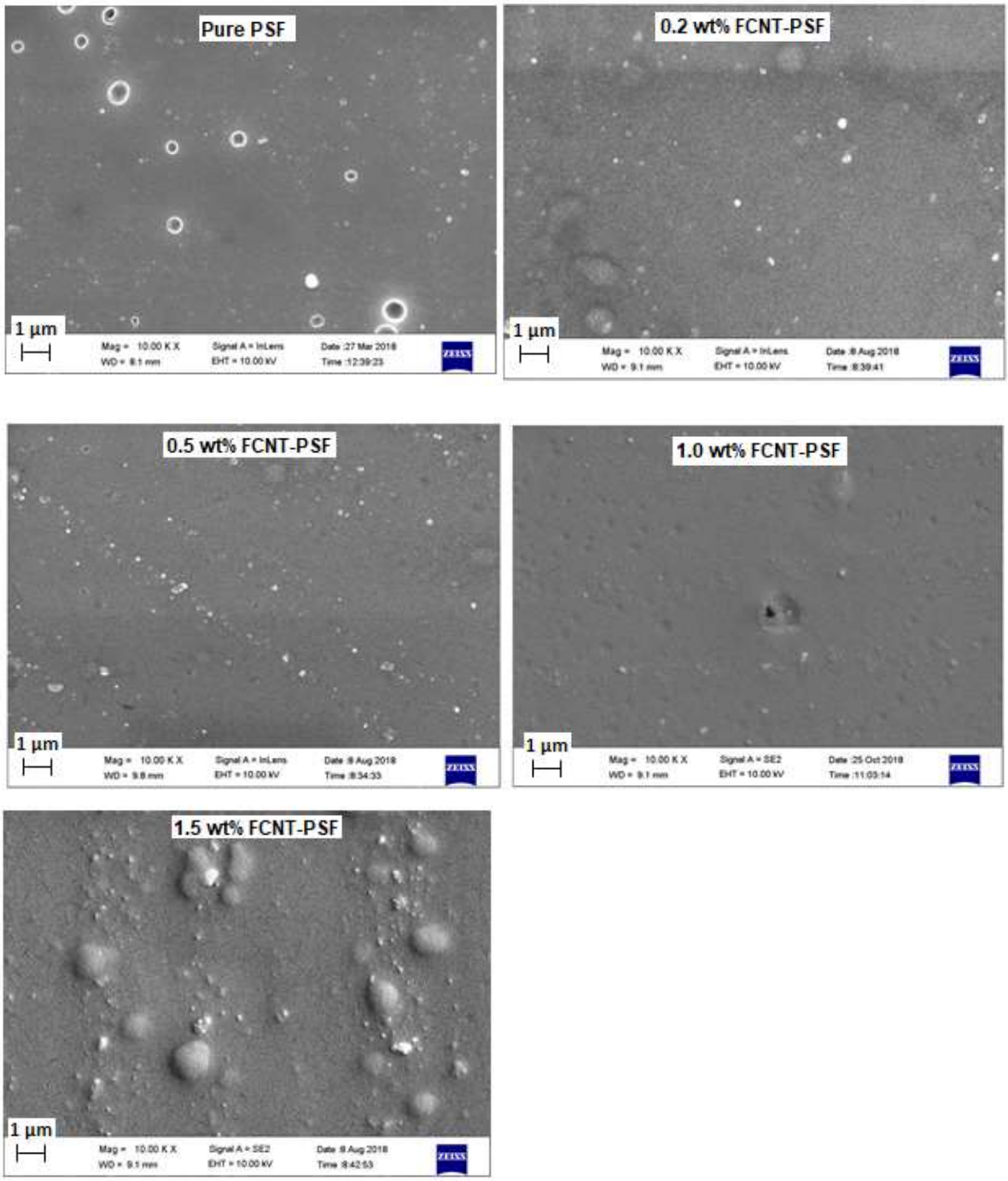

Figure 5.1: SEM micrograph of surface morphology of the synthesized membranes

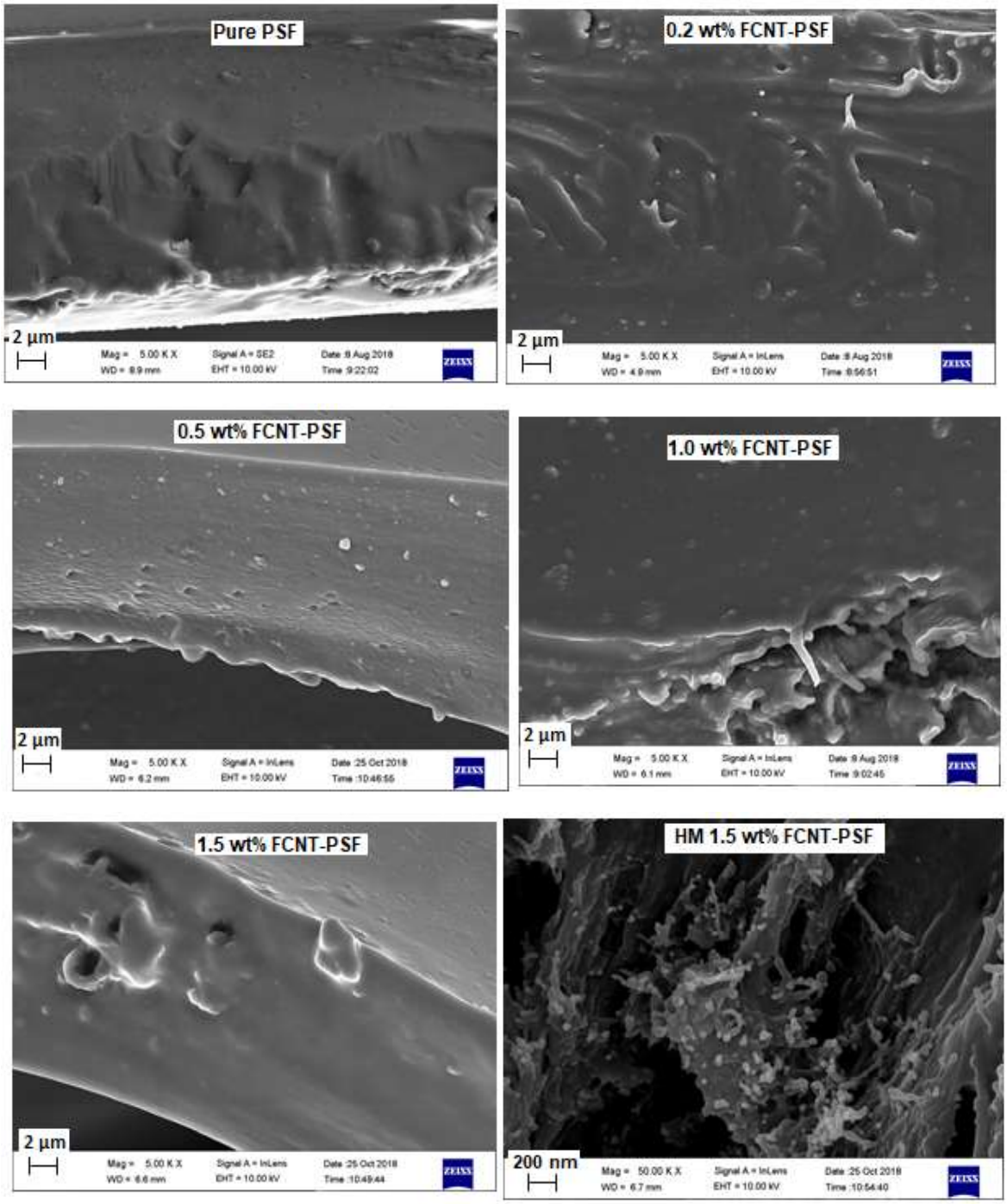

Figure 5.2: SEM micrograph of cross-sectional morphology of the synthesized membranes

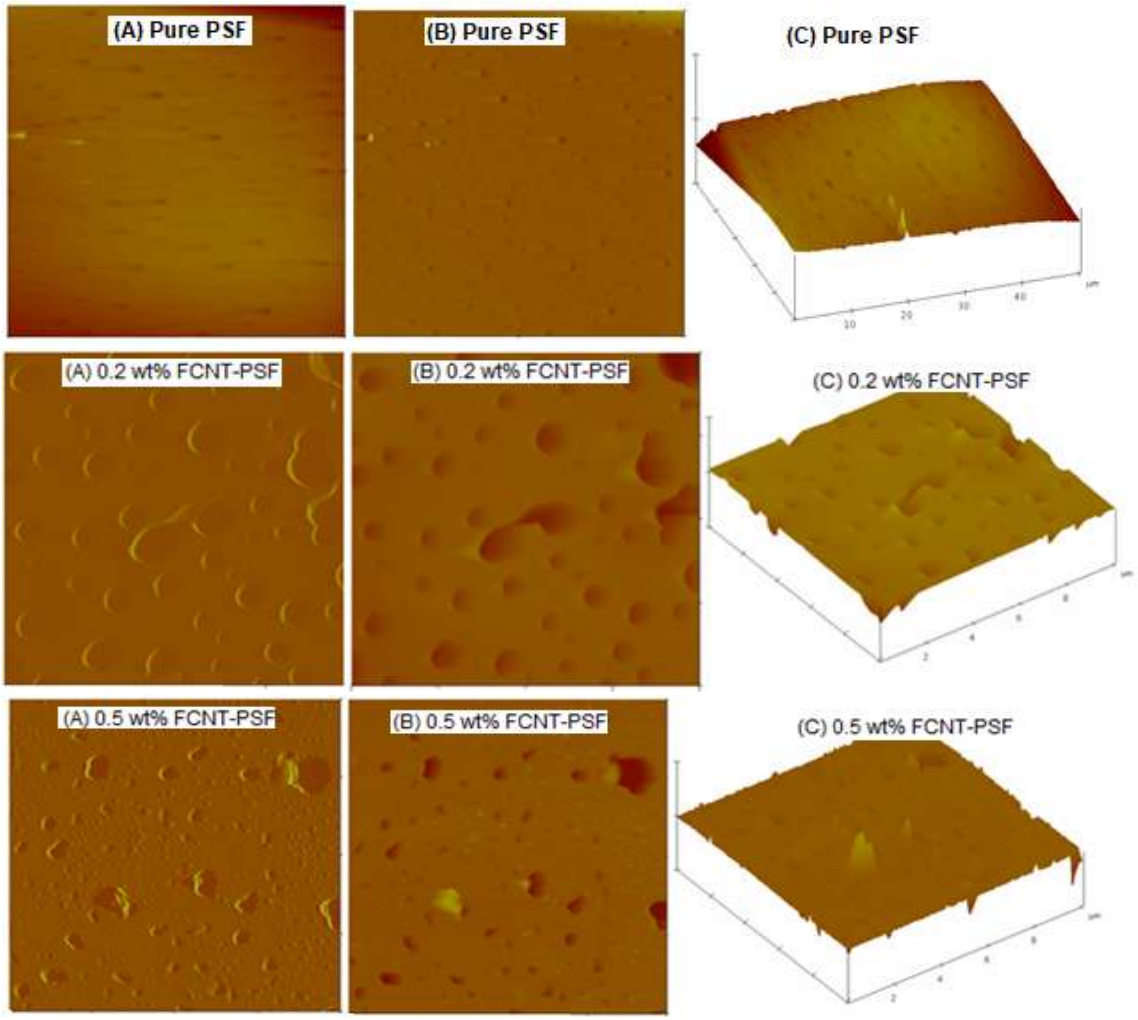
(A) Pure PSF
(B) Pure PSF
(C) Pure PSF
(A) 0.2 wt% FCNT-PSF
(B) 0.2 wt% FCNT-PSF
(C) 0.2 wt% FCNT-PSF
(A) 0.5 wt% FCNT-PSF
(B) 0.5 wt% FCNT-PSF
(C) 0.5 wt% FCNT-PSF

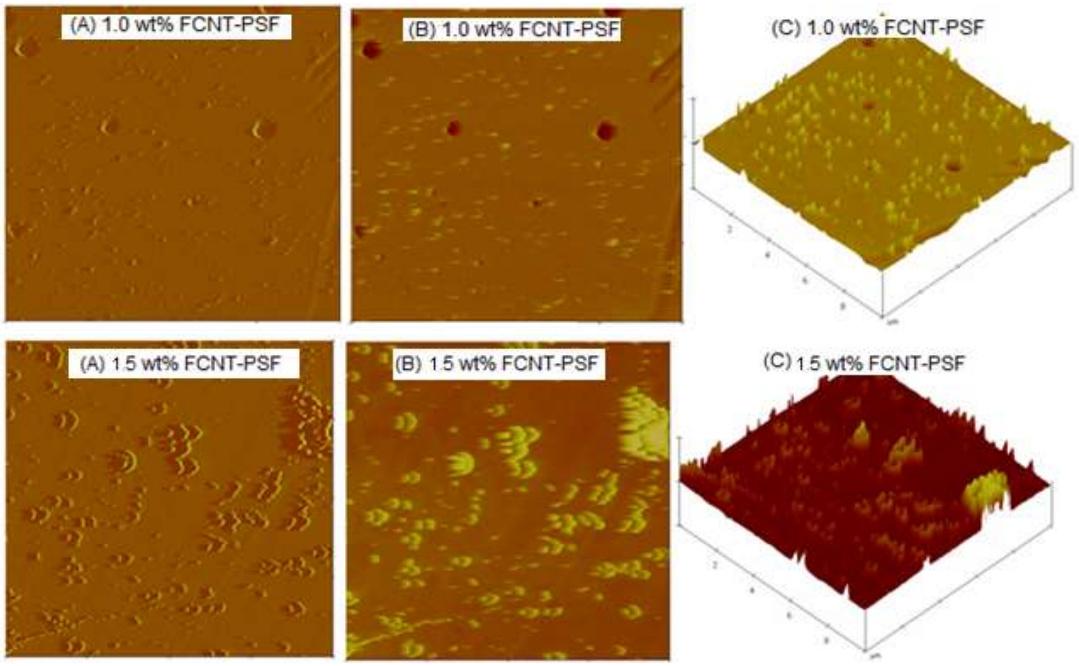

Figure 5.3: AFM surface topographies of synthesized membranes; (A) is amplitude 2D image, (B) is 2D height image and (C) is 3D image of height. Scan size for Pure PSF: 50 µm x 50 µm, scan size of the MMMs: 10 µm x 10 µm

Table 5.1: Surface topographic analysis of synthesized membranes

Membrane	**Depth-at-max (nm)**
Pure PSF	145.82
0.2 FCNT-PSF	81.13
0.5 FCNT-PSF	86.96
1.0 FCNT-PSF	111.65
1.5 FCNT-PSF	155.42

(Figures 5.1 and 5.2). Also, the depth-at-max of MMMs (0.2 wt. % - 1.0 wt. % of FCNTs) is lower than that of the pure PSF, which shows pore filling by FCNTs. However, 1.5 wt. % FCNT-PSF shows greater depth-at-max compared to pure PSF. This could be attributed to poor interface interaction between FCNTs and PSF matrices due to agglomeration of FCNTs (Khan et al., 2012). AFM images of depth-at-max analysis are presented in Appendix E.

5.3.3 Thermal stability and glass transition temperature

Figures 5.4 and 5.5 depicts thermogravimetric (TG) and derivative of TG (DTG) curves of the synthesized membranes, respectively. Figure 5.4 shows that there is no weight loss below 150 ^{o}C, which indicates that there is complete removal of the solvent from the membranes. Decomposition temperature, which is the peak of DTG curves of the membranes (Rafiq et al., 2012), and weight residue content of the membranes at 700 ^{o}C are presented in Table 5.2. Addition of FCNTs to PSF improves the decomposition temperature of the MMMs as depicted in Figure 5.5. A similar result was reported by Amirian et al. (2013). With Increase in FCNTs loading, however, the decomposition temperature of the MMMs remains relatively unchanged. Furthermore, the residue content increases with increasing wt. % loading of FCNTs up until 1.0 wt. % FCNT, which suggests successful dispersion of FCNTS into the polymer matrices thereby improving the thermal stability of the MMMs. But, further increase in FCNT loading to 1.5 wt. % decreases the residual content, which could be attributed to the agglomeration of FCNTs in the polymer matrices as evident in SEM and AFM images shown in Figures 5.1 and 5.3, respectively.

Glass transition temperature (T_g) of the synthesized membranes are presented in Table 5.3. T_g of polymeric membranes is the temperature region where the matrix of the membrane losses its glassy state to rubbery nature (Jansen, 2015). It is also a measure of the rigidity of the polymer matrix (Xue et al., 2013). T_g of the PSF membrane was slightly improved with the addition of FCNTs as shown in Table 5.3, which indicates that the mobility of the polymer chains is reduced. Although the increase in wt. % loading of FCNTs does not significantly impact the T_g of the MMMs, but there is a

trend similar to that of residual content of the MMMs presented in Table 5.2. 1.5 wt.% FCNT-PSF shows a decline in the T_g compared to the other MMMs. Ismail et al. (2011) reported similar behaviour where T_g of polyethersulfone was slightly increased with the addition of 0.5 wt. % CNT, but further increase in wt. % loading of CNTs decreased the T_g of the membrane. DSC thermograms of the membranes are presented in Appendix D.

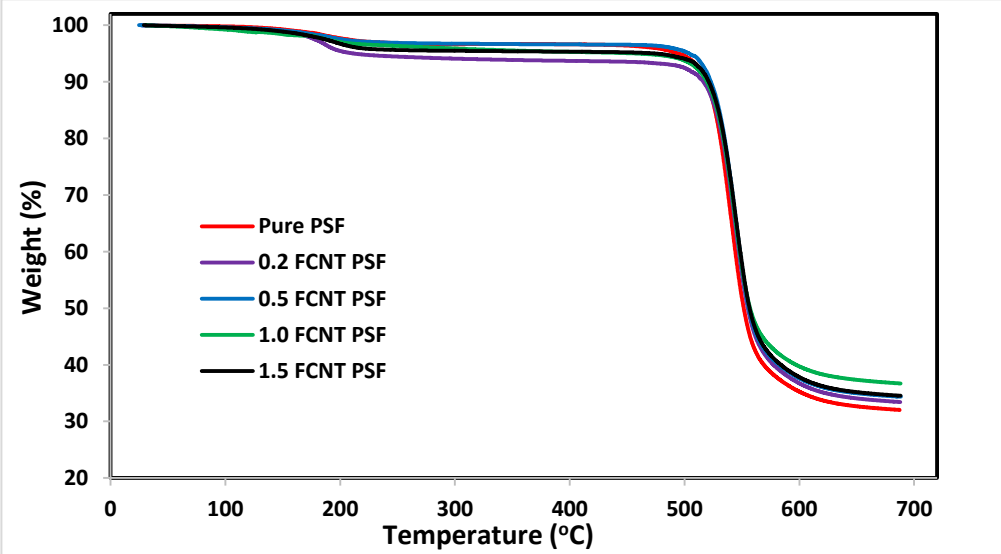

Figure 5.4: Thermogravimetric curves of synthesized membranes

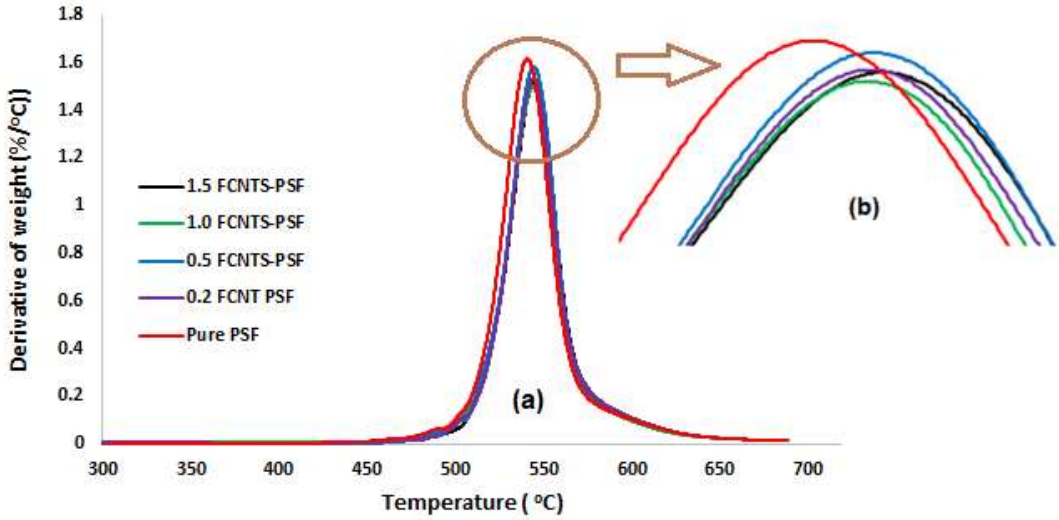

Figure 5.5: Derivative of TG curves of synthesized membranes (a) Full curve and (b) expanded view of peaks of the curves

Table 5.2: Thermogravimetric analysis of synthesized membranes

Samples	Decomposition Temperature (°C)	Residual contents (%)
Pure PSF	540.4	32.0
0.2 FCNT-PSF	544.1	33.4
0.5 FCNT-PSF	544.3	34.3
1.0 FCNT-PSF	544.0	37.7
1.5 FCNT-PSF	544.8	34.5

Table 5.3: Glass transition temperature of synthesized membranes

Sample	T_g (°C)
Pure PSF	183.6
0.2 FCNTS-PSF	186.0
0.5 FCNTS-PSF	186.1
1.0 FCNTS-PSF	186.5
1.5 FCNTS-PSF	185.8

5.3.4 Mechanical property

Mechanical properties of a MMM is largely dependent on the polymer matrix-filler interface interaction (Shen and Lua, 2012). Good interface interaction enables the FCNT as a filler to transfer its excellent mechanical property to the polymer matrix. The variations of tensile strength and Young's modulus as a function of wt.% FCNTs loading are presented in Figure 5.6. 0.2 wt. % FCNT-PSF has maximum tensile strength and maximum Young's modulus of 46.1 MPa and 668 MPa, respectively while pure PSF has tensile strength and Young's modulus of 35.1 MPa and 477 MPa, respectively. This showed that 0.2 wt. % FCNTs have good interface interaction with the polymer matrices. For 1.5 wt. % FCNT-PSF, decrease in the tensile strength and Young's modulus compared to pure PSF was observed. This could be attributed to poor

interface interaction between FCNTs and polymer matrices due to agglomeration of FCNTs. Deep and Mishra (2018) reported a comparable result.

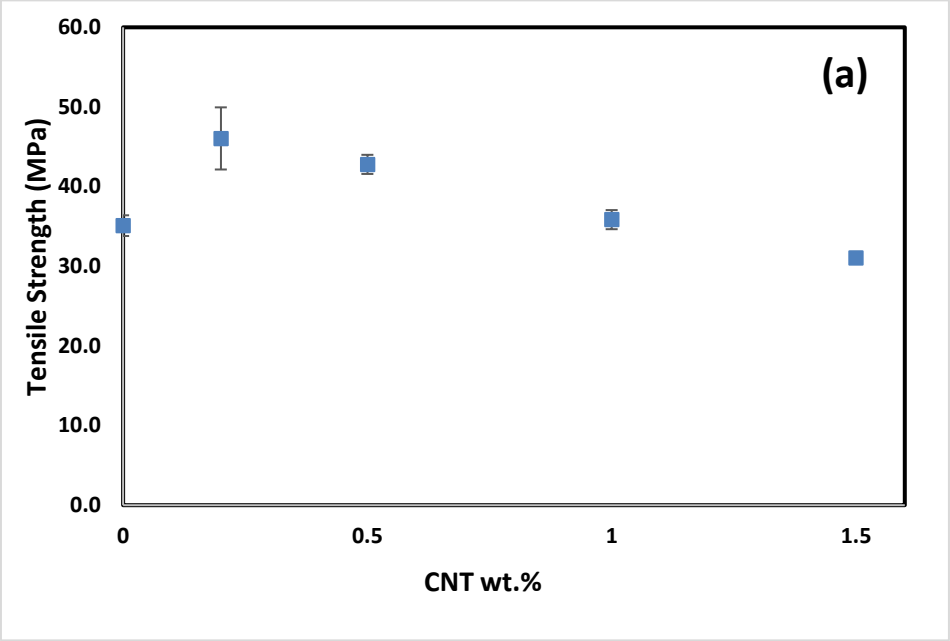

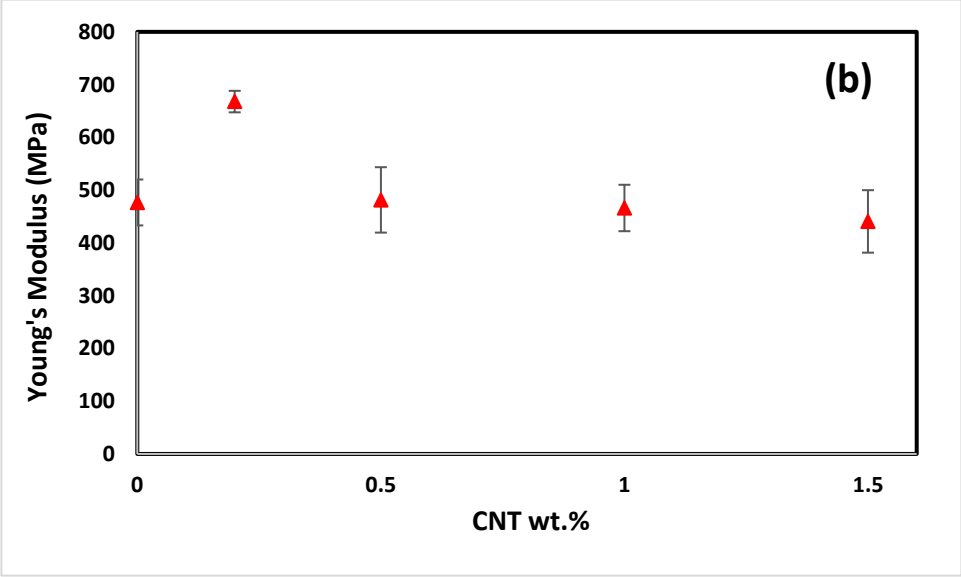

Figure 5.6: Mechanical properties of the synthesized FCNTs-PSF; (a) Tensile strength and (b) Young's Modulus

5.3.5 Single gas permeation results

Gas permeation through polymeric dense membrane has been widely reported to follow solution-diffusion mechanism also known as dual-mode sorption model (Shen and Lua, 2012; Deep and Mishra, 2018). This mechanism involves three stages (Mauze and Stern, 1984; Zhou and Stern, 1989): (a) dissolution of the gas into the high-pressure side of the membrane, (b) diffusion of the gas through the membrane and (c) desorption from the low-pressure side of the membrane. The rate of dissolution of a gas into a membrane is a function of the critical temperature of the gas (Wijmans and Baker, 1995). The higher the critical temperature of gas the higher its solubility coefficient. The rate of diffusion of a gas through a membrane increases as the kinetic diameter of the gas decreases (Pandey and Chauhan, 2001). The critical temperatures of CO_2 and CH_4 are 304.25 K and 191.25 K, respectively while their kinetic diameters are 0.33 nm and 0.38 nm, respectively. Hence, CO_2 has transport advantages over CH_4 through polymeric membranes.

From Figure 5.7a, FCNT-PSF showed higher pure CO_2 permeability compared to pure PSF at a specific pressure over the whole range of pressure. This could be attributed to an increase in excess free volume of the MMM by FCNTs thereby creating more sorption sites for CO_2 (Chung et al., 2003) and increasing the diffusion path (Robeson et al., 2014). Also, the inherent smoothness of CNTs could increase the rate of diffusion of gas through the MMM (Ismail et al., 2009). However, CO_2 permeability reaches the highest at 1.0 wt.% loading of FCNTs. Further increase in wt.% loading of FCNTs to 1.5 wt.% resulted in a decrease in the permeability of CO_2. This could be attributed to agglomeration of FCNTs within the polymer matrix causing a poor interface interaction between FCNT and polymer matrices (Khan et al., 2012). Furthermore, the increase in pressure led to a slight decrease in CO_2 permeability for all the types of membranes. This behaviour is predicted by the dual-mode sorption model owing to the saturation of Langmuir sites reducing the solubility of CO_2 with increasing pressure (Wijmans and Baker, 1995). Figures 5.7b depicts the permeability of pure CH_4 at 35 ^oC. Pure CH_4 permeability shows a similar trend as that of CO_2 permeability with the increase in

wt.% loading of FCNTs. Hence, a decrease in ideal selectivity of CO_2/CH_4 was observed with increase in FCNTs wt.% loading, as presented in Figure 5.7c. However, the increase in feed pressure has little effect on the CH_4 permeability for all the types of membranes. This agrees with the result obtained by Alaslai et al. (2016). CH_4 is a low-condensable gas, hence an increase in feed pressure has little effect on the saturation of Langmuir sites of the membranes (Kanehashi and Nagai, 2005).

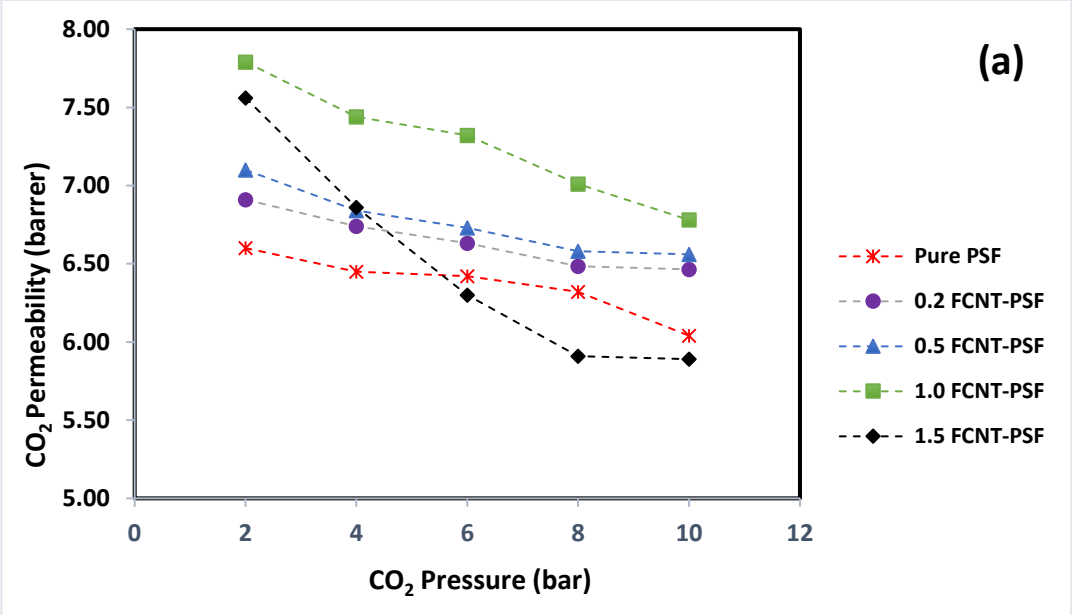

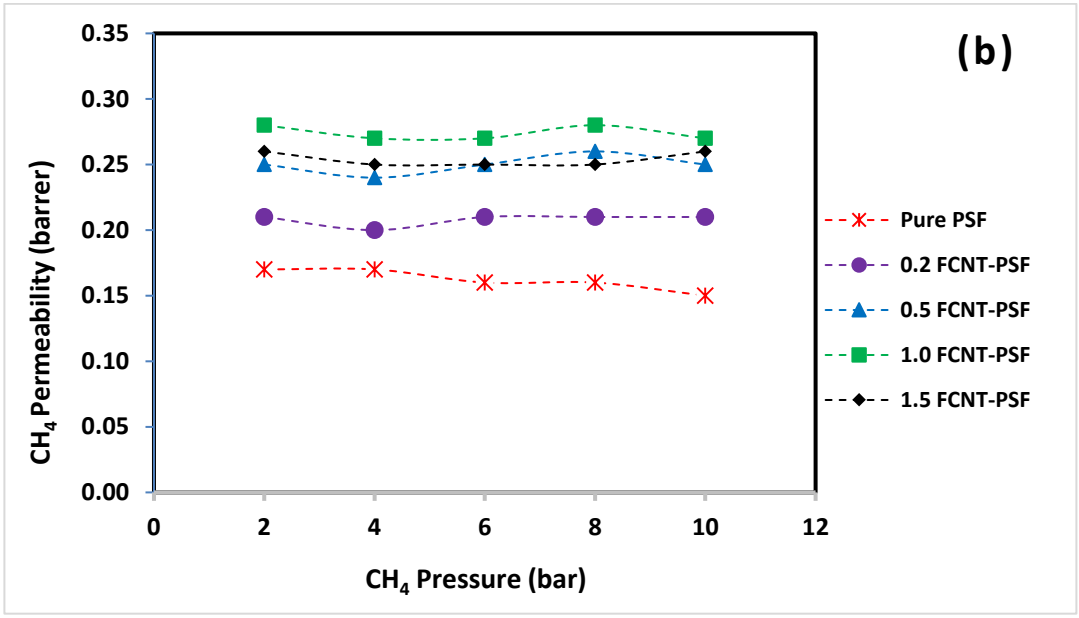

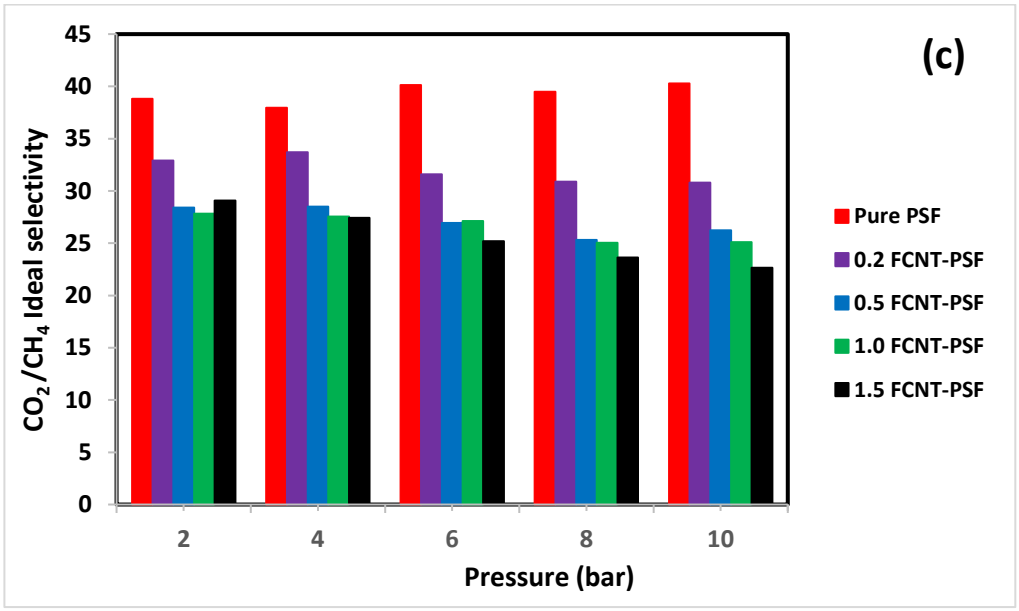

Figure 5.7: Single gas permeation at 35 ^{o}C. (a) Pure CO_2, (b) Pure CH_4, (c) Ideal selectivity

5.3.6 Mixed gas separation performance

Figure 5.8a shows that CO_2 permeability increases with increase in wt. % loading of FCNTs in PSF for a mixture of CO_2/CH_4 (10%/90%). This is due to enhanced diffusion rate of CO_2 through the membrane owing to excellent diffusivity properties of CNTs. A similar result was reported by Cong et al., (2007). Furthermore, CO_2 permeability decreases with an increase in the partial pressure of CO_2 for all the types of membrane. This is similar to the results obtained for pure gas permeation of CO_2 (Figure 5.7a) and for a mixture of CO_2/CH_4 (50%/50%) as shown in Figure 5.9a. However, the increase in CH_4 partial pressure does not significantly affect CH_4 permeability for both gas mixtures in all the types of the membrane as shown in Figures 5.8b and 5.9b. This is similar to the results obtained for pure gas permeation of CH_4 (Figure 5.7b). 1.5 wt. % FCNT-PSF showed highest CO_2 permeability when the CO_2 partial pressure was less than 2 bar. However, the effect of agglomeration of 1.5 wt. % FCNT in PSF on CO_2 permeability became evident at CO_2 partial pressure of 2 bar and above.

Mixed gas separation factor is expected to be lower than the ideal selectivity due to competitive sorption and bulk flow effects of the mixed gas (Kraftschik et al., 2013). However, in this study, mixed gas separation factor is higher than the ideal selectivity for both gas mixtures. For a mixture of CO_2/CH_4 (10%/90%), the partial pressure of CO_2 is much lower than CH_4 partial pressure. Since partial pressure difference across the membrane is a driving force for CO_2 permeation (Merkel et al., 2000), lower CO_2 partial pressure favours the permeability of CO_2 over CH_4. Hence, the mixed gas separation factor increases as depicted in Figure 5.8c. For a mixture of CO_2/CH_4 (50%/50%), the partial pressure of the component gases is the same but the mixed gas separation factor is still higher than ideal selectivity as shown in Figure 5.9c. There would be intermolecular interactions between the CNTs and CO_2, giving CO_2 a sorption competitive advantage over CH_4. Ansaloni et al. (2015) reported a similar experience with amino-functionalized CNT coupled with a hydrophilic polymer matrix to form a facilitated transport membrane. The gas transport mechanism in the membrane is depicted in Figure 5.10.

Therefore, improved mixed gas separation factor over ideal selectivity in our study could be due to intermolecular bonding between CO_2 and the CNTs thereby giving CO_2 additional sorption advantage over CH_4. To further substantiate this possibility, 1.0 wt. % purified CNT (PCNT) PSF membrane was tested using a mixture of CO_2/CH_4 (50%/50%) to eliminate the influence of differences in partial pressure of the component gases. The results of permeability and separation factor of the gas mixture in 1.0 wt. % PCNT-PSF as compared to 1.0 wt. % FCNT-PSF are presented in Figures 5.11a and 5.11b. The results show an improved CO_2 permeability and separation factor for 1.0 wt.% FCNT-PSF membrane over 1.0 wt.% PCNT-PSF membrane. The summary of CO_2/CH_4 permeation results from this study compared to literature reports is presented in Table 5.4. Notwithstanding the differences in the conditions different studies recorded in the literature were conducted, results documented in this study are comparable to literature. Full tables of CO_2/CH_4 permeability and selectivity values for pure and mixed gases are presented in Appendix F.

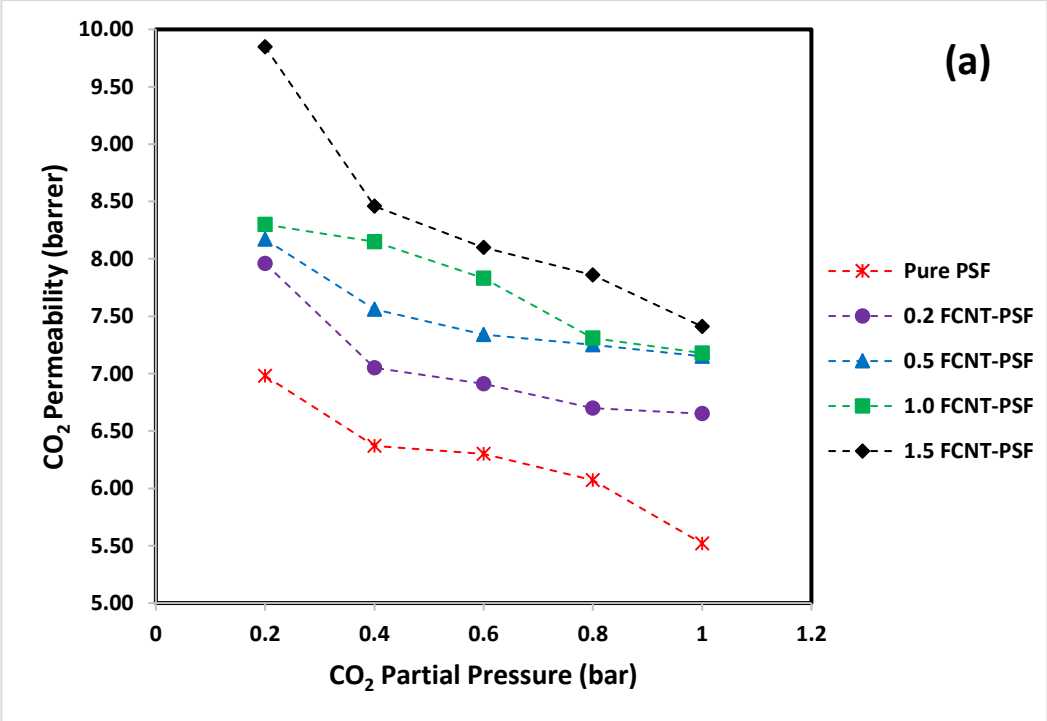

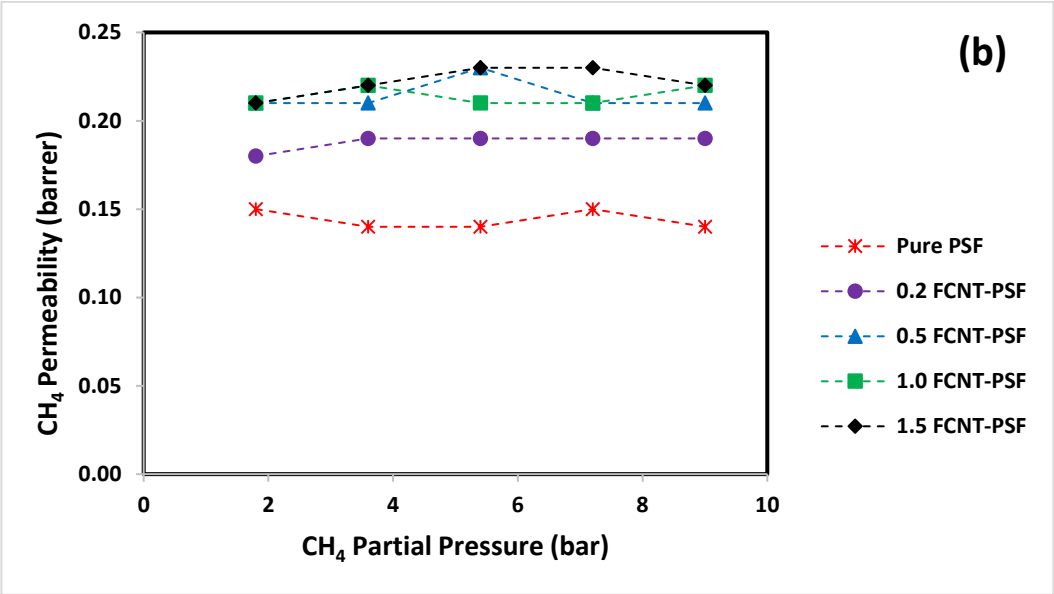

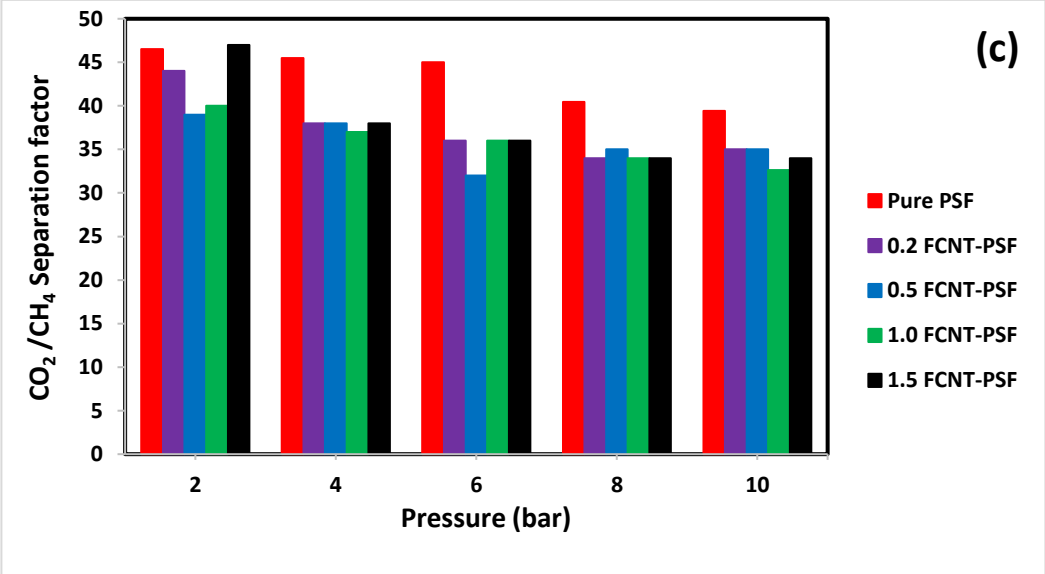

Figure 5.8: Separation performance of 10%/90% CO_2/CH_4 mixture. (a) CO_2 permeability as a function of CO_2 partial pressure; (b) CH_4 permeability as a function of CH_4 partial pressure; (c) CO_2/CH_4 separation factor

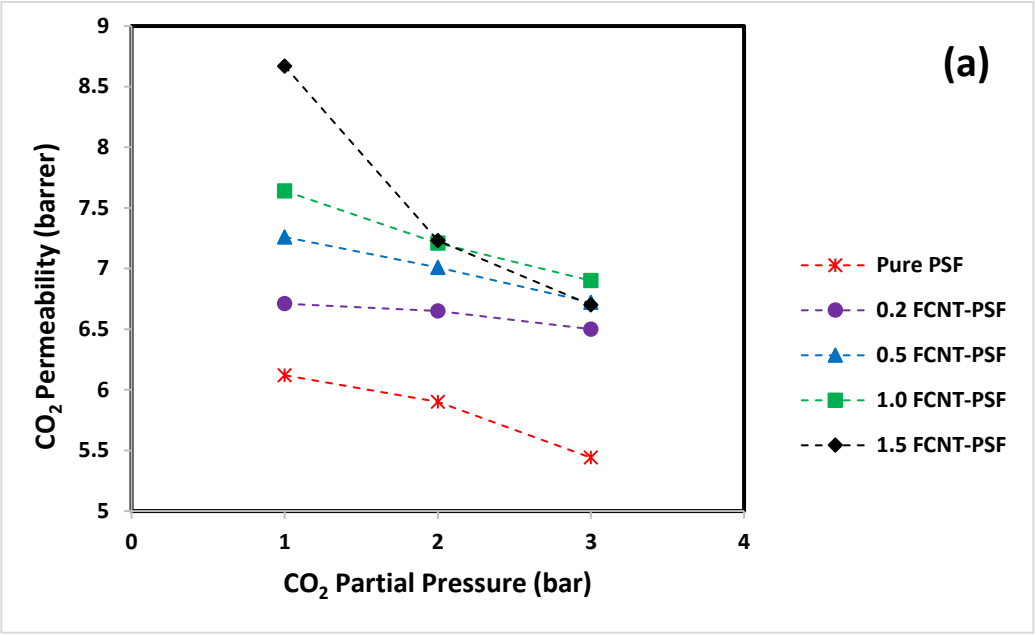
(a)
CO_2 Permeability (barrer)
CO_2 Partial Pressure (bar)
9
8.5
8
7.5
7
6.5
6
5.5
5
0
1
2
3
4
Pure PSF
0.2 FCNT-PSF
0.5 FCNT-PSF
1.0 FCNT-PSF
1.5 FCNT-PSF

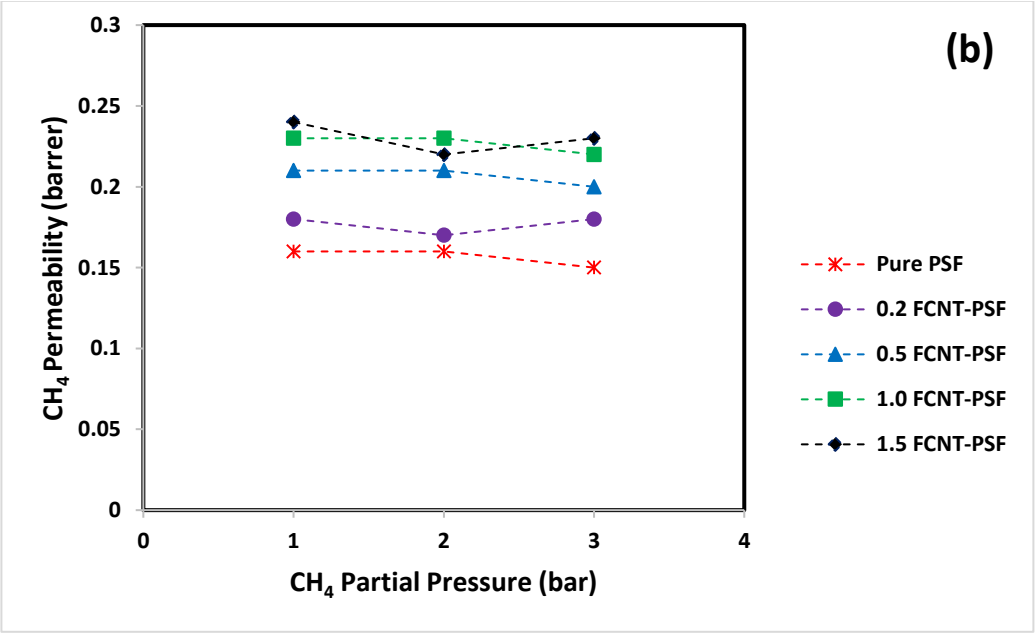
(b)
CH_4 Permeability (barrer)
CH_4 Partial Pressure (bar)
0.3
0.25
0.2
0.15
0.1
0.05
0
0
1
2
3
4
Pure PSF
0.2 FCNT-PSF
0.5 FCNT-PSF
1.0 FCNT-PSF
1.5 FCNT-PSF

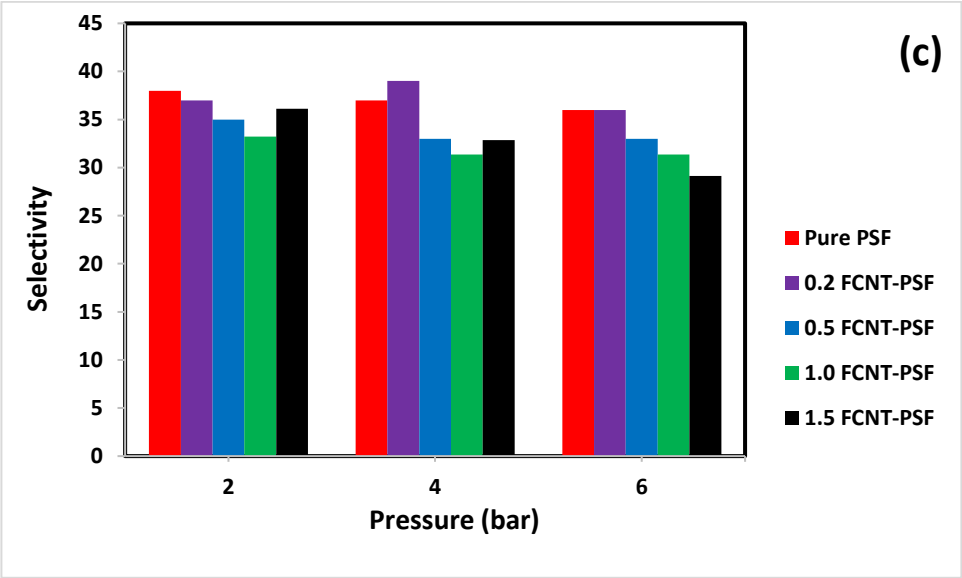

Figure 5.9: Separation performance of 50%/50% CO_2/CH_4 mixture. (a) CO_2 permeability as a function of CO_2 partial pressure; (b) CH_4 permeability as a function of CH_4 partial pressure; (c) CO_2/CH_4 separation factor

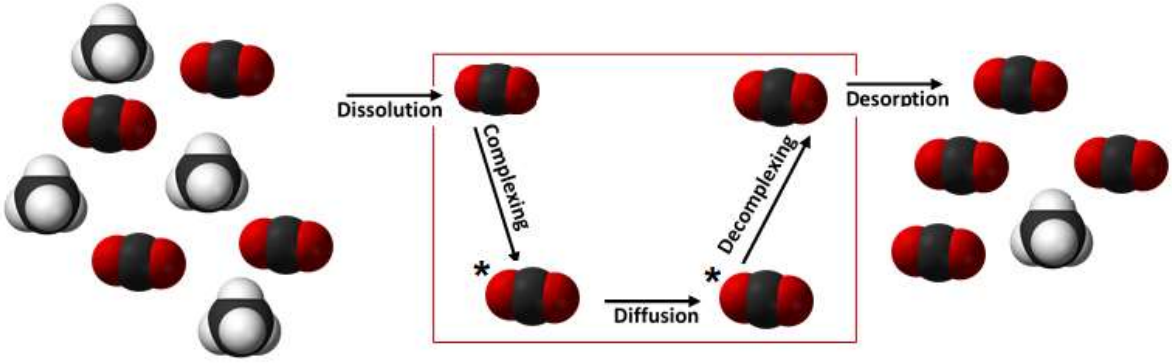

Figure 5.10: Schematic of the gas transport mechanism in the membrane (adapted from Luebke et al., 2007)

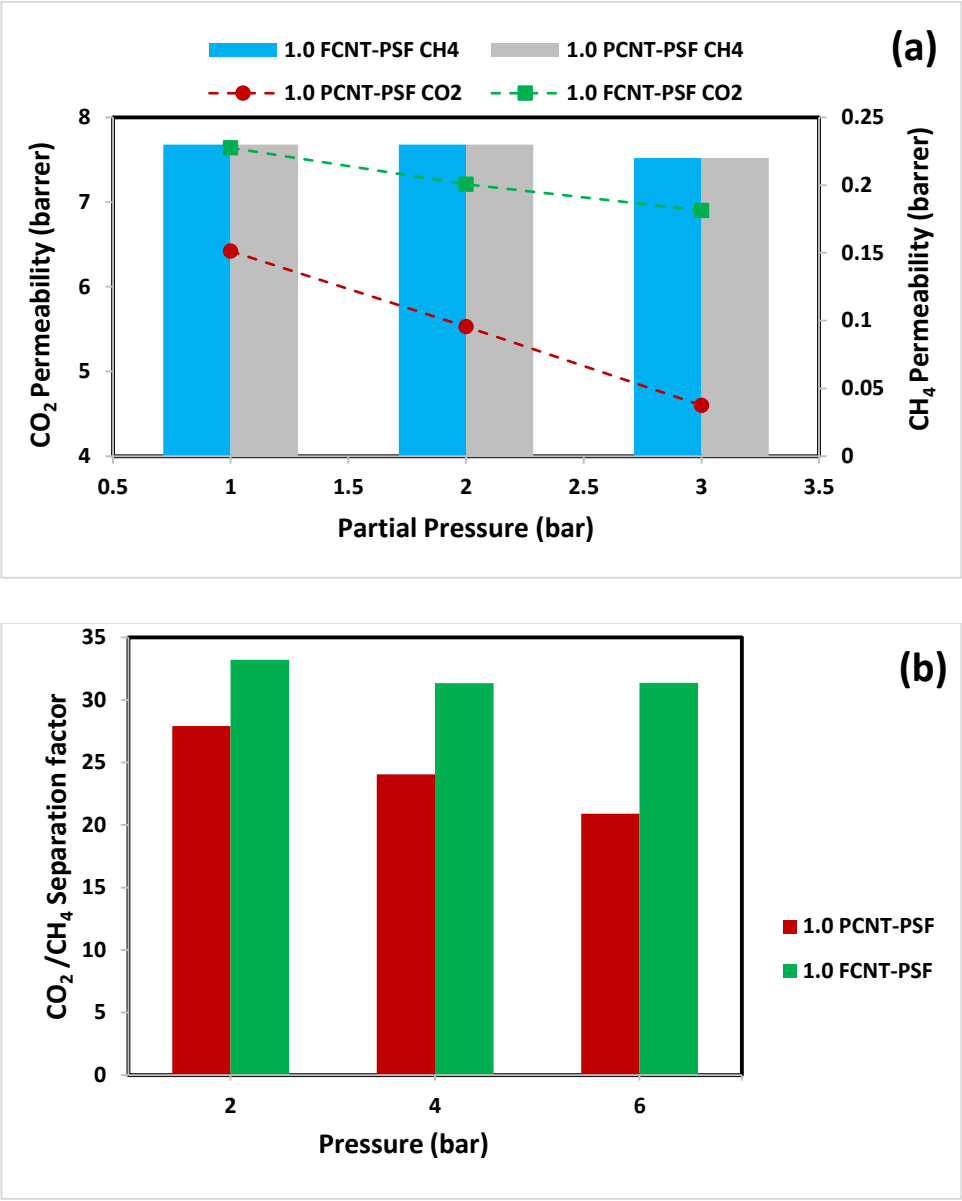

Figure 5.11: Separation performance of 50%/50% CO_2/CH_4 mixture in 1.0 wt. % PCNT-PSF and 1.0 wt. % FCNT-PSF. (a) CH_4 and CO_2 permeability as a function of CO_2 partial pressure; (b) CO_2/CH_4 separation factor

Table 5.4: Summary of CO_2/CH_4 permeation results from this study compared to literature

polymer	CNT Loading (wt. %)	Feed gas	Operation conditions	P(CO_2)	α(CO_2/CH_4)	Ref.
PSF[a]	0	Pure gases	35 °C, 2 bar	6.60	39	This work
	0.2 (F)	Pure gases	35 °C, 2 bar	6.91	33	This work
	0.5 (F)	Pure gases	35 °C, 2 bar	7.10	28	This work
	1.0 (F)	Pure gases	35 °C, 2 bar	7.79	28	This work
	1.5 (F)	Pure gases	35 °C, 2 bar	7.56	29	This work
	0	CO_2/CH_4 (10/90 v/v)	35 °C, 2 bar	6.98	47	This work
	0.2 (F)	CO_2/CH_4 (10/90 v/v)	35 °C, 2 bar	7.96	44	This work
	0.5 (F)	CO_2/CH_4 (10/90 v/v)	35 °C, 2 bar	8.17	39	This work
	1.0 (F)	CO_2/CH_4 (10/90 v/v)	35 °C, 2 bar	8.30	40	This work
	1.5 (F)	CO_2/CH_4 (10/90 v/v)	35 °C, 2 bar	9.85	47	This work
	0	CO_2/CH_4 (50/50 v/v)	35 °C, 2 bar	6.12	38	This work
	0.2 (F)	CO_2/CH_4 (50/50 v/v)	35 °C, 2 bar	6.71	37	This work
	0.5 (F)	CO_2/CH_4 (50/50 v/v)	35 °C, 2 bar	7.26	35	This work
	1.0 (F)	CO_2/CH_4 (50/50 v/v)	35 °C, 2 bar	7.64	33	This work
	1.0 (R)	CO_2/CH_4 (50/50 v/v)	35 °C, 2 bar	6.42	28	This work
	1.5 (F)	CO_2/CH_4 (50/50 v/v)	35 °C, 2 bar	8.67	36	This work
Elvaloy[a]	0	Pure gases	35 °C, 2 bar	80.69	6.57	Ranjbaran et al., 2015

	1.0 (F)	Pure gases	35 ºC, 2 bar	102.78	5.95	Ranjbaran et al., 2015
	1.0 (R)	Pure gases	35 ºC, 2 bar	78.36	6.05	Ranjbaran et al., 2015
	2.0 (F)	Pure gases	35 ºC, 2 bar	76.92	5.97	Ranjbaran et al., 2015
	2.0 (R)	Pure gases	35 ºC, 2 bar	73.73	5.77	Ranjbaran et al., 2015
PES[b]	0	Pure gases	27 ºC, 4 bar	10.98	51.26	Ismail et al., 2011
	1.0 (F)	Pure gases	27 ºC, 4 bar	2.79	30.91	Ismail et al., 2011
	2.0 (F)	Pure gases	27 ºC, 4 bar	11.60	14.22	Ismail et al., 2011
	3.0 (F)	Pure gases	27 ºC, 4 bar	13.56	5.04	Ismail et al., 2011
PDMS[a]	0	Pure gases	35 ºC, 4 bar	166.02	5.89	Kim et al., 2006
	2.0 (R)	Pure gases	35 ºC, 4 bar	190.67	5.58	Kim et al., 2006
	10.0 (R)	Pure gases	35 ºC, 4 bar	191.3	5.21	Kim et al., 2006
PI[a]	0	Pure gases	25 ºC, 15 bar	8.92	19.1	Aroon et al., 2010
	1.0 (F)	Pure gases	25 ºC, 15 bar	14.27	10	Aroon et al., 2010
	1.0 (R)	Pure gases	25 ºC, 15 bar	5.44	22.7	Aroon et al., 2010
PSF[a]	0	Pure gases	35 ºC, 4 bar	3.90	22.94	Kim et al., 2007
	5.0 (F)	Pure gases	35 ºC, 4 bar	5.12	18.96	Kim et al., 2007
	10.0 (F)	Pure gases	35 ºC, 4 bar	5.19	18.54	Kim et al., 2007

	15.0 (F)	Pure gases	35 °C, 4 bar	4.52	16.14	Kim et al., 2007
FTM[a]	2.1 (F)	$CO_2/CH_4/H_2$ (20/58.8/20.2)	107 °C, 2 bar	3157	650	Ansaloni et al., 2015
	0	$CO_2/CH_4/H_2$ (20/58.8/20.2)	107 °C, 15 bar	986	283	Ansaloni et al., 2015
	6.9 (F)	$CO_2/CH_4/H_2$ (20/58.8/20.2)	107 °C, 15 bar	1014	265	Ansaloni et al., 2015

[a] $P(CO_2)$ in Barrer; [b] $P(CO_2)$ in GPU; F – Functionalized; R – Raw; PES – Polyethersulfone; PDMS – Poly (imide siloxane); PI – Polyimide; FTM – Facilitated transport membrane

5.4 Concluding remarks

In this chapter, results of the investigation of the effect of the addition of FCNTs to PSF on the physicochemical and gas separation properties of the MMM are reported. Addition of FCNTs to PSF membrane increased its thermal and mechanical properties. With Increase in FCNTs loading, the decomposition temperature of the MMM remains relatively unchanged. However, the percentage change in weight decreases with increase in FCNTs loading with an optimum point at 1.0 wt. %. Glass transition temperature (T_g) of PSF membrane was improved with the addition of FCNTs, but the increase in FCNTs does not significantly impact the T_g of the MMM. Analysis of tensile strength and Young's modulus of the MMM show an increase in these mechanical properties with the addition of FCNTs. The permeability of pure CO_2 increased with increase in FCNTs wt. % loading. The optimum permeability was achieved at 1.0 wt. %. The permeability of pure CO_2 decreased with an increase in pressure for all the membranes, but the permeability of pure CH_4 was relatively the same with an increase in pressure. Ideal selectivity decreased with increase in FCNTs wt. % loading. Mixed gas permeability trend was similar to that of pure gas permeability. However, 1.5 wt. % loading of FCNTs showed the best CO_2 permeability result. Mixed gas selectivity of MMM was at par with pure PSF at low pressure with

improved CO_2 permeability. This favourable condition could be attributed to molecular interactions between the CNTs and CO_2, giving CO_2 additional sorption competitive advantage over CH_4. For quick dissemination of these results, a manuscript is currently under review at Separation Science and Technology.

References

Adewole, J. K., Ahmad, A. L., Ismail, S. and Leo, C.P., 2013. Current challenges in membrane separation of CO2 from natural gas: A review, *International Journal of Greenhouse Gas Control*, vol. 17, pp. 46‑65.

Ahmad, A.L., Sunarti, A., Lee, K., Fernando, W., 2008. Review of liquid absorbent behaviours in membrane gas absorption process. *In: 12th Asian Pacific Confederation of Chemical Engineering Congress, Dalian, China.*

Ahn, J., Chung, W.J., Pinnau, I. and Guiver, M.D., 2008. Polysulfone/silica nanoparticle mixed-matrix membranes for gas separation. *Journal of Membrane Science*, 314(1-2), pp.123-133.

Alaslai, N., Ghanem, B., Alghunaimi, F., Litwiller, E., and Pinnau, I., 2016. Pure-and mixed-gas permeation properties of highly selective and plasticization resistant hydroxyl-diamine-based 6FDA polyimides for CO2/CH4 separation, *Journal of Membrane Science*, vol. 505, pp. 100–107

Ansaloni, L., Zhao, Y., Jung, B.T., Ramasubramanian, K., Baschetti, M.G. and Ho, W.W., 2015. Facilitated transport membranes containing amino-functionalized multi-walled carbon nanotubes for high-pressure CO 2 separations. *Journal of Membrane Science*, 490, pp.18-28.

Aroon, M. A., Ismail, A. F., Matsuura, T., and Montazer-Rahmati, M. M., 2010. Performance studies of mixed matrix membranes for gas separation: A review, *Separation and Purification Technology*, vol. 75, pp. 229–242.

Baker, R. W. and Lokhandwala, K., 2008. Natural Gas Processing with Membranes: An Overview, *Industrial & Engineering Chemistry Research*, vol. 47 (7), pp. 2109–2121.

Balasubramanian, K. and Burghard, M., 2005. Chemically functionalized carbon nanotubes. *Small*, 1(2), pp.180-192.

Bernardo, P. and Clarizia, G., 2013. 30 Years of Membrane Technology for Gas Separation, *Chemical Engineering Transactions*, vol. 32, pp. 1999-2003

Chen, L., Xie, H., Li, Y. and Yu, W., 2008. Surface chemical modification of multiwalled carbon nanotubes by a wet-mechanochemical reaction. *Journal of Nanomaterials*, 2008, p.63.

Chen, X.Y., Vinh-Thang, H., Ramirez, A.A., Rodrigue, D. and Kaliaguine, S., 2015. Membrane gas separation technologies for biogas upgrading. *RSC Advances*, 5(31), pp.24399-24448.

Chung, T.S., Cao, C. and Wang, R., 2003. Pressure and temperature dependence of the gas-transport properties of dense poly [2, 6-toluene-2, 2-bis (3, 4-dicarboxylphenyl) hexafluoropropane diimide] membranes. *Journal of Polymer Science Part B: Polymer Physics*, 42(2), pp.354-364.

Comesaña-Gándara, B., Hernández, A., Jose, G., de Abajo, J., Lozano, A. E. and Lee, Y. M., 2015. Thermally rearranged polybenzoxazoles and poly (benzoxazole-co-imide) s from ortho-hydroxyamine monomers for high performance gas separation membranes, *Journal of Membrane Science*, vol. 493, pp.329-339

Cong, H., Zhang, J., Radosz, M. and Shen, Y., 2007. Carbon nanotube composite membranes of brominated poly(2,6-diphenyl-1,4-phenylene oxide) for gas separation, *Journal of Membrane Science*, vol. 294, pp. 178–185.

Corry, B., 2011. Water and ion transport through functionalised carbon nanotubes: implications for desalination technology. *Energy & Environmental Science, 4(3), pp.751-759.*

Deng, L. and Hägg, M-B., 2014. Carbon nanotube reinforced PVAm/PVA blend FSC nanocomposite membrane for CO2/CH4 separation, *International Journal of Greenhouse Gas Control*, vol. 26 pp. 127–134.

Dortmundt, D. and Doshi, K., 1999. Recent developments in CO2 removal membrane technology. *UOP LLC*, pp.1-30.

Du, J., Bai, J. and Cheng, H., 2007. The present status and key problems of carbon nanotube based polymer composites. *Express Polymer Letters*, 1(5), pp.253-273.

Eguchi, H., Kim, D. J. and Koros, W. J., 2015. Chemically cross-linkable polyimide membranes for improved transport plasticization resistance for natural gas separation, *Polymer*, vol. 58, pp. 121-129.

George, S.C. and Thomas, S., 2001. Transport phenomena through polymeric systems. *Progress in Polymer Science*, 26(6), pp.985-1017.

Hart, K.E. and Colina, C.M., 2014. Estimating gas permeability and permselectivity of microporous polymers, *Journal of Membrane Science*, vol. 468, pp.259-268

Hu, C.C., Chang, C.S., Ruaan, R.C. and Lai, J.Y., 2003. Effect of free volume and sorption on membrane gas transport. *Journal of Membrane Science*, 226(1-2), pp.51-61.

Ismail, A.F., Goh, P.S., Sanip, S.M. and Aziz, M., 2009. Transport and separation properties of carbon nanotube-mixed matrix membrane. *Separation and Purification Technology*, 70(1), pp.12-26.

Ismail, A.F., Rahim, N.H., Mustafa, A., Matsuura, T., Ng, B.C., Abdullah, S. and Hashemifard, S.A., 2011. Gas separation performance of

polyethersulfone/multi-walled carbon nanotubes mixed matrix membranes. *Separation and Purification Technology*, 80(1), pp.20-31.

Jansen J. C., 2015. Glass Transition Temperature (Tg). In: Drioli E., Giorno L. (eds) Encyclopedia of Membranes. Springer, Berlin, Heidelberg

Kanehashi, S. and Nagai, K., 2005. Analysis of dual-mode model parameters for gas sorption in glassy polymers. *Journal of Membrane Science*, 253(1-2), pp.117-138.

Khan, M.M., Filiz, V., Bengtson, G., Shishatskiy, S., Rahman, M. and Abetz, V., 2012. Functionalized carbon nanotubes mixed matrix membranes of polymers of intrinsic microporosity for gas separation. *Nanoscale Research Letters*, 7(1), p.504.

Kraftschik, B., Koros, W.J., Johnson, J.R. and Karvan, O., 2013. Dense film polyimide membranes for aggressive sour gas feed separations. *Journal of Membrane Science*, 428, pp.608-619.

Li, S., Jo, H.J., Han, S.H., Park, C.H., Kim, S., Budd, P.M. and Lee, Y.M., 2013. Mechanically robust thermally rearranged (TR) polymer membranes with spirobisindane for gas separation, *Journal of Membrane Science*, vol. 434, pp.137-147

Liu, G., Chernikova, V., Liu, Y., Zhang, K., Belmabkhout, Y., Shekhah, O., Zhang, C., Yi, S., Eddaoudi, M. and Koros, W.J., 2018. Mixed matrix formulations with MOF molecular sieving for key energy-intensive separations, *Nature Materials*, vol.17, no. 3, p.283

Liu, Q., Paul, D.R. and Freeman, B.D., 2016. Gas permeation and mechanical properties of thermally rearranged (TR) copolyimides, *Polymer*, vol. 82, pp.378-391

Luebke D, Ilconich J, Myers C, Pennline H., 2007. Carbon dioxide separation with supported ionic liquid membranes. *In: Sixth annual conference on carbon capture & sequestration, Pittsburgh, PA, USA, 7-10 May 2007, 15 pp (2007)* Available from: http://www.netl.doe.gov/publications/proceedings/07/carbon-seq/start.htm

Mauze, G. R. and Stern, S. A., 1984. The dual-mode solution of vinyl chloride monomer in poly(vinylchloride), *Journal of Membrane Science*. vol. 18, pp. 99.

Merkel, T.C., Bondar, V., Nagai, K. and Freeman, B.D., 2000. Sorption and transport of hydrocarbon and perfluorocarbon gases in poly (1-trimethylsilyl-1-propyne). *Journal of Polymer Science Part B: Polymer Physics*, 38(2), pp.273-296.

Mushtaq, A., Mukhtar, H. B., Shariff, A. M. and Mannan, H. A., 2013. A Review: Development of Polymeric Blend Membrane for Removal of CO_2 from Natural Gas, *International Journal of Engineering & Technology*, vol. 13, No. 02, pp. 53-60.

Okabe, K., Matsumiya, N. and Mano, H., 2007. Stability of gel-supported facilitated transport membrane for carbon dioxide separation from model flue gas. *Separation and Purification Technology*, vol. 57(2), pp.242-249.

Pandey, P. and Chauhan, R.S., 2001. Membranes for gas separation. *Progress in Polymer Science*, 26(6), pp.853-893.

Prokopowicz, M., 2016. Atomic force microscopy technique for the surface characterization of sol–gel derived multi-component silica nanocomposites. *Colloids and Surfaces A: Physicochemical and Engineering Aspects*, 504, pp.350-357.

Rafiq, S., Man, Z., Maulud, A., Muhammad, N. and Maitra, S., 2012. Separation of CO2 from CH4 using polysulfone/polyimide silica nanocomposite membranes. *Separation and Purification Technology,* 90, pp.162-172.

Ranjbaran, F., Omidkhah, M. R. and Amooghin, A. E., 2015. The novel Elvaloy 4170/functionalized multi-walled carbon nanotubes mixed matrix membranes: Fabrication, characterization and gas separation study, *Journal of the Taiwan Institute of Chemical Engineers*, vol. 49, pp. 220–228

Rezakazemi, M., Amooghin, A.E., Montazer-Rahmati, M.M., Ismail, A.F. and Matsuura, T., 2014. State-of-the-art membrane based CO2 separation using mixed matrix membranes (MMMs): an overview on current status and future directions, *Progress in Polymer Science*, vol. 39, no. 5, pp. 817-861

Robeson, L.M., Smith, Z.P., Freeman, B.D. and Paul, D.R., 2014. Contributions of diffusion and solubility selectivity to the upper bound analysis for glassy gas separation membranes. *Journal of Membrane Science,* 453, pp.71-83.

Scholes, C. A., Chen, G. Q., Stevens, G. W. and Kentish, S. E., 2010. Plasticization of ultra-thin polysulfone membranes by carbon dioxide, *Journal of Membrane Science*, vol. 346, pp. 208–214.

Shah, P. and Murthy, C. N., 2013. Studies on the porosity control of MWCNT/polysulfone composite membrane and its effect on metal removal, *Journal of Membrane Science*, vol. 437, pp. 90–98.

Shen, Y. and Lua, A.C., 2012. Preparation and characterization of mixed matrix membranes based on poly (vinylidene fluoride) and zeolite 4A for gas separation. *Polymer Engineering & Science*, 52(10), pp.2106-2113.

Skoulidas, A.I., Ackerman, D.M., Johnson, J.K. and Sholl, D.S., 2002. Rapid transport of gases in carbon nanotubes. *Physical Review Letters*, 89(18), p.185901.

Sokhan, V.P., Nicholson, D. and Quirke, N., 2004. Transport properties of nitrogen in single walled carbon nanotubes. *The Journal of Chemical Physics*, 120(8), pp.3855-3863.

Swaidan, R., Ghanem, B., Litwiller, E. and Pinnau, I., 2015. Physical aging, plasticization and their effects on gas permeation in "rigid" polymers of intrinsic microporosity, *Macromolecules*, vol. 48, no. 18, pp.6553-6561

Vinoba, M., Bhagiyalakshmi, M., Alqaheem, Y., Alomair, A.A., Pérez, A. and Rana, M.S., 2017. Recent progress of fillers in mixed matrix membranes for CO2 separation: A review, *Separation and Purification Technology*, vol. 188, pp.431-450

Wang, M., Wang, Z., Zhao, S., Wang, J. and Wang, S., 2017. Recent advances on mixed matrix membranes for CO2 separation, *Chinese Journal of Chemical Engineering*, vol. 22, pp. 1581-1597

Wijmans, J.G. and Baker, R.W., 1995. The solution-diffusion model: a review. *Journal of Membrane Science*, 107(1-2), pp.1-21.

Xiao, Y., Low, B. T., Hosseini, S. S., Chung, T. S. and Paul, D. R., 2009. The strategies of molecular architecture and modification of polyimide-based membranes for CO2 removal from natural gas—A review, *Progress in Polymer Science*, vol. 34, pp. 561–580.

Xue, Q., Lv, C., Shan, M., Zhang, H., Ling, C., Zhou, X. and Jiao, Z., 2013. Glass transition temperature of functionalized graphene–polymer composites. *Computational Materials Science*, 71, pp.66-71.

Zhang, Y., Sunarso, J., Liu, S. and Wang, R., 2013. Current status and development of membranes for CO2/CH4 separation: A review, *International Journal of Greenhouse Gas Control*, vol. 12, pp. 84–107.

Zhou, S. and Stern, S. A., 1989. The effect of plasticization on the transport of gases in and through glassy polymers, *Journal of Polymer Science Part B: Polymer Physics*, vol. 27, pp. 205.

CHAPTER 6

6 EXPERIMENTAL AND MODELLING STUDY OF CO_2 INDUCED PLASTICIZATION OF FUNCTIONALIZED CARBON NANOTUBE / POLYSULFONE DENSE MEMBRANE

6.1 Introduction

In glassy polymers, plasticization causes a decrease in the interface between adjacent segments of polymer chains (Scholes et al., 2010) which theoretically can be seen as swelling and solvation of polymers (Kesting and Fritzche, 1993). CO_2 induced plasticization is a pressure dependent phenomenon (Balçık and Ahunbay, 2018) and it occurs when the concentration of CO_2 reaches a critical point, causing mobility of polymer matrix and increasing the fractional free volume of the polymer. Furthermore, CO_2 induced plasticization has been defined as the increase in CO_2 permeability with an increase in feed pressure (Bos et al., 1999). In polymeric membranes, the increase in feed pressure of many gases decreases the permeability of these gases through the membrane (Minelli and Sarti, 2013). However, the minimum pressure at which gas permeability begins to increase is known as plasticization pressure (Dong et al., 2011). The increase in the permeability is as a result of disruption in chain packing and increase in inter-segmental mobility (Zhuang et al., 2018).

Dual-mode sorption model consisting of Langmuir and Henry's law contributions has been used to describe the plasticization effects of gases in the polymeric membrane (Mauze and Stern, 1984; Zhou and Stern, 1989). The following Equations (6.1 – 6.3) illustrate the dual-mode sorption mechanism:

$$C_d = k_d p \tag{6.1}$$

$$C_h = \frac{C_h' bp}{1+bp} \tag{6.2}$$

$$C = C_d + C_h = k_d p + \frac{C_h' bp}{1+bp} \tag{6.3}$$

Equation (6.1) is an expression of gas molecules dissolution process with respect to Henry's law where C_d is the concentration of gas molecules based on Henry's law sorption, k_d is Henry's law solubility coefficient and p is pressure. Some literature reported the use of fugacity in place of pressure (Petropoulos, 1992). However, Koro et al. (1976) investigated the effect of using fugacity instead of pressure and reported that it makes little or no effect within the pressure range of 1 – 23 bar. Equation (6.2) describes fixed sites gas molecules absorption into the polymer matrix by Langmuir isotherm where C_h is the concentration of these molecules, C_h' is the polymer matrix saturation constant and b is the Langmuir affinity constant. Equation 6.3 gives the total penetrants concentration C.

The solubility of a penetrant in glassy polymers is a thermodynamic parameter (Hu et al., 2003) and may be affected by the inherent condensability of the penetrant, the polymer-penetrant interactions and the excess free volume in the polymer (Chung et al., 2003). The solubility, S, can be expressed in terms of dual mode sorption model parameters as follows:

$$S = \frac{C}{p} \tag{6.4}$$

Substituting Equation (6.3) into Equation (6.4)

$$S = k_d + \frac{C_h' b}{1+bp} \tag{6.5}$$

In this study, CO_2 induced plasticization of functionalized carbon nanotube (FCNT) reinforced polysulfone (PSF) dense membranes was investigated using CO_2 sorption measurement at feed pressure up to 20 bar. This is to determine the total CO_2 concentration in the membrane matrix and to evaluate the dual-mode sorption model parameters. In addition to the sorption measurement, pure CO_2 permeability was measured at feed pressure between 2 – 20 bar to determine the plasticization pressure of the membranes. The use of CNTs as fillers for the synthesis of MMMs for CO_2 induced plasticization suppression is yet to be reported in open literature to the best of our knowledge. Hence, the focus of this work is to leverage the excellent mechanical properties, lightweight, and length to radius ratio of CNTs to synthesize MMMs that can withstand high CO_2 feed pressure without plasticizing. Furthermore, many of the existing phenomenological models focus on the polymer matrix – polymer matrix interface interaction without considering filler particle – filler particle interface interaction in the fundamental development of the models. Therefore, three possible interface interactions in MMMs were considered in this work to develop a phenomenological model for CO_2 permeability determination in FCNT reinforced polymeric dense membrane in the presence of plasticization.

6.2 Experimental

6.2.1 CO_2 sorption experiment

Sorption measurement of CO_2 gas was carried out using a gravimetric sorption analyzer (GHP-FS, with a Cahn D-200 balance, VTI Scientific Instruments, Florida) operated in a static mode at 35 ^oC with 10 pressure points between 0 - 20 bar. At each pressure level, the system was allowed to equilibrate for 1 h until a constant mass of adsorbed CO_2 by the membrane was achieved. CO_2 sorption isotherms as a function of feed pressure were determined. The detailed CO_2 sorption measurement protocol is given in

chapter 3, section 3.6.3. Equation (6.6) was used to convert the mass of adsorbed CO_2 (m_a) in g/g to concentration (C) in cm^3 (STP)/cm^3 polymer (Hölck et. al., 2006).

$$C = \frac{V_{id} m_a \rho_o}{M_{CO_2} m_o} \tag{6.6}$$

Where

V_{id} = Volume of an ideal gas at STP = 22400 cm^3

ρ_o = density of the polymer prior to any measurement

M_{CO2} = molar mass of CO_2

m_o = mass of the polymer prior to any measurement

Analysis of sorption data for the determination of dual-mode sorption parameters in Equation (6.3) was carried out using the graphical method as follows (Koro et al. 1976; Kanehashi and Nagai, 2005):

- k_d which represents the CO_2 dissolved in the polymer matrix at equilibrium was obtained from the gradient of linear asymptote of the sorption data at high pressure.
- C_h representing the CO_2 concentration in the polymer matrix based on Langmuir sorption was obtained from Equation (6.3) to form Equation (6.7);

$$C_h = C - k_d p \tag{6.7}$$

- Equation (6.2) was written in form of linear equation (y = mx + c) as shown in Equation (6.8);

$$\frac{p}{C_h} = \frac{p}{C_h'} + \frac{1}{C_h' b} \tag{6.8}$$

- $\frac{p}{C_h}$ was plotted against p. From the graph, the following parameters were obtained;

$$C_h' = \frac{1}{gradient}$$

$$b = \frac{1}{y - intercept \times C_h'}$$

- Graphs obtained from the analysis of sorption data for each synthesized membrane are presented in Appendix G.

6.2.2 Pure CO_2 gas permeation experiment at elevated pressure

Pure CO_2 gas permeation experiment was conducted using constant volume variable pressure (CVVP) technique. The initial feed pressure was set at 2 bar and increased at 2 bar interval up until 20 bar [It is important to state that the typical partial pressure of CO_2 in most natural gas wells is around 5-10 bar (Baker, 2002)]. Each pressure point was kept for 60 min before the increase to another pressure level, this is to allow the system to equilibrate until a constant mass of adsorbed CO_2 by the membrane was achieved. The temperature was kept constant at 35^o C throughout the experiment. The detailed experimental protocol for the gas permeation is given in chapter 3, section 3.6.1.

6.3 Model development

6.3.1 Theory

Gas transport in a dense membrane is usually governed by a solution-diffusion mechanism (Kanehashi and Nagai, 2005). According to the mechanism, permeability (P) can be expressed as the product of the diffusion coefficient (D_d) and the solubility coefficient (S).

$$P = D_d S \tag{6.9}$$

From Equation (6.5)

$$S = k_d + \frac{C_h' b}{1+bp}$$

Petropoulos (1970) and Paul and Koros (1976) observed that a fraction (F) of the gas held in Langmuir sites have mobility within the membrane. Equation 6.5 then becomes;

$$S = k_d + \frac{F C_h' b}{1+bp} \tag{6.10}$$

F has also been described as the ratio of the diffusivity through the Langmuir sites (microvoids) to the diffusivity through the Henry's Law sites (polymeric matrix) (Scholes et al., 2010).

Substituting Equation (6.10) into Equation (6.9)

$$P = k_d D_d \left(1 + \frac{FC_h^{'} b}{k_d(1+bp)}\right) \quad (6.11)$$

i. If there is total immobilization of penetrant in Langmuir sites, F = 0

$$P = k_d D_d$$

This should result in constant permeability with pressure.

ii. If there is no immobilization of gas held in Langmuir sites, F is unity

$$P = k_d D_d \left(1 + \frac{C_h^{'} b}{k_d(1 + bp)}\right)$$

This should result in a sharp decrease in permeability with pressure.

iii. If there is partial immobilization of penetrant in Langmuir sites, F < 1

$$P = k_d D_d \left(1 + \frac{FC_h^{'} b}{k_d(1 + bp)}\right)$$

This should result in a slight decrease in permeability with pressure.

From the CO_2 permeability results obtained in this study, the synthesized MMMs tends to follow partly theory (ii) and partly theory (iii).

6.3.2 Assumptions and model equations

The synthesized MMMs have three difference interface interactions:

a) Polymer matrix – polymer matrix interface interaction
b) CNT – polymer matrix interface interaction
c) Aligned CNT – CNT interface interaction

Assumption 1: There is partial immobilization of CO_2 in Langmuir sites of polymer matrix – polymer matrix and CNT – polymer matrix interface interactions.

Assumption 2: There is no immobilization of CO_2 held in Langmuir sites of aligned CNT – CNT interface interaction due to inherent smoothness of CNTs.

Assumption 3: Mobile species of CO_2 follow one-dimensional transport and permeability is measured at steady state.

Fick's law for one-dimensional transport can be expressed as Equation (6.12) to account for mobile species of the gas.

$$J = -D(C_m)\frac{dC_m}{dx} \tag{6.12}$$

$$C_m = C_d + FC_h + \emptyset C_h \tag{6.13}$$

Where C_m is the total mobile gas in the membrane, C_d is Henry's law sites contribution to the gas mobility, FC_h is the partial immobilization contribution from the Langmuir sites of polymer matrix – polymer matrix and CNT – polymer matrix interface interactions and $\emptyset C_h$ is the no immobilization contribution from the Langmuir sites of aligned CNT – CNT interface interaction, $\emptyset$ is the fraction of FCNTs dispersed into the polymer matrix.

From Equations (6.1) and (6.2)

$$C_d = k_d p$$

$$C_h = \frac{C_h' bp}{1+bp}$$

Substituting Equations (6.1) and (6.2) into (6.13) results into Equation (6.14)

$$C_m = K_d\left(1 + \frac{(F+\emptyset)K}{1+bp}\right) \tag{6.14}$$

Where $K = \frac{C_h' b}{K_d}$

For penetrant induced plasticization of a glassy polymer, the diffusion coefficient is concentration dependent and it is often assumed to be an exponential function of C_m (Stern and Saxena, 1980).

$$D(C_m) = D_o \exp(\beta C_m) \tag{6.15}$$

Where D_o is the diffusion coefficient as C_m tends to zero and β is an empirical constant representing the plasticization potential of the gas – polymer system.

Substitute Equation (6.15) into Equation (6.12):

$$J = -D_o \exp(\beta C_m)\frac{dC_m}{dx} \tag{6.16}$$

Applying the exponential rule of differentiation to Equation (6.16) gives:

$$J = \frac{D_o}{\beta}\frac{d}{dx}[\exp(\beta C_m)] \tag{6.17}$$

In this study, permeation of gas across the membrane of thickness (L) occurs at upstream pressure p_2 as the downstream pressure, p_1, approaches zero i.e $p_2 >> p_1$. The effective permeability, P_{eff}, is usually given as Equation (6.18) (Zhou and Stern, 1989):

$$P_{eff} = \frac{J_s L}{p_2} \tag{6.18}$$

Where J_s is the steady-state flux of gas through the membrane.

For steady-state conditions (dC/dt = 0), integral solution of Equation (6.17) with boundary conditions:

x = 0 $C_m = C_{m2}$ (for $p = p_2$)

x = L $C_m = C_{m1} = 0$ (for $p = p_1 = 0$)

yields Equation (6.19):

$$J_s = \frac{D_o[\exp(\beta C_{m2})-1]}{\beta L} \tag{6.19}$$

Substituting Equations (6.14) and (6.19) into Equation (6.18) gives:

$$P_{eff} = \frac{D_0}{\beta p_2}\left\{exp\left[\beta k_d p_2\left(1 + \frac{(F+\emptyset)K}{1+bp_2}\right)\right] - 1\right\} \quad (6.20)$$

Let $z = k_d p_2\left(1 + \frac{(F+\emptyset)K}{1+bp_2}\right)$

$$P_{eff} = \frac{D_0}{\beta p_2}\{exp(z\beta) - 1\} \quad (6.21)$$

From Maclaurin series (Kreyszig, 2007):

$$\exp(z) = \sum_{n=1}^{\infty} \frac{z^n}{n!} = 1 + z + \frac{z^2}{2!} + \cdots \quad (6.22)$$

Applying equation (6.22) to equation (6.21) gives:

$$P_{eff} = \frac{D_0}{\beta p_2}\left\{1 + z\beta + \frac{(z\beta)^2}{2!} + \cdots\right\} - \frac{D_0}{\beta p_2} \quad (6.23)$$

Considering equation (6.23) for the following cases:

1. For polymeric membrane without a filler and that undergoes plasticization

$\emptyset = 0$ $\beta > 0$

Equation (6.23) becomes:

$$P_{eff} = \frac{D_0}{\beta p_2}\left\{exp\left[\beta k_d p_2\left(1 + \frac{FK}{1+bp_2}\right)\right] - 1\right\} \quad (6.24)$$

2. For MMM that is not undergoing plasticization

$$\emptyset > 0 \qquad \beta \rightarrow 0$$

Equation (6.23) becomes:

$$P_{eff} = k_d D_o\left[1 + \frac{(F+\emptyset)K}{1+bp_2}\right] \quad (6.25)$$

Equations (6.24) and (6.25) were solved by using Levenberg-Marquardt algorithm in the Matlab environment to obtain the plasticization potential (β) and the fraction (F) of the gas held in Langmuir sites that have mobility within the membrane. K and k_d values were obtained from the sorption experimental data, P_{eff} and p_2 values were obtained from the permeability-pressure results.

6.4 Experimental results and discussion

6.4.1 Effect of FCNT on CO_2 sorption isotherms of synthesized membranes

Figure 6.1 showed a typical dual-mode sorption model behaviour for all the types of synthesized membranes (Kanehashi and Nagai, 2005; Hölck et. al., 2006). From the figure, it was observed that the CO_2 concentration increases rapidly at low pressures, which indicates a hole-filling of the Langmuir sites (microvoids). At higher pressure,

the rate of increase in the concentration declines due to the saturation of the microvoids, the further increase in the concentration at higher pressure is because of the gas sorption in Henry's law sites (polymer matrix). The CO_2 concentration in pure PSF was similar to those of MMMs at low pressures. As pressure increases, the CO_2 concentration in pure PSF deviates farther from those MMMs. This could be due to the formation of new microvoids at higher pressure for more sorption to take place, and also possible mobility of the polymer matrix. This means that pure PSF is likely to have been plasticized at higher CO_2 pressure. The MMMs showed similar CO_2 concentration throughout the pressure range irrespective of the % loading of FCNTs.

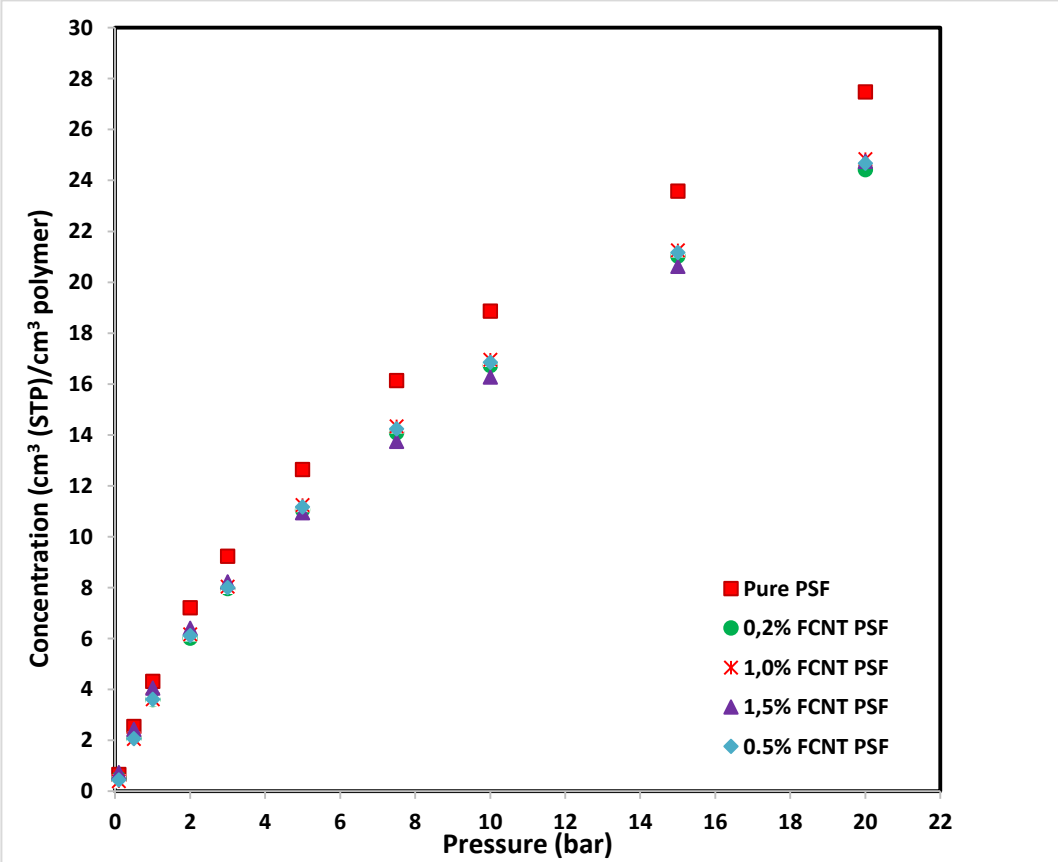

Figure 6.1: CO_2 sorption isotherms of synthesized membranes at 35 ^oC

The dual-mode sorption model parameters as obtained from the graphical method is presented in Table 6.1. The parameters for pure PSF are similar to those reported in the literature using a non-linear regression algorithm (Erb and Paul, 1981; Scholes et al., 2010). The model CO_2 sorption isotherms based on Equation (6.3) and the dual-mode sorption model parameters were compared with the experimental isotherms and displayed in Figure 6.2. The model isotherms fitted well with the experimental isotherms. This means that the graphical method used to obtain the dual-mode sorption model parameters is efficient. From Table 6.1, k_d and C_h' of MMMs are lower than that of pure PSF. For k_d, this could be attributed to the smoothness of FCNTs within the polymer chains which reduces the ability of the CO_2 to associate with the chain (Kiadehi et al., 2015). In the case of C_h', the could be due to the reduction in the microvoid volume (Scholes et al., 2010) because of the dispersion of FCNTs into the pores of the polymer as shown by depth-at-max analysis of the AFM images of the membranes (chapter 5 section 5.3.2). b did not give any particular trend. The reason for this could not be ascertained.

Table 6.1: Dual-mode sorption model parameters of synthesized membranes

Polymer	k_d **(cm^3 STP)/cm^3 bar)**	C_h' **(cm^3(STP)/cm^3 bar)**	b **(bar^{-1})**
Pure PSF	0.86	11.74	0.48
0.2 FCNT-PSF	0.77	10.55	0.54
0.5 FCNT-PSF	0.78	10.64	0.40
1.0 FCNT-PSF	0.79	10.71	0.38
1.5 FCNT-PSF	0.79	10.01	0.48

The effect of pressure on the solubility of CO_2 in the membranes is depicted in Figure 6.3. From Equation (6.4), Solubility is inversely proportional to pressure, hence, increase pressure reduces the solubility of the gas in the membranes as shown in the figure. The solubility of CO_2 in the membranes drops significantly with an increase in pressure within the low-pressure region but tends to level off in the high-pressure region. This shows that the effect of pressure on the solubility of CO_2 in the Langmuir sites is substantial at low pressures, but is negligible at high pressures once all the microvoids are filled by the penetrant (Chung et al., 2004).

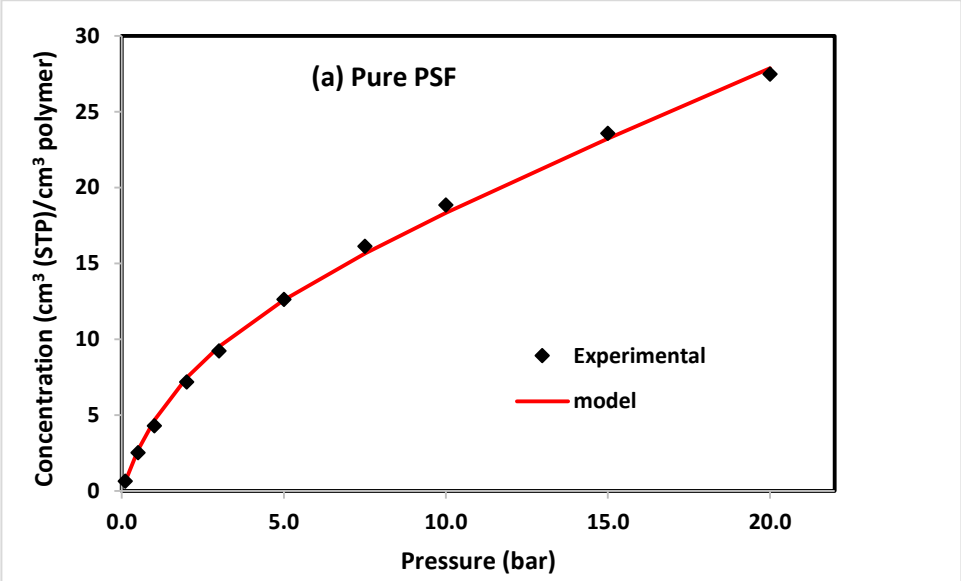

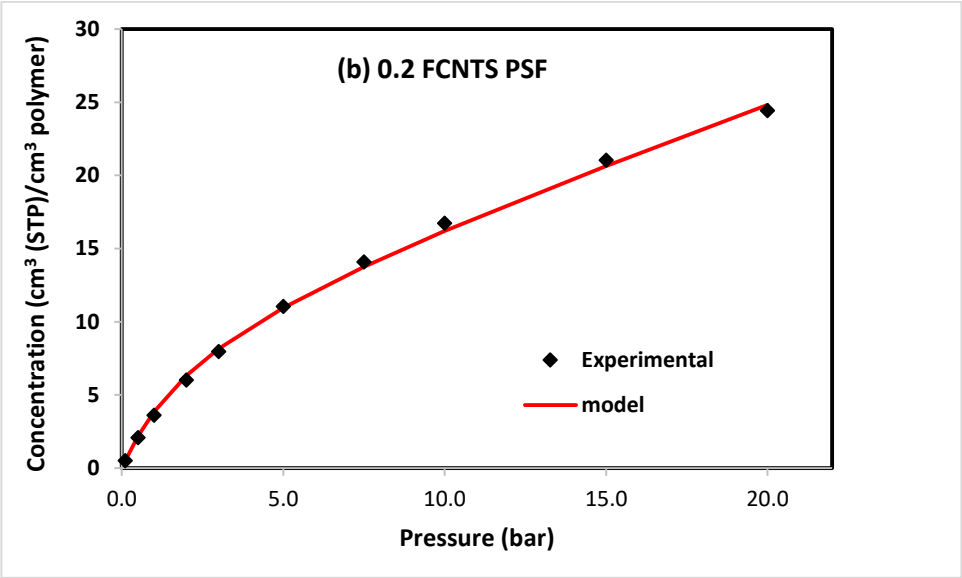
(b) 0.2 FCNTS PSF
Concentration (cm³ (STP)/cm³ polymer)
Pressure (bar)
Experimental
model
0
5
10
15
20
25
30
0.0
5.0
10.0
15.0
20.0

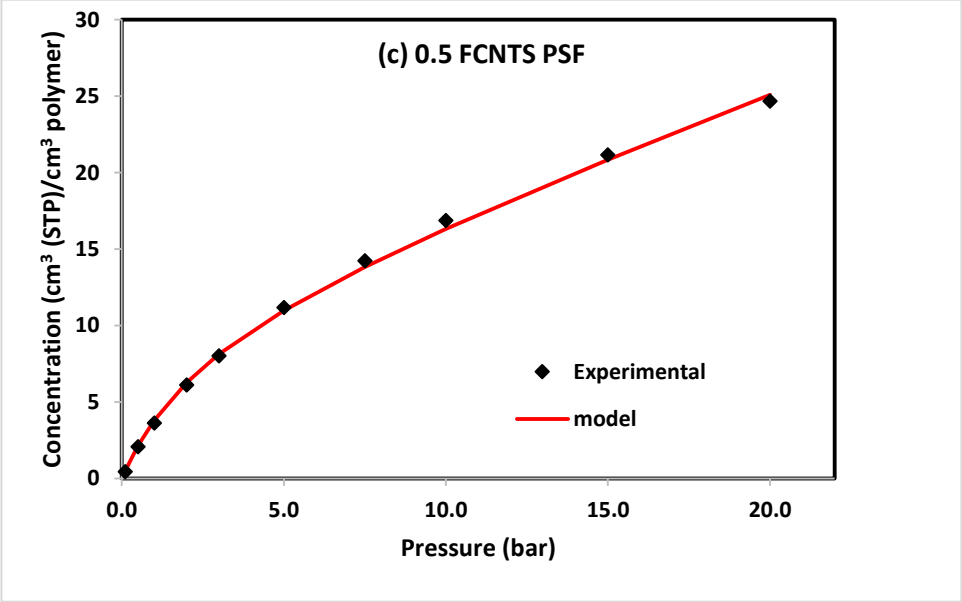
(c) 0.5 FCNTS PSF
Concentration (cm³ (STP)/cm³ polymer)
Pressure (bar)
Experimental
model
0
5
10
15
20
25
30
0.0
5.0
10.0
15.0
20.0

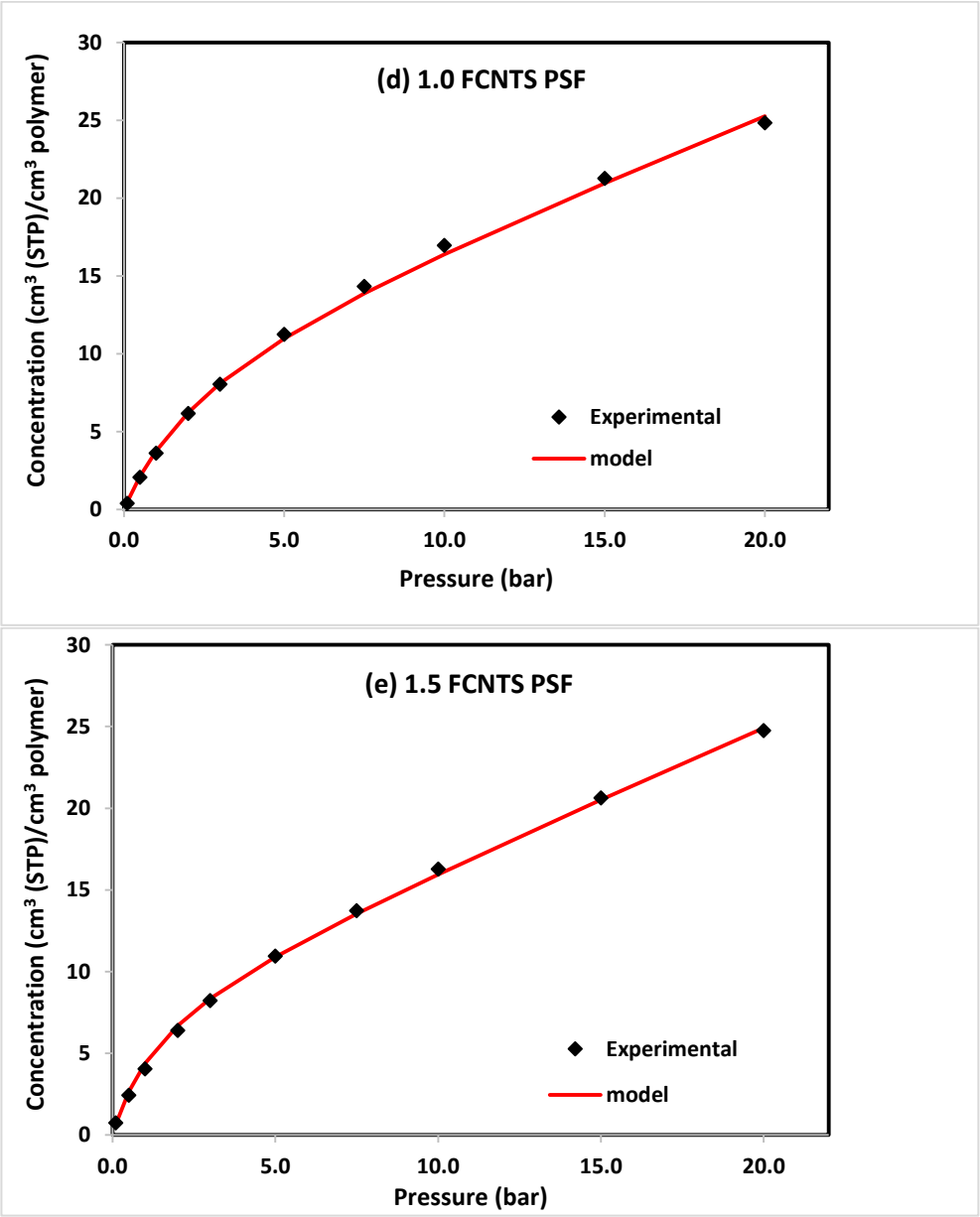

Figure 6.2: Experimental and model CO_2 sorption isotherms

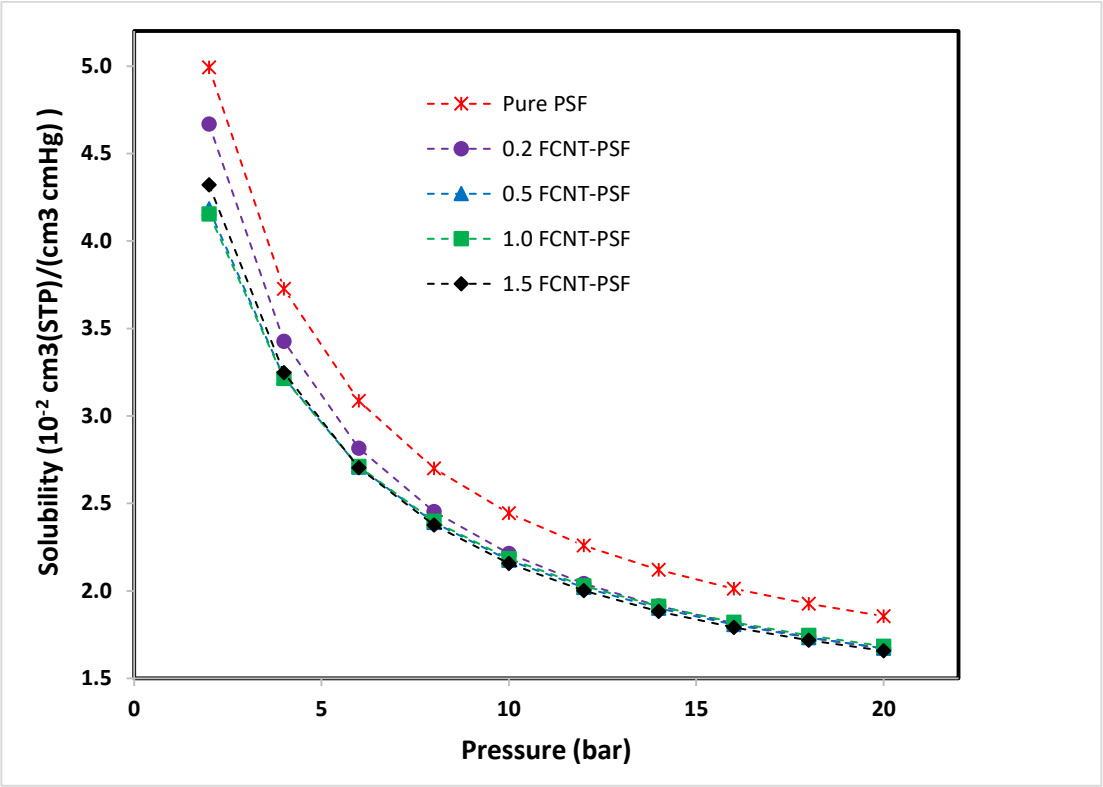

Figure 6.3: Effect of pressure on the solubility of CO_2 in the membranes at 35 ^oC

6.4.2 Effect of FCNT on CO_2 induced plasticization pressure of synthesized membranes

The CO_2 permeation isotherms of the synthesized membranes are shown in Figure 6.4. The isotherms represented a standard permeability-pressure curve for a polymeric membrane with a gradual decrease in permeability as the pressure increases from 2 bar to 12 bar (Minelli and Sarti, 2013). Although, for 1.5 FCNT-PSF, a sharp decline in CO_2 permeability was observed with increasing pressure from 2 bar to 8 bar. This could be attributed to reduced dissolution of CO_2 within the polymer matrix because of the agglomeration of FCNTs. Further increase in CO_2 pressure above 12 bar showed an increase in CO_2 permeability of pure PSF membrane. This indicates an onset of CO_2 induced plasticization of the membrane. The plasticization pressure of pure PSF is therefore 12 bar. Scholes et al. (2010) reported similar plasticization pressure for PSF

in their study. MMMs showed no sign of plasticization over the range of pressure tested. This could be due to enhanced chain rigidity of MMMs (Zhang et al., 2019). This means that the addition of FCNTs to PSF has improved the CO_2 induced plasticization resistance of the MMMs. Detailed tables of CO_2 permeability and solubility at elevated pressure are shown in Appendix H.

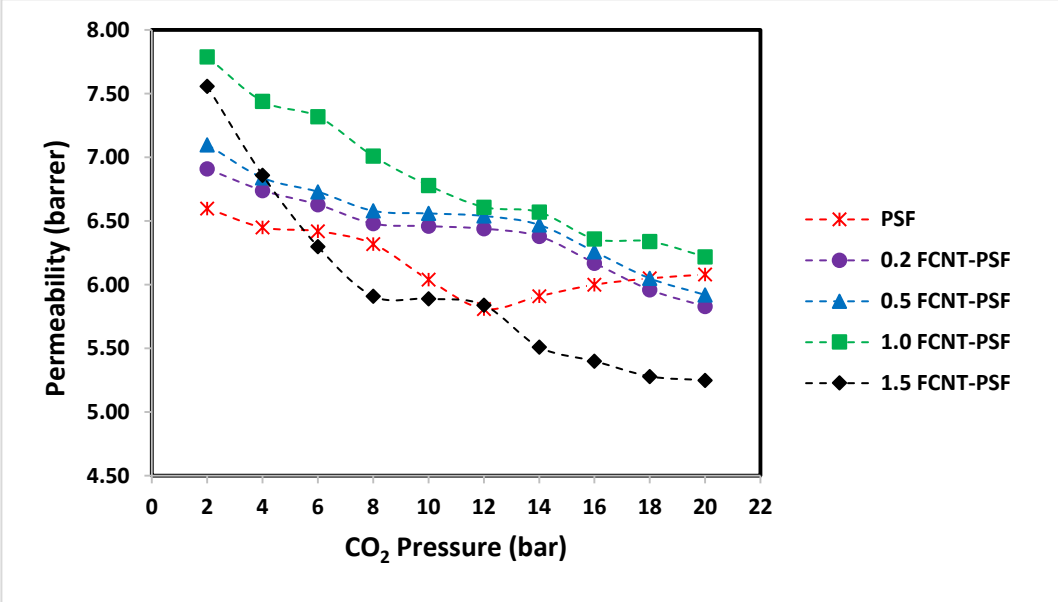

Figure 6.4: Pure CO_2 permeability isotherms at 35 ^oC of the synthesized membranes

6.5 Model results and discussion

The model equations were solved using a Levenberg-Marquardt nonlinear regression algorithm to obtain the plasticization potential of pure PSF (β) and the fraction of CO_2 held in Langmuir sites that have mobility (F) with 95% confidence bounds. β is an empirical parameters which describes the relative potential of condensable penetrant to plasticize polymeric membranes (Scholes et al., 2010). β of pure PSF obtained from equation (6.24) was 0.052 at 35 ^oC. Lock et al. (2018) reported 0.054 for β of their pure PSF at 35 ^0C. This result is similar to the β obtained for this work. The slight variation may be due to PSF to solvent ratio in their work which was 1:4 while for this work,

PSF to solvent ratio was 1:10. Figure 6.5 showed experimental and model CO_2 permeability isotherms of the synthesized membranes at 35 ^oC and the coefficient of determination (R^2). R^2 is an expression of how much variance of the experimental data is explained by the model. Model CO_2 permeability is in good agreement with experimental CO_2 permeability. While R^2 does not tell the whole story about the accuracy of a model, the values of F obtained from the model equation (6.25) support the solution-diffusion phenomenon in polymeric membranes.

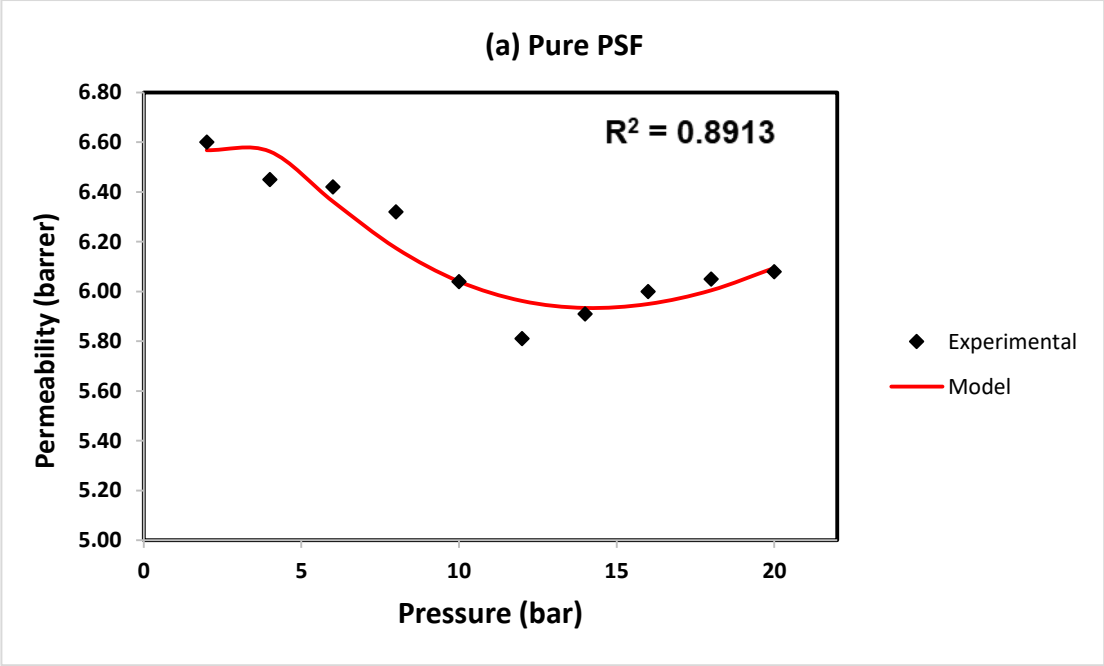

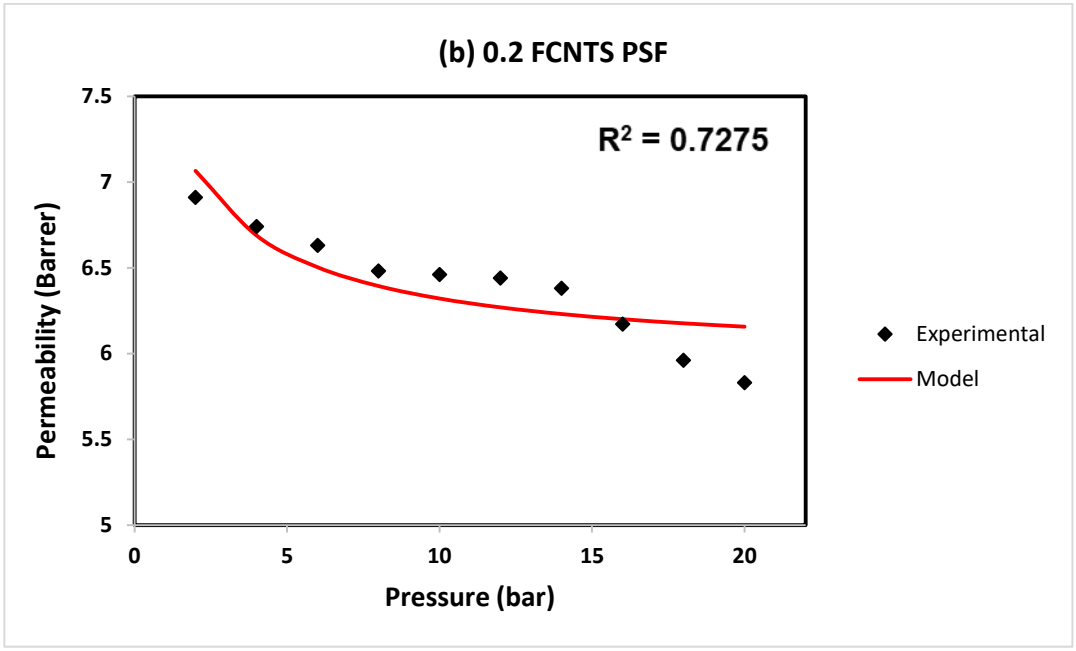
(b) 0.2 FCNTS PSF
R² = 0.7275
Permeability (Barrer)
Pressure (bar)
Experimental
Model
7.5
7
6.5
6
5.5
5
0
5
10
15
20

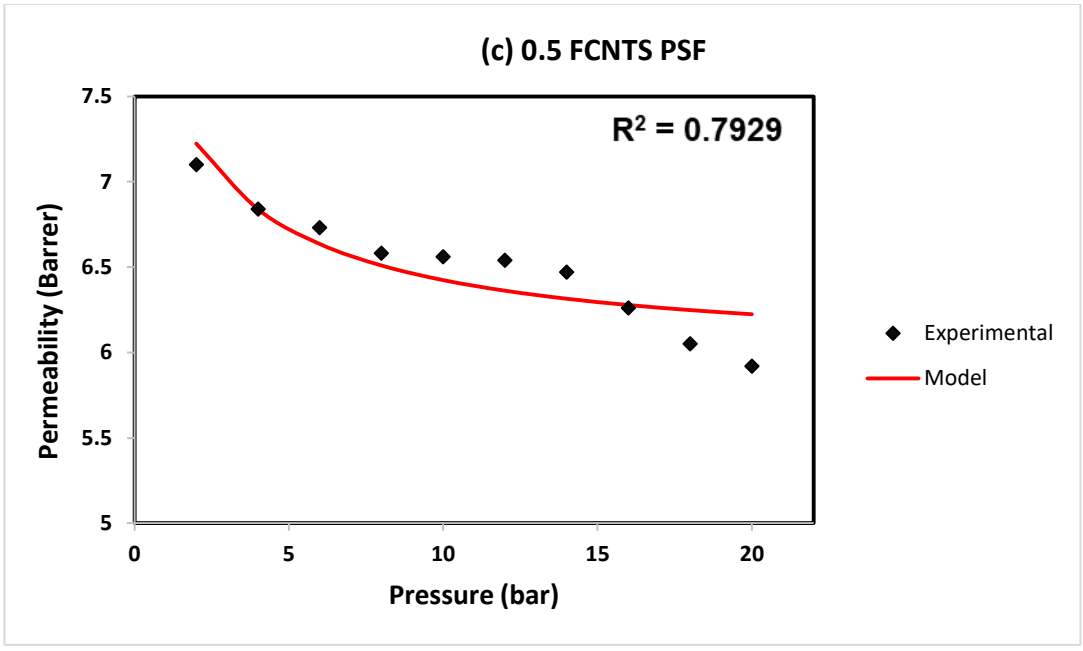
(c) 0.5 FCNTS PSF
R² = 0.7929
Permeability (Barrer)
Pressure (bar)
Experimental
Model
7.5
7
6.5
6
5.5
5
0
5
10
15
20

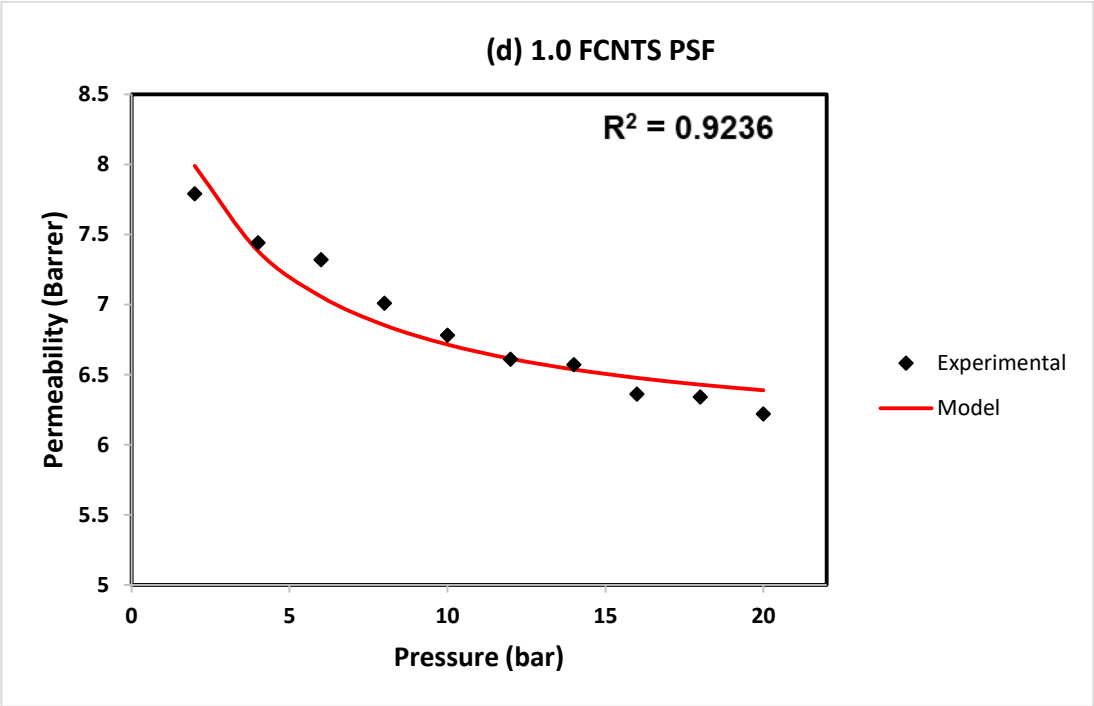

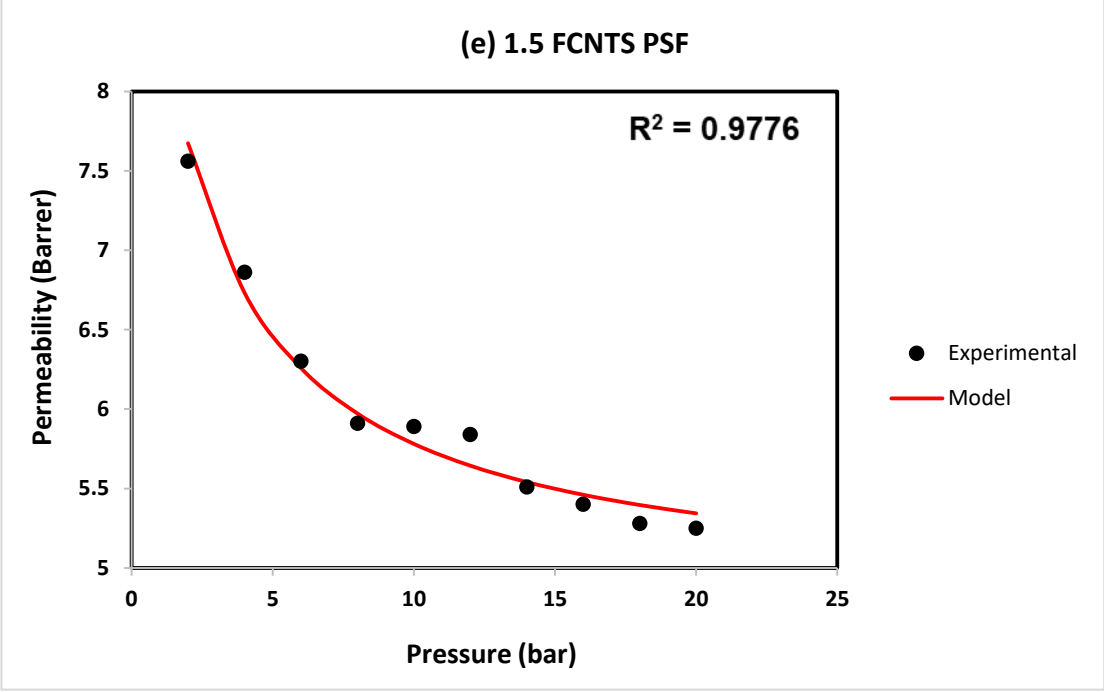

Figure 6.5: Experimental and model CO_2 permeability isotherms at 35 ^oC of the synthesized membranes

6.5.1 Effect of FCNT on the fraction of CO_2 held in Langmuir sites that have mobility

The fraction of CO_2 held in Langmuir sites that have mobility (F) is a measure of the ratio of the diffusivity through the Langmuir sites (microvoids) to the diffusivity through the Henry's Law sites (polymeric matrix). It is an indication of the size and the number of microvoids that exist within a membrane (Lock et al., 2018). The higher the value of F is, the more is the contribution of diffused gas through the Langmuir sites to the overall gas mobility through the membranes. From Table 6.2, F increases with an increase in the wt. % loading of FCNTs in the membrane. This could be attributed to an increase in sizes and numbers of microvoid existing within the membrane as the amount of FCNTs dispersed in the pure PSF increases. The increase in the size and the number of the microvoid provides more sorption sites for the penetrant thereby increasing the penetrant permeability through the membrane as seen in experimental CO_2 permeability results in Figure 6.4. However, 1.5 wt. % FCNT PSF has higher F than 1.0 wt. % FCNT PSF but its experimental CO_2 permeability is lower than that of 1.0 wt. % FCNT PSF. This could be due to the reduced dissolution of CO_2 within the polymer matrix of 1.5 wt. % FCNT PSF because of the agglomeration of FCNTs shown in Figure 5.2 (chapter 5). This causes a decrease in the contribution of gas dissolution within the polymer matrix to the overall gas mobility in the membrane. Pure PSF has the least value of F, this means that more penetrant is immobilized within microvoids of the membrane. As the concentration of CO_2 immobilized within the microvoid reaches a critical point, there could be swelling of the polymer due to disruption in polymer chain packing (Zhuang et al., 2018). Hence, there is plasticization in pure PSF.

Table 6.2: Immobilization factors for the synthesized membranes at 35 ºC

Membrane	F
Pure PSF	0.048
0.2 FCNT-PSF	0.050
0.5 FCNT-PSF	0.064
1.0 FCNT-PSF	0.105
1.5 FCNT-PSF	0.176

6.6 Concluding remarks

This chapter investigated the effect of the addition of FCNTs to PSF on the CO_2 induced plasticization resistance of the MMM using sorption and permeation experiments at elevated pressure, and mathematical modelling. Sorption experiments reveal a higher concentration of CO_2 in the pure PSF as compared to the MMMs. This could lead to plasticization of pure PSF once the CO_2 concentration reaches a critical point. Furthermore, the rate of increase of CO_2 concentration in pure PSF membrane at high pressures suggested a likelihood of formation of new microvoids due to plasticization, which accounted for the additional sorption at high pressure along with the dissolution in the polymer matrix (Henry's law sites). CO_2 permeability isotherm of pure PSF indicated an onset of plasticization at CO_2 pressure of 12 bar. However, MMMs showed no indication of plasticization over the pressure range tested. Three possible interface interaction in MMMs were considered in developing a phenomenological model that describes the plasticization potential and the fraction of the gas held in Langmuir sites that have mobility within the membrane. The model CO_2 permeability is in good agreement with experimental CO_2 permeability. The plasticization potential of PSF obtained is consistent with the values available in the literature. In addition, the fraction of the gas held in Langmuir sites that have mobility within the membrane increases with an increase in FCNT wt. % loading which shows high diffusivity through the microvoids with respect to diffusivity through the polymer

matrix. This is an indication of an increase in Langmuir sorption sites for the penetrant thereby improving the penetrant permeability.

For quick dissemination of these results, a manuscript is currently under review at Chemical Engineering Journal.

References

Baker, R.W., 2002. Future directions of membrane gas separation technology. *Industrial & Engineering Chemistry Research*, *41*(6), pp.1393-1411.

Balçık, M. and Ahunbay, M.G., 2018. Prediction of CO2-induced plasticization pressure in polyimides via atomistic simulations. *Journal of Membrane Science*, *547*, pp.146-155.

Barrer, R.M., 1984. Diffusivities in glassy polymers for the dual mode sorption model. *Journal of Membrane Science*, *18*, pp.25-35.

Bos, A., Pünt, I.G.M., Wessling, M. and Strathmann, H., 1999. CO2-induced plasticization phenomena in glassy polymers. *Journal of Membrane Science*, *155*(1), pp.67-78.

Chen, X.Y., Vinh-Thang, H., Ramirez, A.A., Rodrigue, D. and Kaliaguine, S., 2015. Membrane gas separation technologies for biogas upgrading. *RSC Advances*, *5*(31), pp.24399-24448.

Chung, T.S., Cao, C. and Wang, R., 2004. Pressure and temperature dependence of the gas-transport properties of dense poly [2, 6-toluene-2, 2-bis (3, 4-dicarboxylphenyl) hexafluoropropane diimide] membranes. *Journal of Polymer Science Part B: Polymer Physics*, *42*(2), pp.354-364.

Dong, G., Li, H. and Chen, V., 2011. Plasticization mechanisms and effects of thermal annealing of Matrimid hollow fiber membranes for CO2 removal. *Journal of Membrane Science*, *369*(1-2), pp.206-220.

Erb, A.J. and Paul, D.R., 1981. Gas sorption and transport in polysulfone. *Journal of Membrane Science*, *8*(1), pp.11-22.

Hölck, O., Siegert, M.R., Heuchel, M. and Böhning, M., 2006. CO2 sorption induced dilation in polysulfone: comparative analysis of experimental and molecular modeling results. *Macromolecules*, *39*(26), pp.9590-9604.

Hu, C.C., Chang, C.S., Ruaan, R.C. and Lai, J.Y., 2003. Effect of free volume and sorption on membrane gas transport. *Journal of Membrane Science*, *226*(1-2), pp.51-61.

Kanehashi, S. and Nagai, K., 2005. Analysis of dual-mode model parameters for gas sorption in glassy polymers. *Journal of Membrane Science*, *253*(1-2), pp.117-138.

Kesting, R.E. and Fritzsche, A.K., 1993. *Polymeric gas separation membranes* (pp. 61-233). New York: Wiley.

Kiadehi, A.D., Rahimpour, A., Jahanshahi, M. and Ghoreyshi, A.A., 2015. Novel carbon nano-fibers (CNF)/polysulfone (PSf) mixed matrix membranes for gas separation. *Journal of Industrial and Engineering Chemistry*, *22*, pp.199-207.

Koros, W.J., Paul, D.R. and Rocha, A.A., 1976. Carbon dioxide sorption and transport in polycarbonate. *Journal of Polymer Science: Polymer Physics Edition*, *14*(4), pp.687-702.

Kreyszig, E., 2007. *Advanced Engineering Mathematics*. John Wiley & Sons.

Lock, S.S.M., Lau, K.K., Shariff, A.M., Yeong, Y.F. and Jusoh, N., 2018. Experimental Study of CO2 Plasticization in Polysulfone Membrane for Biogas Processing. In *Biogas*. IntechOpen.

Mauze, G.R. and Stern, S.A., 1984. The dual-mode solution of vinyl chloride monomer in poly (vinyl chloride). *Journal of Membrane Science*, *18*, pp.99-109.

Minelli, M. and Sarti, G.C., 2013. Permeability and solubility of carbon dioxide in different glassy polymer systems with and without plasticization. *Journal of Membrane Science*, *444*, pp.429-439.

Paul, D. R. and Koros, W. J., 1976. Effect of partially immobilized sorption on permeability and the diffusion time lag, *Journal of Polymer Science Part B: Polymer Physics*, vol. 14, pp. 675–685.

Petropoulos, J.H., 1970. Quantitative analysis of gaseous diffusion in glassy polymers. *Journal of Polymer Science Part A-2: Polymer Physics*, *8*(10), pp.1797-1801.

Petropoulos, J.H., 1992. Plasticization effects on the gas permeability and permselectivity of polymer membranes. *Journal of Membrane Science*, *75*(1-2), pp.47-59.

Scholes, C.A., Chen, G.Q., Stevens, G.W. and Kentish, S.E., 2010. Plasticization of ultra-thin polysulfone membranes by carbon dioxide. *Journal of Membrane Science*, *346*(1), pp.208-214.

Stern, S.A. and Saxena, V., 1980. Concentration-dependent transport of gases and vapors in glassy polymers. *Journal of Membrane Science*, *7*(1), pp.47-59.

Vieth, W.R. and Sladek, K.J., 1965. A model for diffusion in a glassy polymer. *Journal of Colloid Science*, *20*(9), pp.1014-1033.

Xiao, Y., Low, B.T., Hosseini, S.S., Chung, T.S. and Paul, D.R., 2009. The strategies of molecular architecture and modification of polyimide-based membranes for CO2 removal from natural gas—A review. *Progress in Polymer Science*, *34*(6), pp.561-580.

Zhang, M., Deng, L., Xiang, D., Cao, B., Hosseini, S.S. and Li, P., 2019. Approaches to Suppress CO2-Induced Plasticization of Polyimide Membranes in Gas Separation Applications. *Processes*, *7*(1), p.51.

Zhou, S. and Stern, S.A., 1989. The effect of plasticization on the transport of gases in and through glassy polymers. *Journal of Polymer Science Part B: Polymer Physics*, *27*(2), pp.205-222.

Zhuang, G.L., Tseng, H.H., Uchytil, P. and Wey, M.Y., 2018. Enhancing the CO_2 plasticization resistance of PS mixed-matrix membrane by blunt zeolitic imidazolate framework. *Journal of CO2 Utilization*, *25*, pp.79-88.

CHAPTER 7

7 CONCLUSIONS AND RECOMMENDATIONS

7.1 Conclusions

The aim of this study was to synthesize dense mixed matrix membrane (MMM) with an excellent balance of permeability, selectivity and CO_2 induced plasticization resistance during natural gas separations, especially separation of CO_2/CH_4 mixture. This was achieved by the addition of functionalized carbon nanotube (FCNT) to polysulfone to fabricate the MMM.

Raw CNTs (RCNTs) were produced by catalyst chemical vapour deposition (CCVD) method. Impacts of types of carbon source used and production conditions were investigated. CNTs produced from a mixture of acetylene and argon showed the presence of more carbon nanoballs than CNTs. This could be attributed to the deactivation of the catalyst nucleation site for the growth of CNTs due to carbon deposition on the catalyst active site. The maximum yield of 1.15 mg/s was achieved at 850 ^oC and the yield decreased with increase in temperature from 850 ^oC to 1000 ^oC. This could be as a result of the loss of catalyst activity due to the sintering effect. Addition of hydrogen to acetylene and argon showed the presence of more CNTs in the samples with increasing yield up to 1.78 mg/s as the temperature increases to 1000 ^oC. This showed that the addition of hydrogen reduced catalyst deactivation caused by carbon deposition and sintering effect. Methane was used as the carbon source together with argon as a carrier gas, the result showed an improved CNT quality with I_D/I_G ratio of 0.17 at 900 ^oC reactor temperature. However, the yield was lower than the yield from acetylene as a carbon source. The maximum yield obtained was 0.31 mg/s at 900 ^oC. This could be attributed to less reactivity of methane compared to acetylene, and the number of carbon in acetylene is twice that of methane.

To improve the dispersion of CNTs within the polymer matrix and to enhance intermolecular interaction between CO_2 and the CNTs, the best of the as-produced CNTs was functionalized using carboxylation protocol. The CNTs were first purified

to remove the iron residue and amorphous carbon from RCNTs. Thereafter, carboxyl group was attached to purified CNTs (PCNTs) by the acid oxidation reaction. Thermogravimetric analysis (TGA) of PCNT showed an improvement in its purity compared to RCNT. TGA also gave a quantitative analysis of the degree of functionalization of FCNT. Fourier transform infrared spectroscopy (FTIR) confirmed the presence of carboxyl functional group on FCNT. Nitrogen adsorption and desorption isotherms of RCNT, PCNT, and FCNT at 77 K showed Type IV physisorption isotherms with a characteristic H1 hysteresis as classified by IUPAC. This classification means that most pores of the CNTs are in mesopore sizes. Furthermore, BET analysis of the textural properties showed an increase in pore volume and average pore size of FCNTs as compared to PCNTs and RCNTs. These characteristics could enhance the transport properties of FCNT reinforced polymeric membranes when compared to that of non-reinforced polymeric membranes. The X-ray diffraction (XRD) patterns reveal that purification and functionalization of RCNT preserve its crystallographic characteristics. However, interatomic distances of FCNT was altered.

MMMs were synthesized by incorporating FCNTs at different wt. % (0.2, 0.5, 1.0, and 1.5) into polysulfone (PSF) using evaporation method. Field emission scanning electron microscope (FESEM) micrographs of surface and cross-sectional morphologies of the synthesized membranes showed that they have a dense structure with non-continuous pores. The micrographs also revealed that FCNTs were well dispersed into the polymer matrix with agglomeration of FCNTs only noticeable at 1.5 wt. % loading of FCNTs. Atomic force microscope (AFM) images also corroborated the non-continuous porosity of the membranes. The depth-at-max of the AFM height images are much smaller than the thickness of the membranes. Furthermore, an addition of FCNTs to PSF improved the thermal stability and mechanical properties of the MMMs. TGA showed an improved decomposition temperature of the MMMs compared to pure PSF membrane, but increase in FCNT wt. % loading did not enhance the decomposition temperature. A similar pattern was observed for the glass transition

temperature (T_g) of the membranes as determined by differential scanning calorimeter (DSC). Tensile strength and Young's modulus of the membranes were measured using texture analyzer (TA). 0.2 wt. % FCNT-PSF has maximum tensile strength and maximum Young's modulus of 46.1 MPa and 668 MPa, respectively.

Single gas permeation results show an increase in CO_2 permeability with an increase in FCNTs wt. % loading with the highest CO_2 permeability achieved at 1.0 wt. %. CO_2 permeability decreased for 1.5 wt. % FCNT-PSF. This could be attributed to the agglomeration of FCNTs within the polymer matrix. The ideal selectivity of CO_2/CH_4 decreased with increase in FCNTs. This could be due to excess free volume created by the addition of FCNTs to the polymeric membrane which increased the flux of both CO_2 and CH_4. However, mixed gas separation performance of the MMMs for both 10%/90% and 50%/50% CO_2/CH_4 mixtures displayed a significant increase in CO_2 permeability without sacrificing CO_2/CH_4 selectivity. This could be as a result of interaction between carboxyl group covalently bounded to FCNTs and CO_2, giving CO_2 additional sorption competitive advantage over CH_4.

CO_2 sorption measurements reveal a higher concentration of CO_2 in pure PSF membranes as compared to the MMMs as the pressure increases. This showed that pure PSF membrane is more susceptible to plasticization than MMMs. However, the increase in FCNT wt. % loading did not significantly affect the CO_2 concentration within the MMMs. CO_2 gas permeation experiment at elevated feed pressure indicates the plasticization pressure of pure PSF membrane as 12 bar. Above the pressure of 12 bar, the CO_2 permeability of pure PSF membrane increases gradually and continuously throughout the pressure tested (14 - 20 bar). MMMs showed no sign of plasticization within the pressure range tested (0 – 20 bar). This indicates that the addition of FCNT to PSF improved CO_2 induced plasticization resistance of the MMMs. A phenomenological model that considers three possible interface interaction in the MMM was development. The plasticization potential of PSF obtained from the model is similar to those reported in the literature. Furthermore, the fraction of the gas held in Langmuir sites that have mobility within the membrane increases with an increase in

the wt. % loading of FCNTs. This indicates that the addition of FCNTs to PSF increases Langmuir sorption sites of the MMMs thereby enhancing the diffusivity through Langmuir region as compared to diffusivity through Henry's law region which further improves penetrant permeability through the membrane

In addition, the results of this work provide a platform for the development of robust CNT reinforced polymeric membranes for suppression of CO_2 induced plasticization in membranes during gas separation. The significant contributions of this work to the body of knowledge have been communicated through posters, oral presentations, and scientific journal publications. A list of presentations at conferences, published and submitted papers related to this work can be found in the initial pages of this thesis.

7.2 Recommendations for future work

The following recommendations should be considered for future work:

1. CNTs produced from methane was of good quality but low yield as compared to CNTs produced from acetylene. Therefore, more work should be done in the future to improve the quantity of CNTs produced from methane without sacrificing the quality.
2. Carboxylic functionalization protocol was adopted in this research work because carboxyl group has the potential to interact with CO_2 to enhance molecular sieving by chemical recognition during natural gas separation. Effect of other functional groups on the improvement of separation performance of mixed matrix membranes should be studied in future work.
3. To fully demonstrate the potential industrial application of CNT reinforced polysulfone membrane, future work should be carried out to evaluate the permeation performance of the membrane with multi-component feeds including C_{2+} hydrocarbon.
4. CO_2 induced plasticization of polymeric membranes is a pressure-dependent phenomenon from a technical perspective (Zhang et al., 2010). However, the lower temperature has been reported to accelerate the plasticization of

polymeric membranes (Duthie et al., 2007). Therefore, future work should investigate temperature-dependent CO_2 induced plasticization of FCNT/PSF MMM.

5. Our experimental study of CO_2 induced plasticization of the synthesized membranes was limited to absolute feed pressure of 20 bar owing to the maximum pressure capacity of the equipment used. Besides, the majority of the current natural gas wells have CO_2 partial pressure of about 5–10 bar (Baker, 2002). Higher feed pressure above 20 bar should be investigated in the future for CNT reinforced polysulfone membrane.

References

Baker, R.W., 2002. Future directions of membrane gas separation technology. *Industrial & Engineering Chemistry Research*, 41(6), pp.1393-1411.

Duthie, X., Kentish, S., Powell, C., Nagai, K., Qiao, G. and Stevens, G., 2007. Operating temperature effects on the plasticization of polyimide gas separation membranes. *Journal of Membrane Science*, 294(1-2), pp.40-49.

Zhang, L., Xiao, Y., Chung, T.S. and Jiang, J., 2010. Mechanistic understanding of CO2-induced plasticization of a polyimide membrane: A combination of experiment and simulation study. *Polymer*, 51(19), pp.4439-4447.

APPENDICES

Appendix A: EDS elemental compositions and spectra of as-produced CNTs

Elemental composition tables and spectra of acetylene carbon source and argon only.

Table A1: Elemental composition table for A-800-Ar

Element	Weight%	Atomic%
C	85.34	89.98
O	11.87	9.39
Fe	2.79	0.63
Totals	100.00	

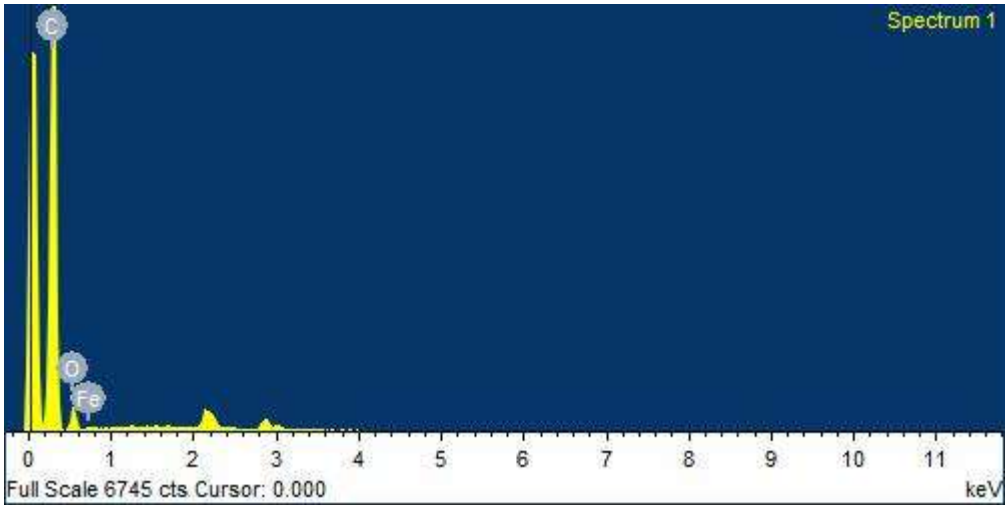

Figure A1: Elemental composition spectrum for A-800-Ar

Table A2: Elemental composition table for A-850-Ar

Element	Weight%	Atomic%
C	87.03	89.94
O	12.97	10.06
Totals	100.00	

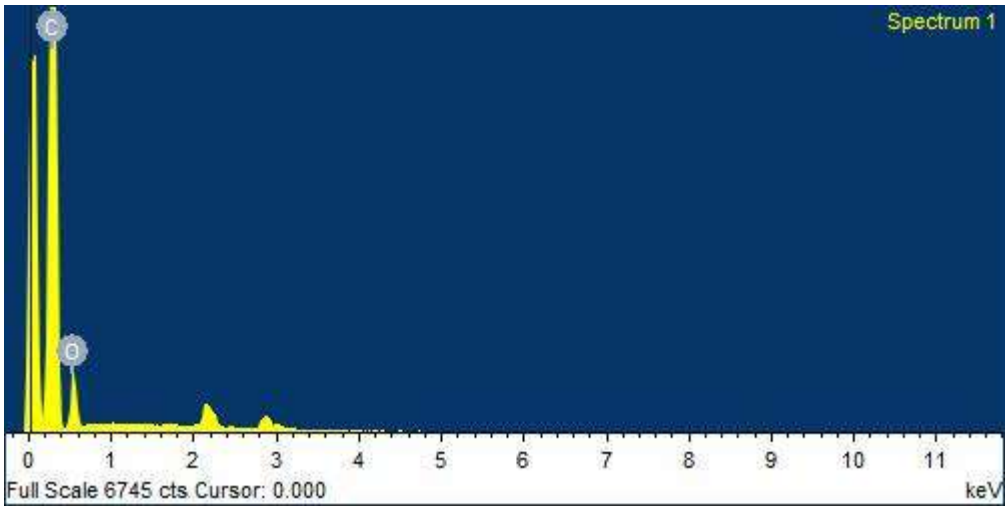

Figure A2: Elemental composition spectrum for A-850-Ar

Table A3: Elemental composition table for A-900-Ar

Element	Weight%	Atomic%
C	90.51	94.52
O	5.99	4.70
Fe	3.50	0.79
Totals	100.00	

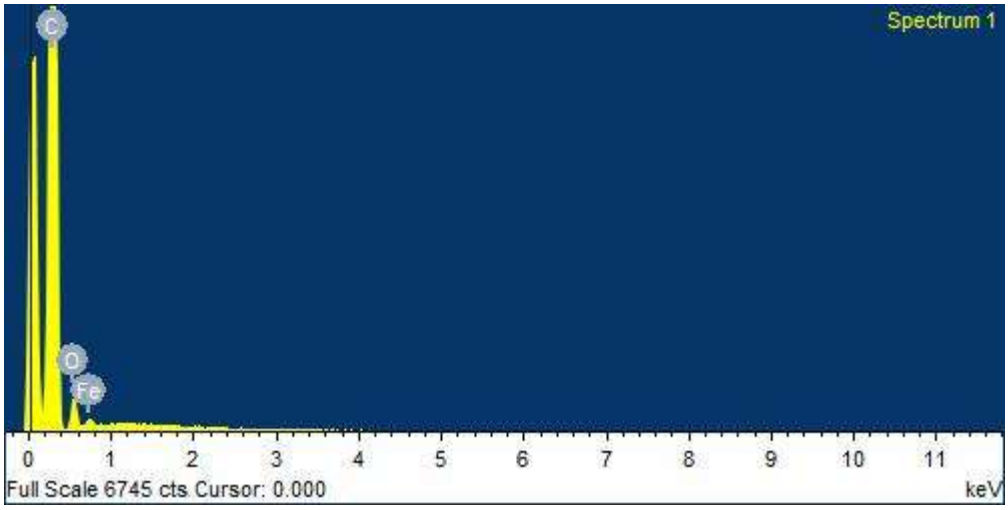

Figure A3: Elemental composition spectrum for A-900-Ar

Table A4: Elemental composition table for A-950-Ar

Element	Weight%	Atomic%
C	88.32	90.97
O	11.68	9.03
Totals	100.00	

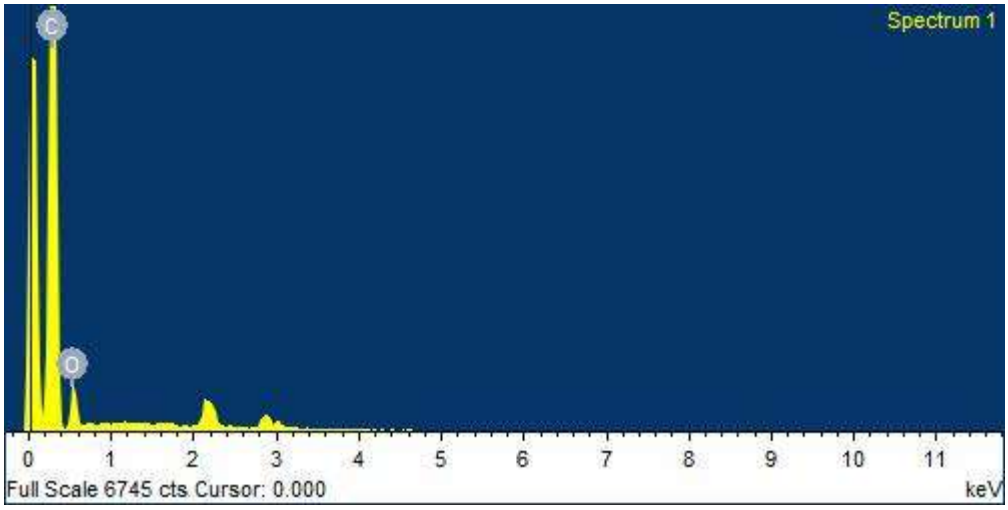

Figure A4: Elemental composition spectrum for A-950-Ar

Table A5: Elemental composition table for A-1000-Ar

Element	Weight%	Atomic%
C	92.56	95.66
O	4.85	3.76
Fe	2.59	0.58
Totals	100.00	

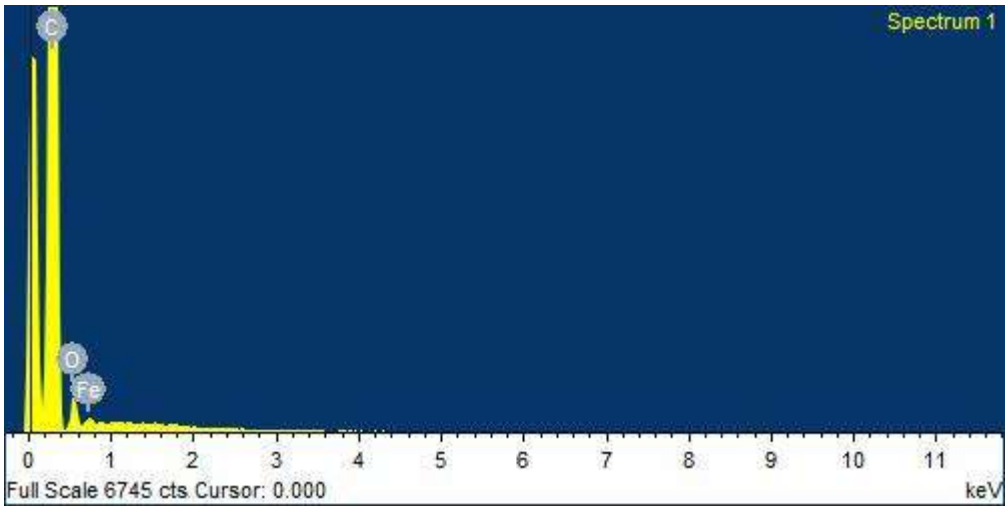

Figure A5: Elemental composition spectrum for A-1000-Ar

Compositional tables and spectra of acetylene carbon source and argon/hydrogen.

Table A6: Elemental composition table for A-800-Ar/H

Element	Weight%	Atomic%
C	95.96	99.10
Fe	4.04	0.90
Totals	100.00	

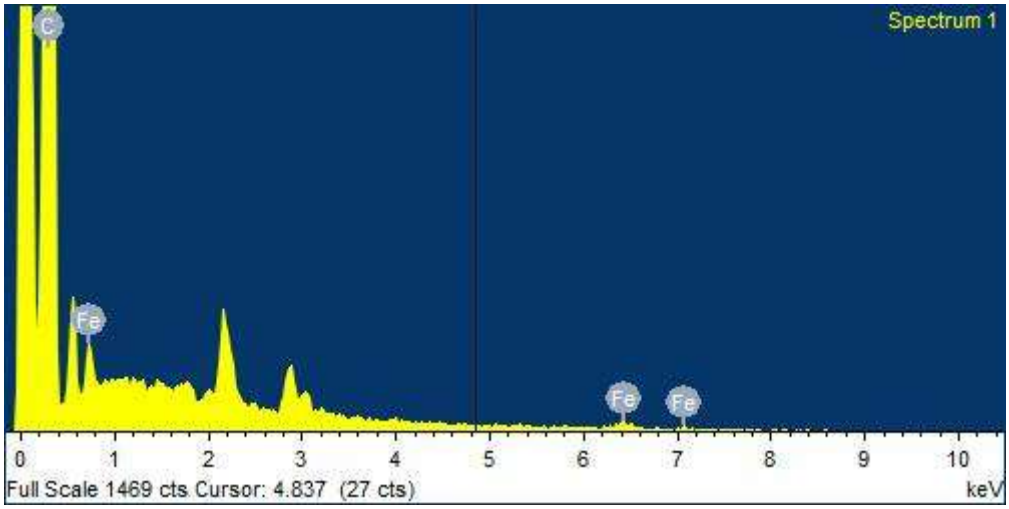

Figure A6: Elemental composition spectrum for A-800-Ar/H

Table A7: Elemental composition table for A-850-Ar/H

Element	Weight%	Atomic%
C	94.76	97.30
O	2.80	2.16
Fe	2.44	0.54
Totals	100.00	

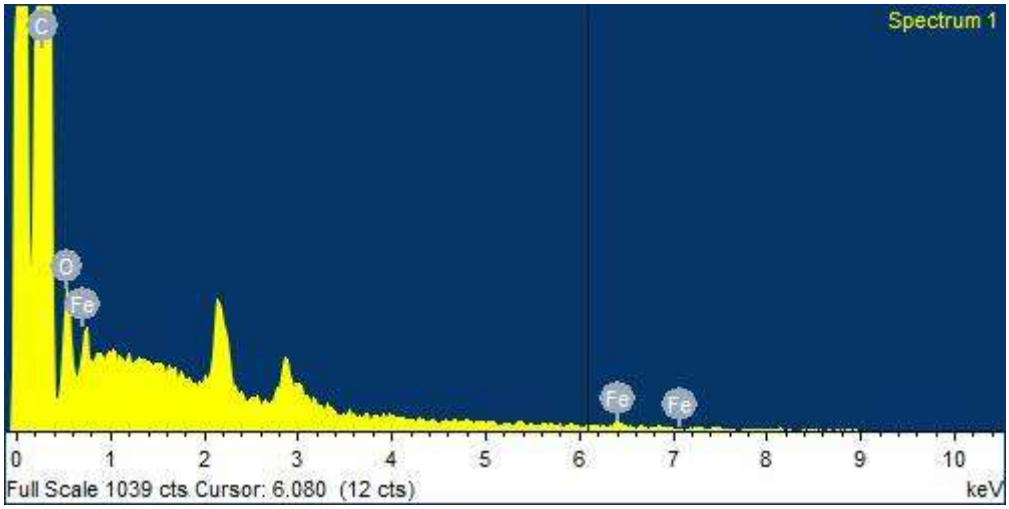

Figure A7: Elemental composition spectrum for A-850-Ar/H

Table A8: Elemental composition table for A-900-Ar/H

Element	Weight%	Atomic%
C	89.08	94.37
O	5.55	4.41
Fe	5.37	1.22
Totals	100.00	

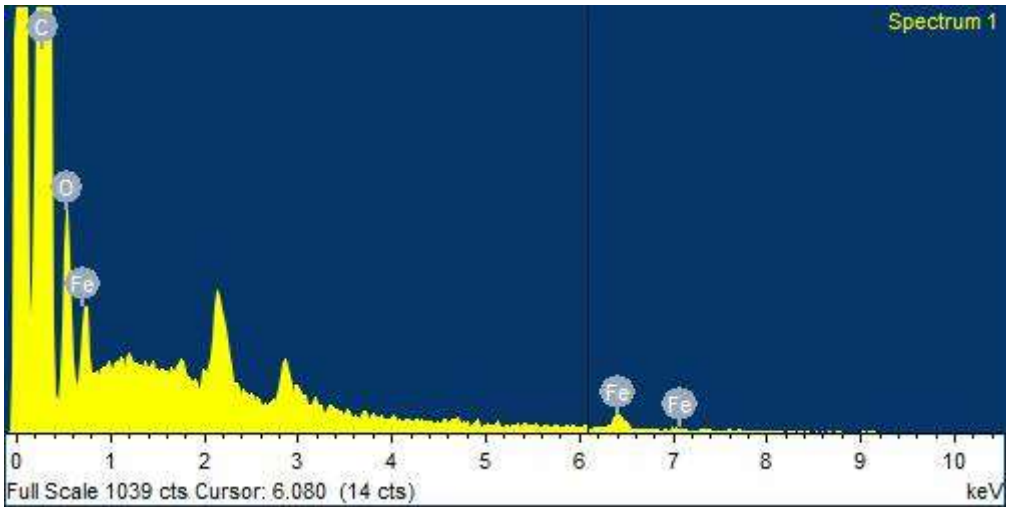

Figure A8: Elemental composition spectrum for A-900-Ar/H

Table A9: Elemental composition table for A-950-Ar/H

Element	Weight%	Atomic%
C	98.45	99.52
Si	0.67	0.29
Fe	0.88	0.19
Totals	100.00	

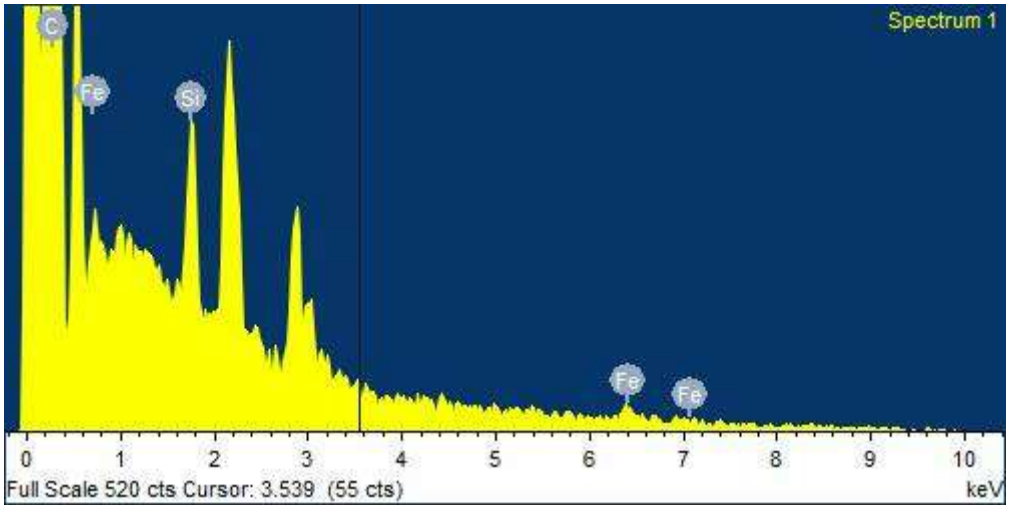

Figure A9: Elemental composition spectrum for A-950-Ar/H

Table A10: Elemental composition table for A-1000-Ar/H

Element	Weight%	Atomic%
C	98.94	99.77
Fe	1.06	0.23
Totals	100.00	

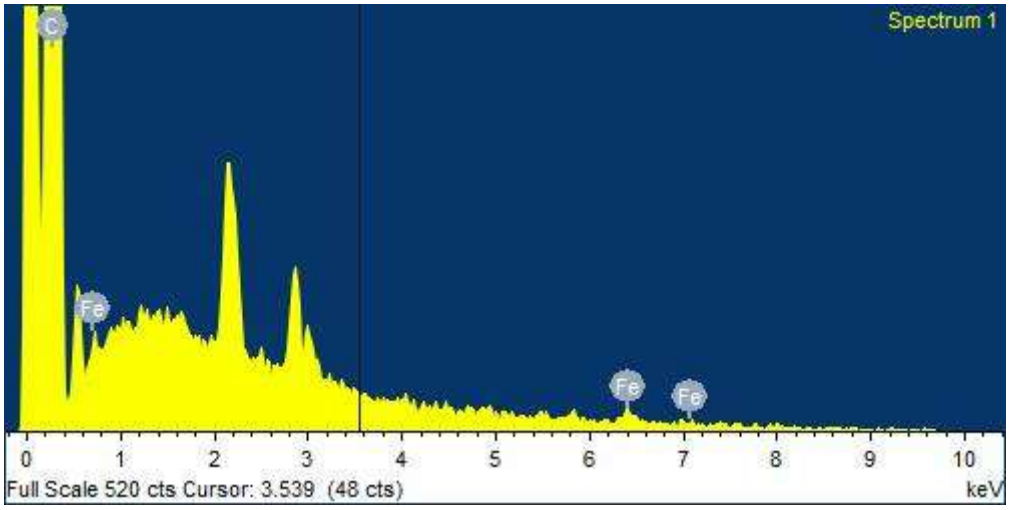

Figure A10: Elemental composition spectrum for A-1000-Ar/H

Compositional tables and spectra of methane carbon source and argon only.

Table A11: Elemental composition table for M-800-Ar

Element	Weight%	Atomic%
C	79.39	94.72
Fe	20.43	5.24
Cu	0.18	0.04
Totals	100.00	

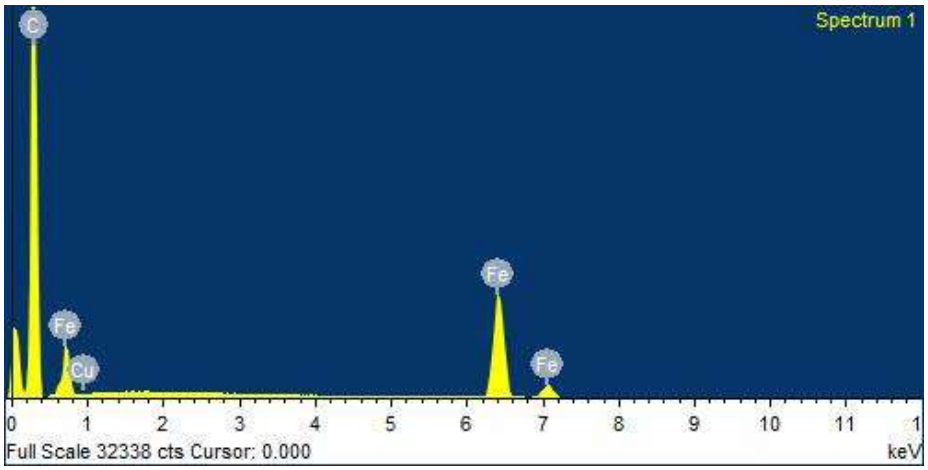

Figure A11: Elemental composition spectrum for M-800-Ar

Table A12: Elemental composition table for M-900-Ar

Element	Weight%	Atomic%
C	78.43	90.31
O	7.02	6.07
Si	0.09	0.05
Fe	14.46	3.58
Totals	100.00	

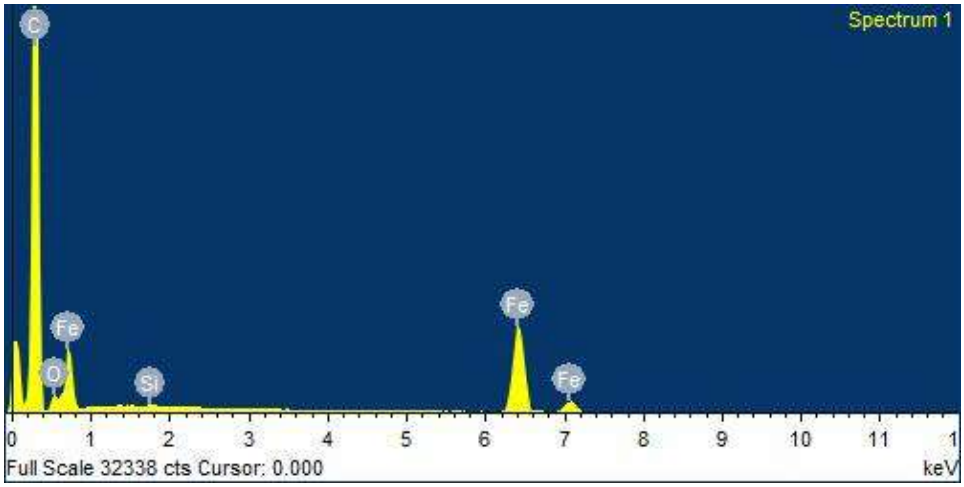

Figure A12: Elemental composition spectrum for M-900-Ar

Table A13: Elemental composition table for M-1000-Ar

Element	Weight%	Atomic%
C	70.74	91.83
Fe	29.26	8.17
Totals	100.00	

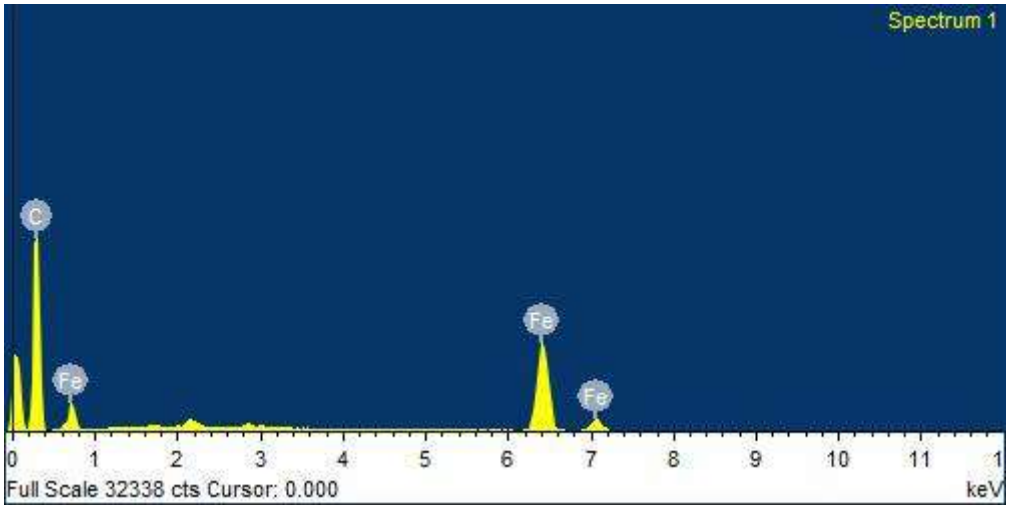

Figure A13: Elemental composition spectrum for M-1000-Ar

Appendix B: BET surface area calculations

BET equation is given as equation (B1):

$$\frac{1}{Q\left[\frac{P_O}{P}-1\right]} = \frac{C-1}{Q_m C}\left[\frac{P}{P_O}\right] + \frac{1}{Q_m C} \qquad \text{(B1)}$$

Where

Q = Volume of gas adsorbed at STP.

Q_m = Volume of gas adsorbed at STP to produce apparent monolayer on the sample surface.

P/P_o = Relative pressure

C = BET constant (its related to the enthalpy of adsorption of the adsorbate on the sample)

Equation (B1) can be writing in the form of straight line equation

$$y = mx + c$$

if

$$y = \frac{1}{Q\left[\frac{P_O}{P}-1\right]} \quad \text{and} \quad x = \left[\frac{P}{P_O}\right]$$

Then

Gradient of the linear graph (m) = $\frac{C-1}{Q_m C}$

The intercept (c) = $\frac{1}{Q_m C}$

Plotting $\frac{1}{Q\left[\frac{P_O}{P}-1\right]}$ against $\left[\frac{P}{P_O}\right]$ within the monolayer adsorption region i.e at relative pressure between 0 – 0.3, will yield a linear graph as shown in Figures B1-B3.

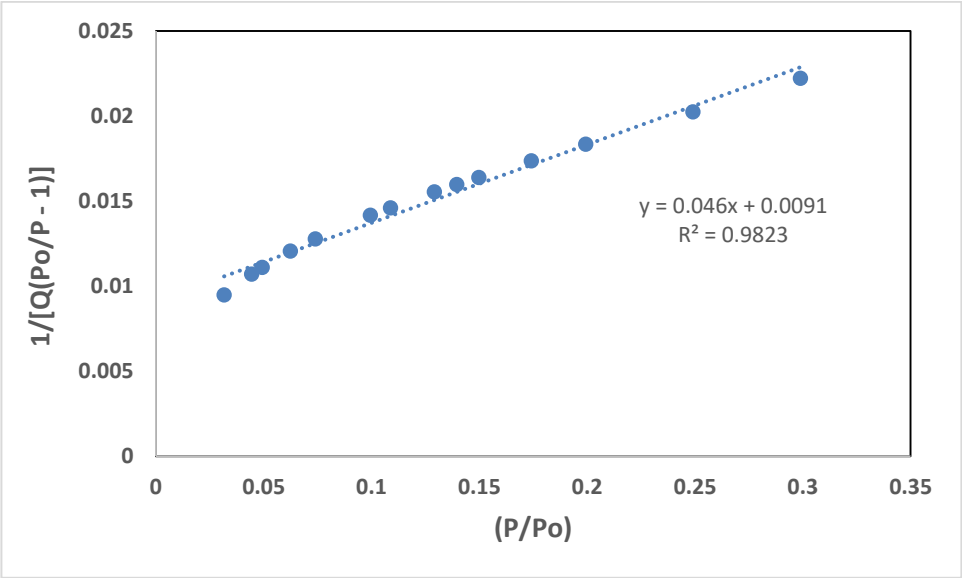

Figure B1: Graph of BET analysis within the monolayer adsorption region for raw CNT

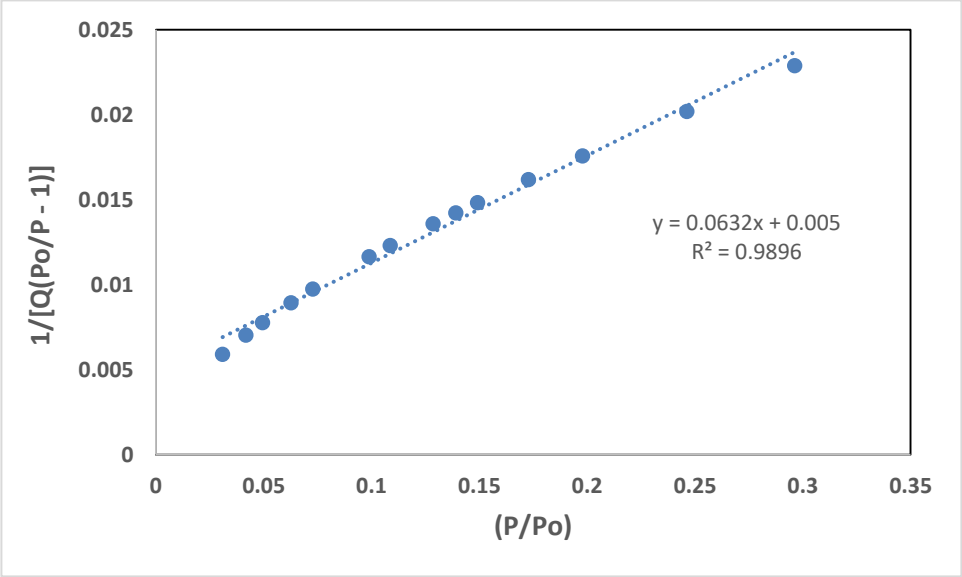

Figure B2: Graph of BET analysis within the monolayer adsorption region for purified CNT

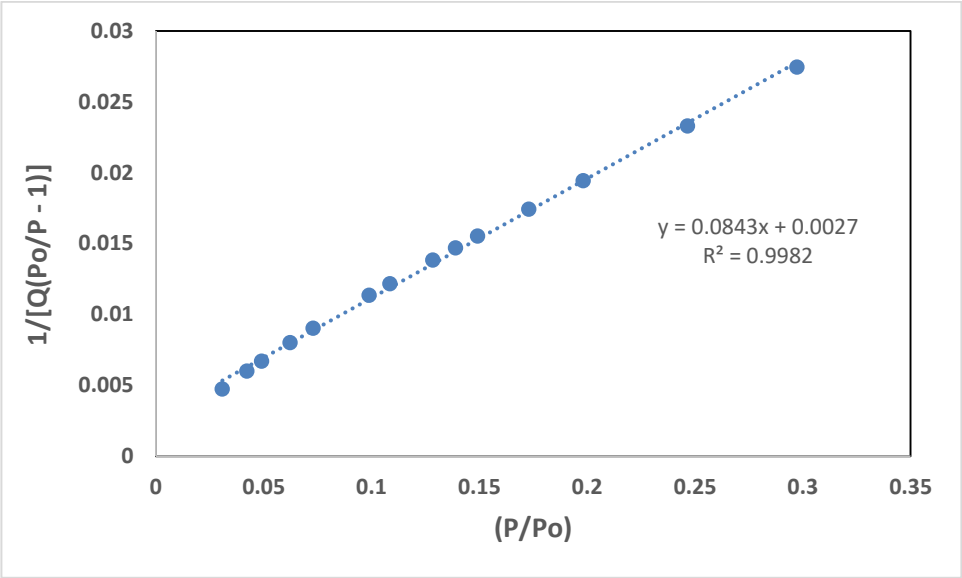

Figure B3: Graph of BET analysis within the monolayer adsorption region for Functionalized CNT

$$Q_m = \frac{1}{m + c}$$

$$S = \frac{Q_m A_{cs} N}{w \times 22400}$$

Where

m = gradient of the graph

c = y-intercept of the graph

w = mass of tested sample

N = Avogadro constant

A_{cs} = effective cross-sectional area of one adsorbate molecule

Appendix C: Sample of measurement of membrane thickness using SEM

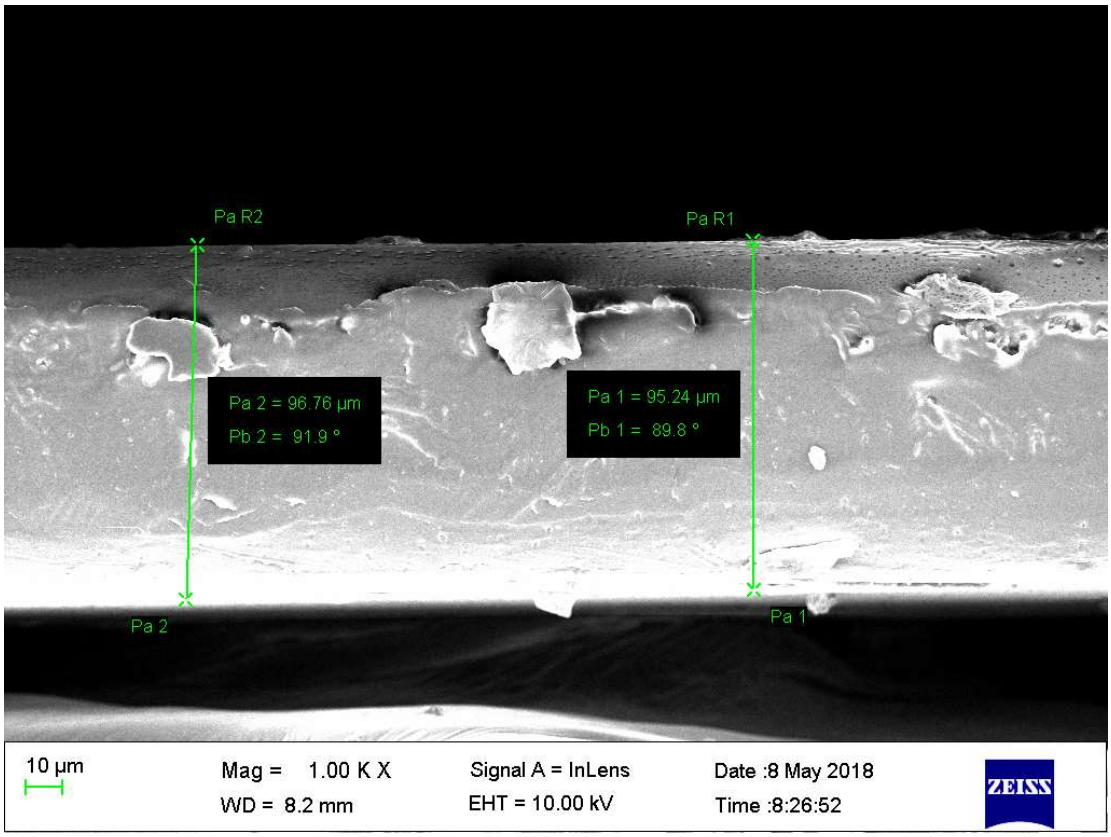

Figure C1: SEM micrograph of Pure PSF thickness measurement

Appendix D: DSC thermogram analysis

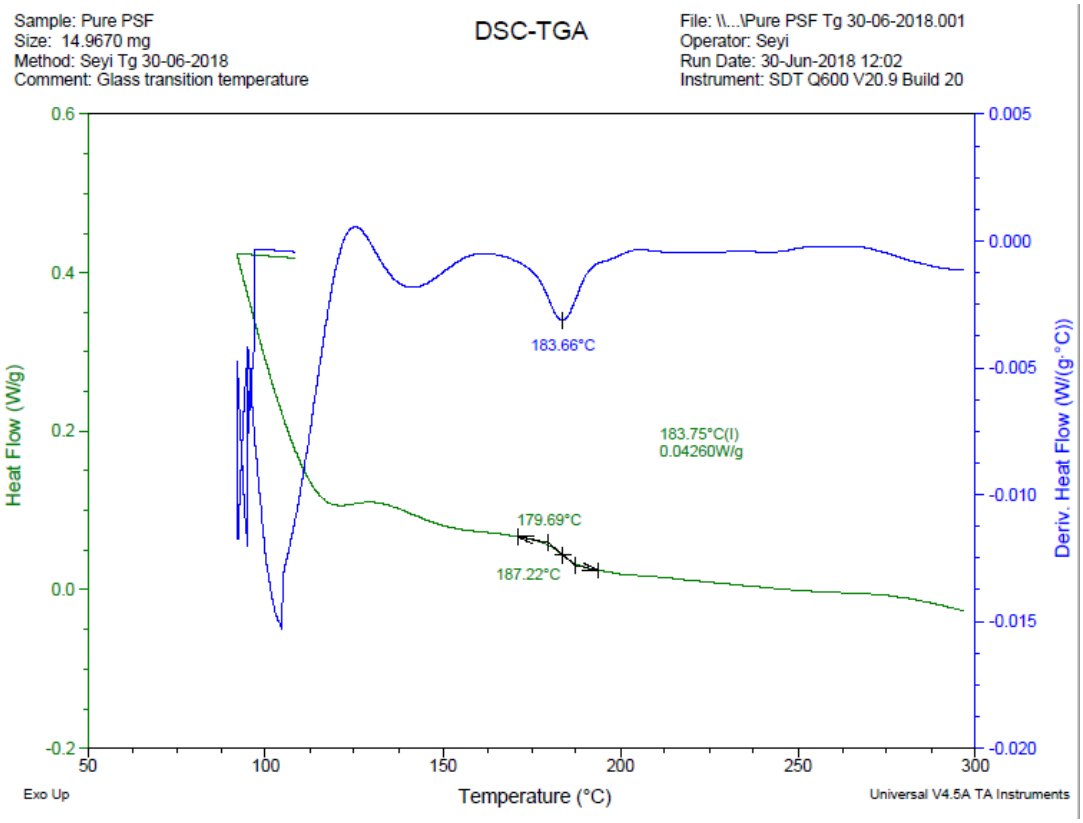

Figure D1: Pure PSF DSC thermogram

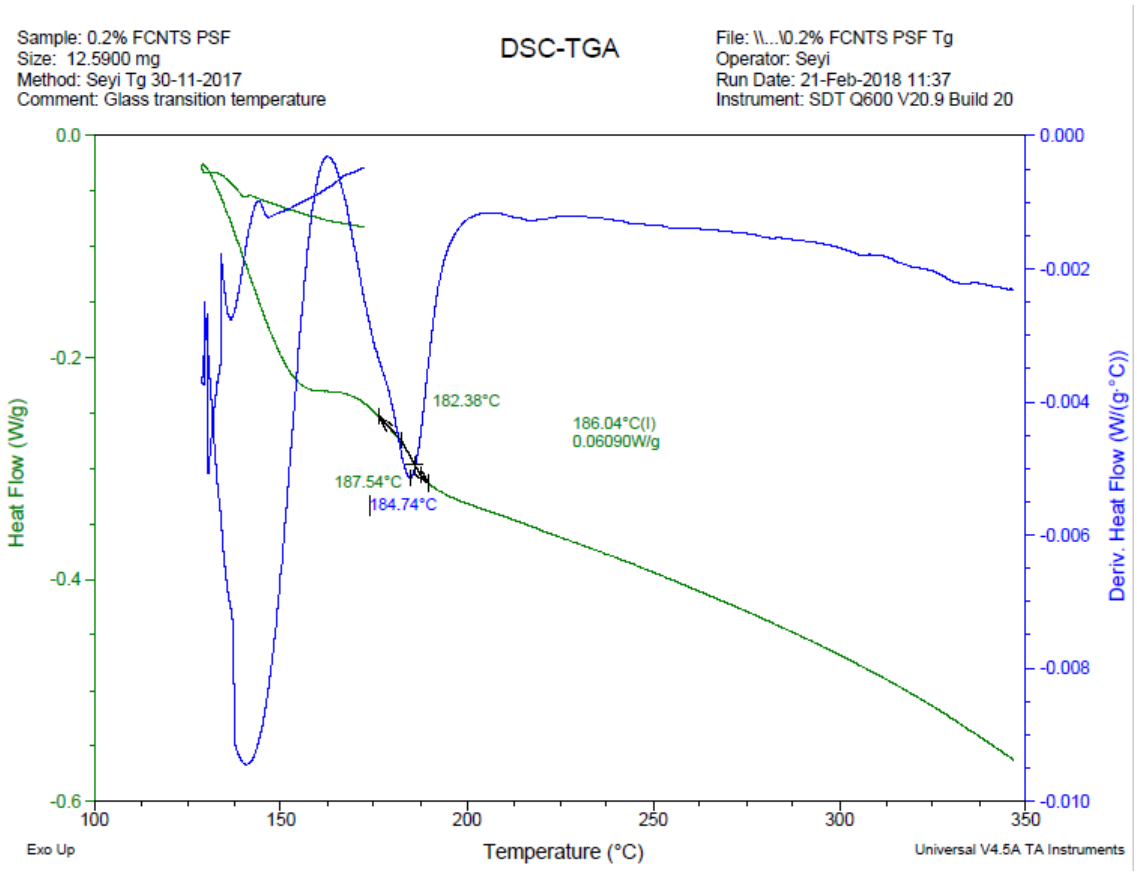

Figure D2: 0.2 FCNT PSF DSC thermogram

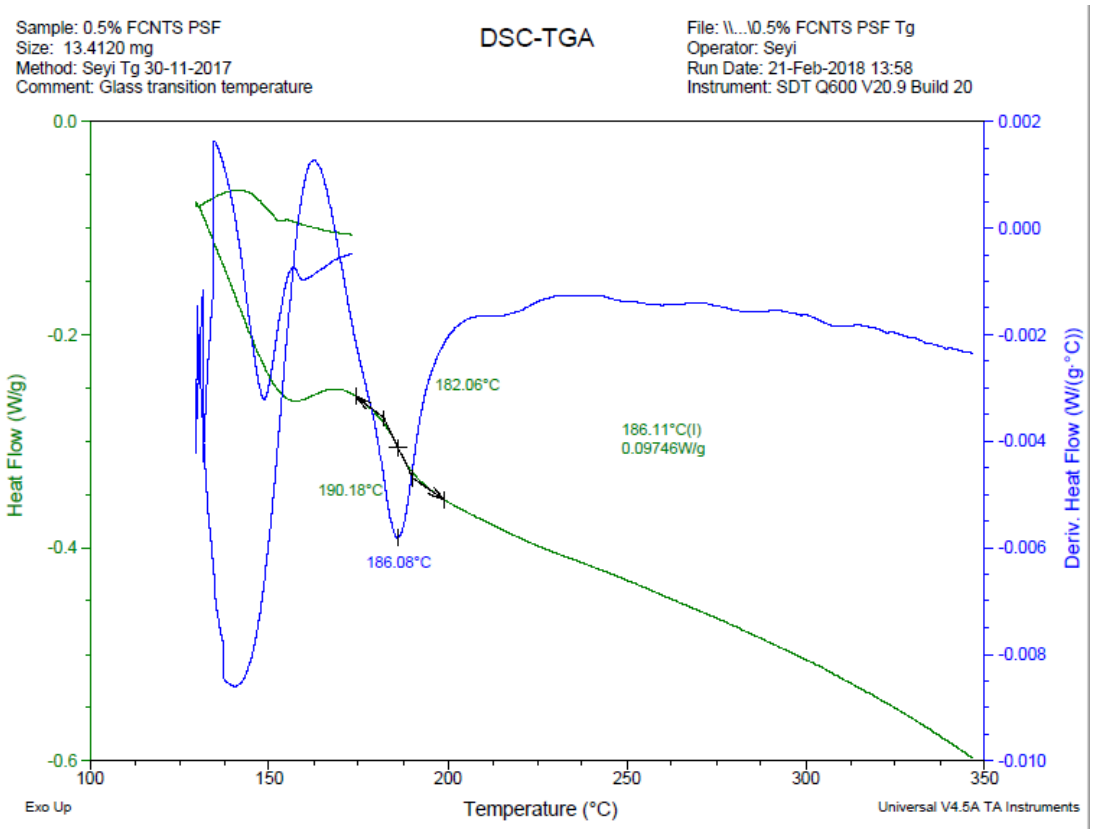

Figure D3: 0.5 FCNT PSF DSC thermogram

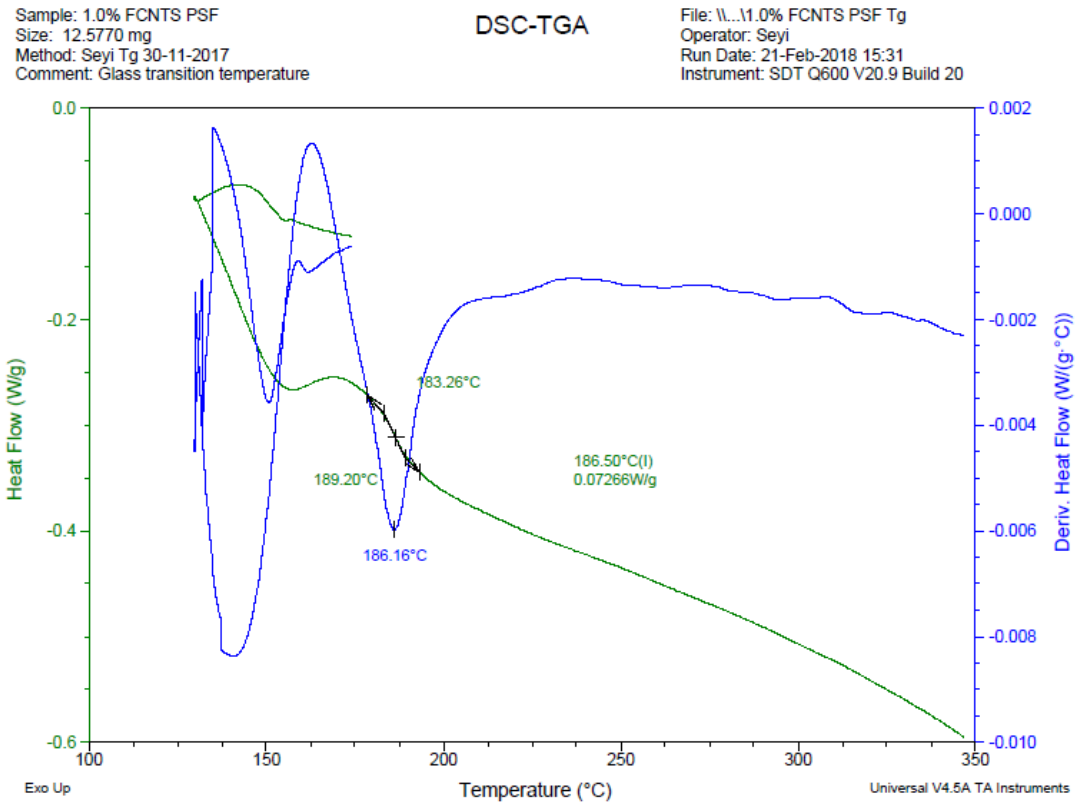

Figure D4: 1.0 FCNT PSF DSC thermogram

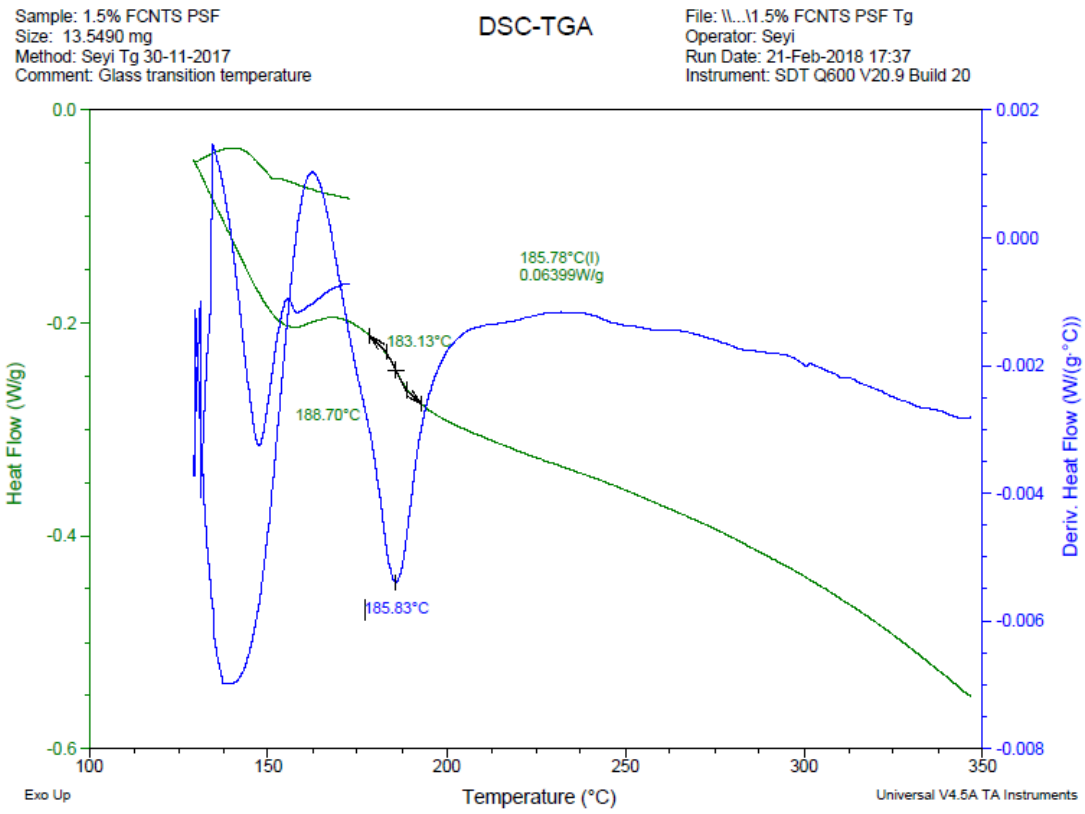

Figure D5: 1.5 FCNT PSF DSC thermogram

Appendix E: AFM depth-at-max analysis

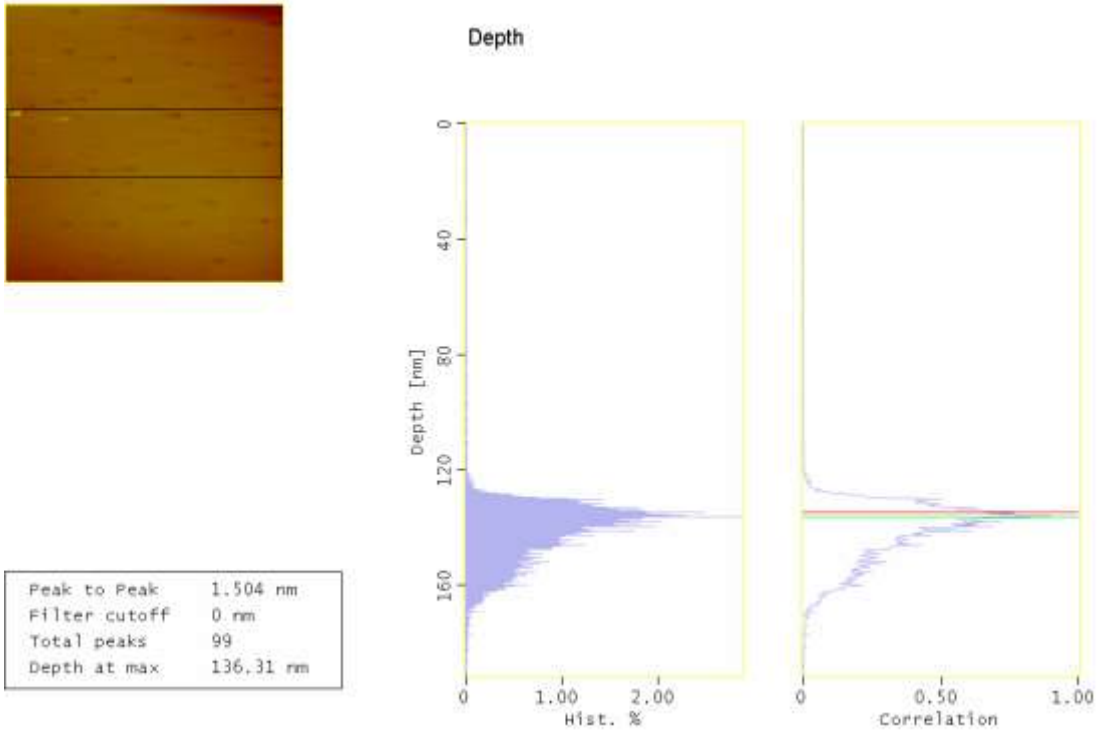

Figure E1: Pure PSF depth at max spectrum

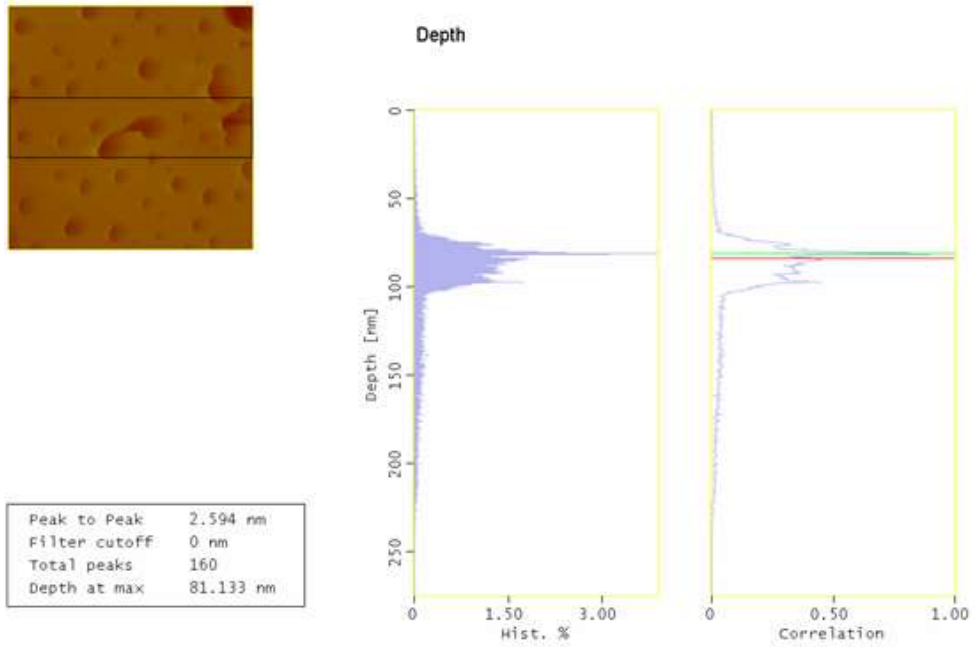

Figure E2: 0.2 FCNT PSF depth at max spectrum

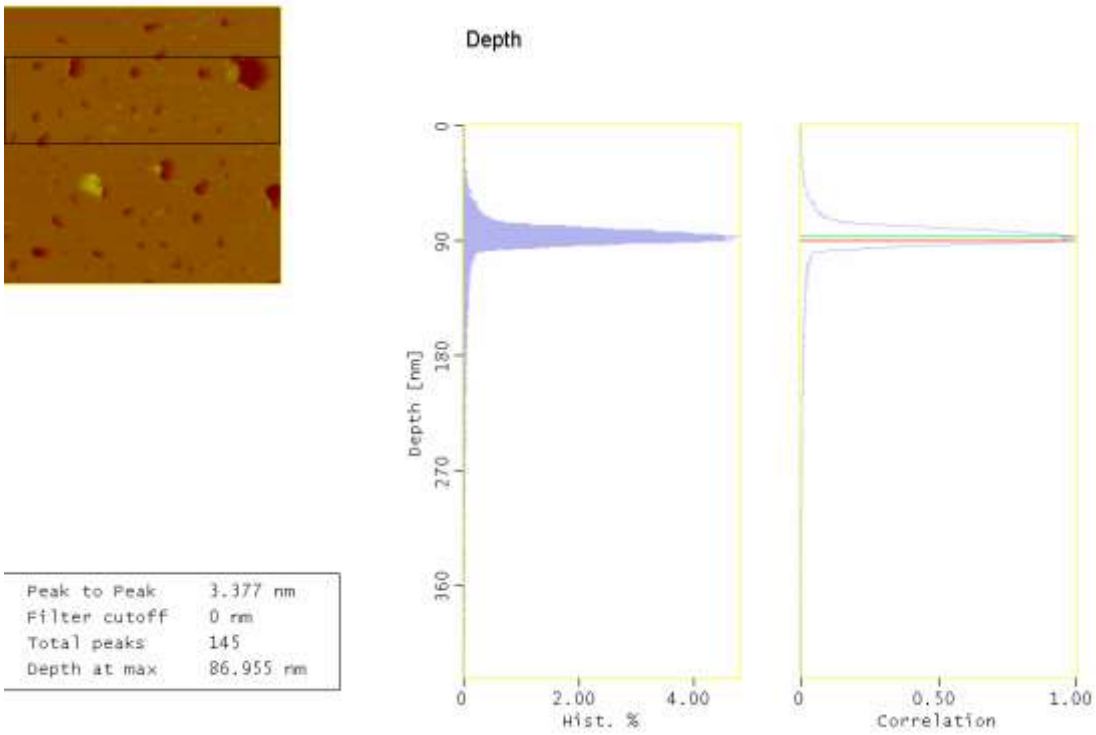

Figure E3: 0.5 FCNT PSF depth at max spectrum

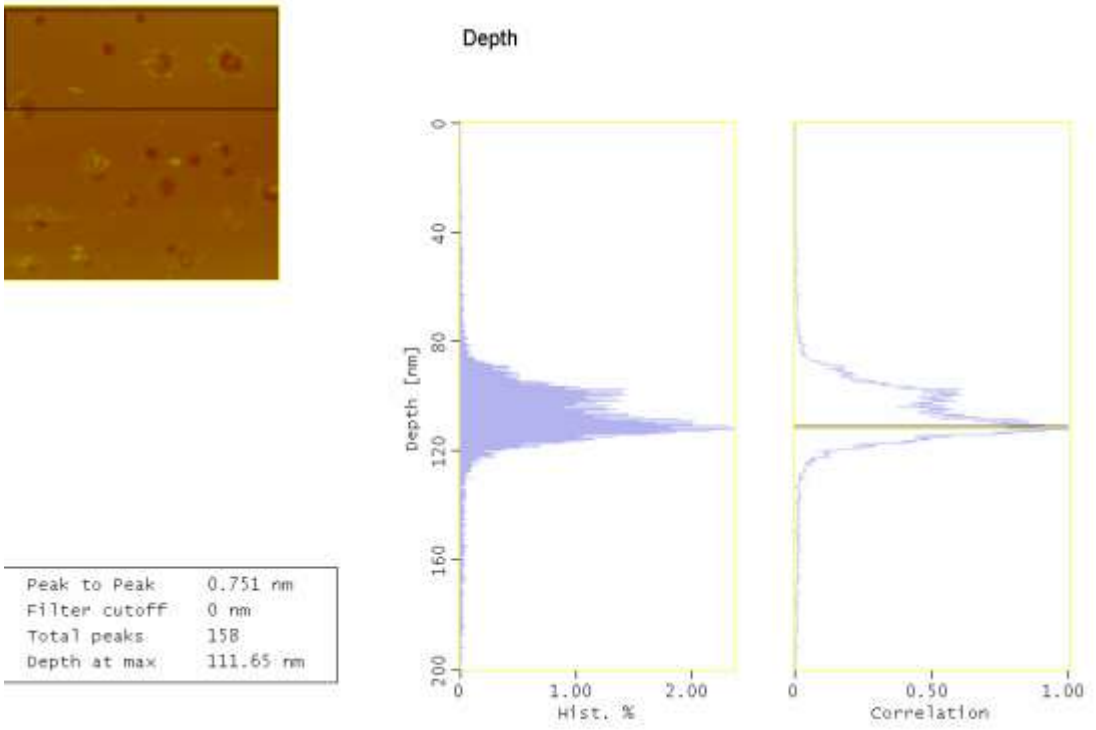

Figure E4: 1.0 FCNT PSF depth at max spectrum

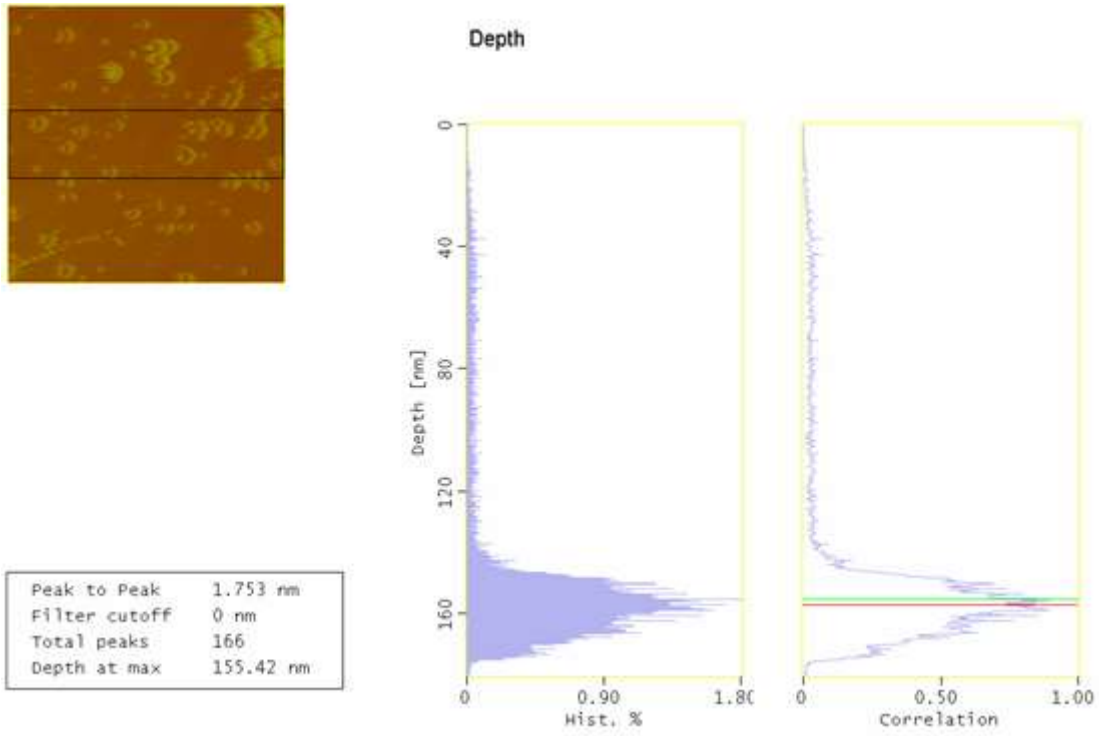

Figure E5: 1.5 FCNT PSF depth at max spectrum

Appendix F: Tables of CO_2/CH_4 permeability and selectivity values for pure and mixed gases

Table F1: Pure gas permeability and selectivity values of pure PSF

Pressure (bar)	P (CO2)	P (CH4)	Ideal α
2	6.60	0.17	39
4	6.45	0.17	38
6	6.42	0.16	40
8	6.32	0.16	40
10	6.04	0.15	40

Table F2: Pure gas permeability and selectivity values of 0.2% FCNT PSF

Pressure (bar)	P (CO2)	P (CH4)	Ideal α
2	6.91	0.21	33
4	6.74	0.20	34
6	6.63	0.21	32
8	6.48	0.21	31
10	6.46	0.21	31

Table F3: Pure gas permeability and selectivity values of 0.5% FCNT PSF

Pressure (bar)	P (CO2)	P (CH4)	Ideal α
2	7.10	0.25	28
4	6.84	0.24	29
6	6.73	0.25	27
8	6.58	0.26	25
10	6.56	0.25	26

Table F4: Pure gas permeability and selectivity values of 1.0% FCNT PSF

Pressure (bar)	P (CO2)	P (CH4)	Ideal α
2	7.79	0.28	28
4	7.44	0.27	28
6	7.32	0.27	27
8	7.01	0.28	25
10	6.78	0.27	25

Table F5: Pure gas permeability and selectivity values of 1.5% FCNT PSF

Pressure (bar)	P (CO2)	P (CH4)	Ideal α
2	7.56	0.26	29
4	6.86	0.25	27
6	6.30	0.25	25
8	5.91	0.25	24
10	5.89	0.26	23

Table F6: CO_2/CH_4 (10%/90%) mixed gas permeability and separation factor of pure PSF

CO_2 partial pressure (bar)	CH_4 partial pressure (bar)	Feed pressure (bar)	P (CO2)	P (CH4)	Separation factor (α)
0.2	1.8	2	6.98	0.15	47
0.4	3.6	4	6.37	0.14	46
0.6	5.4	6	6.30	0.14	45
0.8	7.2	8	6.07	0.15	40
1	9	10	5.52	0.14	39

Table F7: CO_2/CH_4 (10%/90%) mixed gas permeability and separation factor of 0.2% FCNT PSF

CO_2 partial pressure (bar)	CH_4 partial pressure (bar)	Feed pressure (bar)	P (CO2)	P (CH4)	Separation factor (α)
0.2	1.8	2	7.96	0.18	44
0.4	3.6	4	7.05	0.19	38
0.6	5.4	6	6.91	0.19	36
0.8	7.2	8	6.70	0.19	34
1	9	10	6.65	0.19	35

Table F8: CO_2/CH_4 (10%/90%) mixed gas permeability and separation factor of 0.5% FCNT PSF

CO_2 partial pressure (bar)	CH_4 partial pressure (bar)	Feed pressure (bar)	P (CO2)	P (CH4)	Separation factor (α)
0.2	1.8	2	8.17	0.21	39
0.4	3.6	4	7.56	0.21	38
0.6	5.4	6	7.34	0.23	32
0.8	7.2	8	7.25	0.21	35
1	9	10	7.15	0.21	35

Table F9: CO_2/CH_4 (10%/90%) mixed gas permeability and separation factor of 1.0% FCNT PSF

CO_2 partial pressure (bar)	CH_4 partial pressure (bar)	Feed pressure (bar)	P (CO2)	P (CH4)	Separation factor (α)
0.2	1.8	2	8.30	0.21	40
0.4	3.6	4	8.15	0.22	37
0.6	5.4	6	7.83	0.21	36
0.8	7.2	8	7.31	0.21	34
1	9	10	7.18	0.22	33

Table F10: CO_2/CH_4 (10%/90%) mixed gas permeability and separation factor of 1.5% FCNT PSF

CO_2 partial pressure (bar)	CH_4 partial pressure (bar)	Feed pressure (bar)	P (CO2)	P (CH4)	Separation factor (α)
0.2	1.8	2	9.85	0.21	47
0.4	3.6	4	8.46	0.22	38
0.6	5.4	6	8.10	0.23	36
0.8	7.2	8	7.86	0.23	34
1	9	10	7.41	0.22	34

Table F11: CO_2/CH_4 (50%/50%) mixed gas permeability and selectivity values of pure PSF

CO_2 partial pressure (bar)	CH_4 partial pressure (bar)	Feed pressure (bar)	P (CO2)	P (CH4)	Separation factor (α)
1.0	1.0	2	6.12	0.16	38
2.0	2.0	4	5.90	0.16	37
3.0	3.0	6	5.44	0.15	36

Table F12: CO_2/CH_4 (50%/50%) mixed gas permeability and selectivity values of 0.2% FCNT PSF

CO_2 partial pressure (bar)	CH_4 partial pressure (bar)	Feed pressure (bar)	P (CO2)	P (CH4)	Separation factor (α)
1.0	1.0	2	6.71	0.18	37
2.0	2.0	4	6.65	0.17	39
3.0	3.0	6	6.5	0.18	36

Table F13: CO_2/CH_4 (50%/50%) mixed gas permeability and selectivity values of 0.5% FCNT PSF

CO_2 partial pressure (bar)	CH_4 partial pressure (bar)	Feed pressure (bar)	P (CO2)	P (CH4)	Separation factor (α)
1.0	1.0	2	7.26	0.21	35
2.0	2.0	4	7.01	0.21	33
3.0	3.0	6	6.72	0.2	33

Table F14: CO_2/CH_4 (50%/50%) mixed gas permeability and selectivity values of 1.0% FCNT PSF

CO_2 partial pressure (bar)	CH_4 partial pressure (bar)	Feed pressure (bar)	P (CO2)	P (CH4)	Separation factor (α)
1.0	1.0	2	7.64	0.23	33
2.0	2.0	4	7.21	0.23	31
3.0	3.0	6	6.9	0.22	31

Table F15: CO_2/CH_4 (50%/50%) mixed gas permeability and selectivity values of 1.5% FCNT PSF

CO_2 partial pressure (bar)	CH_4 partial pressure (bar)	Feed pressure (bar)	P (CO2)	P (CH4)	Separation factor (α)
1.0	1.0	2	8.67	0.24	36
2.0	2.0	4	7.23	0.22	33
3.0	3.0	6	6.7	0.23	29

Table F16: CO_2/CH_4 (50%/50%) mixed gas permeability and selectivity values of 1.0% PCNT PSF

CO_2 partial pressure (bar)	CH_4 partial pressure (bar)	Feed pressure (bar)	P (CO2)	P (CH4)	Separation factor (α)
1.0	1.0	2	6.42	0.23	28
2.0	2.0	4	5.53	0.23	24
3.0	3.0	6	4.6	0.22	21

Appendix G: Dual-mode sorption model parameters analysis

Table G1: CO_2 concentration in the MMMs based on sorption experiment

Pressure (bar)	Pure PSF Concentration (cm^3 (STP)/cm^3 polymer)	0,2% FCNT PSF Concentration (cm^3 (STP)/cm^3 polymer)	0,5% FCNT PSF Concentration (cm^3 (STP)/cm^3 polymer)	1,0% FCNT PSF Concentration (cm^3 (STP)/cm^3 polymer)	1,5% FCNT PSF Concentration (cm^3 (STP)/cm^3 polymer)
0.1	0.65637446	0.502575922	0.439904008	0.397913826	0.73552674
0.5	2.537139741	2.07772241	2.065888971	2.057960567	2.43018035
1	4.316924335	3.597708126	3.606452631	3.612311449	4.054223393
2	7.201185185	6.018653118	6.10788137	6.167664298	6.402024748
3	9.233421495	7.961538085	8.004261002	8.032885356	8.22024685
5	12.63520836	11.05054131	11.1646277	11.24106558	10.9446379
7.5	16.13166462	14.08438377	14.2321271	14.33111513	13.73963951
10	18.86445444	16.71984288	16.85684835	16.94864201	16.27573571
15	23.57267894	21.02851206	21.16551242	21.25730266	20.63005401
20	27.47936923	24.42396403	24.67220538	24.83852709	24.74900376

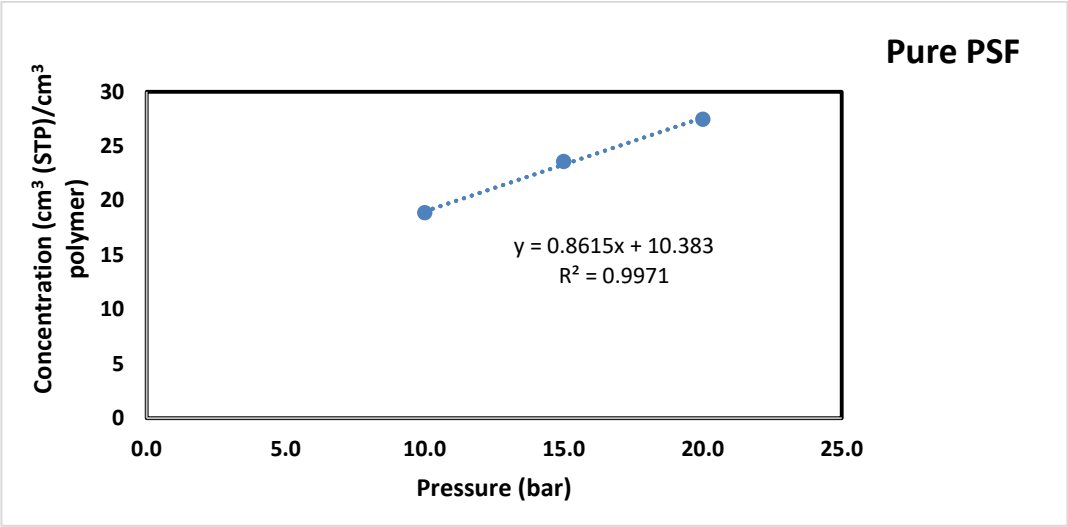
Pure PSF
Concentration (cm³ (STP)/cm³ polymer)
30
25
20
15
10
5
0
0.0
5.0
10.0
15.0
20.0
25.0
Pressure (bar)
y = 0.8615x + 10.383
R² = 0.9971

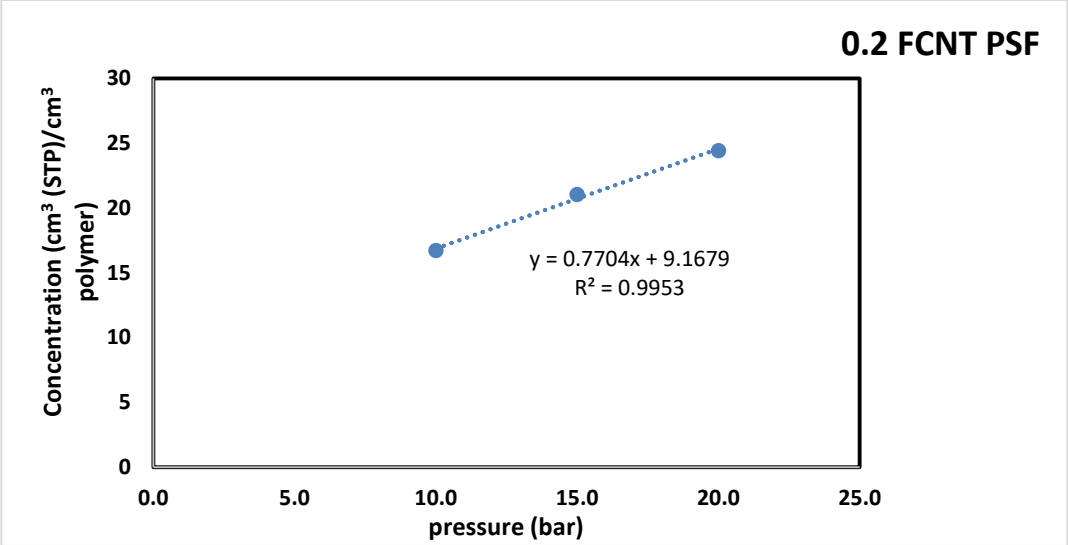
0.2 FCNT PSF
Concentration (cm³ (STP)/cm³ polymer)
30
25
20
15
10
5
0
0.0
5.0
10.0
15.0
20.0
25.0
pressure (bar)
y = 0.7704x + 9.1679
R² = 0.9953

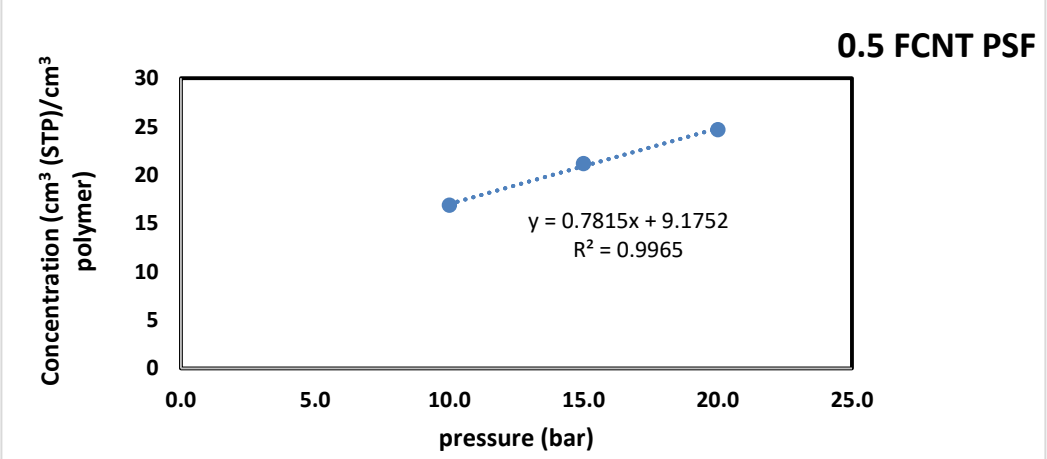
0.5 FCNT PSF
Concentration (cm³ (STP)/cm³ polymer)
30
25
20
15
10
5
0
0.0
5.0
10.0
15.0
20.0
25.0
pressure (bar)
y = 0.7815x + 9.1752
R² = 0.9965

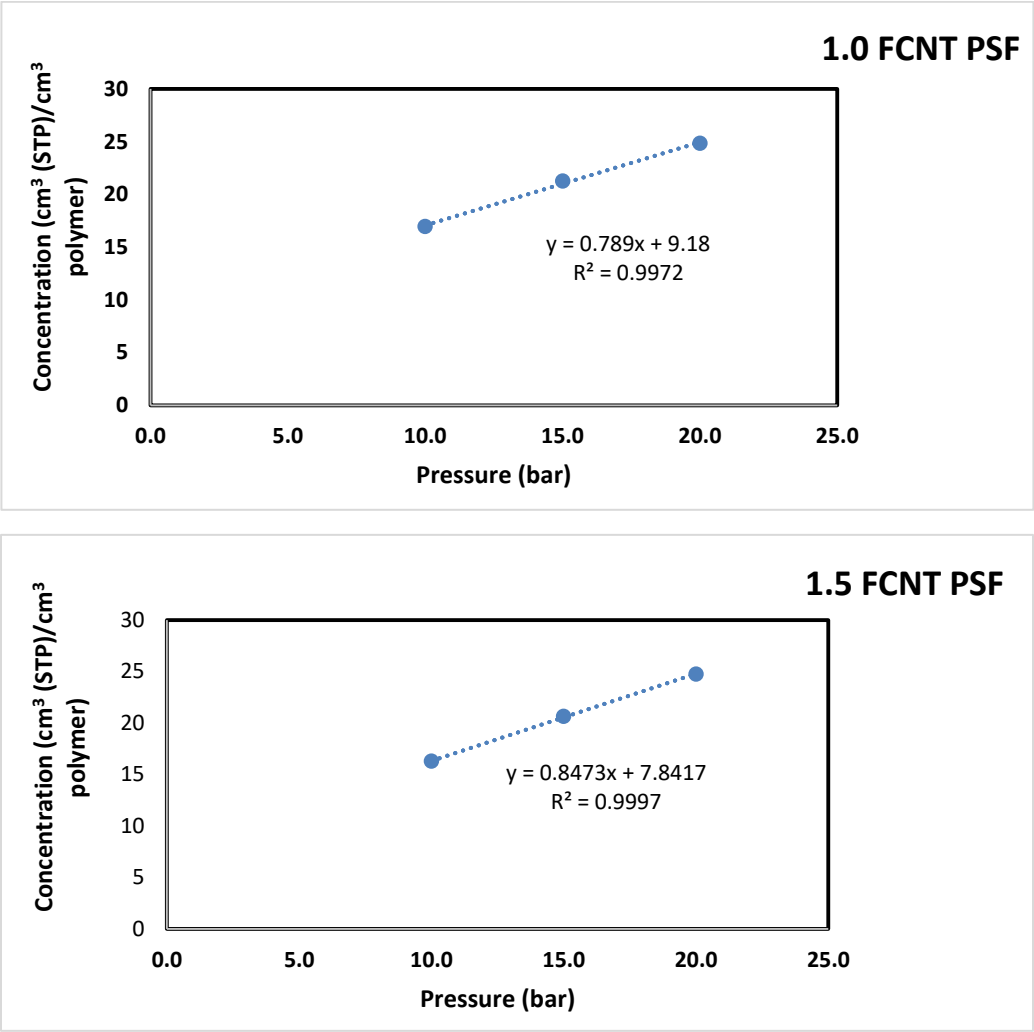

Figure G1: Linear asymptotes of the sorption data at elevated pressure for k_d determination

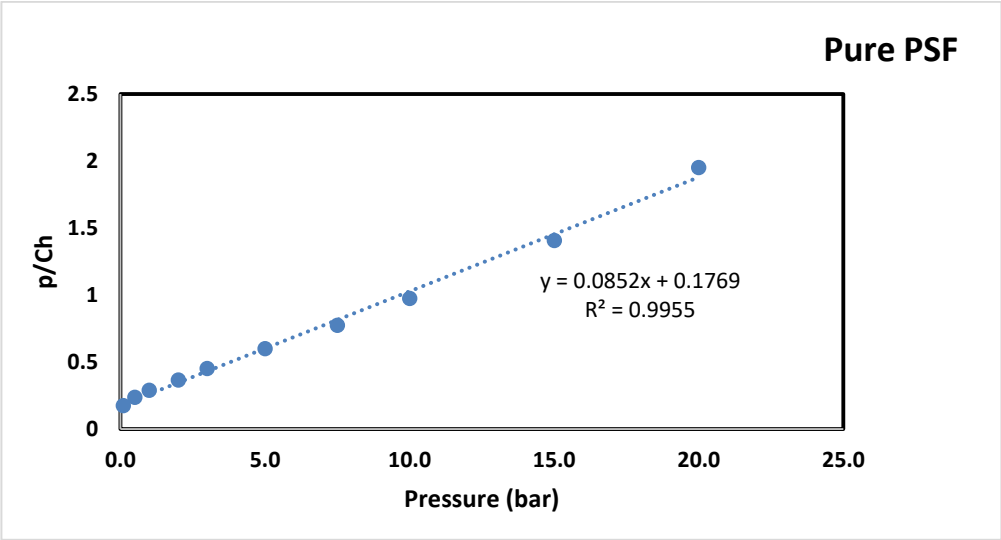
Pure PSF
2.5
2
1.5
1
0.5
0
p/Ch
y = 0.0852x + 0.1769
R² = 0.9955
0.0
5.0
10.0
15.0
20.0
25.0
Pressure (bar)

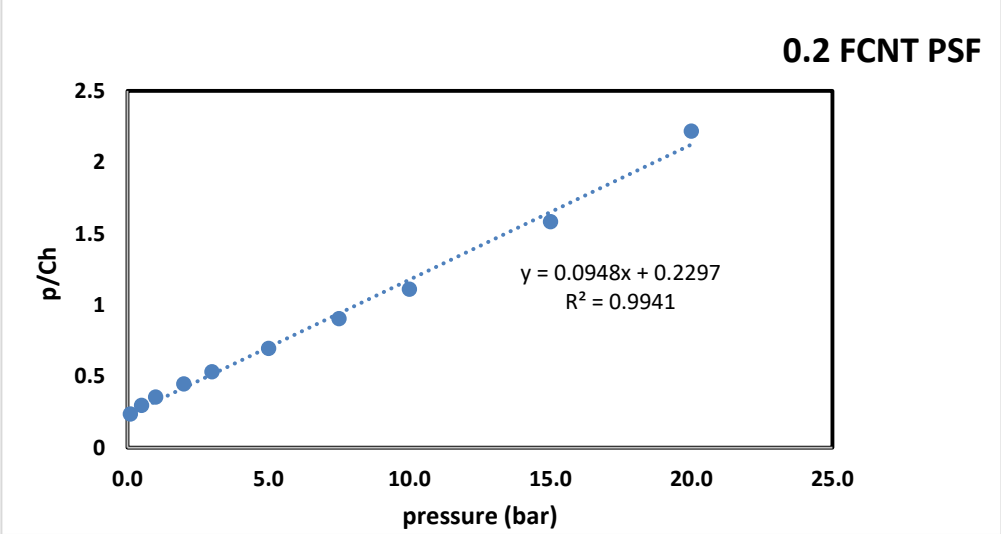
0.2 FCNT PSF
2.5
2
1.5
1
0.5
0
p/Ch
y = 0.0948x + 0.2297
R² = 0.9941
0.0
5.0
10.0
15.0
20.0
25.0
pressure (bar)

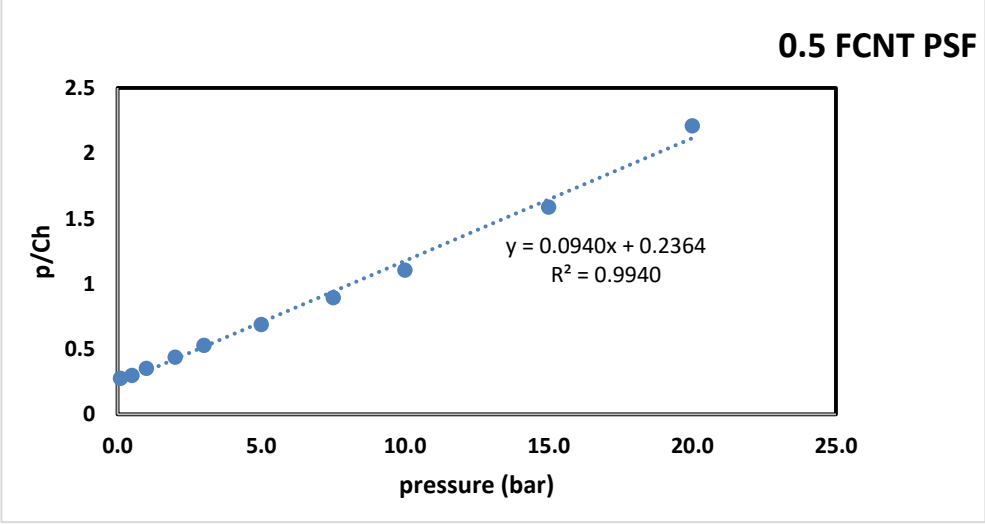
0.5 FCNT PSF
2.5
2
1.5
1
0.5
0
p/Ch
y = 0.0940x + 0.2364
R² = 0.9940
0.0
5.0
10.0
15.0
20.0
25.0
pressure (bar)

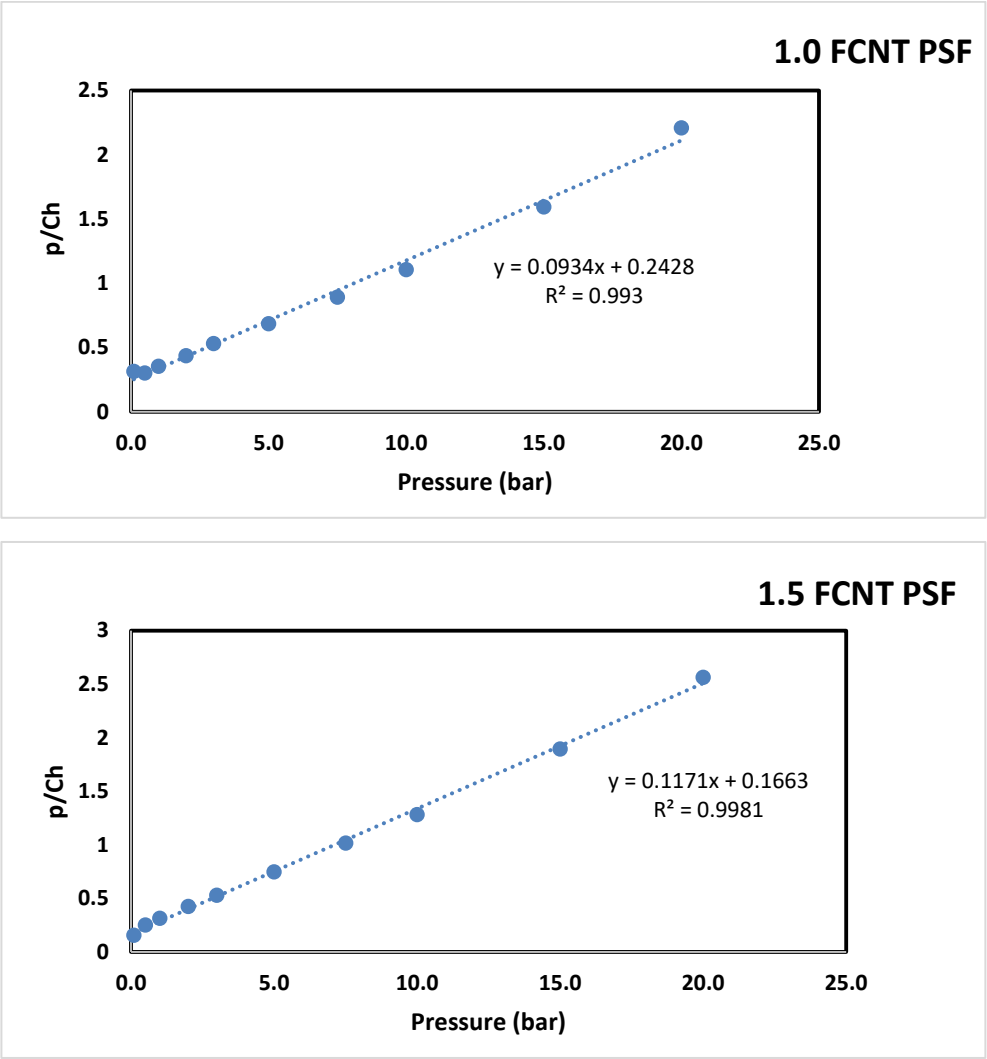

Figure G2: Plot of p/C_h against p for the determination of C_h' and b

Appendix H: Tables of CO_2 solubility coefficient and permeability values at elevated pressure

Table H1: CO_2 permeability and solubility values of pure PSF

Pressure (bar)	CO_2 Permeability (Barrer)	Solubility (10^{-2} cm^3 (STP)/(cm^3 cmHg))
2	6.60	4.99
4	6.45	3.73
6	6.42	3.09
8	6.32	2.70
10	6.04	2.44
12	5.81	2.26
14	5.91	2.12
16	6.00	2.01
18	6.05	1.93
20	6.08	1.86

Table H2: CO_2 permeability and solubility values of 0.2% FCNT PSF

Pressure (bar)	CO_2 Permeability (Barrer)	Solubility (10^{-2} cm^3 (STP)/(cm^3 cmHg))
2	6.91	4.67
4	6.74	3.43
6	6.63	2.82
8	6.48	2.45
10	6.46	2.21
12	6.44	2.04
14	6.38	1.91
16	6.17	1.81
18	5.96	1.74
20	5.83	1.67

Table H3: CO_2 permeability and solubility values of 0.5% FCNT PSF

Pressure (bar)	**CO_2 Permeability (Barrer)**	**Solubility (10^{-2} cm^3 (STP)/(cm^3 cmHg))**
2	7.1	4.18
4	6.84	3.22
6	6.73	2.71
8	6.58	2.39
10	6.56	2.18
12	6.54	2.02
14	6.47	1.90
16	6.26	1.81
18	6.05	1.73
20	5.92	1.67

Table H4: CO_2 permeability and solubility values of 1.0% FCNT PSF

Pressure (bar)	**CO_2 Permeability (Barrer)**	**Solubility (10^{-2} cm^3 (STP)/(cm^3 cmHg))**
2	7.79	4.15
4	7.44	3.21
6	7.32	2.71
8	7.01	2.40
10	6.78	2.18
12	6.61	2.03
14	6.57	1.91
16	6.36	1.82
18	6.34	1.74
20	6.22	1.68

Table H5: CO_2 permeability and solubility values of 1.5% FCNT PSF

Pressure (bar)	**CO_2 Permeability (Barrer)**	**Solubility (10^{-2} cm^3 (STP)/(cm^3 cmHg))**
2	7.56	4.46
4	6.86	3.23
6	6.3	2.66
8	5.91	2.34
10	5.89	2.13
12	5.84	1.98
14	5.51	1.87
16	5.4	1.78
18	5.28	1.72
20	5.25	1.66

Appendix I: Permissions to include published works in this thesis

This Agreement between Mr. Oluseyi Aberefa ("You") and Elsevier ("Elsevier") consists of your license details and the terms and conditions provided by Elsevier and Copyright Clearance Center.

License Number	4531230943897
License date	Feb 17, 2019
Licensed Content Publisher	Elsevier
Licensed Content Publication	Separation and Purification Technology
Licensed Content Title	Transport and separation properties of carbon nanotube-mixed matrix membrane
Licensed Content Author	A.F. Ismail,P.S. Goh,S.M. Sanip,M. Aziz
Licensed Content Date	Nov 19, 2009
Licensed Content Volume	70
Licensed Content Issue	1
Licensed Content Pages	15
Start Page	12
End Page	26
Type of Use	reuse in a thesis/dissertation
Portion	figures/tables/illustrations
Number of figures/tables/illustrations	1
Format	both print and electronic

Are you the author of this Elsevier article?	No
Will you be translating?	No
Original figure numbers	Figure 4
Title of your thesis/dissertation	IMPROVING POLYSULFONE MEMBRANE RESISTANCE TO CARBON DIOXIDE INDUCED PLASTICIZATION DURING NATURAL GAS SEPARATION USING FUNCTIONALIZED CARBON NANOTUBES
Expected completion date	Jun 2019
Estimated size (number of pages)	220
Requestor Location	Mr. Oluseyi Aberefa University of the witwatersrand Johannesburg, Gauteng 2000 South Africa Attn: Mr. Oluseyi Aberefa
Publisher Tax ID	ZA 4110266048
Total	0.00 USD

Order Completed

Thank you for your order.

This Agreement between Mr. Oluseyi Aberefa ("You") and Elsevier ("Elsevier") consists of your license details and the terms and conditions provided by Elsevier and Copyright Clearance Center.

Your confirmation email will contain your order number for future reference.

This Agreement between Mr. Oluseyi Aberefa ("You") and Elsevier ("Elsevier") consists of your license details and the terms and conditions provided by Elsevier and Copyright Clearance Center.

License Number	4531231076698
License date	Feb 17, 2019
Licensed Content Publisher	Elsevier
Licensed Content Publication	Composites Part A: Applied Science and Manufacturing
Licensed Content Title	Dispersion and functionalization of carbon nanotubes for polymer-based nanocomposites: A review
Licensed Content Author	Peng-Cheng Ma,Naveed A. Siddiqui,Gad Marom,Jang-Kyo Kim
Licensed Content Date	Oct 1, 2010
Licensed Content Volume	41
Licensed Content Issue	10
Licensed Content Pages	23
Start Page	1345
End Page	1367
Type of Use	reuse in a thesis/dissertation
Intended publisher of new work	other

Portion	figures/tables/illustrations
Number of figures/tables/illustrations	1
Format	both print and electronic
Are you the author of this Elsevier article?	No
Will you be translating?	No
Original figure numbers	Figure 2
Title of your thesis/dissertation	IMPROVING POLYSULFONE MEMBRANE RESISTANCE TO CARBON DIOXIDE INDUCED PLASTICIZATION DURING NATURAL GAS SEPARATION USING FUNCTIONALIZED CARBON NANOTUBES
Expected completion date	Jun 2019
Estimated size (number of pages)	220
Requestor Location	Mr. Oluseyi Aberefa University of the witwatersrand Johannesburg, Gauteng 2000 South Africa Attn: Mr. Oluseyi Aberefa
Publisher Tax ID	ZA 4110266048
Total	0.00 USD